THE SYNTHESIS AND REACTIVITY OF SOME PLATINUM GROUP CLUSTERS.

A Thesis submitted to the

UNIVERSITY OF GLASGOW

for the degree of

DOCTOR OF PHILOSOPHY

in the Faculty of Science

by

PAUL NICHOLAS EWING

Department of Chemistry
University of Glasgow.

 March 1989.

ProQuest LLC.
789 East Eisenhower Parkway
P.O. Box 1346
Ann Arbor, MI 48106 – 1346

Dedicated to the memory of

Maurice Miller (1912-1988),

a philosopher of life.

ACKNOWLEDGEMENTS.

I am most indebted to Dr. Louis J. Farrugia for his help, guidance, patience and inexhaustible enthusiasm during the course of this work.

I am grateful to the staff of the i.r, n.m.r, and micro-analytical laboratories for their technical assistance and to Dr. K.W. Muir for some help with the crystallographic analyses.

My thanks also to Mrs. Liz Hughes for typing this thesis.

I acknowledge financial support from the SERC.

Finally, I thank my family and Alison for their love and support.

CONTENTS

SUMMARY

This thesis describes the synthesis, characterisation and reactivity of several M_3Pt, (M = Os,Ru) clusters.

Chapter 1 contains a brief survey of the chemistry of unsaturated clusters together with an account of commonly applied electron counting schemes. Catalytically activated cluster transformations and the reactivity of lightly stabilised clusters are also considered.

In Chapter 2, the chemistry of the unsaturated 58 electron *closo*-tetrahedral cluster $Os_3Pt(\mu\text{-}H)_2(CO)_{10}(PCy_3)$, 1, is described. The 60 electron adducts of 1, $Os_3Pt(\mu\text{-}H)_2(CO)_{10}(PCy_3)(L)$, are known to adopt butterfly (L = CO) or *closo*-tetrahedral (L = CH_2) metal core geometries. A molecular orbital analysis of the interactions of μ-CO and μ-CH_2 fragments with the *closo*-tetrahedral complex $[Ru_3Pt(CO)_{10}(PH_3)]^{2-}$, which models 1, is presented. This analysis suggests that the symmetry of the frontier orbitals of the incoming ligand is important in defining the framework geometry of the 60 electron adducts. With this in mind, the reactivity of $Os_3Pt(\mu\text{-}H)_2(CO)_{10}(PCy_3)$ towards CO and CH_2 analogues (CNR; and SO_2, $SnCl_2$) is reported. CNR and SO_2 give rise to the expected butterfly and tetrahedral adducts respectively. However, with $SnCl_2$ a more complex cluster transformation takes place. The CNR adduct readily decarbonylates to give the first CO substituted derivative of 1. The protonation of several Os_3Pt systems is reported. All the clusters examined protonate at Os-Os edges. In the final sections of this chapter the reactivity of 1 towards heterocumulene and anionic acetylide species is described.

Chapter 3 describes the synthesis and reactivity of the spiked triangular complex $Ru_3Pt(\mu\text{-}H)(\mu_4\text{-}\eta^2\text{-}C{\equiv}Ct\text{-}Bu)(cod)(CO)_9$, 2. The cod ligand of 2 is readily displaced by dppe giving the analogous substituted complex $Ru_3Pt(\mu\text{-}H)(\mu_4\text{-}\eta^2\text{-}C{\equiv}Ct\text{-}Bu)(dppe)(CO)_9$, 3 and the tautomeric vinylidene butterfly species $Ru_3Pt(\mu_4\text{-}\eta^2\text{-}C{=}C(H)t\text{-}Bu)(dppe)(CO)_9$, 4. 3 and 4 interconvert via an intramolecular hydride migration. 4 protonates at the hinge Ru-Ru vector. The reaction of 2 with $Os_3(\mu\text{-}H)_2(CO)_{10}$ results in scission of the Pt-Ru bond of 2 and formation of $Os_3Pt(\mu\text{-}H)_2(\mu\text{-}CO)(cod)(CO)_9$.

In Chapter 4 the X-ray structure determinations of $Os_3Pt(\mu\text{-}H)(\mu_4\text{-}\eta^2\text{-}C{\equiv}CPh)(CO)_{10}(PCy_3)$; $Ru_3Pt(\mu\text{-}H)(\mu_4\text{-}\eta^2\text{-}C{\equiv}Ct\text{-}Bu)(cod)(CO)_9$; and $[Ru_3Pt(\mu\text{-}H)(\mu_4\text{-}\eta^2\text{-}C{=}C(H)t\text{-}Bu)(dppe)(CO)_9]^+BF_4^-$ are reported. These analyses were performed by the author.

Chapter 5 details the experimental procedures used in this work.

KEY TO COMPOUND NUMBERING SYSTEM.

Compound No.	Formula.
1	$Os_3(CO)_{12}$
2	$Ru_3(CO)_{12}$
3	$Fe_3(CO)_{12}$
4	$Os_3(\mu\text{-}H)_2(CO)_{10}$
5	$Os_3(\mu\text{-}H)(\mu\text{-}\eta^2\text{-}CH{=}CH_2)(CO)_{10}$
6	$Os_3(\mu\text{-}H)(\mu\text{-}\eta^2\text{-}PhC{=}C(H)Ph)(CO)_{10}$
7(I)	$Os_3(\mu\text{-}H)(\mu\text{-}\eta^2\text{-}CH_3)(CO)_{10}$
7(II)	$Os_3(\mu\text{-}H)_2(\mu\text{-}CH_2)(CO)_{10}$
8	$Os_3(\mu\text{-}H)(\mu_3\text{-}\eta^3\text{-}(Ph)_2PCH_2P(Ph)C_6H_4)(CO)_8$
9	$[NEt_4]_2[Re_3(\mu\text{-}H)_3(CO)_{10}]$
10	$[NEt_4][Re_3(\mu\text{-}H)_4(CO)_{10}]$
11	$Fe_3(\mu_3\text{-}\eta^2\text{-}\perp\text{-}PhC{\equiv}CPh)(CO)_9$
12	$Os_3(PhC{\equiv}CPh)(CO)_9$
13	$Os_3(\mu_3\text{-}\eta^2\text{-}\perp\text{-}PhC{\equiv}CPh)(dppm)(CO)_7$
14	$Fe_4(\mu\text{-}CO)(\mu_4\text{-}PPh)_2(CO)_{10}$
15	$Fe_3Rh(\mu_4\text{-}PPh)_2(Cp^*)(CO)_8$
16	$Ru_4(\mu\text{-}CO)(\mu_4\text{-}PPh)_2(CO)_{10}$
17	$Os_3(CO)_{11}(MeCN)$
18	$Os_3(CO)_{10}(MeCN)_2$
19	$Os_3Pt(\mu\text{-}H)_2(CO)_{10}(PR_3)$; a, R=Cy; b, R=Ph
20	$Os_3Pt(\mu\text{-}H)_2(CO)_{11}(PCy_3)$
21	$Os_3Pt(\mu\text{-}H)_2(CO)_{10}(PPh_3)_2$
22	$Os_3Pt(\mu\text{-}H)_4(CO)_{10}(PCy_3)$

23 $Os_3Pt(\mu\text{-}H)_2(\mu\text{-}CH_2)(CO)_{10}(PCy_3)$ -C_s isomer

24 $Os_3Pt(\mu\text{-}H)_2(\mu\text{-}CH_2)(CO)_{10}(PCy_3)$ - C_1 isomer

25 $Os_3Pt(\mu\text{-}H)_2(CO)_{10}(RNC)(PCy_3)$; a, R=t-Bu;
b, R=Cy.

26 $Os_3Pt(\mu\text{-}H)_2(CO)_9(RNC)(PCy_3)$; a, R=t-Bu;
b, R=Cy.

27 $Os_3Pt(\mu\text{-}H)_2(\mu\text{-}CH_2)(CO)_9(CyNC)(PCy_3)$

28 $Os_3Pt(\mu\text{-}H)_2(\mu\text{-}SO_2)(CO)_{10}(PCy_3)$

29 $Os_3PtSn(\mu\text{-}H)_2(CO)_{10}(Cl)(OEt_2)(SnCl_3)(PCy_3)$

30 $[Os_3Pt(\mu\text{-}H)_3(CO)_{10}(PCy_3)]BF_4$

31 $[Os_3Pt(\mu\text{-}H)_3(CO)_9(CyNC)(PCy_3)]BF_4$

32 $[Os_3Pt(\mu\text{-}H)_3(\mu\text{-}CH_2)(CO)_9(CyNC)(PCy_3)]CF_3CO_2$

33 $Os_3Pt(\mu_3\text{-}S)_2(\eta^1\text{-}C_{11}H_{18})(CO)_9(PCy_3)$

34 $Os_3Pt(\mu\text{-}H)(\mu_4\text{-}\eta^2\text{-}C{\equiv}CPh)(CO)_{10}(PCy_3)$

35 $Ru_3(\mu\text{-}H)(\mu_3\text{-}\eta^2\text{-}C{\equiv}Ct\text{-}Bu)(CO)_9$

36 $Ru_3Pt(\mu\text{-}H)(\mu_4\text{-}\eta^2\text{-}C{\equiv}Ct\text{-}Bu)(cod)(CO)_9$

37 $Ru_3Pt(\mu\text{-}H)(\mu_4\text{-}\eta^2\text{-}C{\equiv}Ct\text{-}Bu)(dppe)(CO)_9$

38 $Ru_3Pt(\mu_4\text{-}\eta^2\text{-}C{=}C(H)t\text{-}Bu)(dppe)(CO)_9$

39 $[Ru_3Pt(\mu\text{-}H)(\mu_4\text{-}\eta^2\text{-}C{=}C(H)t\text{-}Bu)(dppe)(CO)_9]BF_4$

40 $Os_3(\mu\text{-}H)_2(\mu\text{-}CO)(cod)(CO)_9$

41 $Ru_3(\mu\text{-}H)[\mu_3\text{-}\eta^3\text{-}CH(Me){=}C{=}C(Et)](CO)_9$

42 $Ru_3(\mu\text{-}PPh_2)[\mu_3\text{-}\eta^3\text{-}CH_2{=}C{=}C(i\text{-}Pr)](CO)_8$

43 $Ru_3(\mu\text{-}CH_2)(\mu\text{-}PPh_2)[\mu_3\text{-}\eta^3\text{-}CH_2{=}C{=}C(i\text{-}Pr)](CO)_7$

44 $Os_3Ni(\mu\text{-}H)(\mu_4\text{-}\eta^2\text{-}C{=}C(H)t\text{-}Bu)(Cp)(CO)_9$

45 $Ru_3Ni(\mu\text{-}H)(\mu_4\text{-}\eta^2\text{-}C{=}C(H)t\text{-}Bu)(Cp)(CO)_9$

46 $Ru_3Ni(\mu\text{-}H)(\mu_4\text{-}\eta^2\text{-}C{=}C(H)i\text{-}Pr)(Cp)(CO)_9$

47 $Co_3Fe(\mu\text{-}CO)_2(\mu_4\text{-}\eta^2\text{-}C{=}CH_2)(Cp)(CO)_7$

48 $Ru_4(\mu\text{-}PPh_2)(\mu_3\text{-}OH)(\mu_4\text{-}\eta^2\text{-}C{=}C(H)i\text{-}Pr)(CO)_{10}$

INDEX OF ABBREVIATIONS.

acac	acetylacetonate
Bu	butyl
cod	1,5-cyclooctadiene
Cp	cyclopentadiene
Cp^*	pentamethyl cyclopentadiene
Cy	cyclohexyl
dppe	bis(diphenyl phosphino)ethane
dppm	bis(diphenyl phosphino)methane
E.A.N	Effective Atomic Number
EHMO	Extended Huckel Molecular Orbital
esd	estimated standard deviation
Et	ethyl
E.T.C	Electron Transfer Catalysis
h	hours
HOMO	Highest Occupied Molecular Orbital
IR	infra-red
LUMO	Lowest Unoccupied Molecular Orbital
Me	methyl
mins	minutes
MO	Molecular Orbital
n.m.r	nuclear magnetic resonance
Ph	phenyl
PPN^+	$[(Ph_3P)_2N]^+$
Pr	propyl
P.E.S.P.T	Polyhedral Skeletal Electron Pair Theory
py	pyridine
S.E.P.	Skeletal Electron Pair
T.E.C	Topological Electron Counting

THF	tetrahydrofuran
Tol	tolyl
VT	variable temperature

For IR data : vs = very strong; s = strong; m = medium;
w = weak; vw = very weak; br = broad;
sh = shoulder.

For n.m.r data : s = singlet; d = doublet; t = triplet
m = multiplet.

CHAPTER ONE.

INTRODUCTION.

1.1 Prologue.

The chemistry of low valent transition metal cluster compounds has developed rapidly over the last 25 years or so, and now merits a detailed discussion in undergraduate textbooks.[1] Three major reasons for this suggest themselves.

i) Muetterties[2-4] has proposed that cluster complexes may represent molecular models for the interactions of chemisorbed species with metal surfaces under catalytic conditions. This model, the "cluster-surface analogy", suggests that the ligand-metal bonding in cluster systems parallels the localised bonding of chemisorbed substrates at surface metal sites. This analogy is proving increasingly useful in the identification of surface species by comparison of spectroscopic data obtained from chemisorbed molecules with that of cluster complexes with well characterised ligand coordination.[5-7] However, as pointed out by Moskovits,[8] this analogy has limitations imposed by the differences in electronic structure, metal geometry and localisation of metal-ligand/adsorbate bonding that exist between metal surfaces and molecular clusters.

ii) Clusters can afford species that are catalytically active in a number of homogeneous processes,[9-11] including alkene isomerisation[12,13] and the water-gas shift reaction.[14,15] In addition to this, there is a growing interest in the application of cluster complexes as precursors of homo and heterometallic hetrogeneous catalysts.[9,16,17]

iii) Lastly, and of increasing importance, metal clusters are chemically interesting in their own right and display a wide range of cluster framework geometries and ligand transformations. A number of reviews have been published recently that illustrate this point. They

encompass a wide range of topics including cluster chemistry in general,[18-22] high nuclearity cluster compounds,[23] heterometallic clusters,[24,25] electrochemistry of cluster complexes,[26] structural and bonding considerations in cluster chemistry,[27,28] clusters with open transition metal polyhedra,[29] metalloborane clusters,[30] butterfly clusters,[31] organic substrate interactions with clusters,[32,33] alkyne and acetylide containing clusters,[34-36] carbido carbonyl clusters,[37] and nitrosyl and nitrido clusters.[38] These exemplify the breadth of current research activity in the area of transition metal cluster chemistry.

For the purposes of this introduction, Johnson's[39] definition of a cluster as "a discrete unit containing at least three metal atoms in which metal-metal bonding is present" will be adopted. In addition, the scope of this introduction will be limited to consideration of metal carbonyl clusters.

1.2 Reactivity of Clusters.

Initially, studies of metal clusters focussed on synthetic and structural aspects, with a range of preparative routes to clusters and an accompanying variety of metal framework geometries and novel ligand bonding modes being discovered.

Recently, however, the systematic investigation of cluster reactivity has become an increasingly important objective.[21] One major aim of such research is to advance the understanding of cluster reactions to an extent that renders their outcome predictable. However, achieving this goal remains a long term prospect.

The binary carbonyls of the iron triad, $M_3(CO)_{12}$, (M = Fe,Ru,Os), (Fig.1.), constitute one of the best studied series of clusters. By considering a conceptually simple reaction such as ligand substitution of

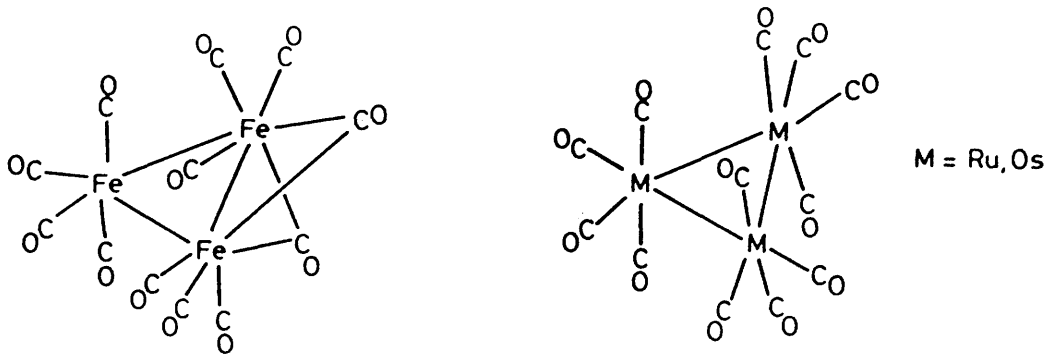

Figure 1 : The binary carbonyls of the iron triad.

these $M_3(CO)_{12}$ (M = Fe,Ru,Os) clusters, the diverse factors that influence product formation in such systems are illustrated.

Thermodynamic studies indicate that both the metal-metal and metal-carbonyl bonds in $Os_3(CO)_{12}$, 1, are stronger than those in the corresponding Fe and Ru analogues.[40] (Table 1).

Table 1. Comparison of M-M and M-CO bond strengths in $M_3(CO)_{12}$(M = Fe,Ru,Os).

	ΔH_D kJmol^{-1}	M-M kJmol^{-1}	M-CO kJmol^{-1}
$Fe_3(CO)_{12}$	1676	52	126
$Ru_3(CO)_{12}$	2414	78	182
$Os_3(CO)_{12}$	2690	94	201

*ΔH_D refers to $M_3(CO)_{12}(g,298K) \longrightarrow 3M(g,298K) + 12CO(g,298K)$.

The comparative strength of the Os-Os bond in 1 accounts to some extent for the relative inertness to Os-Os bond cleavage of the *triangulo* - Os_3 framework. The consequences of the relative strengths of the M-CO and M-M bonds are evident in mechanistic studies of ligand substitution in the $M_3(CO)_{12}$ (M = Fe,Ru,Os) series.

The kinetics of the substitution reactions of 1 with PR_3 (R = Ph,[41,42] n-Bu[42]) follow the rate equation

$$k_{obs} = k_1 + k_2[PR_3] \qquad \text{Equation 1.}$$

For PPh_3, the value of k_2 is negligible and the reaction follows first

order kinetics.[41,42] This is consistent with a CO dissociative mechanism, although it does not preclude a pathway with a rate determining step involving reversible isomerisation of the cluster yielding a complex with a vacant coordination site.[42] However, Os-CO dissociation is considered the most likely mechanism.[41,42] Due to the slow rate of Os-CO bond scission at ambient temperatures, fairly forcing thermal conditions ($\geq 100^{o}C$) are required for these reactions. This may be a reflection of the thermodynamic stability of the Os-CO bond.

In contrast, the reaction of 1 with the more nucleophilic phosphine $Pn\text{-}Bu_3$ obeys second order kinetics at relatively low temperatures ($70^{o}C$) and high concentrations of $Pn\text{-}Bu_3$.[42] This implies associative nucleophilic attack at a cluster site is occurring. Since 1 is coordinatively saturated, an associative pathway leads to cluster fragmentation and the mononuclear products $Os(CO)_4(Pn\text{-}Bu_3)$ and $Os(CO)_3(Pn\text{-}Bu_3)_2$ are observed. Reducing the concentration of $Pn\text{-}Bu_3$ and increasing the temperature to $170^{o}C$ promotes the CO dissociative route and again first order kinetics are followed.[42] This leads, through successive substitutions, to formation of the trisubstituted derivative $Os_3(CO)_9(Pn\text{-}Bu_3)_3$.

Where first order kinetics are obeyed, mono, di- and trisubstituted phosphine derivatives are observed, indicating that the rates for second and third ligand substitutions are approximately equal to that of the first. In addition, to this, the temperatures required to effect substitution of PPh_3 [43] and PMe_2Ph [44] are sufficiently high to allow ligand transformations involving C-H and C-P bond scission,[43,44] and C-C bond formation[43,45] to occur on the triangular cluster framework. Examples of clusters displaying each type of transformation are given in Figure 2.

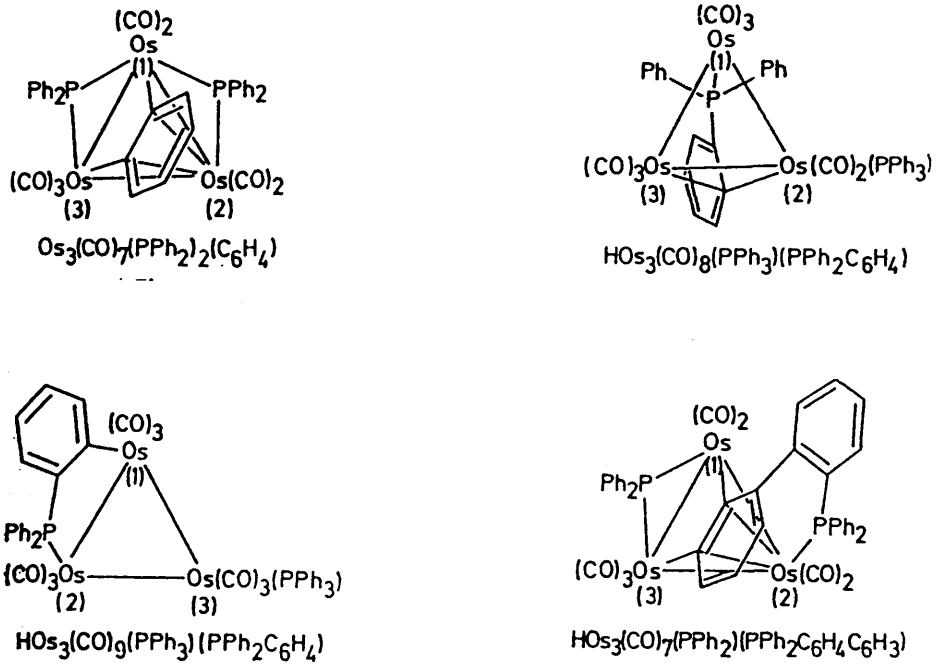

Figure 2. Examples of ligand transformations on thermolysis of 1 with PPh_3.

Thus, for 1, carbonyl substitution will occur when there is enough thermal energy supplied to allow Os-CO dissociation to take place at an appreciable rate. This has two potential drawbacks. The initially formed species may react further under reaction conditions to yield a variety of Os_3 products, as in the cases cited above. Secondly, the elevated temperatures required for reaction may facilitate cluster degradation. For example, the substitution of 1 with isocyanides occurs at 110°C yielding $Os_3(CO)_{12-n}(RNC)_n$, (n = 1-4), while at 125°C, the hexanuclear complexes $Os_6(CO)_{18-n}(RNC)_n$, (n = 1-5), form.[46-48]

The substitution reactions of 1 contrast with the observed chemistry of $Ru_3(CO)_{12}$, 2, and $Fe_3(CO)_{12}$, 3. The reaction of 2 with PPh_3 proceeds directly to the tri-substituted cluster $Ru_3(CO)_9(PPh_3)_3$, with no detectable mono or disubstituted intermediates. However, with stronger nucleophiles fragmentation occurs. For example with $Pn\text{-}Bu_3$, $Ru(CO)_4(Pn\text{-}Bu_3)$, and $Ru(CO)_3(Pn\text{-}Bu_3)_2$, in addition to $Ru_3(CO)_9(Pn\text{-}Bu_3)_3$ are the observed

products.[49] Fragmentation products were observed even at very low concentrations of Pn-Bu_3, in contrast to the fragmentation reaction of 1 with the same phosphine.[42] Treatment of 3 with phosphines leads to formation of the monosubstituted cluster followed by rapid fragmentation and the formation of the mononuclear species $Fe(CO)_4L$ and $Fe(CO)_3L_2$.[41]

Therefore, as the M-M bond strength decreases from 1 through 3 the tendency of the clusters to undergo fragmentation rather than substitution increases. These reactions are summarised below:

$$Fe_3(CO)_{12} + L \xrightarrow{a)} Fe_3(CO)_{11}L \longrightarrow Fe(CO)_4L + Fe(CO)_3L_2$$

$$Ru_3(CO)_{12} + L \xrightarrow{b)} Ru_3(CO)_9L_3 + Ru(CO)_4L + Ru_3(CO)_3L_2$$

$$Os_3(CO)_{12} + L \xrightarrow{c)} Os_3(CO)_{11}L + Os_3(CO)_{10}L_2 + Os_3(CO)_9L_3$$

Reaction temperatures: a) Ambient temperatures, b) 25-60°C, c) 100°C or over.

In view of the complexities revealed in these studies of cluster reactivity, it is desirable to utilise clusters that can react under sufficiently mild conditions to prevent degradation and reduce product spread. There are a number of classes of such clusters available to the synthetic chemist, the most important being:

i) Electronically unsaturated clusters

ii) Lightly stabilised clusters

iii) Catalytically activated clusters

The remainder of this introduction will concentrate on the reactivity of clusters from each of the above categories. It is not intended to present a comprehensive treatment of these topics, but it is hoped that an overview of the progress made in understanding the reactivity of these systems will be given.

1.3 Electronically unsaturated clusters.

These are defined as clusters in which the number of valence

electrons is less than that predicted by electron counting rules. Due to their unsaturation such clusters are susceptible to nucleophilic attack. Before considering the chemistry of unsaturated clusters, a brief survey of commonly used electron counting schemes will be presented.

1.3.1 Electron Counting Rules.

Extensive structural studies of metal cluster complexes by X-ray (and, infrequently, neutron) diffraction techniques have established that metal frameworks in these systems exhibit an intriguing variety of geometries.[1,51,52] Several conceptual approaches have been developed to rationalise the relationship between the metal framework geometries and the numbers of valence electrons that contribute to the framework bonding.

1.3.1.(i) Effective Atomic Number (E.A.N) Rule.

The simplest electron counting scheme is based on the "18 electron" or "Effective Atomic Number" (E.A.N) rule.[53] This rule states that transition metals use 9 valence atomic orbitals (A.O's), namely the nd, (n+1)s and (n+1)p orbitals, for metal-ligand bonding and accommodating non-bonding electrons. The E.A.N rule can be successfully applied to many low oxidation state mononuclear organometallic complexes. To extend the application of this rule to clusters, two further assumptions are made:-[54]

i) all nine of the metal's valence A.O's are used in metal-metal (M-M) bonding, metal-ligand bonding or accommodating non-bonding electrons.

ii) the edges of the metal skeleton are connected via 2 centre - 2 electron (2c-2e) bonds.

Using these assumptions the following expression can be derived to calculate the number of M-M bonds, m, in a cluster M_nL_x

$$m = \frac{(18n-k)}{2} \qquad \text{Equation 2.}$$

where k is the total valence electron count of the cluster (i.e. the sum of metal valence electrons plus electrons contributed by ligands and net charge). The number of electrons contributed to the valence electron count by various ligands in common bonding modes has recently been tabulated by Owen[28] (Table 2).

Table 2. Number of electrons donated by ligands in common bonding modes.

Ligand	Bonding Mode.	Electrons Donated.	Ligand	Bonding Mode.	Electrons Donated.
H	μ_1	1e	OR	μ_2	3e
H	μ_2	1e	NO	μ_1	3e
H	μ_3	1e	$CRCR_2$	μ_2-η^2	3e
$AuPR_3$	μ_2	1e	Br	μ_2	3e
$AuPR_3$	μ_3	1e	I	μ_2	3e
Au	μ_4	1e	BCO	μ_3	3e
I	μ_1	1e	Bi	μ_3	3e
SiR_3	μ_1	1e	$AsMe_2$	μ_2	3e
$SnMe_3$	μ_1	1e	RC:O	μ_2-η^2	3e
$HOs(CO)_5$	μ_1	1e	NO	μ_2	3e
$W(CO)_3Cp$	μ_1	1e	CO	μ_3-η^1, μ_1-η^1	4e
PR_3	μ_1	2e	PR	μ_3	4e
CO	μ_1	2e	S	μ_3	4e
CO	μ_2	2e	O	μ_2	4e
CO	μ_3	2e	C	Interstitial	4e
CS	μ_2	2e	RCCR	μ_3-η^2	4e
CR_2	μ_2	2e	Te	μ_3	4e
NR_3	μ_1	2e	C_2R_2	μ_2-η^2	4e
R_2CCR_2	μ_1-η^2	2e	Se	μ_3	4e
SO_2	μ_2	2e	P	Interstitial	5e
NCMe	μ_1	2e	Cp	η^5	5e
$SnCl_2$	μ_3	2e	CCR	μ_3-η^2	5e
Hg	μ_4	2e	N	Interstitial	5e
PR_2	μ_2	3e	Arene	η^6	6e
SR	μ_2	3e	CS	μ_4-η^2	6e
CR	μ_3	3e			

One consequence of Equation 2 is that, for a given n, an increase of two in k reduces m by one. This can be accounted for by assuming the two additional valence electrons occupy a localised M-M antibonding orbital, thus effecting bond cleavage.[55] Pomeroy et al[56] have recently prepared a series of tetraosmium complexes which illustrate the opening of a *closo*-tetrahedral framework to a butterfly and finally spiked-triangular geometry, with increasing electron count (Figure 3).

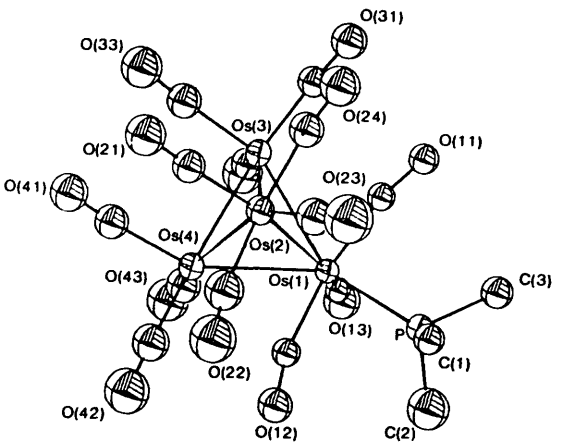

Molecular structure of $Os_4(CO)_{13}(PMe_3)$

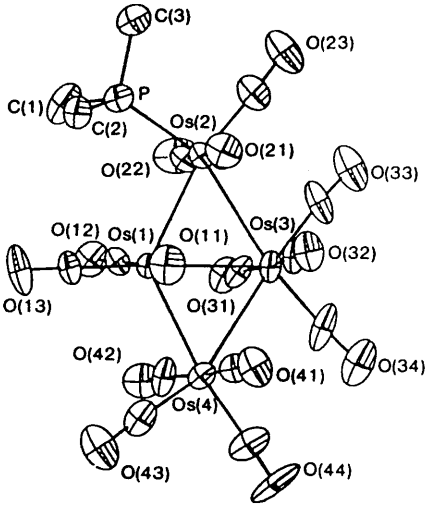

Molecular structure of $Os_4(CO)_{14}(PMe_3)$

n = 4, k = 60, m = 6

n = 4, k = 62, m = 5

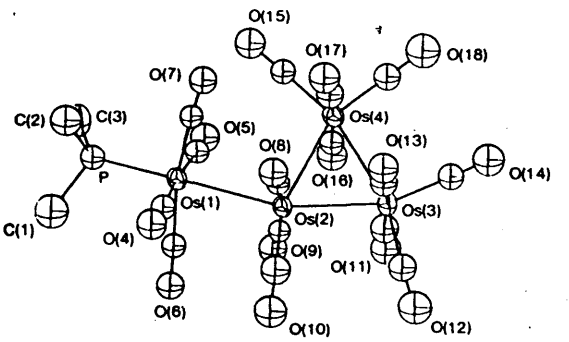

Molecular structure of molecule 2 of $Os_4(CO)_{15}(PMe_3)$

n = 4, k = 64, m = 4

Figure 3. Molecular Structures of $Os_4(CO)_n(PMe_3)$, (n = 13,14,15).

The E.A.N rule successfully predicts the experimentally observed metal-metal connectivity in a large number of low nuclearity clusters. However, as the nuclearity of cluster systems increases, the assumption that metal-metal bonding involves localised 2c-2e bonds becomes increasingly untenable.[54] For this reason the E.A.N approach is unsuitable for

clusters with n>6, and electron counting schemes that take into account the delocalised nature of the skeletal bonding are more reliable. It should be noted that, while the E.A.N. rule is a useful rule of thumb for predicting m in low nuclearity systems, the bonding in these systems is more accurately described in terms of cluster based Molecular Orbitals (M.O's).

1.3.1 (ii) The Polyhedral Skeletal Electron Pair Theory (P.S.E.P.T).

The Polyhedral Skeletal Electron Pair Theory, P.S.E.P.T., developed through the work of Wade[57] and Mingos,[55] approaches the correlation between valence electron count and metal framework geometry from a different standpoint. It allocates electrons involved in framework bonding to skeletal bonding M.O's (as opposed to localised 2c-2e bonds). Although originally developed to rationalise bonding in main group clusters, the P.S.E.P.T, can be successfully applied to transition metal cluster structures, as well as to clusters containing both transition metal and main group skeletal atoms.

The P.S.E.P.T assumes that, for a closed (or *closo*) deltahedral transition metal framework with n vertices, each skeletal M atom uses all 9 of its valence A.O's. 6n A.O's are used for M-L bonding and occupation by non-bonding electrons. The remaining 3n A.O's available for skeletal bonding interact to give (n+1) bonding M.O's. The total number of cluster valence molecular orbitals (C.V.M.O's) for a *closo*-deltahedron with n-vertices is, therefore, (7n+1). This result is supported in a recent theoretical analysis by Stone using his Tensor Surface Harmonic Theory.[58]

This P.S.E.P.T treatment can be extended to include *nido* and *arachno* clusters. These are clusters with metal skeletons derived from *closo* polyhedra by removal of one (*nido*) or two (*arachno*) vertices.

It has been shown that the number of C.V.M.O's for *nido* and

arachno frameworks is (7n+2) and (7n+3) respectively.[54]

One major advantage of the P.S.E.P.T over the E.A.N approach is that it can be adapted to rationalise the skeletal bonding in high nuclearity clusters. Many of these clusters have frameworks that are derived from the condensation of smaller polyhedra.[59,60] By considering fragment M.O analyses of these condensed polyhedra, Mingos has developed a modification to the P.S.E.P.T that accounts for the valence electron count of these systems.[60] It can be stated as follows:-

"The total electron count in a condensed polyhedron is equal to the sum of the electron counts for the parent polyhedra minus the electron count characteristic of the atom, pair of atoms or face of atoms common to each unit".

The characteristic electron count of the shared unit corresponds to the expected electron count of that unit when it exists in isolation; these counts are listed in Table 3.

Table 3. The Characteristic electron counts of shared units.

Shared Unit.	Subtract.
Vertex	$18e^-$
Edge	$34e^-$
Triangular Face	$48e^-$, $50e^-$ [a]
Square Face	$62e^-$,[b] $64e^-$, [c]
"Butterfly Face"	$62e^-$

a) when parent polyhedra are deltahedra with n>6.

b) when either of the parent polyhedra is a deltahedron.

c) when both parent polyhedra are 3 connected.

A summary of the general P.S.E.P.T electron counting rules for various polyhedra is presented in Table 4.

Table 4. Summary of electron counts for P.S.E.P.T. (from Ref. 28)

Polyhedral type	Electron count
Deltahedron *closo-*	$14n+2$
nido-	$14n+4$
arachno-	$14n+6$
Three-connected	$15n$
Ring compounds	$16n$
Capped structures	$N+12x$
Edge bridged structures	$N+14x$
Condensed polyhedra:	
vertex shared	$A+B-18$
edge shared	$A+B-34$
Δ-face shared	$A+B-48$ or $A+B-50$
□-face shared	$A+B-62$ or $A+B-64$

Where: n is the nuclearity of the cluster. N is the electron count of the uncapped or unbridged parent polyhedron. x is the number of capping or edge-bridging groups. A and B are the electron counts of the parent polyhedra.

This Thesis is concerned with the chemistry of heteronuclear clusters containing platinum, and special considerations apply to electron counting rules for such clusters. Clusters containing late transition metals such as platinum and gold, are, in general, electron deficient according to the predictions of the P.S.E.P.T.[61,62] This is due to the large energy separation of the metal valence s- and p-orbitals which restricts the involvement of the p-orbitals in forming M.O's of sufficiently low energy to be occupied by valence electrons. The P.S.E.P.T can be adapted to account for the electron counts observed in these systems with some success.[61-66] It is interesting to note that Boag[67] has recently reported the synthesis and structure of the 60 electron tetrahedral cluster $[Pt_4(\mu_3\text{-}CO)(\eta^5\text{-}C_5Me_5)_3(CO)_2]^+[BF_4]^-$, the first example of an electronically saturated homonuclear platinum cluster.

Despite these various refinements, there are structures which cannot be rationalised by the P.S.E.P.T. For example $[Ni_5(CO)_{12}]^{2-}$ [68] has a distorted trigonal bipyramidal framework and an electron count of

76, whereas the P.S.E.P.T predicts 72 valence electrons. This exemplifies the fact that, although the P.S.E.P.T is conceptually useful, it cannot be viewed as a substitute for rigorous M.O. treatments. The P.S.E.P.T is the most commonly applied electron counting scheme in current use. It successfully accounts for, and predicts, a wide range of metal framework geometries in terms of the cluster valence electron count.

1.3.1 (iii) Topological Electron Counting (T.E.C) Scheme.

Another, more recently developed counting scheme is the Topological Electron Counting (T.E.C) approach devised by Teo.[69-72] This is based on Euler's Theorem:

$$E = V + F - 2 \qquad \text{Equation 3.}$$

where:- E is the number of edges of a polyhedron.

V is the number of vertices of a polyhedron.

F is the number of faces of a polyhedron.

From this, the number of C.V.M.O's, T, can be determined as

$$T = 8V - F + 2 + X \qquad \text{Equation 4.}$$

X is an adjustment factor, which is equal to the number of electron pairs in excess of that predicted by the E.A.N. rule.[69] Various rules have been proposed for evaluating X and these are presented in Table 5.

Table 5. Rules for determining X in the T.E.C. Scheme.

1.	For all 3-connected polyhedra, X = 0	
2.	Capping an N-gonal face of a polyhedron increases X by N-3	
3.	X = 0 for all Pyramids.	
4.	For Bipyramids :	X = 0 (or 2), for Trigonal
		X = 1 (or 3), for Tetragonal
		X = 3 for Pentagonal

contd...

5. For Antiprisms : X = 1, for Trigonal

X = 1, (or 3) for Square

X = 3 for Pentagonal

6. X = S for Vertex or Edge-sharing (connected) Polyhedra, where S is the number of shared Vertices, or Edges respectively.

7. X = H for Face sharing Polyhedra, where H is the number of "hidden edges".

Mingos has shown the close relationship between the T.E.C. approach and the P.S.E.P.T.[73] However, as argued by Teo[74] the T.E.C. theory allows for multiple electron counts in certain polyhedra where X is not uniquely defined. This allows rationalisation of several compounds where the P.S.E.P.T fails, for instance in $[Ni_5(CO)_{12}]^{2-}$,[68] with X = 2, the observed electron count of 76 is predicted.

1.3.1 (iv) Other Schemes.

A rationalisation of bonding in metal clusters has been presented by Lauher,[75] using an approach that is quite different from that of the P.S.E.P.T and T.E.C. theory.

Lauher analysed the orbital interactions of bare metal atoms in clusters with a variety of nuclearities and metal geometries using extended Huckel calculations. The calculated energy levels of the resultant cluster orbitals were found to fall into two categories : the low lying C.V.M.O's and the high lying antibonding orbitals. The results of these calculations are summarised in Table 6.

By subtracting the valence electron count of the metals in the cluster from the predicted cluster valence electron count, the number of electrons required from ligand bonding can be calculated, and hence stoichiometries of, for example, binary carbonyl clusters can be predicted, given a specific metal geometry. The number of C.V.M.O's for a given metal framework calculated by this method is in close

Table 6. Bonding Capabilities of Transition Metal Cluster Frameworks. (ref. 75)

geometry	N	$9 \times N$	HLAO	CVMO	CVE	CVMO/N
monomer	1	9	0	9	18	9.0
dimer	2	18	1	17	34	8.5
trimer	3	27	3	24	48	8.0
tetrahedron	4	36	6	30	60	7.5
butterfly	4	36	5	31	62	7.75
square plane	4	36	4	32	64	8.0
trigonal bipyramid	5	45	9	36	72	7.2
square pyramid	5	45	8	37	74	7.4
bicapped tetrahedron	6	54	12	42	84	7.0
octahedron	6	54	11	43	86	7.17
capped square pyramid	6	54	11	43	86	7.17
edge shared bitetrahedron	6	54	11	43	86	7.17
pentagonal pyramid	6	54	10	44	88	7.33
trigonal prism	6	54	9	45	90	7.5
capped octahedron	7	63	14	49	98	7.0
pentagonal pyramid	7	63	14	49	98	7.0
capped trigonal prism	7	63	12	51	102	7.29
bicapped octahedron	8	72	17	55	110	6.88
triangular dodecahedron	8	72	16	56	112	7.0
square antiprism	8	72	15	57	114	7.13
bicapped trigonal prism	8	72	15	57	114	7.13
cube	8	72	12	60	120	7.5
tricapped octahedron	9	81	18	63	126	7.0
tricapped trigonal prism	9	81	17	64	128	7.11
capped square antiprism	9	81	16	65	130	7.22
capped cube	9	81	15	66	132	7.33
tetrahedron	10	90	20	70	140	7.0
bicapped cube	10	90	19	71	142	7.1
bicapped square antiprism	10	90	19	71	142	7.1
truncated trigonal bipyramid	12	108	28	80	160	6.67
icosahedron	12	108	23	85	170	7.08
cube octahedron	12	108	23	85	170	7.08
truncated hexagonal bipyramid	12	108	23	85	170	7.08
icosahedron	13	117	32	85	170	6.54
cube octahedron	13	117	32	85	170	6.54
truncated hexagonal bipyramid	13	117	32	85	170	6.54
face centered cube	14	126	36	90	180	6.43
rhombic dodecahedron	14	126	30	96	192	6.86
rhombic dodecahedron	15	135	39	96	192	6.40

[a] N is the number of atoms; $9 \times N$ is the number of atomic orbitals; HLAO is the number of high lying antibonding orbitals; CVMO is the number of cluster valence molecular orbitals; CVE is the number of cluster valence electrons.

agreement with that predicted by the P.S.E.P.T.

Separate counting rules for high nuclearity metal carbonyl clusters have recently been developed. Teo has extended the Hume-Rothery rule for bulk metals to derive an electron counting scheme for high nuclearity clusters,[76] while Mingos and Zhenyoung[77] have applied Stone's Tensor Surface Harmonic approach to rationalise the bonding in such systems.

If a cluster is predicted by these electron counting schemes to be unsaturated, this implies that not all the C.V.M.O's (or localised M-M bonding orbitals) are occupied. Therefore, one would expect low

lying, vacant M.O's to be characteristic of such systems. Thus reactions which relieve the unsaturation of the cluster (e.g. nucleophilic addition, electrochemical reduction) may be anticipated to be the main feature of the chemistry of unsaturated clusters.

This proposal is examined in the following section in which the reactivity of unsaturated cluster systems is considered.

1.3.2 Chemistry of Unsaturated Clusters.

Although there are not many unsaturated clusters known, these systems have been studied fairly intensely. It is intended in this section to give an overview of the chemistry associated with unsaturated clusters, emphasising reactions that are typical of individual systems as well as those characteristic of unsaturated cluster complexes in general.

1.3.2 (i) $Os_3(\mu\text{-}H)_2(CO)_{10}$.

The triosmium cluster $Os_3(\mu\text{-}H)_2(CO)_{10}$,[78] 4, is the most widely studied unsaturated cluster. It is prepared in good yield by hydrogenolysis of 1.[79] 4 has a triangular metal framework, as defined by both X-ray[80,81] and neutron[82,83] diffraction studies (Figure 4). Both the E.A.N rule and the P.S.E.P.T predict a valence electron count of 48 for this geometry, however 4 has only 46 valence electrons and is, therefore, unsaturated. The experimentally observed Os-Os separations show the doubly hydride bridged Os-Os bond to be considerably shorter than the other two Os-Os distances[80-83] (see Figure 4). This short Os-Os separation has been interpreted as evidence of a metal-metal double bond,[80-81] which is required to satisfy the E.A.N. rule. However, a molecular orbital treatment of the bonding in 4 [84] indicates that the direct Os(2)-Os(3) bonding interaction is small and the bonding in the $Os(\mu\text{-}H)_2Os$ system is more accurately described in terms of two three centre-two electron Os-H-Os bonds. Furthermore, these M.O. calculations show that the energy difference between the highest occupied molecular orbital (HOMO)

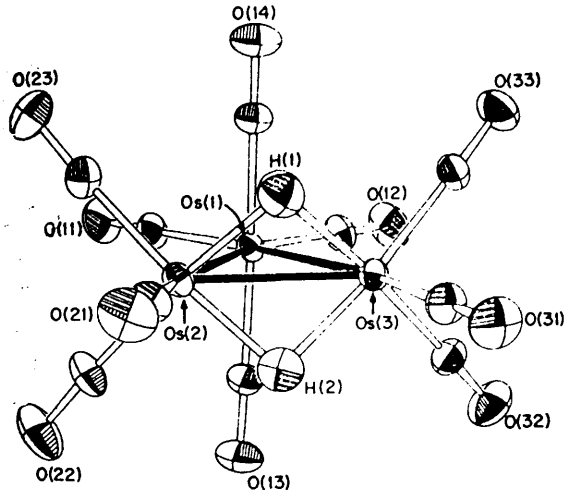

Os-Os bond lengths Å. [83]

Os(1)-Os(2)	2.815(1)
Os(1)-Os(3)	2.814(1)
Os(2)-Os(3)	2.683(1)

Figure 4 : Crystal structure of $Os_3(\mu\text{-}H)_2(CO)_{10}$ (after Broach and Williams)

and the lowest unoccupied molecular orbital, (LUMO), in 4 is small, suggesting that 4 should be susceptible to nucleophilic attack. This expectation is realised in the reactivity of 4.

1.3.2 (ii) Reactions of $Os_3(\mu\text{-}H)_2(CO)_{10}$

(a) Simple Adduct Formation.

The unsaturated nature of 4 is evident in its reactivity towards 2 electron donor nucleophiles. In general, these reactions result in the formation of the saturated 48 electron adducts, $Os_3(\mu\text{-}H)(CO)_{10}(H)L$, according to Scheme 1.

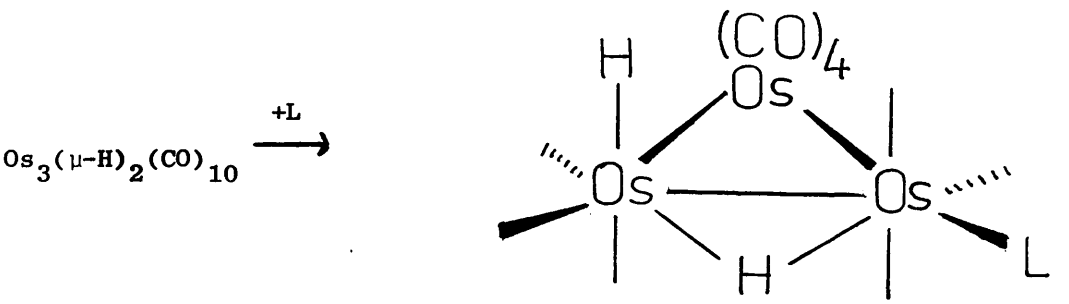

L = CO [85, 12] PR_3 [85, 12] AsR_3 [85,88] $P(OR)_3$ [88] PhCN [12] RNC [85,89]

Scheme 1. The reactions of 4 with 2 electron donor nucleophiles.

Crystallographic studies of the CO, [87] PPh_3 [90] and tBuNC [91] adducts reveal

that, unlike 4, there are no unusually short Os-Os separations and the Os-Os bond lengths in these adducts are comparable with those found in the saturated triosmium system 1, (see Table 7). The major difference in Os-Os distances between 1 and the $Os_3(\mu\text{-H})(CO)_{10}(H)L$ complexes is due to the expected elongation[87] of the hydride bridged Os-Os vector in the adduct clusters.

Table 7. Os-Os Bond Lengths in Selected Saturated 48 Electron Adducts of 4 (Å)

	Os(μ-H)Os	Os -Os	Os -Os	Ref.
$Os_3(\mu\text{-H})(CO)_{10}(H)(PPh_3)$	3.0185(6)	2.9170(5)	2.8645(7)	90
$Os_3(\mu\text{-H})(CO)_{11}(H)$	2.9886(9)	2.9097(7)	2.8574(7)	87
$Os_3(\mu\text{-H})(t\text{-BuNC})(CO)_{10}(H)$	3.000(1)	2.930(1)	2.876(1)	91
$Os_3(CO)_{12}$	Os-Os(AVE): 2.8771			87

Addition of anionic nucleophiles, X^-, readily yield the corresponding adducts $[Os_3(\mu\text{-H})(CO)_{10}(H)X]^-$ ($X^- = Cl^-$,[92] Br^-,[92] I^-,[92] H^-,[92] CN^-,[93]). Interestingly, the hydride adduct $[Os_3(\mu\text{-H})(CO)_{10}(H)_2]^-$ releases dihydrogen on further treatment with H^- to form the 48 electron dianionic species $[Os_3H_2(CO)_{10}]^{2-}$, which can also be accessed through reduction of 4 with $K[Ph_2CO]$.[92]

(b) Reactions of $Os_3(\mu\text{-H})_2(CO)_{10}$ with Organic Molecules.

As discussed in recent reviews by Deeming[94] and Burgess[33], 4 is reactive towards many unsaturated organic species. This fact, coupled with the general ease of isolation of products from such reactions, has led to a rapid growth in the organometallic chemistry of 4. As outlined in Section 1.1, clusters have been considered as molecular models for metal surfaces under catalytic conditions, and numerous examples of catalytically important transformations involving hydrogen transfer to or from the organic moiety, C-C bond cleavage and formation have been

observed on a triosmium framework in reactions that are accessed via 4. Some of these reactions, summarised in Scheme 2, are considered below.

Treatment of 4 with ethylene yields $Os_3(\mu\text{-}H)(\mu\text{-}\eta^2\text{-}CH{=}CH_2)(CO)_{10}$, 5, and ethane.[95] 5 is also formed in the reaction of 4 with acetylene, and the vinyl ligand can be viewed as a partially hydrogenated acetylene fragment.[96] Thermal treatment of 5 leads to decarbonylation and ligand rearrangement to yield the vinylidene complex $Os_3(\mu\text{-}H)_2(\mu_3\text{-}\eta^2\text{-}C{=}CH_2)(CO)_9$.[96]

With the disubstituted acetylene, PhC≡CPh, 4 yields the corresponding vinyl cluster $Os_3(\mu\text{-}H)(\mu\text{-}\eta^2\text{-}PhC{=}C(H)Ph)(CO)_{10}$, 6 as the initial product.[97] An X-ray analysis of 6,[97] reveals that it differs structurally from 5 in the orientation of the alkenyl ligand with respect to the Os_3 framework. In 5, the ligand is oriented such that the α-substituent, a hydrogen atom, is syn with respect to the $Os(CO)_4$ group. In 6, however, the α-substituent is a phenyl group, which lies anti to the $Os(CO)_4$ moiety, presumably to relieve steric congestion.

Further treatment with PhC≡CPh leads to alkyne coupling on the cluster framework and the formation of $Os_3(\mu\text{-}\eta^4\text{-}PhC{=}C(Ph)\text{-}C(Ph){=}C(Ph))(CO)_9$. $Os_3(\mu_3\text{-}\eta^2\text{-}PhC{\equiv}CPh)(CO)_{10}$ and stilbene are intermediates in this process.[98,99] These mono and dialkenyl clusters may be intermediates[98] in the cyclotrimerisation of diphenyl acetylene to hexaphenyl benzene, catalysed by $Os_3(CO)_{12}$.[100]

4 reacts with diazomethane to yield an isomeric mixture of two products, the initially formed $Os_3(\mu\text{-}H)(\mu\text{-}\eta^2\text{-}CH_3)(CO)_{10}$, 7(I), and $Os_3(\mu\text{-}CH_2)(\mu\text{-}H)_2(CO)_{10}$, 7(II).[101,102] The structure of 7(I) has not been crystallographically defined, however it is believed that 7(I) has the structure shown in Scheme 2, with a methyl group containing an agostically bound hydrogen spanning an Os-Os edge.[102] The solid state structure of 7(II), as determined by neutron diffraction techniques,[103,104] is shown in Figure 5. The methylene function adopts the expected[105] Os-Os edge bridging coordination mode.

Scheme 2 : Some organometallic chemistry of $Os_3(\mu\text{-}H)_2(CO)_{10}$, 4.

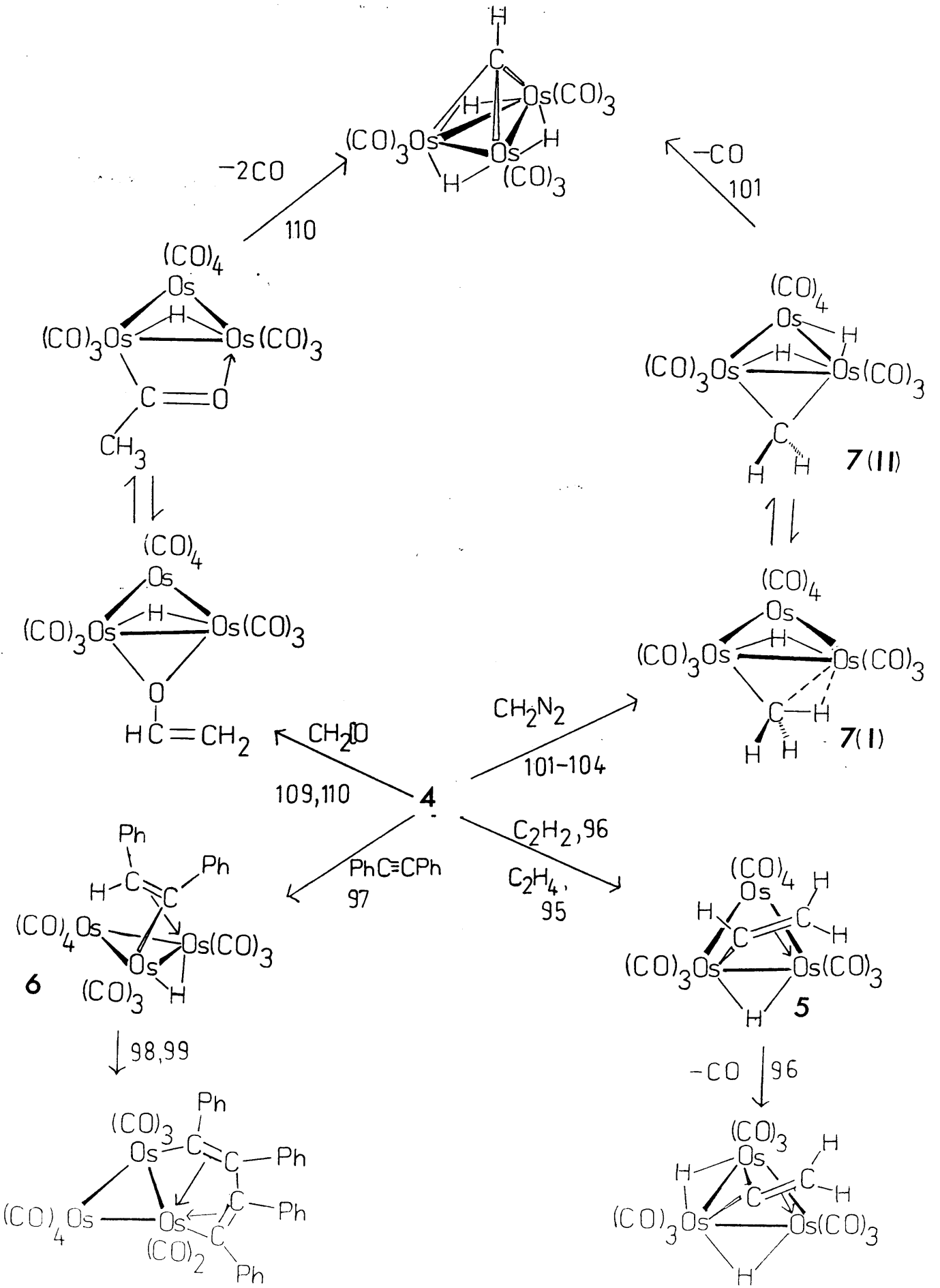

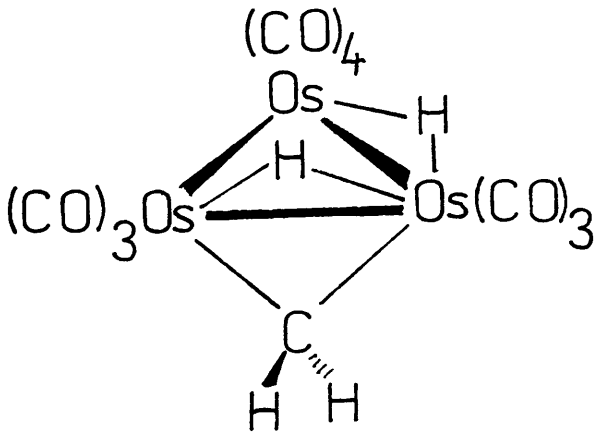

Figure 5. The molecular structure of $Os_3(\mu\text{-}H)_2(\mu\text{-}CH_2)(CO)_{10}$

7(I) and 7(II) interchange via hydrogen migration from an Os-Os edge to the bridging methylene group and vice versa.[102]

It is noteworthy that the structures of isomers 7(I) and 7(II) are comparable with those observed in the SnR_2, ($R = CH(SiMe_3)_2$),[106] and SO_2[107] adducts of 4. SnR_2, SO_2 and CH_2 are related by Hoffmann's isolobal theory.[108] For fragments to be isolobal requires that their frontier orbitals are approximately equal in size, energy, symmetry and occupation by electrons. Thus, where frontier orbitals are important in defining the chemistry of a system (as in neutral metal carbonyl clusters), isolobally related fragments are expected to behave similarly.

The molecular structure of $Os_3(\mu\text{-}H)_2(\mu\text{-}Sn[CH(SiMe_3)_2]_2)(CO)_{10}$ is shown in Figure 6(i).[106]

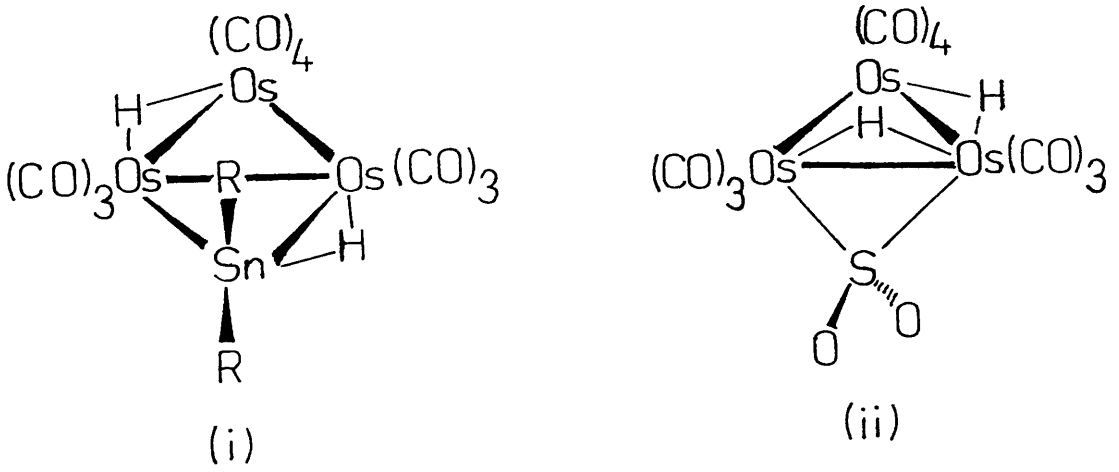

Figure 6. Solid state structure of (i) $Os_3(\mu\text{-}H)_2(\mu\text{-}SnR_2)(CO)_{10}$, $R = CH(SiMe_3)_2$, and (ii) $Os_3(\mu\text{-}H)_2(\mu\text{-}SO_2)(CO)_{10}$.

This structure is similar to that proposed for 7(I) as both can be considered to have a $\mu\text{-}\eta^2$ $X(R_2)H$ function with an agostically bound hydrogen bridging an Os-X bond, (X = C, R = H; X = Sn, R = $CH(SiMe_3)_2$). The magnitude of $^{117/119}Sn$ coupling to one hydride resonance in the ^1H n.m.r spectrum supports the assumption that the structure in the solid state is maintained in solution.[106]

In contrast, X-ray diffraction studies on the initially formed SO_2 adduct of 4 indicate both hydrides remain bridging Os-Os vectors,[107] (Figure 6.(ii)) in a manner similar to that observed in 7(II).

An important structural difference between the CH_2, SO_2 and $Sn[CH(SiMe_3)_2]_2$ adducts is that the C and S atoms of the CH_2 and SO_2 groups lie at angles of 105.5° [104] and 105.9° [107] respectively to the Os_3 plane, whereas the Sn atom is essentially coplanar with the triosmium triangle in the $Sn[CH(SiMe_3)_2]_2$ adduct, which minimises steric interactions between the carbonyl groups and bulky alkyl functions.

Thermal decarbonylation of mixtures of 7(I) and 7(II) leads to the formation of $Os_3(\mu\text{-}H)_3(\mu_3\text{-}CH)(CO)_9$.[101] (Scheme 2). This cluster can also be prepared by reaction of 4 with ketene or vinylene carbonate, which yields $Os_3(\mu\text{-}H)(\mu\text{-}OCH{=}CH_2)(CO)_{10}$,[109-111] which, on heating, isomerises to $Os_3(\mu\text{-}H)(\mu\text{-}\eta^2\text{-}O{=}CMe)(CO)_{10}$.[110] Decarbonylation of this complex yields $Os_3(\mu\text{-}H)_3(\mu_3\text{-}CH)(CO)_9$,[110] through C-C bond scission.

The reactions cited above represent a small subsection of the known organometallic chemistry of 4, and, for a more comprehensive treatment of this topic, reference should be made, again, to the recent excellent reviews by Deeming[94] and Burgess.[33] The Os_3 unit has proved a useful stable framework on which organic transformations can occur and the presence of hydride ligands on 4, capable of migration on to organic moieties,[96,97,101] coupled with its inherent reactivity, make 4 an attractive reagent for entry into Os_3 organometallic chemistry.

(c) Substituted Analogues of $Os_3(\mu\text{-}H)_2(CO)_{10}$.

It is possible to substitute either the carbonyl groups or hydride ligands of 4 to prepare corresponding unsaturated substituted analogues. The reactivity of such clusters may be expected to differ from that of 4 due to the steric and electronic changes imposed by the substituent ligand.

One method of obtaining the carbonyl substituted derivatives $Os_3(\mu\text{-}H)_2(CO)_9L$, (L = PR_3,[86] CNR[89]), is to thermolyse the simple adduct clusters $Os_3(\mu\text{-}H)(CO)_{10}(H)L$ to effect decarbonylation. Derivatives of 4 in which one[112] or both[113] hydride ligands are substituted by $AuPR_3$ units can be accessed through treating the anionic cluster $[Os_3H(CO)_{11}]^-$ with either one or two equivalents of $Au(PR_3)Cl$ to give $Os_3(\mu\text{-}H)_{2-n}(\mu\text{-}AuPR_3)_n(CO)_{10}$, (n = 1,[112] 2,[113] R = Et,Ph). Diphos disubstituted analogues, $Os_3(\mu\text{-}H)_2(CO)_8(diphos)$, can be prepared by hydrogenolysis of the corresponding $Os_3(CO)_{10}(diphos)$ cluster, similar to the synthesis of 4 from 1.[114,126]

The structures of several substituted derivatives of 4 have been crystallographically defined. In all cases, the substituent ligand has replaced a carbonyl or hydride at the $Os(\mu\text{-}H)_2Os$ unit of 4. The metal-metal separations in these systems, listed in Table 8, closely resemble those observed in 4 with characteristically short bridged Os-Os bonds (range 2.666 - 2.699 Å) and longer unbridged Os-Os vectors (range 2.812 - 2.844 Å). This indicates that the effect of ligand substitution on metal framework bonding is small. However, the bridged Os-Os unit is normally the initial reactive site in 4, and the proximity of bulky ligands to that site in these derivatives is expected to modify their reactivity. Thus, for example, while $Os_3(\mu\text{-}H)_2(CO)_9(CNR)$ readily adds CO to give $Os_3(\mu\text{-}H)(CO)_{10}(CNR)(H)$,[91] derivatives with bulkier ligands which protect the reactive site, e.g. $Os_3(\mu\text{-}H)_2(CO)_8(dppm)$[116] and $Os_3(\mu\text{-}AuPPh_3)_2(CO)_{10}$[113] are unreactive towards CO. Several other instances of the differing reactivities of 4 and its derivatives are detailed below.

On treatment with p-tolyl isocyanate, 4 yields $Os_3(\mu\text{-}H)(\mu\text{-}p\text{-}CH_3C_6H_4NC(H)O)(CO)_{10}$ as the principal product,[119] whereas, with $Os_3(\mu\text{-}H)_2(CO)_9(PMe_2Ph)$, the major product is the carboximido complex $Os_3(\mu\text{-}H)(\mu\text{-}p\text{-}CH_3C_6H_4N(H)C{=}O)(CO)_9(PMe_2Ph)$,[119] (see Figure 7).

In refluxing CS_2, 4 affords $\{Os_3(\mu\text{-}H)(CO)_{10}\}_2CH_2S_2$ (Figure 8(i)),[120] however, $Os_3(\mu\text{-}H)_2(CO)_9(PMe_2Ph)$, in addition to forming the related $\{Os_3(\mu\text{-}H)(CO)_9(PMe_2Ph)\}_2CH_2S_2$,[121] yields $Os_3(\mu\text{-}H)(\mu\text{-}S_2CH)(CO)_9(PMe_2Ph)$,[121] and $Os_3(\mu\text{-}SCH_2)(\mu_3\text{-}S)(CO)_9(PMe_2Ph)$[122] (see Figure 8(ii) and (iii) respectively). This latter compound, formed through cleavage of two Os-Os bonds and one C-S bond, is a rare example of a triosmium cluster containing only one Os-Os bond.

Table 8. Os-Os bond distances in 4 and its substituted analogues.

Cluster	Substituent	Os-Os bond length (Å) bridged	unbridged	Ref.
$Os_3(\mu\text{-}H)_2(CO)_{10}$	-	2.683(1)	2.815(1), 2.814(1)	83
$Os_3(\mu\text{-}H)_2(CO)_9(CN^tBu)$	CN^tBu	2.690(1)	2.826(1), 2.827(1)	91
$Os_3(\mu\text{-}H)_2(CO)_9(PPh_3)$	PPh_3	2.683(2)	2.813(2), 2.822(2)	115
$Os_3(\mu\text{-}H)_2(CO)_8(dppm)$	dppm	2.681(1)	2.820(1), 2.812(1)	116
$Os_3(\mu\text{-}H)(\mu\text{-}AuPPh_3)(CO)_{10}$	$AuPPh_3$	2.699(1)	2.824(1), 2.844(1)	112
$Os_3(\mu\text{-}AuPEt_3)_2(CO)_{10}$	$AuPEt_3$	2 684(1)	2.830(1), 2.830(1)	113
$([Os_3(\mu\text{-}H)(CO)_{10}]_2Au)^-$	$AuClus^-$	2.698(1) 2.689(1)	2.830(1), 2.826(1) * 2.840(2), 2.828(2) *	117
$([Os_3(\mu\text{-}H)(CO)_{10}]_2Ag)^-$	$AgClus^-$	2.676(1) 2.666(1)	2.830(1), 2.827(1) * 2.827(1), 2.839(1) *	118

Clus = $Os_3(\mu\text{-}H)(CO)_{10}$

* Parameters given for two independent molecules in unit cell.

Average Os-Os bridged separation in substituted complexes = 2.685Å

Figure 7 : Distribution of products in reaction of p-tolyl isocyanate with $Os_3(\mu\text{-}H)_2(CO)_9L$, L = CO, PMePh.

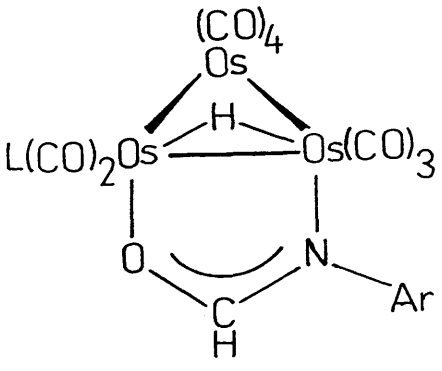

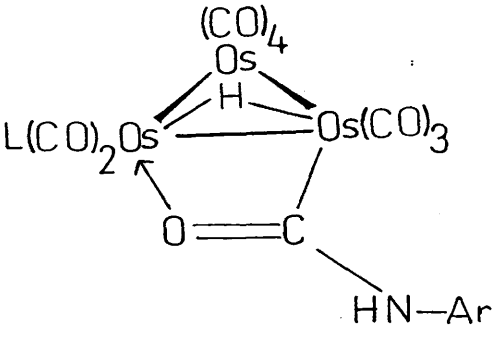

L = CO **major**	**minor**
L = PMe_2Ph **minor**	**major**

Figure 8 : The molecular structures of (i) $\{Os_3(\mu\text{-}H)(CO)_{10}\}_2CH_2S_2$, (ii) $Os_3(\mu\text{-}H)(\mu\text{-}\eta^2SC(H)S)(CO)_9(PMe_2Ph)$, and (iii) $Os_3(\mu\text{-}\eta^2SCH_2)(\mu_3\text{-}S)(CO)_9(PMe_2Ph)$.

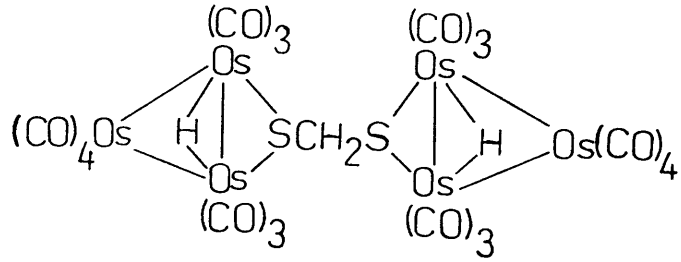

(i)

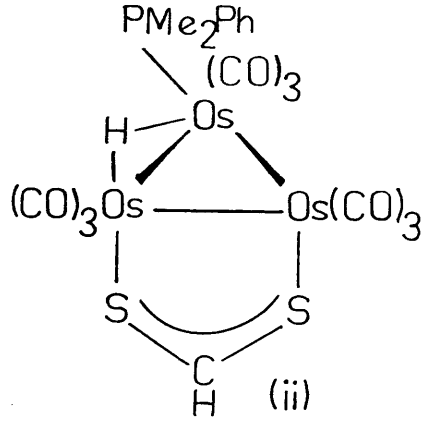

(ii)

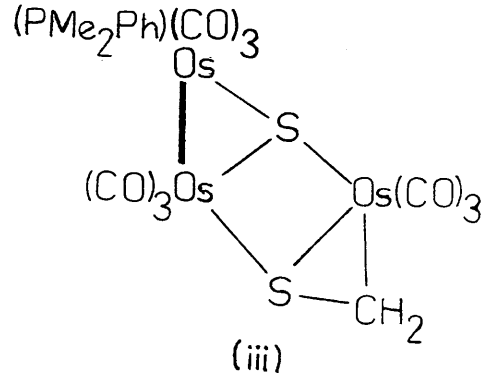

(iii)

The ethylene adduct of $Os_3(\mu\text{-}H)_2(CO)_9(PR_3)$ has been characterised spectroscopically,[123] while that of 4 has not been observed. From the spectroscopic data available, the most likely site of coordination of the alkene is on the phosphine bearing osmium. Only after prolonged treatment with ethylene does $Os_3(\mu\text{-}H)(\mu\text{-}\eta^2\text{-}CH{=}CH_2)(CO)_9(PR_3)$ form,[123] supporting the proposed intermediacy of $Os_3(\mu\text{-}H)(\eta^2\text{-}CH_2CH_2)(CO)_{10}(H)$ in the formation of 5.[95] Thus by employing a substituted derivative of 4, cluster reactivity towards ethylene is retarded through stabilisation of the ethylene adduct.

The 46 electron triosmium cluster $Os_3(\mu\text{-}H)(\mu_3\text{-}\eta^3(Ph)_2PCH_2P(Ph)C_6H_4)(CO)_8$, 8, is synthesised by thermolysis of $Os_3(CO)_{10}(dppm)$.[124] 8 can be considered a trisubstituted derivative of 4 in which two phosphine groups, coordinated at different Os centres, and a metallated ortho carbon of a phenyl ring replace two carbonyl functions and one μ-H ligand of 4 respectively. The structure of 8, is shown in Figure 9 along with the M-M bond lengths.[124]

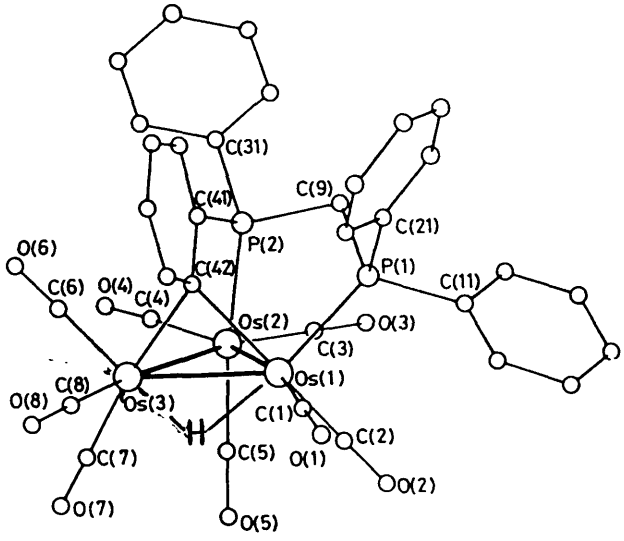

Os-Os bond lengths	Å
Os(1)-Os(2)	2.844(1)
Os(1)-Os(3)	2.747(1)
Os(2)-Os(3)	2.834(1)

Figure 9. Molecular structure and Os-Os bond distances of 8.

Consideration of these Os-Os separations indicates that the doubly bridged Os(1)-Os(3) distance of 2.747(1) Å is significantly shorter than the other two. However, compared to the average bond length of the corresponding Os-Os edge in other substituted derivatives of 2.685 Å (see Table 8), this value is somewhat large. This elongation may be due to a combination of the steric crowding effects of the enforced axial ligation of one phosphine group of the diphos unit and the electronic effect of replacing two good π-acceptor carbonyl ligands with two phosphine groups, which have poor π-accepting capabilities.

Several reactions involving 8 have been investigated and are

summarised in Scheme 3. These illustrate both similarities and distinctions between the chemistries of 4 and 8.

Like 4, 8 reacts reversibly with CO[124] yielding $Os(\mu_3\text{-}\eta^3\text{-}(Ph)_2PCH_2P(Ph)C_6H_4)(CO)_9(H)$. The structure of this complex is thought to be analogous to that of the CO adduct of 4, (see Scheme 3).

Hydrogenolysis of 8 yields $Os_3(\mu\text{-}H)_2(CO)_8(dppm)$, the dppm substituted analogue of 4;[125] this is also accessed through treatment of $Os_3(CO)_{10}(dppm)$ with dihydrogen.[114,126] With diphenyl acetylene 8 forms the 46 electron species $Os_3(\mu_3\text{-}\eta^2\text{-}\perp\text{-}PhC{\equiv}CPh)(CO)_7(dppm)$,[127] whereas 4 forms $Os_3(\mu\text{-}H)(\mu\text{-}\eta^2\text{-}PhC{=}C(H)Ph)(CO)_{10}$ with $PhC{\equiv}CPh$.[97] (The corresponding unsubstituted 46 electron cluster, $Os_3(\mu_3\text{-}\eta^2PhC{\equiv}CPh)(CO)_9$, is known,[98] but is highly reactive, vide infra).

The mixed metal Os_3Sn_2 cluster, $Os_3(\mu\text{-}SnR_2)_2(CO)_8(dppm)$, R = $CH(SiMe_3)_2$, has been prepared by thermal treatment of 8 with $Sn[CH(SiMe_3)_2]_2$.[128] This complex is unique in that it is a closed paramagnetic cluster that obeys the E.A.N. rule. The crystal structure shows the Os_3Sn_2 core is planar (Figure 10) and calculations by Evans and Mingos[129] indicate that HOMO's of approximately equal energies are feasible in such "raft-like" systems. This is a prerequisite for paramagnatism in an even electron system such as this. The origin of the paramagnatism has been attributed to the elongated Os(1)-Os(2) vector which is considered non-bonding and allows electron counts of 17,17 and 18 at Os(1), (2) and (3) respectively.

Scheme 3 : Some reactions of $Os_3(\mu\text{-}H)(\mu_3\text{-}\eta^3\text{-}(Ph)_2PCH_2P(Ph)C_6H_4)(CO)_8$, 8

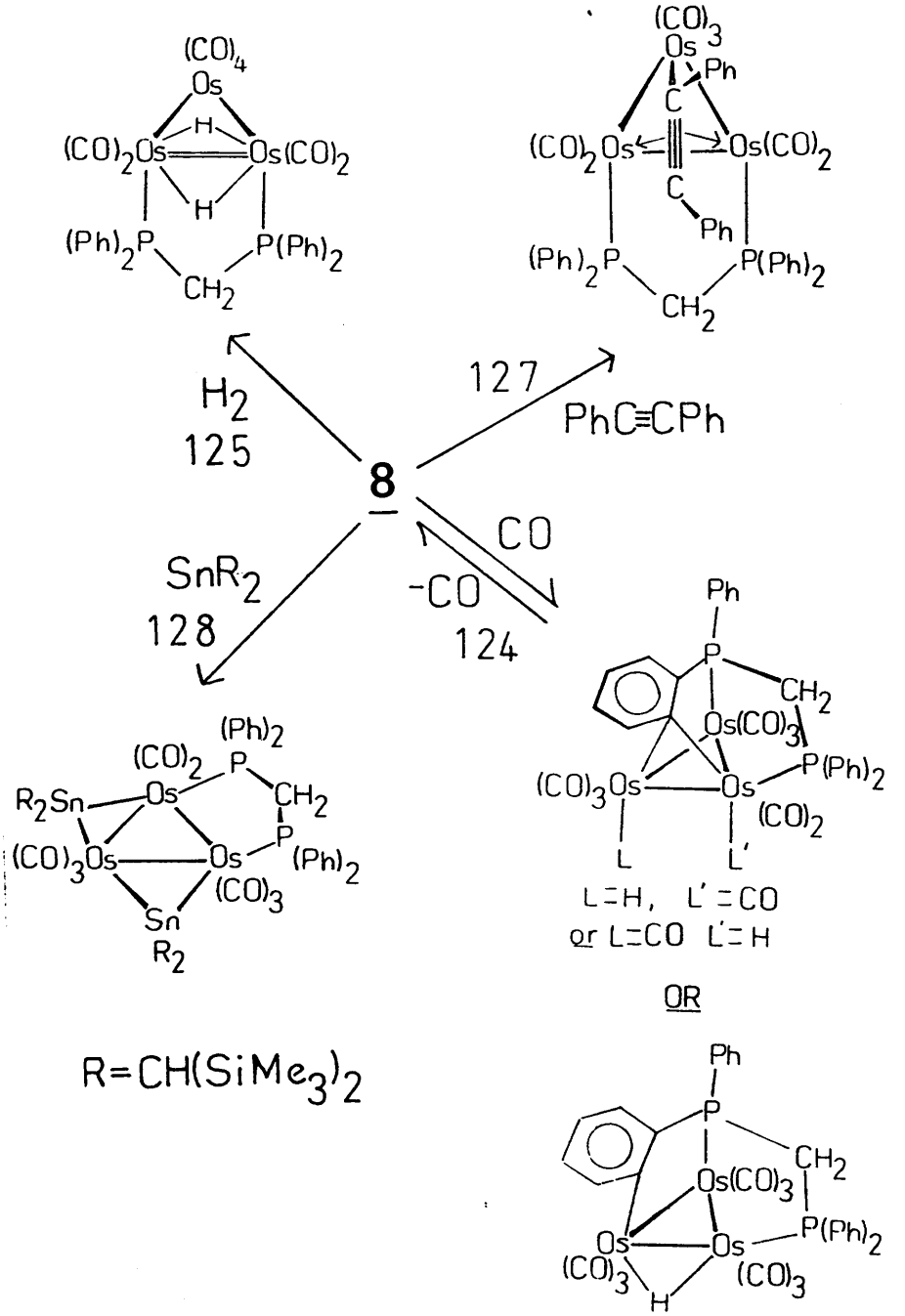

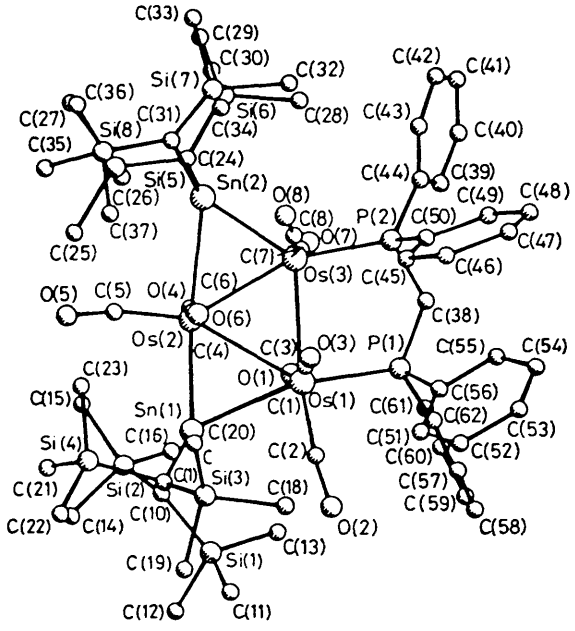

Selected bond lengths Å

Os(1)-Os(2)	3.048(2)
Os(1)-Os(3)	2.909(2)
Os(2)-Os(3)	2.854(2)
Os(1)-Sn(1)	2.873(3)
Os(2)-Sn(1)	2.649(3)
Os(2)-Sn(2)	2.866(3)
Os(3)-Sn(2)	2.651(2)

Figure 10. Molecular structure of $Os_3(\mu\text{-}SnR_2)_2(CO)_8(dppm)$ R = $CH(SiMe_3)_2$.

In summation the use of derivatives of 4 allows access to a wider cluster chemistry with, in some instances, the substituted cluster systems displaying a totally different reactivity, to that of the parent 4. It is apparent that, with an increasing degree of substitution the differences in chemical reactivities between 4 and its derivatives become more pronounced. Thus the reactivity of 8 is, in some respects, quite distinct from that of 4. This is hardly surprising when the increasing steric and electronic changes brought about by substitution are considered.

d) $Os_3(\mu\text{-}H)_2(CO)_{10}$ as a synthon for heterometallic clusters.

4 has proved a useful starting material for the synthesis of heterometallic clusters containing a triosmium unit. Mixed metal osmium clusters are of interest for a number of reasons:- they can be used as precursors for the preparation of heterometallic heterogeneous catalysts;[130-133] some have been found to be active homogeneous catalysts;[134,135] and the chemistry of mixed metal osmium clusters is

expected to differ from that of homometallic Os systems because of the different size, bonding capabilities and reactivities of the component heterometallic centres.

Various strategies have been developed to generate mixed metal clusters using 4 as a precursor. The most frequently adopted synthetic routes are outlined below.

Thermal treatment of 4 with metal carbonyls, or functionalised metal carbonyls has proved successful in the preparation of tetranuclear MOs_3 systems with tetrahedral metal frameworks. Table 9 provides a listing of several MOs_3 clusters prepared in this fashion.

Shore and coworkers, investigating the reactions of 4 with cyclopentadienyl metal carbonyls in the presence of dihydrogen have prepared several unusual MOs_3 systems. The mixed cobalt-triosmium cluster $CoOs_3(\mu\text{-}H)_3(Cp)(CO)_9$ has 59 valence electrons instead of the 60 expected for a tetrahedral framework, and is, therefore, both paramagnetic and unsaturated.[142] On treatment with H_2, this cluster readily converts to the 60 electron saturated, diamagnetic species, $CoOs_3(\mu\text{-}H)_4(Cp)(CO)_9$.[142]

When 4 is treated with $(Cp)M(CO)_2$, the product formed is $MOs_3(\mu\text{-}H)_2(\mu\text{-}CO)(Cp)(CO)_9$, (M = Co, Rh, Ir). However, with M = Rh, if the reaction is attempted in the presence of H_2 in benzene or toluene, both potential η^6-ligands, an unprecedented displacement of the Cp group by the $\eta^6\text{-}C_6H_5X$ (X = H,CH_3) ligand is observed yielding $Os_3Rh(\mu\text{-}H)_3(\eta^6\text{-}C_6H_5X)(CO)_9$, (X = H,$CH_3$) as the major product.[143] On replacement of the Cp function with Cp^* on the mononuclear rhodium precursor, the tetra-hydrido species $Os_3Rh(\mu\text{-}H)_4(Cp^*)(CO)_9$ is formed under the same conditions.[144]

The presence of H_2 in these reactions is believed to aid CO dissociation from the mononuclear species to create reactive monometallic

Table 9 : Examples of *closo*-tetrahedral MOs_3 clusters derived from reactions of 4 with (functionalised) metal carbonyls.

Reagents.	Product.		Ref.
4 + $Fe_2(CO)_9$	$FeOs_3(\mu\text{-}H)_2(CO)_{13}$		136
4 + $Fe(CO)_5$	$FeOs_3(\mu\text{-}H)_2(CO)_{13}$		137
4 + $Ru_3(CO)_{12}$	$Os_3Ru(\mu\text{-}H)_2(CO)_{13}$		137
4 + $Ru(CO)_5$	$Os_3Ru(\mu\text{-}H)_2(CO)_{13}$		138
4 + $Co_4(CO)_{12}$	$CoOs_3(\mu\text{-}H)_3(CO)_{12}$		139
4 + $(Cp)Co(CO)_2$	$CoOs_3(\mu\text{-}H)_2(\mu\text{-}CO)(Cp)(CO)_9$		140
4 + $(Cp)Rh(CO)_2$	$Os_3Rh(\mu\text{-}H)_2(\mu\text{-}CO)(Cp)(CO)_9$		141
4 + $(Cp)Ir(CO)_2$	$IrOs_3(\mu\text{-}H)_2(\mu\text{-}CO)(Cp)(CO)_9$		142
4 + $(Cp)Co(CO)_2$	$CoOs_3(\mu\text{-}H)_3(Cp)(CO)_9$	(a)	142
	$CoOs_3(\mu\text{-}H)_4(Cp)(CO)_9$	(a)	142
4 + $[(Cp)Ni(CO)]_2$	$NiOs_3(\mu\text{-}H)_3(Cp)(CO)_9$	(a)	142
4 + $(Cp)Rh(CO)_2$	$Os_3Rh(\mu\text{-}H)_3(\eta^6\text{-}C_6H_5X)(CO)_9$	(b)	143
4 + $(Cp^*)Rh(CO)_2$	$Os_3Rh(\mu\text{-}H)_4(Cp^*)(CO)_9$	(a)	144
4 + $[(Cp)Mo(CO)_n]_2$	$MoOs_3(\mu\text{-}H)_3(Cp)(CO)_{11}$	(c)	145

$Cp = (\eta^5\text{-}C_5H_5)$; $Cp^* = (\eta^5\text{-}C_5Me_5)$

(a) - Reaction proceeds in the presence of H_2

(b) " " " " " " with benzene (X = H) or toluene ($X = CH_3$) as solvent.

(c) Reaction proceeds in the presence of H_2, n = 2,3.

carbonyl hydrides in situ.[143,144]

A second approach to mixed metal cluster syntheses using 4 as a precursor utilises metal complexes containing labile ligands. This synthetic strategy was developed by Stone through his use of platinum metal olefin complexes to generate heterometallic triosmium clusters.[146-148] Heterometallic clusters prepared in this manner are listed in Table 10.

Ligand rearrangement on complexation of the mononuclear metal fragment to the Os_3 triangle is a feature of all these reactions. For example, in reactions involving cluster formation via displacement of coordinated ethylene, carbonyl migration from the Os_3 framework to a bridging or terminal site on the incoming metal is observed.

Table 10 : Heterometallic clusters prepared by displacement of labile ligands.

Reagents	Product	Metal Geometry	Ref.
4 + $Rh(C_2H_4)_2(acac)$	$Os_3Rh(\mu\text{-}H)_2(acac)(CO)_{10}$	B	146
4 + $Ni(C_2H_4)(PPh_3)_2$	$NiOs_3(\mu\text{-}H)_2(\mu\text{-}CO)_2(PPh_3)_2(CO)_8$	T	146
4 + $Pt(C_2H_4)_2(PCy_3)$	$Os_3Pt(\mu\text{-}H)_2(PCy_3)(CO)_{10}$	T	147
4 + $Pt(C_2H_4)(PPh_3)_2$	$Os_3Pt(\mu\text{-}H)_2(PPh_3)_2(CO)_{10}$	B	148
4 + $Co(\eta^5\text{-}C_5Me_4Et)(C_2H_4)(Me)_2$	$CoOs_3(\mu\text{-}H)_2(\mu\text{-}CO)(\eta^5\text{-}C_5Me_4Et)(CO)_9$	T	149
4 + $Ir(N_2)(PPh_3)_2Cl$	$IrOs_3(\mu\text{-}Cl)(\mu\text{-}H)_2(\mu\text{-}CO)(CO)_9(PPh_3)$	T	150
4 + $Ir(Cl)(CO)_2(NH_2C_6H_4Me)$	$IrOs_3(\mu\text{-}Cl)(\mu\text{-}H)_2(CO)_{12}$	B	151

T = closo tetrahedral B = butterfly

The synthetic methods listed above are not the only routes to mixed metal clusters using 4, others can be employed. For example, Shore has prepared a series of anionic heterometallic clusters using metallocarbonylates as nucleophiles.[92] The products are thought to have a similar structure to those of the halide adducts of 4, (see Figure 11).

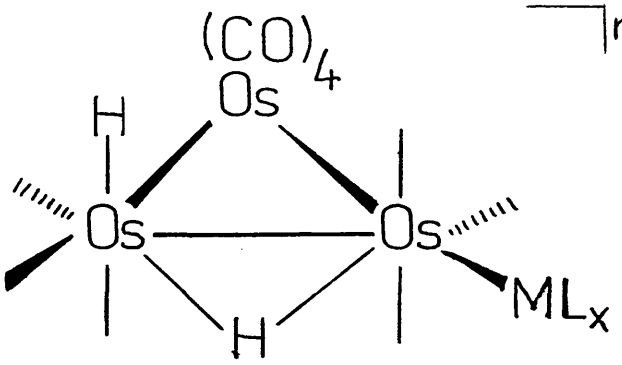

ML_x = $Mn(CO)_5$, $Fe(CO)_4$*, $(Cp)Mo(CO)_3$, $(Cp)V(CO)_3$*, $(Cp)Fe(CO)_2$

*n = 2; in all other cases n = 1

Figure 11 : Mixed metal MOs_3 complexes obtained from reaction of 4 with metallocarbonylates.

Another route utilises the ligand functionality of the hetero-metal reagent to assist binding to the Os framework. This is exemplified in the reaction of the manganese vinylidene complex $(Cp)Mn(\eta^1\text{-}C{=}C(H)Ph)(CO)_2$ with 4.[152] The product, $MnOs_3(\mu\text{-}H)(\mu\text{-}CO)(\mu\text{-}\eta^2\text{-}HC{=}C(H)Ph)(Cp)(CO)_{11}$, (I) in Scheme 4, has a spiked triangular metal core in which a vinyl group bridges the Mn-Os bond.[152]. This complex can be viewed as an intermediate in the transfer of the -C=C(H)Ph vinylidene moiety from the mononuclear Mn system to the Os_3 cluster as, on standing at 20°C, Mn-Os bond scission is effected yielding $Os_3(\mu\text{-}H)(\mu\text{-}\eta^2\text{-}HC{=}C(H)Ph)(CO)_{10}$ and $Os_3(\mu\text{-}H)_2(\mu_3\text{-}\eta^2PhC{\equiv}CH)(CO)_9$,[142] as shown in Scheme 4.

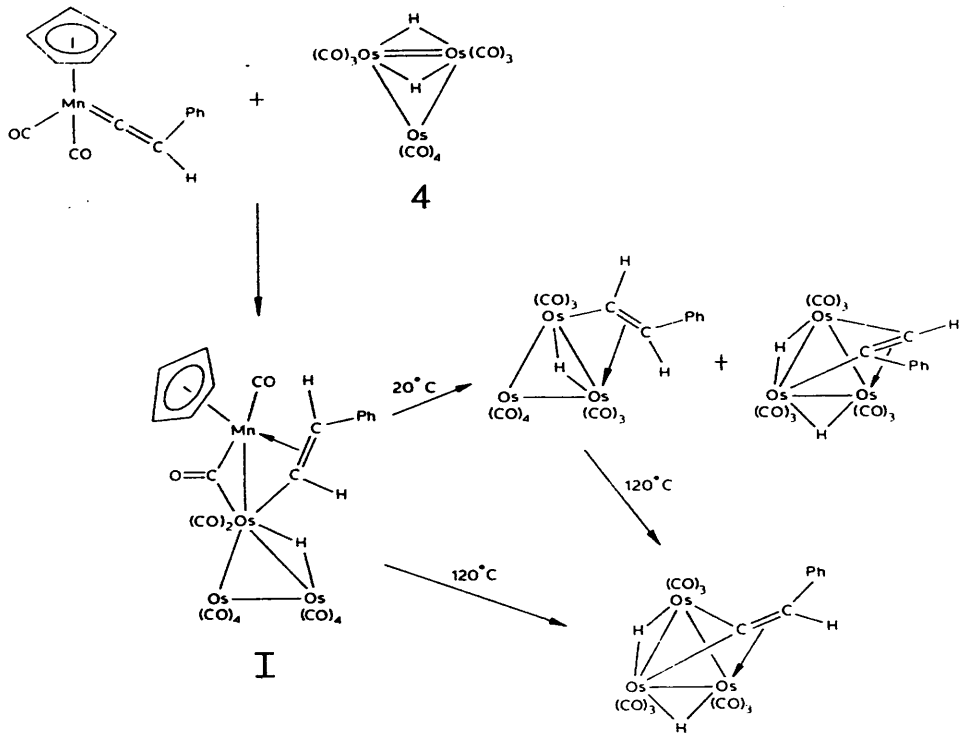

Scheme 4 : Transfer of a $C_2(H)Ph$ fragment from Mn to Os_3 complexes via formation of the mixed metal $MnOs_3$ cluster(I).

The unsaturation of 4 has made it a versatile reagent for the synthesis of new heterometallic triosmium clusters. Recent reviews on Os_3 chemistry serve as a testament to the widespread application of $Os_3(\mu\text{-}H)_2(CO)_{10}$ in osmium cluster chemistry.[24,94,153].

1.3.2 (iii) Reactivity of the Trirhenium Anions $[Re_3(\mu\text{-}H)_m(CO)_{10}]^{n-}$ (m=3, n=2; m=4, n=1).

The unsaturated, 46 electron *triangulo* trirhenium anions $[Re_3(\mu\text{-}H)_3(CO)_{10}]^{2-}$, 9, and $[Re_3(\mu\text{-}H)_4(CO)_{10}]^{-}$, 10, are isoelectronic with 4. These Re_3 systems were first prepared by Ciani and coworkers[154,155] according to the following equations:-

$$[NEt_4][Re_4(\mu\text{-}H)_4(CO)_{15}] \xrightarrow[\text{reflux 3h.}]{EtOH} [NEt_4]_2[Re_3(\mu\text{-}H)_3(CO)_{10}]^{2-} \qquad \text{ref.154}$$

$$[NEt_4]_2[Re_3(\mu\text{-}H)_3(CO)_{10}] \xrightarrow{HCl} [NEt_4][Re_3(\mu\text{-}H)_4(CO)_{10}] \qquad \text{ref.155}$$

The structures of both 9 and 10 have been determined by X-ray diffraction experiments (with $[NEt_4]^+$ as the counter cation), and the solid state configurations of each anion are shown below (Figure 12).

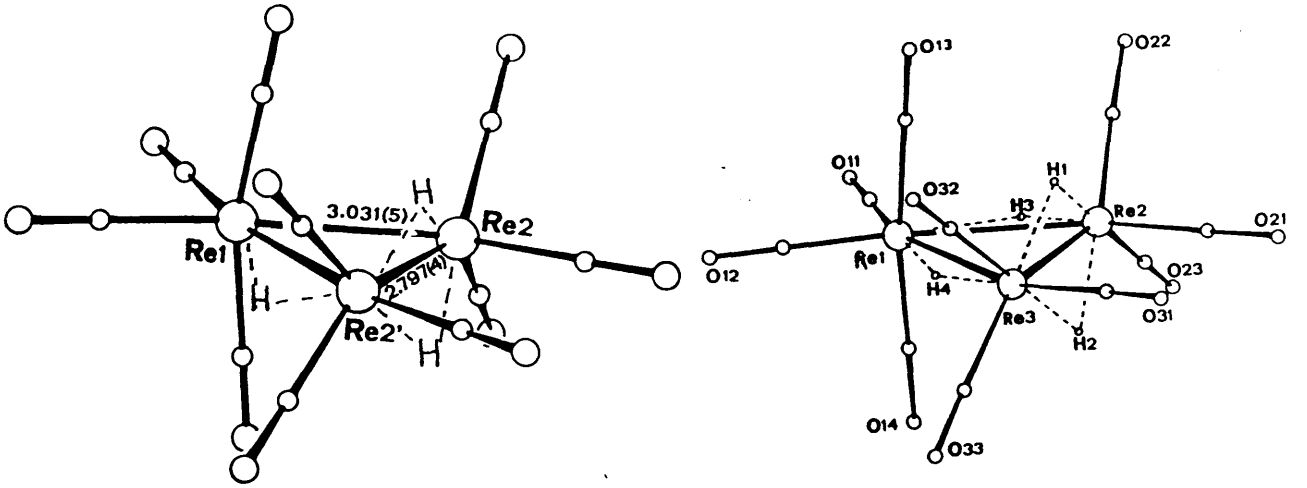

Re-Re bond lengths Å.

9*		10	
Re_1-$Re_{2,2'}$	3.031(5)	Re_1-Re_2	3.173(7)
Re_2-$Re_{2'}$	2.797(4)	Re_1-Re_3	3.194(7)
		Re_2-Re_3	2.821(7)

* disordered structure.

Figure 12 : Solid State Structures of Anions 9 and 10.

It is evident that the Re-Re vector in the $Re(\mu\text{-}H)_2Re$ unit in both 9 and 10 is considerably shorter than the other Re-Re separations and is reminiscent of the short doubly hydride bridged Os-Os distance in 4. It has been argued that the short Re-Re vectors in 9 and 10 are

evidence of localised formal double M-M bonds, analogous to that in 4.[154,155] Despite the structural similarities between 4 and these trirhenium clusters, complexes 9 and 10 show a very distinctive reactivity which differs markedly from that associated with 4.

In general, 9 and 10 react via electrophilic attack at a hydride of the $Re(\mu\text{-}H)_2Re$ unit, followed by addition of a nucleophile to form 48 electron saturated products. This type of transformation is illustrated in reactions i-vi in Scheme 5, in which some known reactions of 10 are presented. The Re-Re bond lengths found in these saturated products are listed in Table 11. An examination of these reveals the absence of abnormally short Re-Re vectors in keeping with the relief of unsaturation.

Under CO pressure 10 converts to the saturated $[Re_3(\mu\text{-}H)_2(CO)_{12}]^-$ with elimination of H_2.[164] Regeneration of 10 is effected by hydrogenolysis of $[Re_3(\mu\text{-}H)_2(CO)_{12}]^-$ at 100°C, [164] in a similar manner to the production of 4 by hydrogenation of 1.[79] Phosphines have been shown to react similarly yielding $[Re_3(\mu\text{-}H)_2(CO)_{10}(PR_3)_2]^-$.[165]

The reduction of a carbonyl group on the Re_3 face to give $[Re_3(\mu\text{-}H)_3(\mu_3\text{-}\eta^2\text{-}CH_2O)(CO)_9]^{2-}$ is effected by treatment of 10 with Li[BH-(s-Bu)$_3$]. [162] Further reduction is achieved by protonation of the dianionic oxymethyl species to yield $[Re_3(\mu\text{-}H)_3(\mu_3\text{-}\eta^2\text{-}CH_2OH)(CO)_9]^-$, which has been identified spectroscopically.[162] This hydroxymethyl cluster reacts with CO to yield $[Re_3(\mu\text{-}H)_2(CO)_{12}]^-$ and methanol.[162] Hydrogenolysis of $[Re_3(\mu\text{-}H)_2(CO)_{12}]^-$ regenerates 10, and, therefore, this reaction sequence has potential as a route to a cluster catalysed reduction of CO to CH_3OH, as shown in Scheme 6.

Scheme 5. Reactions of $[Re_3(\mu\text{-}H)_4(CO)_{10}]^-$

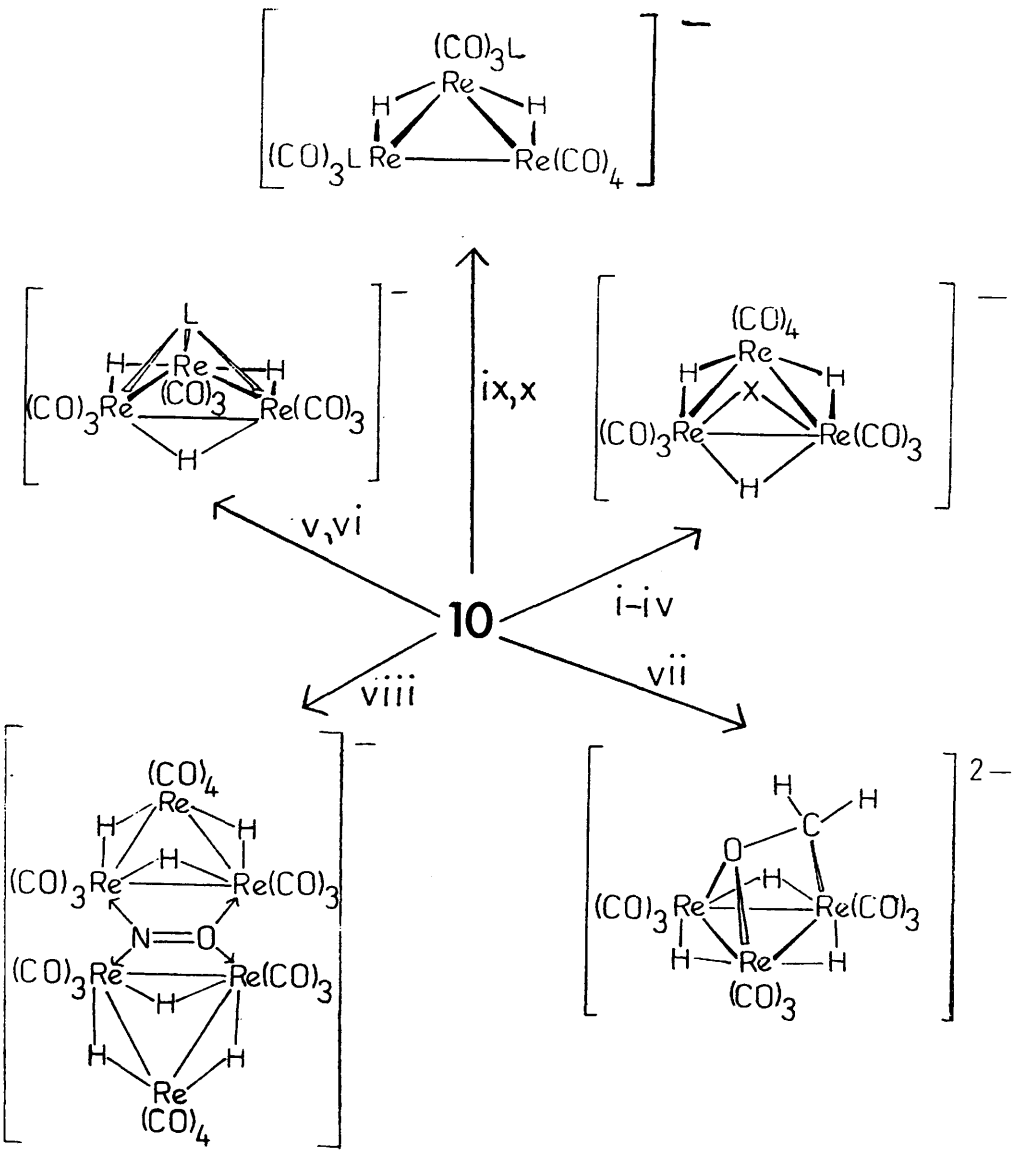

i. HX, X = Cl,Br I	Ref.156	vii. $Li[BH(s\text{-}Bu)_3]$	ref. 162
ii. HO_2CR; X=μ-η^2-O_2CR	157	viii. $NOBF_4$	163
iii. I_2; X=I	158	ix. CO, L = CO	164
iv. $CH_3C(O)CH_3$; X=$OCH(CH_3)_2$	159	x. PR_3, L=PR_3	165
v. HOR, L = OR	160		
vi. HSR, L = SR	161		

Table 11 : Re-Re bond lengths in adducts of $[Re_3(\mu\text{-}H)_4(CO)_{10}]^-$, Å.

Type of Cluster.	Re(μ-H)(μ-X)Re	Re(μ-H)Re	Ref.
$[Re_3(\mu\text{-}H)_3(\mu\text{-}X)(CO)_{10}]^-$			
X = Cl	2.995(2)	3.194(2), 3.219(2)	156
O_2CH	3.181(1)	3.264(1), 3.229(1)	157
O_2CCF_3	3.181*	3.239*	157
$OCHMe_2$	2.930(1)	3.202(1), 3.219(1)	159
NO	3.097*	3.199*, 3.202*	163
$[Re_3(\mu\text{-}H)_3(\mu_3\text{-}L)(CO)_9]^-$	Re(μ-H)Re		
L = OEt	2.998(1), 2.998(1), 2.985(1)		160
St-Bu	3.092(1)		161
$[Re_3(\mu\text{-}H)_3(\mu_3\text{-}\eta^2\text{-}CH_2O)(CO)_9]^{2-}$	Re(μ-CH_2O)(μ-H)Re	Re(μ-CH_2O)(μ-H)Re	
X = CH_2O	2.950(1)	3.221(1), 3.201(1)	162
$[Re_3(\mu\text{-}H)_2(CO)_{10}L_2]^-$	Re-Re	Re(μ-H)Re	
L = CO	3.035(7)	3.173(7), 3.181(7)	166
PPh_3	3.009(3)	3.190(4), 3.203(4)	165

* - average Re-Re distance over 2 independent molecules per unit cell.

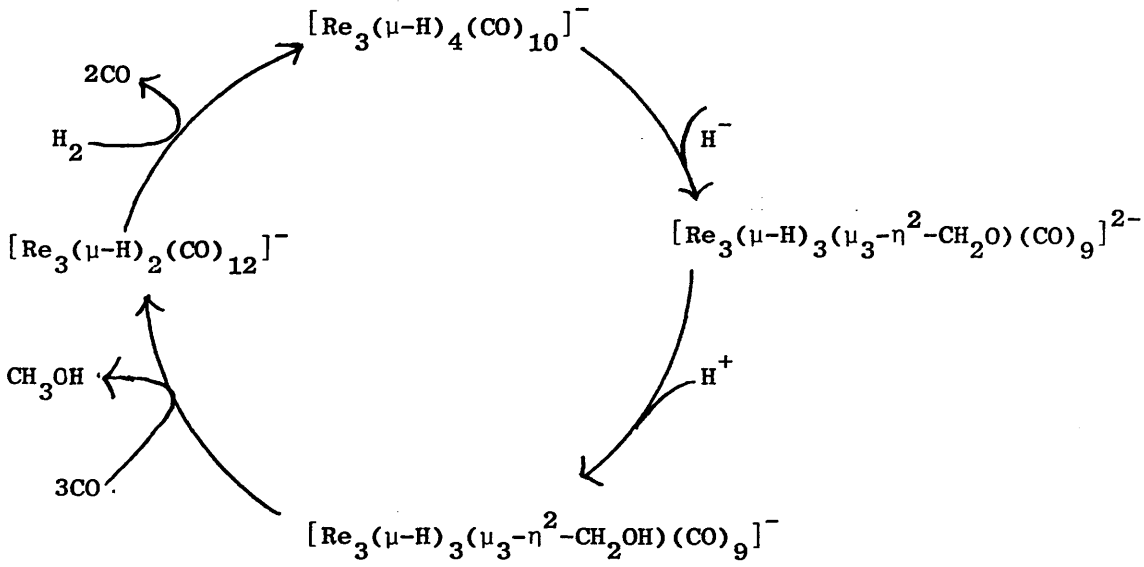

Scheme 6 : Potential catalytic cycle for reduction of CO to CH_3OH on a Re_3 framework.

The organometallic chemistry associated with 10 is somewhat limited compared with that of 4 (vide supra). Only one example of a π-bound unsaturated hydrocarbon adduct of 10 is known. This results from treatment of 10 with $(C_7H_7)BF_4$, which yields $Re_3(\mu\text{-}H)(\mu_3\text{-}H)(\eta^5\text{-}C_7H_9)(CO)_{10}$.[167] Crystallographic analysis[167] of this product reveals the cycloheptadienyl function is bound to one Re centre, and two hydride ligands of 10 have transferred to the organic moiety. The remaining metal bound hydrides are assumed to adopt edge and face bridging coordination sites, as shown in Figure 13.

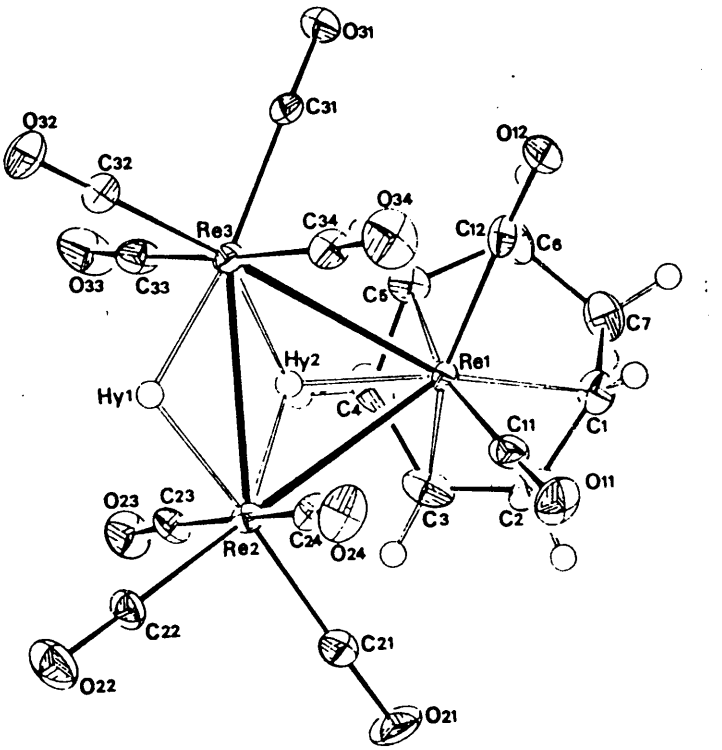

Figure 13 : The crystal structure of $Re_3(\mu\text{-}H)(\mu_3\text{-}H)(\eta^5\text{-}C_7H_9)(CO)_{10}$.

As with 4, it is possible to prepare substituted derivatives of 10. These are accessed via the lightly stabilised cluster $[Re_3(\mu\text{-}H)_4(CO)_9(MeCN)]^-$, [168] which can be prepared according to the equation:-[168]

$$[Re_3(\mu\text{-}H)_4(CO)_{10}]^- \xrightarrow[MeCN]{Me_3NO.2H_2O} [Re_3(\mu\text{-}H)_4(CO)_9(MeCN)]^- + CO_2 + Me_3N$$

Spectroscopic data obtained from this acetonitrile substituted analogue of 10 indicate that the weakly coordinating MeCN ligand is located on the unique Re site, as shown in Figure 14. As expected, the MeCN function is readily displaced by nucleophiles, such as PR_3, CO, and py.[168] X-ray diffraction experiments on $[Re_3(\mu\text{-}H)_4(CO)_9L]^-$, L = PPh_3 [168] and py[168] confirm that the site of substitution is an axial CO group on the unique Re atom, (Figure 14). A consideration of the

corresponding Re-Re vectors in clusters where the substituent ligand L = CO, PPh_3 and py, listed in Table 12, indicates that the bond lengths are similar for all three structures. Indeed, the structures show little variation except those attributable to the differences in bulk of the substituent L.[168]

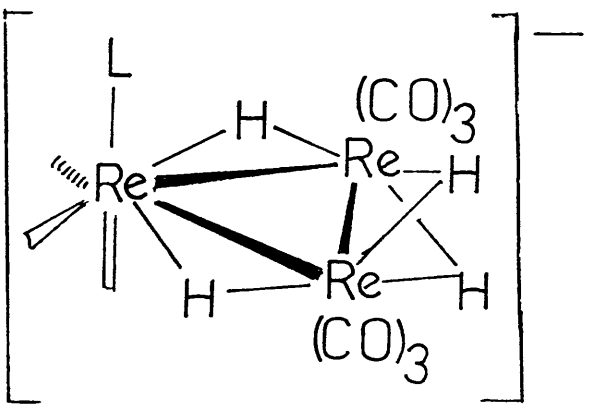

Figure 14 : The structure of $[Re_3(\mu\text{-}H)_4(CO)_9L]^-$ L = MeCN, PPh_3, py.

Table 12 : Comparison of bond lengths (Å) in $[Re_3(\mu\text{-}H)_4(CO)_9L]^-$

	L = CO	PPh_3	py
Re(μ-H)Re	3.190*	3.214*	3.182*
$Re(\mu\text{-}H)_2Re$	2.789(1)	2.797(1)	2.802(1)

* -averaged over both Re(μ-H)Re vectors in each cluster.

These carbonyl substituted derivatives of 10 differ from those of 4 in that the site of substitution in the Re_3 clusters is the unique $M(CO)_4$ group, whereas with the Os_3 systems, substitution occurs at metal centres of the $M(\mu\text{-}H)_2M$ units, where unsaturation is localised. 10 and its substituted analogues are expected to differ in reactivity for reasons

outlined previously i.e. changes in steric and electronic character of the clusters imposed by substituent ligands.

Formal substitution of hydride ligands of 10 can be achieved by treating 9 with $AuClPPh_3$ at low temperatures, yielding $[Re_3(\mu\text{-}H)_3(\mu\text{-}AuPPh_3)(CO)_{10}]^-$.[169] However this complex is unstable and, on warming to room temperature, decarbonylates to give the 44 electron species $[Re_3(\mu\text{-}H)_3(\mu_3\text{-}AuPPh_3)(CO)_9]^-$.[169] An X-ray diffraction study has delineated the structure of this highly unsaturated species,[169] which is shown in Figure 15. This compound, which can also be viewed as a 56 electron Re_3Au *closo.* tetrahedral cluster, is 4 electrons short of a saturated, closed shell configuration.

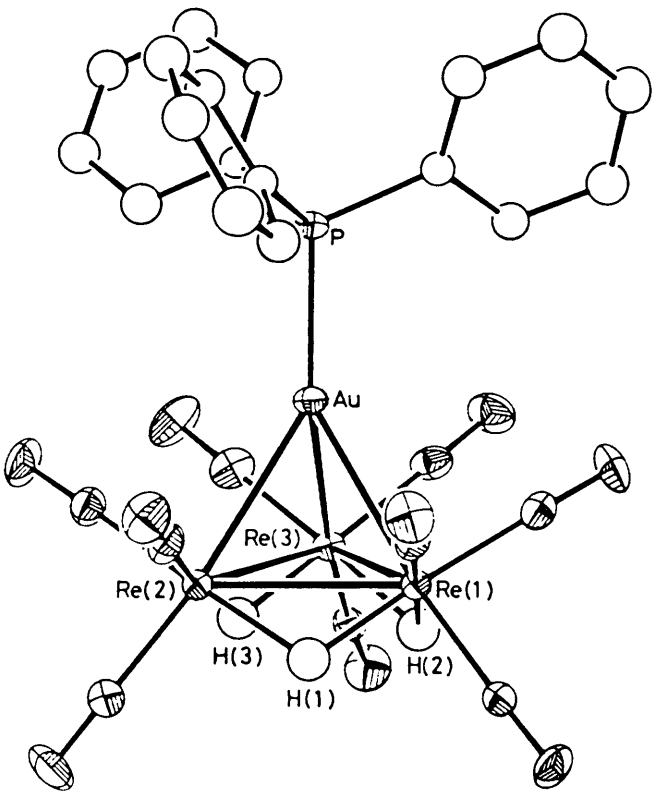

Re-Re Bond lengths	Å
Re(1)-Re(2)	2.889(1)
Re(1)-Re(3)	2.899(1)
Re(2)-Re(3)	2.893(1)

Figure 15 : The crystal structure and Re-Re bond lengths of $[Re_3(\mu\text{-}H)_3(\mu_3\text{-}AuPPh_3)(CO)_9]^-$

This unsaturation is non-localised, as is evident in the three short Re-Re bond lengths. The Re_3Au nonacarbonyl species is stable with respect to CO addition up to 50 atmospheres of CO pressure.[169] The facile formation of the nonacarbonyl from the decacarbonyl contrasts with the chemistry of the triosmium analogue, $Os_3(\mu\text{-}H)(\mu\text{-}AuPPh_3)(CO)_{10}$ which at ambient temperature is stable with respect to decarbonylation.[112]

The nature of products formed by nucleophilic attack at 10 or 4 indicate that, despite gross structural similarities these unsaturated clusters differ significantly in their reactivity. In the triosmium system, addition of a nucleophile, L, leads to formation of adducts with general formula $Os_3(\mu\text{-}H)(CO)_{10}(H)L$. In contrast the observed chemistry of 10 involves electrophilic attack at one bridging hydride site of the $Re(\mu\text{-}H)_2Re$ unit and facilitates replacement of that hydride by an incoming ligand (e.g. reactions i - vi in Scheme 5). Adducts of the type $[Re_3(\mu\text{-}H)_3(CO)_{10}(H)L]^-$, analogous to those of 4, have never been observed in the Re_3 system, although they have been proposed as reactive intermediates.[165] Electrophilic attack may be favoured in 10 due to its negative charge, and the characteristic basic behaviour of the $Re(\mu\text{-}H)_2Re$ hydrides evident in the chemistry of 10 certainly suggests localisation of the negative charge on this unit. It is interesting to note that, when treated with OH^-, 10 yields 9 and H_2O, indicating that the hydrides bridging the long Re-Re separations are apparently positively polarized and, hence, the hydrides in 10 show "amphoteric" behaviour.[164]

In conclusion, despite their structural similarities and isoelectronic relationship, the trirhenium systems, 10 and 9 show interestingly distinct reactivities to that of 4. The products of reactions of 10 seem to be readily crystallised using, in most instances $[NEt_4]^+$ as the counter cation. This has allowed X-ray crystallographic studies to be performed on a number of these products, some of which incorporate

ligands in bonding modes that have not previously been observed, e.g. μ_3-η^2-CH_2O [162] and μ_4-η^2-NO.[163]

1.3.2 (iv) Electron Deficient Clusters obeying the P.S.E.P.T.

There are a number of clusters which are electron deficient according to the E.A.N rule but, if certain main group atoms are considered an integral part of the cluster framework, obey the P.S.E.P.T. predictions for the number of bonding skeletal electron pairs (S.E.P's). In general, these systems involve multi-site bound ligands, such as alkynes, in which the number of electrons donated to the valence electron count of the cluster is unclear. In such cases, the P.S.E.P.T can be applied to illuminate both the structures and the chemistry of these clusters.

a) $M_3(\mu_3$-η^2-$\perp$RC≡CR)$(CO)_9$, (M = Fe,Os) Systems.

An early example of this type of species is the 46 electron *triangulo* cluster $Fe_3(\mu_3$-η^2-PhC≡CPh)$(CO)_9$, 11 which has been synthesised in the following ways:

		Yield	Ref
$Fe_2(CO)_9$ + PhC≡CPh	⟶ 11	1%	170
$Fe_3(CO)_{12}$ + PhC≡CPh	⟶ 11	20%	171

The crystal structures of $Fe_3(\mu_3$-η^2-PhC≡CPh$)(CO)_9$,[170] and the related $Fe_3(\mu_3$-η^2-EtC≡CEt$)(CO)_9$,[172] (Figure 16), show the RC≡CR moiety coordinates to the Fe_3 triangle such that it lies perpendicular ($\perp$) to an Fe-Fe bond.

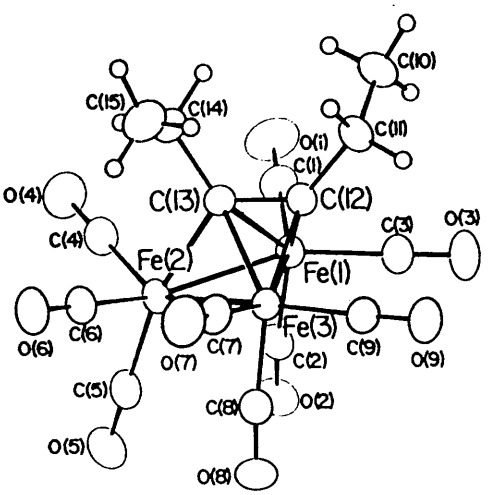

Figure 16 : The molecular structure of $Fe_3(\mu_3\text{-}\eta^2\text{-}EtC{\equiv}CEt)(CO)_9$

This is in contrast to the coordination observed in the saturated 48 electron clusters $M_3(\mu\text{-}H)_2(\mu_3\text{-}\eta^2\text{-}RC{\equiv}CR)(CO)_9$, (M=Ru,[173] Os,[174]), where the alkyne coordinates parallel (||) to the M-M edge.

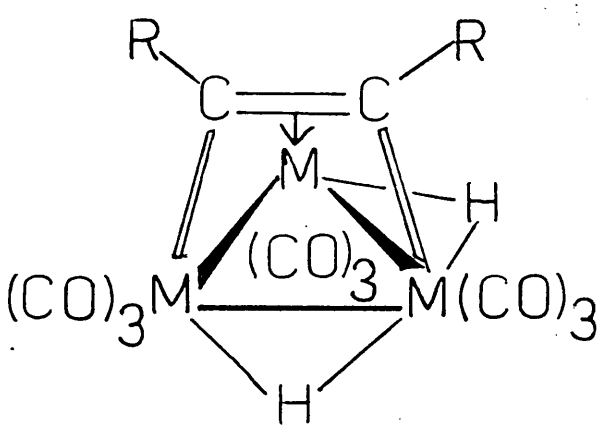

Figure 17 : The structure of the 48 electron system $M_3(\mu\text{-}H)_2(\mu_3\text{-}\eta^2\text{-}RC{\equiv}CR)\text{-}(CO)_9$, M=Ru,Os.

Theoretical analysis of the bonding in $M_3(\mu_3\text{-}\eta^2\text{-}RC{\equiv}CR)$ clusters by Hoffmann,[175] and others,[176,177] has allowed these observations to be rationalised. By application of the Fragment Orbital Formalism, the orbital interactions of the $Fe_3(CO)_9$ fragment with the HC≡CH ligand in the model complex $Fe_3(\mu_3\text{-}\eta^2\text{-}HC{\equiv}CH)(CO)_9$ can be analysed (see Figure 18).[175] The symmetry of the frontier orbitals of HC≡CH with respect to the molecular mirror plane is dependent upon the orientation of the alkyne moiety on the Fe_3 face. Figure 18 shows that for (⊥) acetylene coordination, both π and π* orbitals of HC≡CH comprise of one symmetric and one antisymmetric orbital. These interact with the frontier orbitals of the cluster fragment to destabilise $1s$, stabilise $2s$ and render $1a$ only slightly perturbed. With (||) coordination, the π orbitals of the acetylene unit are symmetric, while the π* orbitals are antisymmetric. In this case, interaction with $Fe_3(CO)_9$ destabilises the fragment $2s$ orbital, renders $1s$ little altered and stabilises 1a. In addition, the vacant 2s fragment orbital is stabilised by interaction with π* $1a$ of the acetylene fragment, such that the resultant cluster orbital can be considered bonding in 48 electron systems. Hence the orientation of the alkyne ligand greatly influences the bonding characteristics and, therefore, the relative stabilities of these complexes. It is calculated that, for a 46 electron cluster, the energetically preferred conformation will be that with the alkyne perpendicular to the Fe-Fe bond.[175,176]

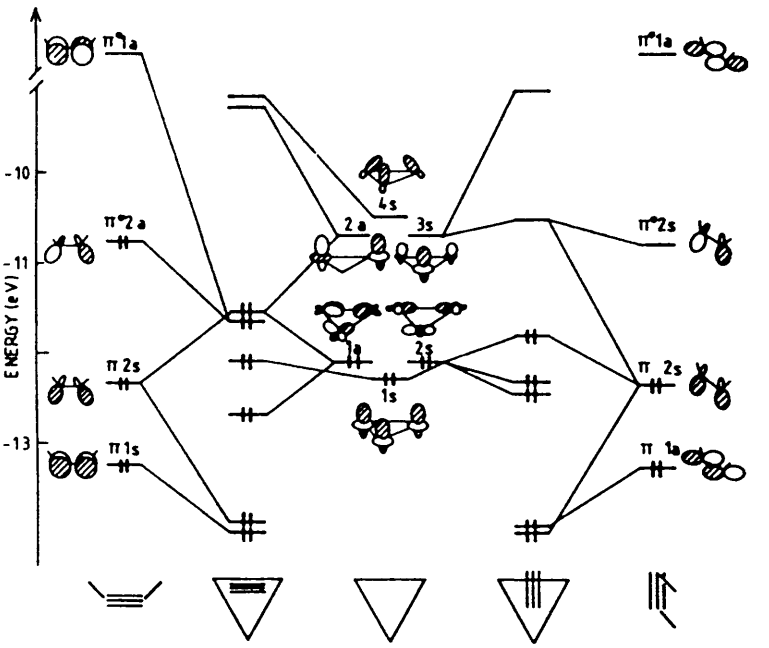

Figure 18 : Orbital energy level diagram for ($\perp$) and ($\parallel$)-alkyne bound $Fe_3(\mu_3\text{-}\eta^2\text{-}HC{\equiv}CH)(CO)_9$ (from ref. 176)

The situation is reversed for $[Fe_3(\mu_3\text{-}\eta^2\text{-}HC{\equiv}CH)(CO)_9]^{2-}$ and, hence, ($\parallel$) coordination is preferred for 48 electron compounds. Saillard et al[176] have estimated that, for the 46 electron system $\mu_3\text{-}\eta^2\text{-}\perp$HC≡CH coordination is favoured by 15 k cal mol^{-1}, whereas in the 48 electron cluster $\mu_3\text{-}\eta^2\text{-}\parallel$-HC≡CH binding is relatively stabilised by 33 k cal mol^{-1}.

The M_3C_2 framework of the 46 electron species can be viewed as a distorted *closo* trigonal bipyramidal core as shown in Figure 19. The P.S.E.P.T. predicts that such a geometry should have (n+1)=6 skeletal electron pairs.[55,57]

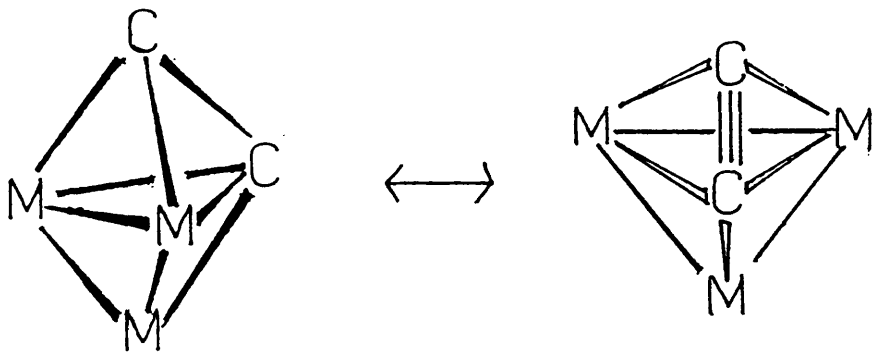

Figure 19. The *closo*-tbp framework of $M_3(\mu_3\text{-}\eta^2\text{-}\perp RC{\equiv}CR)$.

This count is found in $Fe_3(\mu_3\text{-}\eta^2\text{-}\perp RC{\equiv}CR)(CO)_9$ species, which casts doubt on the unsaturated nature of these clusters. To satisfy the E.A.N rule, the acetylene fragment could be considered a 6 electron donor which would allow a 48 electron count for these species. If this were the case, it implies a weak C-C interaction in the acetylene moiety, which is suggested by the experimentally observed facile transformation of $Fe_3(\mu_3\text{-}\eta^2\text{-}\perp\text{-}HC_2OEt)(CO)_9$ to the bisalkylidyne $Fe_3(\mu_3\text{-}CH)(\mu_3\text{-}COEt)(CO)_9$.[178] In addition to this, theoretical analysis of the C-C scission reactions of $\mu_3\text{-}\eta^2\text{-}||$ RC_2R bound alkynes to yield $(\mu_3\text{-}CR)_2$ functions implicate $\mu_3\text{-}\eta^2\text{-}\perp$ RC_2R alkynes as intermediates in this process.[179]

However, comparative analysis of C-C bound lengths in $\mu_3\text{-}\eta^2\text{-}\perp$ and $\mu_3\text{-}\eta^2\text{-}||$ alkyne ligands listed in Table 13 does not support the proposal that this interaction is particularly weak. For $\mu_3\text{-}\eta^2\text{-}\perp$ coordination, bond distances lie in the range 1.391 - 1.441 (ave. 1.411)Å while for $\mu_3\text{-}\eta^2\text{-}||$ alkynes the range is 1.34 - 1.439 (ave. 1.382)Å. Furthermore, the $\mu_3\text{-}\eta^2\text{-}\perp$ $RC_2R' \rightarrow (\mu_3\text{-}CR)(\mu_3\text{-}CR')$ transformation observed

Table 13. Alkyne C-C bond distances in μ_3-η^2-(⊥) and μ_3-η^2-(||) RC≡CR ligands.

		C-C (Å)	ref.
μ_3-η^2-(⊥)RCCR systems			
$Fe_3(PhCCPh)(CO)_9$		1.409(22)	170
$Fe_3(EtCCEt)(CO)_9$		1.391(4)	172
$RuFe_2(PhCCPh)(CO)_9$		1.413(20)	180
$FeW_2(RCCR)(Cp)_2(CO)_6$*		1.399(9)	181
$FeW_2(RCCR)(Cp)(CO)_5(O)$*		1.441(11)	181
*R = C_6H_4Me	Ave.	1.411	
μ_3-η^2-(||)RCCR systems			
$Os_3(PhCCPh)(CO)_{10}$		1.439(10)	182
$FeCo_2(EtCCEt)(CO)_8(PPh_3)$		1.367(8)	183
$FeCo_2(EtCCEt)(CO)_9$		1.37(1)	184
$RuCo_2(\mu\text{-}CO)(PhCCPh)(CO)_8$		1.38(1) 1.370(3)	185 186
$Ru_3(\mu\text{-}PPh_2)_2(HCCPh)(CO)_7$		1.37(1)	187
$CoFeNi(PhCCPh)(Cp)(CO)_5(PPh)_3$		1.34(2)	188
$CoNiRu(PhCCPh)(Cp)(CO)_6$		1.377(9)	188
$CoNiOs(PhCCPh)(Cp)(CO)_6$		1.377(10)	188
$Os_3(\mu\text{-}H)_2(MeCCMe)(CO)_9$		1.434(36)	190
	Ave.	1.382	

on an Fe_3 framework for R=H, R'=OEt [178] is somewhat atypical of the alkyne behaviour in these systems. More generally, in 46 electron clusters the alkyne moiety is stable in the $\perp$ bonding mode. Thus, the alkyne fragment should be considered to donate 4 electrons to the valence electron count when it is $\perp$ bound to the M_3 triangle and, therefore, these species should be considered as 46 electron clusters.

As has been shown for 4 and 10, 46 electron clusters typically react with nucleophiles to relieve their unsaturation

Electrochemical studies of $Fe_3(\mu_3\text{-}\eta^2\text{-}\perp RC{\equiv}CR)(CO)_9$ compounds reveal they undergo two near reversible one electron reductions,[171] in keeping with the expected behaviour of unsaturated systems. Furthermore, ^1H and ^{13}C n.m.r spectroscopic evidence suggest that the alkyne fragment is reorientated to $\mu_3\text{-}\eta^2\text{-}||$ coordination on addition of two electrons in accord with theoretical predictions.[171,175,176]

By considering the M_3C_2 core, this transformation can be described as a skeletal rearrangement from a *closo* trigonal bipyramid to a *nido* octahedral geometry as represented in Figure 20. This can be rationalised in

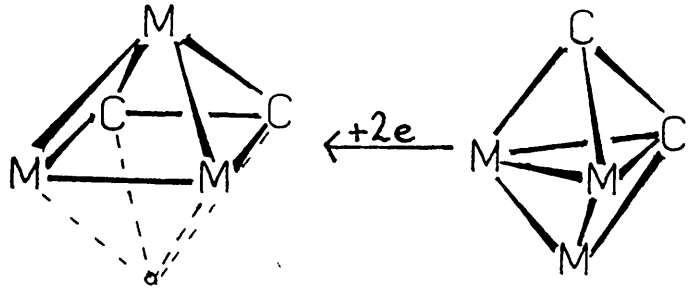

Figure 20 : Framework rearrangement on addition of 2 electrons to $M_3(\mu_3\text{-}\eta^2\text{-}\perp RC{\equiv}CR)$

terms of numbers of S.E.P by P.S.E.P.T arguments. Structural rearrangements of this kind are more typical of saturated clusters.

Addition reactions involving nucleophiles, such as PR_3, are characteristic of electronically unsaturated clusters (vide supra). However, Sappa has investigated such reactions with $Fe_3(\mu_3\text{-}\eta^2\text{-}\perp EtCCEt)(CO)_9$ and found that CO substitution rather than PR_3 addition was effected on treatment with excess PPh_3 affording $Fe_3(\mu_3\text{-}\eta^2\text{-}\perp EtCCEt)(CO)_8(PPh_3)$ in good yield.[189] Sappa has reasoned that addition reactions do not occur with $Fe_3(\mu_3\text{-}\eta^2\text{-}\perp RC_2R)(CO)_9$ systems because the structure has no vacant coordination site.[189]

This stability to nucleophilic attack contrasts with the reactivity of the isoelectronic Os analogue $Os_3(PhC_2Ph)(CO)_9$, 12.[98] 12 is prepared by "flash" thermal decarbonylation of $Os_3(\mu_3\text{-}\eta^2\text{-}||PhC_2Ph)(CO)_{10}$,[98] however this has not proved to be a general synthetic route to 46 electron $Os_3(RC_2R')(CO)_9$ derivatives. Decarbonylation of the analogous but-2-yne or terminal alkyne decacarbonyls yields $Os_3(\mu\text{-}H)(\mu_3\text{-}\eta^3\text{-}MeC{=}C{=}CH_2)(CO)_9$ and $Os_3(\mu\text{-}H)(\mu_3\text{-}\eta^2\text{-}C{\equiv}CR)(CO)_9$ respectively.[96] Thus C-H rupture in the organic moiety and subsequent oxidative addition to the cluster has compensated for CO loss, and the products are electron precise.

12 reacts with CO,[98] and CH_2N_2 [191] readily at room temperature to yield 48 electron products with the expected $\mu_3\text{-}\eta^2\text{-}||PhC_2Ph$ alkyne coordination. The CH_2N_2 reaction yields the methylene and diazomethane adducts, shown in Figure 21.

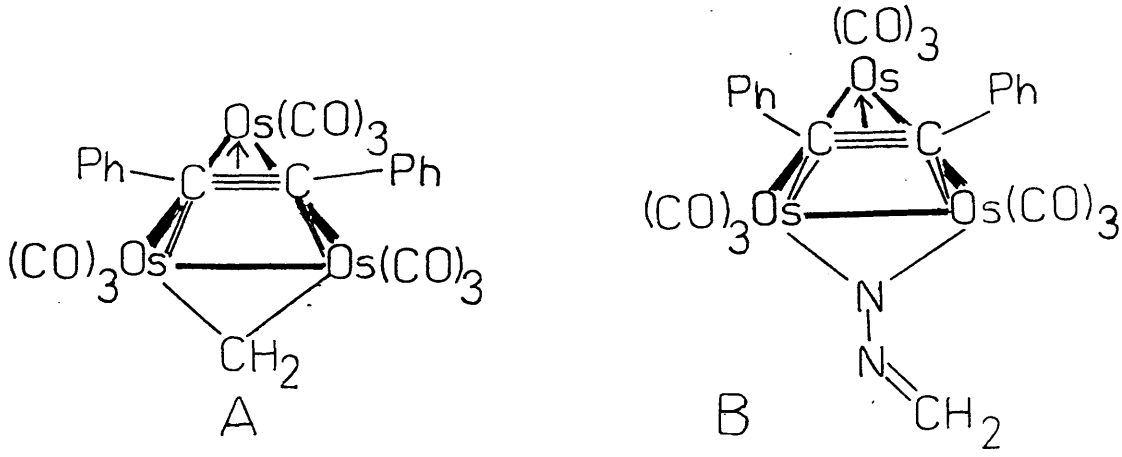

Figure 21 : The CH_2(A) and CH_2N_2 (B) adducts of 12.

B does not convert to A on heating, however photolysis of B effects loss of dinitrogen and yields A.[191]

12 is considerably more reactive than 11. In the absence of structural data on 12, this can be accounted for by assuming either (⊥) or (||) coordination of the PhC≡CPh moiety. Firstly, if it is assumed that 11 and 12 are isostructural, the increased electronegativity of Os compared with Fe would decrease the metal-ligand back-bonding and may render 12 relatively unstable, and more capable of undergoing attack by 2 electron donors to form stable $Os_3(\mu_3\text{-}\eta^2\text{-}||\text{-}PhC{\equiv}CPh)(CO)_9L$ complexes. Secondly, 12 may incorporate a $\mu_3\text{-}\eta^2\text{-}||\text{-}PhC{\equiv}CPh$ coordination mode. EHMO calculations on an Fe_3 analogue predict such systems will have a low lying LUMO in the 46 valence electron configuration[175,176] (see Figure 18). Therefore it may be expected that similar species would be susceptible to nucleophilic attack.

The alkyne orientation in 12 could be determined by ^{13}C n.m.r spectroscopy. In the species $Fe_3(\mu_3\text{-}\eta^2\text{-}\perp\text{-}EtC{\equiv}CEt)(CO)_9$ there

is a large chemical shift difference (> 100 ppm) between the σ-bonded and π-bonded acetylenic carbons,[177] whereas with ||—RC≡CR coordination both acetylenic carbons should have identical chemical shifts. However, the ^{13}C n.m.r spectrum of 12 has not been reported.

The related 46 electron triosmium cluster, $Os_3(\mu_3\text{-}\eta^2\text{-}\perp\text{-}PhC{\equiv}CPh)(dppm)(CO)_7$,[127] 13, synthesised by thermolysis of 8 with PhC≡CPh, is isoelectronic with 12. X-ray crystallography has determined the solid state structure of 13 (shown in Figure 22) in which the alkyne function is ligated to the Os_3 framework in the expected $\perp\mu_3\text{-}\eta^2$ fashion.[127] 13 is more stable than 12. This stability is attributed to the good σ-donor and poor π-acceptor capabilities of the phosphine groups, which provide the Os centres to which they are bound sufficient electron density for the stabilisation of the $\mu_3\text{-}\eta^2\text{-}\perp$ alkyne through Os-π^* (alkyne) interactions.[127]

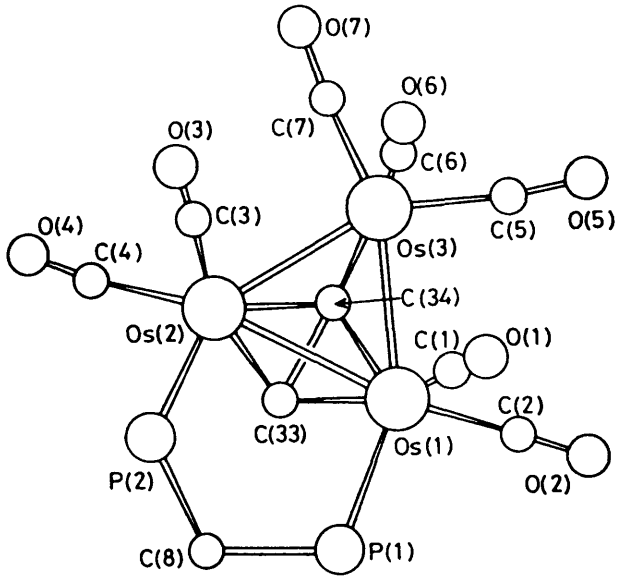

Figure 22 : The molecular structure of $Os_3(\mu_3\text{-}\eta^2\text{-}\perp\text{-}PhC{\equiv}CPh)(CO)_7(dppm)$;

b) *Closo*-octahedral M_4E_2 Unsaturated Clusters.

Several unsaturated *closo*-octahedral tetranuclear M_4E_2 clusters are known, where E is a μ_4 ligand, typically PR, S, Te etc, capping a planar M_4 unit (Figure 23).

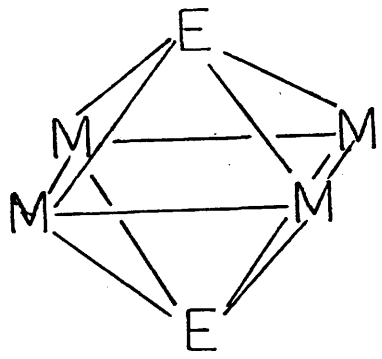

Figure 23 : M_4E_2 - type cluster.

Of these systems, the chemistry of $Fe_4(\mu\text{-CO})(\mu_4\text{-PPh})_2(CO)_{10}$ 14, is the most developed.[192] This cluster has an electron count of 62, but has only 4 Fe-Fe bonds, indicating that 14 is unsaturated by 2 electrons according to the E.A.N rule. However, if the P units are considered part of the cluster core there are 7 skeletal bonding electron pairs in 14, in accord with the (n+1) prediction of the P.S.E.P.T. for a *closo* octahedron (n=6). Crystallographic analyses of 14 [242] and the related unsaturated cluster $Fe_4(\mu\text{-CO})(\mu_4\text{-PTol})_2(CO)_9[P(OMe)_3]$ [192] reveal that the carbonyl bridged Fe-Fe separations (of 2.440(3)Å and 2.458(3)Å respectively) are somewhat shorter than the unbridged Fe-Fe bonds (mean value of 2.689Å in both clusters). However, Vahrenkamp has argued [192] that this bond shortening is not conclusive evidence of localised unsaturation in the Fe(μ-CO)Fe units as comparable bond shrinkage is observed in CO bridged single M-M bonds.

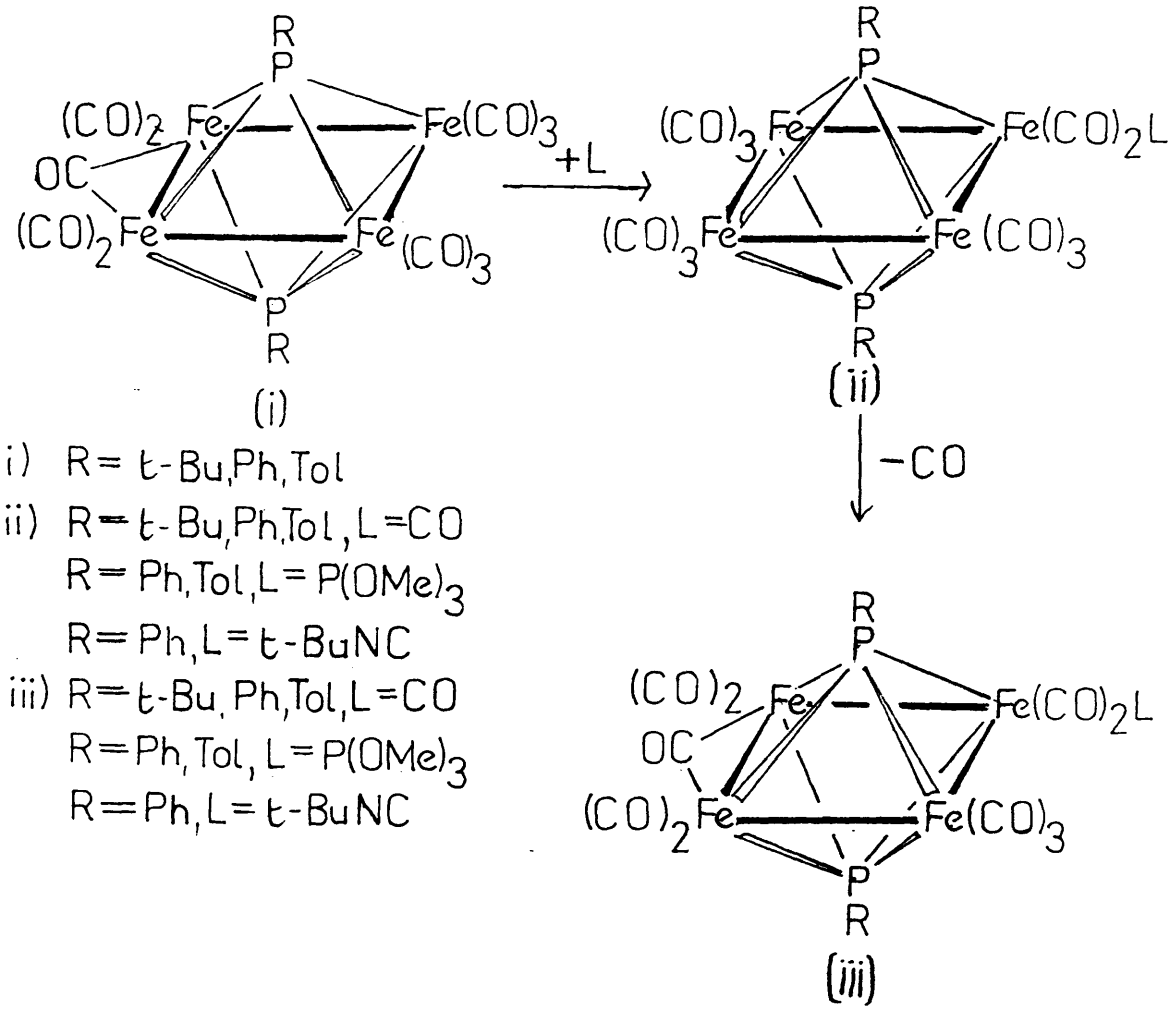

i) R = t-Bu, Ph, Tol

ii) R = t-Bu, Ph, Tol, L = CO
R = Ph, Tol, L = $P(OMe)_3$
R = Ph, L = t-BuNC

iii) R = t-Bu, Ph, Tol, L = CO
R = Ph, Tol, L = $P(OMe)_3$
R = Ph, L = t-BuNC

Scheme 7 : Replacement of CO by L on 14 through formation of a saturated intermediate.

14 readily adds two electron donor ligands, as shown in Scheme 7, yielding 64 electron species with 8 SEP's. Thermal treatment of these adducts in vacuo leads to decarbonylation and the formation of substituted unsaturated clusters. Further substitution and decarbonylation is possible up to $Fe_4(\mu_4\text{-PPh})_2LL'_2(CO)_8$ for L=L'=t-BuNC and L = t-BuNC, L' = $P(OMe)_3$, and $Fe_4(\mu_4\text{-PPh})_2L_4(CO)_7$ for L = $P(OMe)_3$.[192]

Similar chemistry has been observed with $Fe_3Rh(\mu_4\text{-PPh})_2(\eta^5\text{-}C_5Me_5)(CO)_8$,[193] 15, which is isoelectronic with 14. 15 has been shown to add CO reversibly and to undergo two one electron reductions,[193] in keeping with its unsaturated nature.

Substitution of either one or two carbonyls by PMe_2Ph has been observed in the related 62 electron unsaturated $Ru_4(\mu\text{-CO})_2(\mu_4\text{-S})_2(CO)_9$ cluster.[194] Although saturated adducts have not been observed in this reaction, clearly a mechanism invoking such species in the ligand substitution process, is an attractive one.

These compounds are unusual since the 62 electron unsaturated species obey the P.S.E.P.T with 7 S.E.P's, while the saturated 64 electron *closo*-octahedral complexes have 8 S.E.P's, violating the P.S.E.P.T. A more sophisticated molecular orbital treatment of the bonding in these systems has been presented by Halet, Hoffmann and Saillard[195] which accounts for these apparent anomalies. They considered the interaction of a planar $[Fe_4(CO)_{12}]^{8-}$ unit with $[HP....PH]^{8+}$ to generate the model *closo*-octahedral complex $Fe_4(\mu_4\text{-PH})_2(CO)_{12}$. The M.O. interaction diagram is presented in Figure 24. It was found that the energy difference between the HOMO, b_u orbital, of the 64 electron, 8 S.E.P. species and the occupied b_g MO immediately below it depended on the interaction of d-orbitals on the μ_4-PH ligand with π-type metal orbitals. The magnitude of this energy difference dictates whether a *closo* octahedron with seven or eight S.E.P's is most stable.[195]

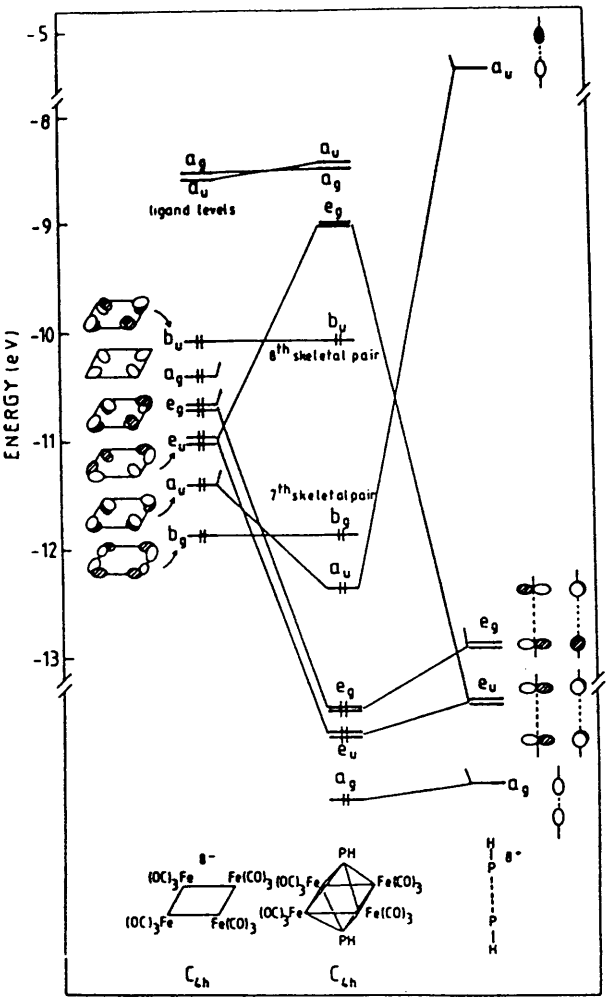

Figure 24 : Orbital interaction diagram for $HP....PH^{8+}$ and $Fe_4(CO)_{12}^{8-}$ fragments.

An examination of the P....P distances in such clusters, listed in Table 14, reveals that the P....P separation is shorter for clusters with 8 S.E.P's than for those with 7, supporting the premise that increased interaction of the d-orbitals of the PR unit with the π orbitals of the M_4 unit stabilises the frontier b_u orbital of the *closo*-octahedral system.

Table 14 : P....P distances in octahedral $M_4(PR)_2$ systems.

	SEP	P---P (Å)	ref.
$Fe_4(\mu\text{-CO})(\mu_4\text{-P-p-tol})_2(CO)_9(P(OMe)_3)$	7	2.646(8)	196
$Fe_4(\mu_4\text{-P-p-Tol})_2(CO)_{11}(P(OMe)_3)$	8	2.598(3)	196
$Fe_3Rh(\mu_4\text{-PPh})_2(\eta^5\text{-}C_5Me_5)(CO)_8$	7	2.666(1)	193
$Fe_3Rh(\mu_4\text{-PPh})_2(\eta^5\text{-}C_5Me_5)(CO)_9$	8	2.579	193

The isostructural ruthenium analogue of 14, $Ru_4(\mu\text{-CO})(\mu_4\text{-PPh})_2(CO)_{10}$, 16 has been prepared.[197] However, unlike 14, addition of CO to 16 results in both Ru-Ru and Ru-P bond scission, yielding $Ru_4(\mu_3\text{-PPh})_2(CO)_{13}$.[198] If $Ru_4(\mu_4\text{-PPh})_2(CO)_{12}$ is an intermediate in the formation of $Ru_4(\mu_3\text{-PPh})_2(CO)_{13}$, then, unlike the saturated $Fe_4(PR)_2$ system, it is clearly unstable with respect to M-M cleavage in the presence of CO. This is somewhat unexpected due to the relative strength of Ru-Ru bonds compared with Fe-Fe bonds.[40] However, this can be explained by reference to the MO description of these systems.[195] The P....P separation in 16 is 2.77 Å (averaged over three independent molecules in the unit cell),[199] which is considerably longer than that observed in 14. It may be that, on treatment of 16 with CO, $Ru_4(\mu_4\text{-PPh})_2(CO)_{12}$ does form. However, if the P....P distance in this saturated species is longer than that of the analogous Fe_4 cluster, (in keeping with the differences in P....P separation observed between 14 and 16), the stabilisation of the HOMO afforded through P d-orbital interaction with the Ru_4 π-orbitals

will be limited, thus rendering the 64 electron Ru_4 species unstable and susceptible to further reaction with CO yielding $Ru_4(\mu_3\text{-}PPh)_2(CO)_{13}$.

The reactivity of these M_4E_2 systems is not limited to carbonyl replacement via saturated adduct formation. For example both 14 and 16 add alkyne units at a phosphorus site to yield $M_4(\mu_4\text{-}PR)[(\mu_4\text{-}\eta^3\text{-}P(R)C(R')CH](CO)_{11}$ (M = Ru, R = Ph, R' = H;[200] M = Fe, R = Ph, Tol, R' = Me, Ph [201]).

In summary unsaturated M_4E_2 type clusters fall into the same category as $M_3(\mu_3\text{-}\eta^2\text{-}RC{\equiv}CR)(CO)_9$ clusters in that although infringing the E.A.N. rule, they obey P.S.E.P.T predictions when the μ_4-E ligands are considered an integral part of the cluster framework. However, several M_4E_2 clusters, for example 14 and 15, are capable of binding two electron donor ligands without changing the skeletal geometry of the core. This type of behaviour is typical of unsaturated systems, e.g. chemistry of 4 and 10, (and atypical of $Fe_3(\mu_3\text{-}\eta^2\text{-}PhC{\equiv}CPh)(CO)_9$, vide supra). A molecular orbital analysis of the bonding in $Fe_4(\mu_4\text{-}PH)_2(CO)_{12}$ indicates that the orbital interaction of the μ_4-E groups with the M_4 unit is important in determining the relative stabilities of saturated/unsaturated electronic configurations in these systems.[195]

1.3.2 (v) Concluding Comments.

The chemistry of unsaturated clusters has been developed to a point where, in certain well researched systems, e.g. $Os_3(\mu\text{-}H)_2(CO)_{10}$, it is possible to predict the outcome of a nucleophilic attack by a simple two electron donor ligand. However, for the majority of unsaturated cluster complexes, the products of reactions involving ligands capable of multi-site bonding are, in general, difficult to predict. This is due to the number of potential bonding modes available to such functions

in clusters and the lack of sufficient experimental data to enable systematic trends in reactivity to be identified and, ultimately, understood.

1.4 Lightly Stabilised Clusters.

A lightly stabilised cluster can be defined as one with a labile mono or poly-hapto ligand whose dissociation from the cluster is preferred over metal-metal bond cleavage. These clusters are extremely useful in effecting site specific reactions.

There are a large number of such systems known and a variety of synthetic routes to these complexes have been developed. Illustrative examples from triosmium chemistry using 4 as a precursor, are cited below:-

i) $\underline{4}$ + c-C_6H_8 ⟶ 1,1 $Os_3(\eta^4\text{-}C_6H_8)(CO)_{10}$ ref.202

ii) $\underline{4}$ + c-C_8H_{14} $\xrightarrow{C_2H_4}$ 1,2 $Os_3(\eta^2\text{-}C_8H_{14})_2(CO)_{10}$ ref.203

However, the most versatile preparative route to this class of compound is treatment of a cluster with Me_3NO in the presence of a coordinating solvent, e.g. MeCN. Me_3NO effects oxidation of carbonyl functions to CO_2 leaving a vacant cluster coordination site at which a molecule of solvent can ligate. The use of Me_3NO in organometallic chemistry is widespread and has been the subject of a recent review.[204]

This synthetic approach can be used to prepare lightly stabilised analogues of 1,[207,208] 2,[206] and 3,[205] as detailed below:-

$$M_3(CO)_{12} + nMe_3NO \xrightarrow{MeCN} M_3(CO)_{12-n}(MeCN)_n + nCO_2 + nMe_3N$$

n = 1,2 M = Os, Ru; n = 1, M = Fe

These compounds, which retain the structure of the parent binary carbonyls, have proved synthetically useful in the preparation of ligand

substituted derivatives of 1, 2 and 3, and many such species are known.[202,205]

A kinetic analysis of the substitution reactions of $Os_3(CO)_{11}(MeCN)$, 17, and $Os_3(CO)_{10}(MeCN)_2$, 18 with PPh_3, $P(OPh)_3$ and $AsPh_3$ has been presented by Poë et al.[211] For 17 the kinetic data are consistent with a reversible dissociative process:

$$Os(CO)_{11}(MeCN) \underset{k_{-1}}{\overset{k_1}{\rightleftharpoons}} [Os_3(CO)_{11}] + MeCN$$

$$[Os_3(CO)_{11}] + L \xrightarrow{k_2} Os_3(CO)_{11}L$$

The mechanism of substitution in 18 is considered to be distinct from that of 17 due to considerable differences in the activation parameters for the substitution reactions of these different clusters. For 18, initial loss of MeCN is believed to be accompanied by the concerted formation of a CO bridged intermediate (I in Figure 25). The simple coordinatively unsaturated intermediate (II in Figure 25) may also be formed by a higher energy dissociative pathway.[211]

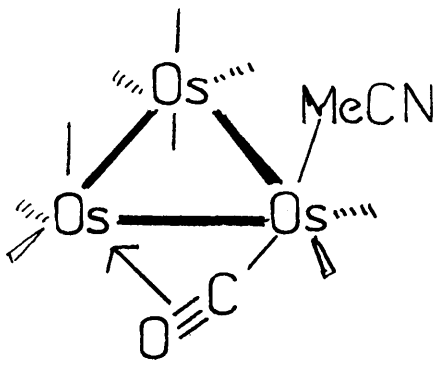

I

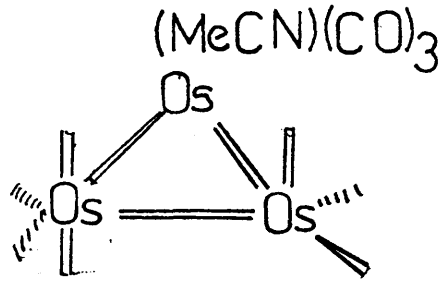

II

Figure 25. Proposed intermediates, I and II in the substitution reactions of 18.

Nucleophilic attack at either of these intermediates yields $Os_3(CO)_{10}(L)_2$. That $Os_3(CO)_{10}(L)(MeCN)$ clusters are not observed products in these reactions indicates that replacement of one MeCN group by L has a significantly labilising effect on the remaining cluster bound MeCN moiety.

Recently reported examples of reactions involving 17 and 18 serve to illustrate their breadth of synthetic application. By employing 17 and 18 as precursors, the build up of higher nuclearity clusters through rational synthetic routes can be achieved. For example, in the synthesis of $Os_6(\mu\text{-}H)(\mu_6\text{-}P)(CO)_{18}$,[212] the stepwise construction of a trigonal prismatic Os_6 cage with an encapsulated μ_6-phosphido ligand is effected by thermal coupling of two Os_3 units sharing a common μ_3-PH moiety [(3) or (4) in Scheme 8]. As indicated in Scheme 8, (3) and (4) are initially prepared by ligating phosphine to the Os_3 framework by displacement of MeCN from 17; subsequent base/H^+ treatment yields the phosphido species $Os_3(\mu\text{-}H)(\mu\text{-}PH_2)(CO)_{10}$ [(2) in Scheme 8]. Further reaction with 17 or 18 yields (3) or (4) respectively and, on thermolysis, the *closo*-trigonal prismatic Os_6 cluster is obtained.

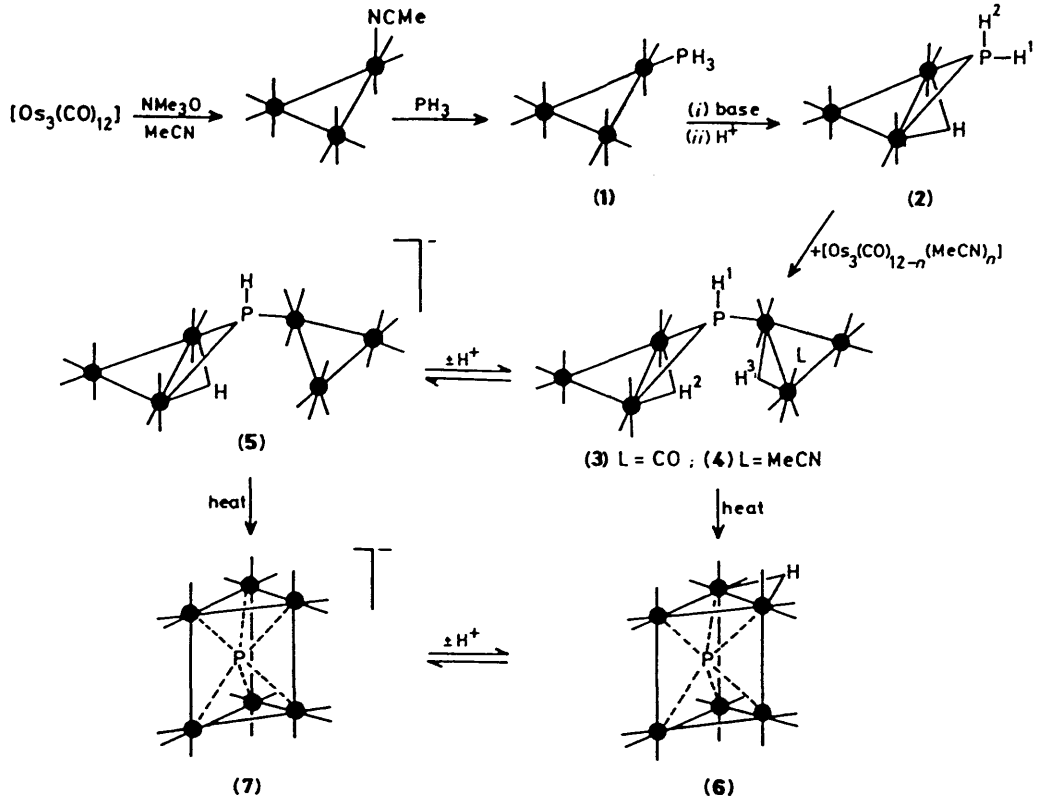

Scheme. Overall yield $[Os_3(CO)_{12}] \longrightarrow [Os_6(CO)_{18}(\mu_6\text{-P})]^-$ (7) *ca.* 60%

Scheme 8 : Stepwise construction of an Os_6 trigonal prism using 17 and 18.

Other examples of increasing cluster nuclearity by syntheses involving 17 or 18 are listed in Table 15.

17 and 18 have proved reactive towards organic, as well as inorganic species. Scheme 9 (a) and (b) summarise some of these reactions. For example the simple alkene coordinated cluster $Os_3(\eta^2\text{-}CH_2CH_2)(CO)_{11}$ has been prepared by treating 17 with ethylene.[210]

The reactions of 17 and 18 with allene have been investigated by Deeming and co-workers.[221] With 17, one allene moiety inserts into an Os-Os bond, yielding the 50 electron cluster $Os_3(\mu\text{-}\eta^3\text{-}CH_2CCH_2)(CO)_{11}$. In contrast, with 18, allene coupling occurs on the Os_3 frame to give $Os_3(\mu_3\text{-}\eta^5\text{-}CH_2CCH_2C(CH_2)_2)(CO)_{10}$.

Both 17,[222,223] and 18,[111] are precursors to $Os_3(\mu\text{-}CH_2)(\mu\text{-}CO)(CO)_{10}$. Although electronically saturated, $Os_3(\mu\text{-}CH_2)(\mu\text{-}CO)(CO)_{10}$,

Table 15 : Examples of Cluster Construction using $Os_3(CO)_{11}(MeCN)$ and $Os_3(CO)_{10}(MeCN)_2$.

Reagents	Product.	Metal Geom.	Ref.
17 + $Os(CO)_4(PMe_3)$	$Os_4(CO)_{15}(PMe_3)$	S.T.	56
18 + catalytic $PdCl_2$	$Os_6(CO)_{20}(MeCN)$	P.R.	213
	$Os_6(CO)_{19}(MeCN)$	P.R.	213
18 + $OsH_2(CO)_4$	$Os_4(\mu\text{-}H)(CO)_{14}(H)(MeCN)$	S.T.	218
18 + $2SnR_2$	$Os_3Sn_2(\mu\text{-}CO)(CO)_9(R)_4$	P.R.	214
$R = CH(SiMe_3)_2$			
18 + $[PPN][Co(CO)_4]$	$[PPN][Os_3Co(CO)_{13}]$	S.T.	215
18 + $[Na]_2[M(CO)_4]$*	$[PPN][Os_3MH(CO)_{13}]$[a]	S.T.	215
	M = Fe,Ru,Os		
17 + $ReH(CO)_5$	$Os_3Re(\mu\text{-}H)(CO)_{15}$	S.T.	216
18 + $2ReH(CO)_5$	$Os_3Re_2(\mu\text{-}H)_2(CO)_{20}$	D.S.T	216
18 + $Os_3(\mu_3\text{-}CO)(\mu_3\text{-}S)(CO)_9$	$Os_6(\mu_3\text{-}S)(CO)_{19}$	E.F.D.B	217
	$Os_6(\mu_3\text{-}S)(CO)_{17}$	F.C.S.P.	217

* cation exchanged by metathesis with [PPN][Cl]

a - H presumed to be abstracted from solvent.

S.T. = spiked triangle

P.R = planar raft

D.S.T = Di spiked triangle

E.F.D.B = edge fused di butterfly

F.C.S.P = face capped square pyramid

Scheme 9 : Some reactions of (a) 17, and (b) 18 with organic molecules.

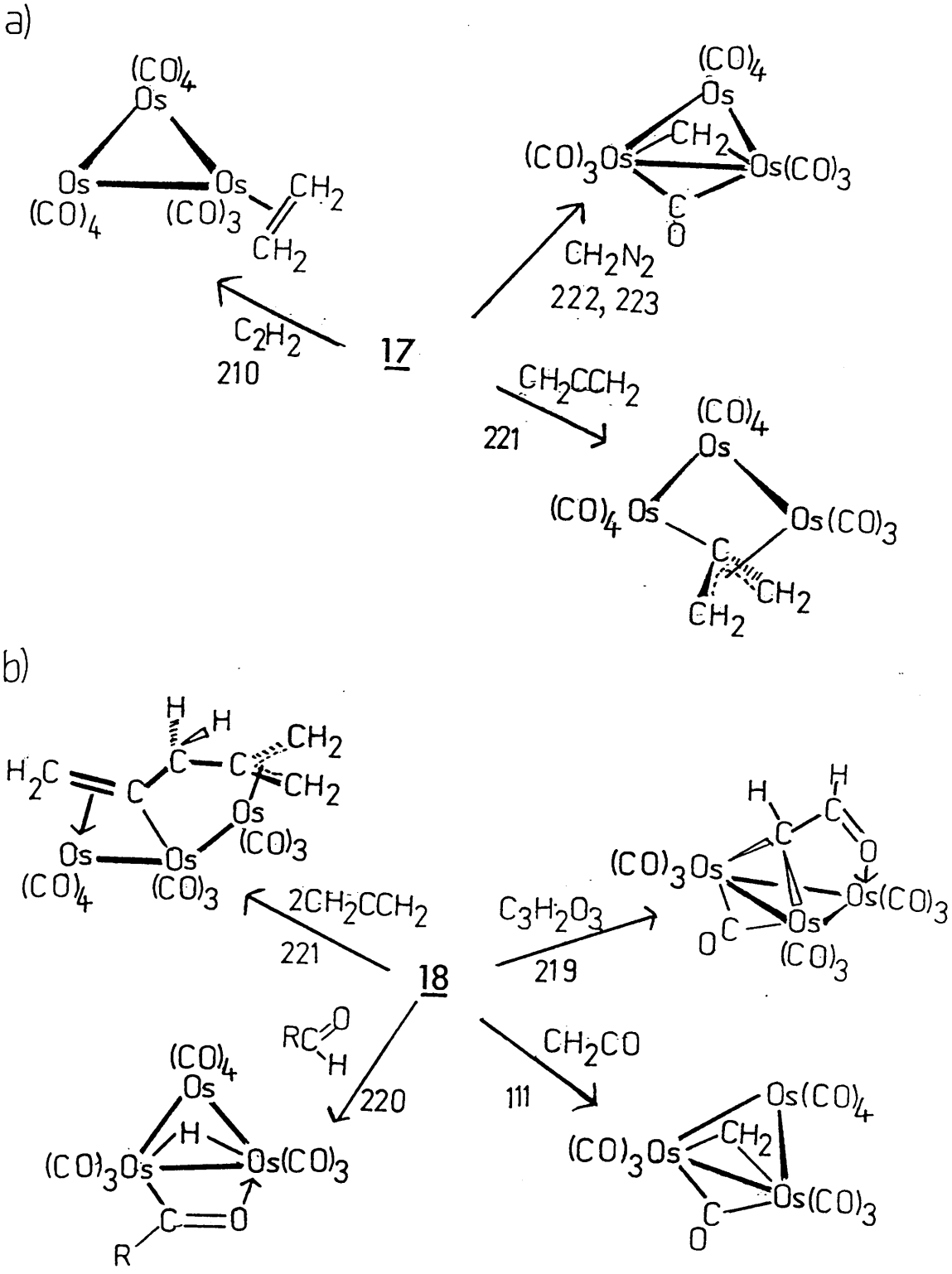

is unusually reactive under mild conditions as shown by Geoffrey and co-workers.[224-226]

The previously cited reviews by Deeming[94] and Burgess[33] should be referred to for a more thorough assessment of the roles of 17 and 18 as precursors in Os_3 organometallic chemistry.

Lightly stabilised clusters are of increasing importance in the development of designed syntheses in cluster chemistry. This is due to the ability of such clusters to direct reactivity to particular sites (i.e. those of the labile ligands) on the cluster framework. The ease with which many cluster systems form lightly stabilised derivatives by Me_3NO/MeCN treatment makes this an attractive method of cluster activation. An abbreviated list of other clusters containing the MeCN ligand, and some of their reactions, is presented in Table 16.

Table 16 : Examples of cluster systems with labile MeCN groups (and some of their reactions).

Lightly stabilised cluster system	Reacts with	ref
$Os_3(\mu\text{-}H)(\mu\text{-}OR)(CO)_9(MeCN)$, R=H,Me,Et,Ph	$P(OMe)_3$	227
$Os_3(\mu\text{-}H)(\mu\text{-}SR)(CO)_9(MeCN)$ R=Me,Et,Ph	$P(OMe)_3$	227
$Os_3[\mu_3\text{-}\eta^5\text{-}C(Me)C(Me)C(O)C(Me)C(Me)](CO)_8(MeCN)$	$P(OMe)_3$, RC CR'	228
$[NEt_4]^+$		
$[Re_3(\mu\text{-}H)_4(CO)_9(MeCN)]^-$	PPh_3, py	168
$Re_3(\mu\text{-}H)_3(CO)_{10}(MeCN)_2$	dppm,py	168
$Os_6(CO)_{16}(MeCN)_2$	$Pt(cod)_2$	229
	$OsH_2(CO)_4$	230

The major disadvantage of this technique is that it is not obvious which CO ligand(s) on a cluster will undergo replacement by MeCN, and it may be that the desired site of CO replacement is not affected by Me_3NO treatment. Nevertheless, lightly stabilised clusters are a widely used class of cluster synthon. It should be noted that treatment of clusters with Me_3NO in the presence of a nucleophile, L, often leads to direct CO substitution by L without the need of a lightly stabilised intermediate.[204,205,230,231]

1.5 Catalytically Activated Cluster Transformations.

It has recently been demonstrated that various cluster and cluster-ligand transformations can be catalytically promoted by electron transfer agents or anionic nucleophiles. The preparation of these catalytically "activated" clusters and their associated chemistry is considered in this section.

i) Electron Transfer Catalysed (E.T.C) Reactions.

Research in Bruce's laboratory has proven that, by catalytic generation of highly reactive anionic radical clusters, the lability of cluster bound ligands can be greatly increased.[232] This synthetic approach has made possible the high yield syntheses of substituted derivatives of several clusters under mild conditions.[232-234] The most frequently employed catalyst for such reactions is sodium diphenyl ketyl, which is readily prepared from sodium and benzophenone in dry THF.

By employing the E.T.C reaction, Bruce and co-workers have investigated the substituent chemistry of 2 in some depth. Syntheses of $Ru_3(CO)_{12-n}(L)_n$, (n = 1-4; L = PR_3, AsR_3) have been reported and structural analyses of the effects of systematically increasing the degree of ligand substitution on the Ru_3 framework have recently been presented.[235-238] For complexes with n = 1-3,[235-237] the structures are similar to that of

2; each substituent ligand is bound to a different metal centre occupying an equatorial position, and changes in Ru-Ru bond lengths are related to electronic and steric effects imposed by the substituent ligands. With n = 4,[238] and L = $PPh(OMe)_2$, the structure is similar to that of 3, with two bridging carbonyl moieties spanning one Ru-Ru vector as shown in Figure 26.

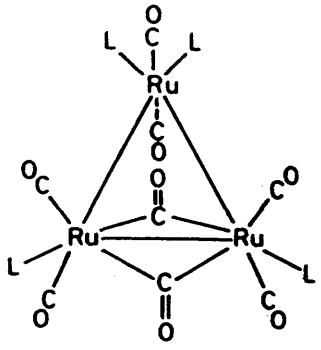

Figure 26 : The molecular structure of $Ru_3(\mu\text{-}CO)_2(CO)_6[PPh(OMe)_2]_4$.

This is the first example of such a structure in Ru_3 chemistry and its occurrence has been rationalised in terms of ligand polyhedra packing arguments.[236]

The mechanism of electron transfer to 2 and the subsequent substitution reaction of the cluster radical is believed to proceed as follows:-[232]

1. $Ru_3(CO)_{12} + [Ph_2CO]^{\cdot-} \rightleftharpoons [Ru_3(CO)_{12}]^{\cdot-} + Ph_2CO$

2. $[Ru_3(CO)_{12}]^{\cdot-} + L \longrightarrow [Ru_3(CO)_{11}L]^{\cdot-} + CO$

3. $[Ru_3(CO)_{11}L]^{\cdot-} + Ru_3(CO)_{12} \longrightarrow Ru_3(CO)_{11}L + [Ru_3(CO)_{12}]^{\cdot-}$

Formation of $[Ru_3(CO)_{12}]^{\cdot-}$ is thought to involve cleavage of a Ru-Ru bond, generating a highly reactive 17-electron Ru centre at which substitution occurs.[232] If $[Ru_3(CO)_{11}L]^{\cdot-}$ is less stable than the parent binary carbonyl, an electron transfer to $Ru_3(CO)_{12}$ takes place. This cycle is terminated when either the cluster or the ligand is entirely consumed.

The chemistry of clusters involving electron transfer catalysis is dominated, at present, by ligand substitution. The mild conditions required for these reactions have enabled the isolation of products that are unobserved in thermally promoted reactions, e.g. $Ru_3(CO)_{12-n}(L)_n$, n = 1,2,4. However, limitations in the applicability of E.T.C reactions to cluster chemistry are already evident. For example, in the electron transfer catalysed substitution of CO by PPh_3 in 1, poor selectivity is observed with the formation of mono, di and trisubstituted derivatives in approximately equal amounts, and, therefore, the E.T.C reaction offers no advantage over simple thermolysis of 1 with PPh_3.[239]

ii) Catalytic Cluster Activation by Anions.

In 1984, Kaesz and Lavigne reported that various [PPN]X ($X = CN^-$, $CH_3CO_2^-$, F^-, Cl^-, I^-, and NO_2^-) salts are active catalysts for the substitution of carbonyl functions in 2 by a range of phosphines.[240]

A mechanistic explanation of this catalytic activation has been advanced by Kaesz and Lavigne,[241] and is presented in Scheme 10.

Scheme 10 : Proposed Mechanism for Anionic Activation of $Ru_3(CO)_{12}$ towards Ligand Substitution.

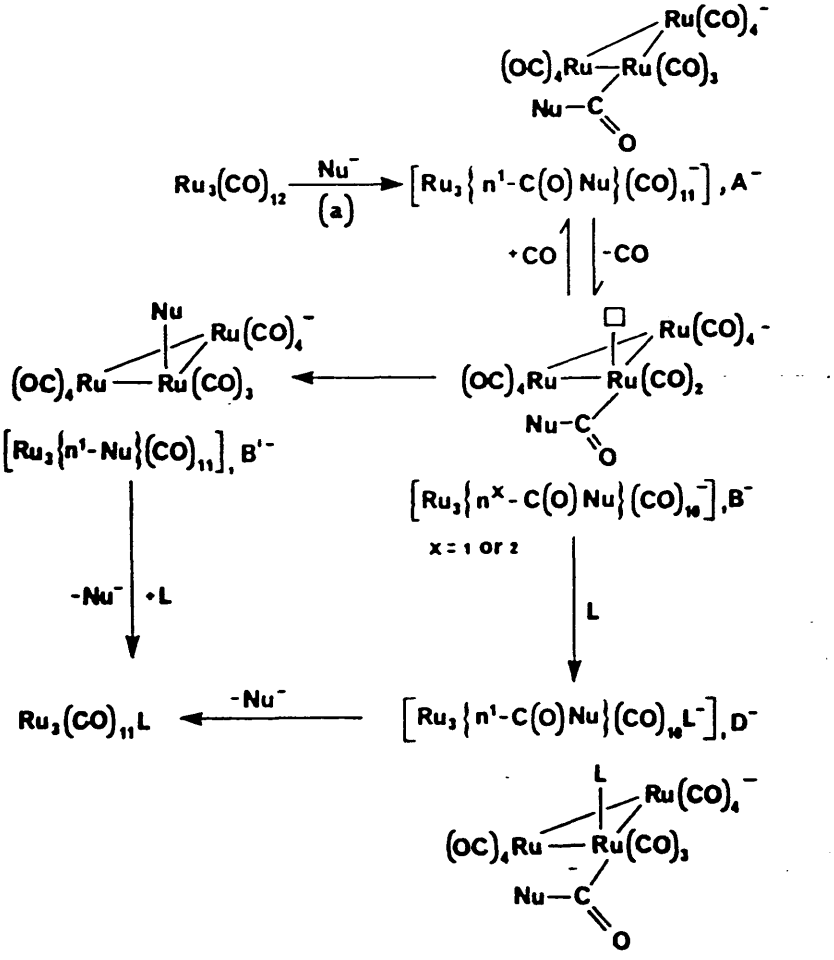

It is proposed that cluster activation occurs through an initial attack of the anionic nucleophile Nu^- at a C site on a CO function, yielding a cluster bound acyl derivative, A^-. Loss of CO from A^-, to give B^-, creates a vacant coordination site at which an incoming ligand, L, can bind, to form D^-. Loss of Nu^- from D^- yields the substituted $Ru_3(CO)_{11}L$. Alternatively, if the Nu-C bond in B^- cleaves, Nu^- may migrate to occupy the vacant coordination site, as in B'^-, and subsequent ligand substitution of Nu^- gives $Ru_3(CO)_{11}L$. Thus, through the formation of an acyl-type intermediate, A^-, labilisation of CO is effected and the cluster is activated towards ligand substitution.

Both the E.T.C reactions and anionic catalytic activation of clusters are relatively recent developments in synthetic cluster chemistry. These approaches have proved successful in expanding the derivative chemistry of saturated clusters, e.g. 2. Nevertheless, further research into reactions involving these methods of cluster activation is required to enable a more thorough evaluation of their synthetic scope.

1.6 Concluding Remarks.

The development of rational synthetic approaches in cluster chemistry has been aided by the use of unsaturated, lightly stabilised and catalytically activated clusters. However, as this introduction has striven to demonstrate, the reactivities of systems within these categories can vary greatly from complex to complex.

Although trends of chemical behaviour are evident in certain well studied systems, there remains, in general, a paucity of experimental data on which to base a systematic analysis of cluster reactivity. There is an obvious need, therefore, to develop the chemistry of individual systems, and add to the increasing body of knowledge of cluster reactivity.

The remainder of this Thesis describes the chemistry associated with M_3Pt (M = Os, Ru) systems.

CHAPTER TWO.

CHAPTER 2.

Reactivity of $Os_3Pt(\mu\text{-}H)_2(CO)_{10}(PCy_3)$

2.1 Prologue.

2.1.1 Mixed Metal Os-Pt Systems.

As outlined previously, the factors influencing the reactivity of homometallic clusters are complex, even for conceptually simple transformations such as ligand substitution. The situation is more complicated for heterometallic systems. Nevertheless, such clusters are of particular interest for several reasons:-

i) mixed metal $M_xM'_y$ cluster systems can be used as precursors to heterogeneous catalysts of a specific $M_xM'_y$ stoichiometry.

ii) heterometallic clusters may offer increased selectivity over homometallic complexes as homogeneous catalysts.

iii) the reactivities of hetero- and homometallic clusters are expected to differ due to changes in size, reactivity and bonding capability of the component metal centres in MM' systems.

As a result of their catalytic potential, heterometallic clusters have received much attention in recent years[24,25]. The extensive chemistry associated with homometallic osmium clusters suggests that heterometallic Os-containing systems may also display interesting reactivities.

In this section, the syntheses and reactivity of mixed-metal Os-Pt systems will be briefly considered.

Table 17 summarises the syntheses of the known Os-Pt clusters. The most widely used Pt reagents are the lightly stabilised, zero valent $Pt(C_2H_4)_n(PR_3)_{3-n}$ (n = 1,2) and $Pt(cod)_2$ complexes which act as sources of "$Pt(PR_3)_n$" (n = 1,2) and "Pt(cod)" respectively. Successful early syntheses of Os-Pt clusters involved reactions of the mononuclear

osmium complex $OsH_2(CO)_4$ with various Pt complexes.[243,244] Recently however, Os clusters have been favoured as Os precursors, allowing the preparation of a number of Os_mPt_n systems that are Os rich, i.e. m>n. The osmium clusters used include electronically unsaturated systems,[147,148,255,256] lightly stabilised complexes,[229,247,248] and sulphido-containing clusters,[245,249,252,253] (where "ligand assisted" bonding at the sulphido site is believed to be important in the initial anchoring of Pt to the cluster).

With the exception of the unsaturated cluster $Os_3Pt(\mu\text{-}H)_2(CO)_{10}(PR_3)$, 19, (R = Cy, 19a ; R = Ph, 19b), the reactivities of these systems have not been investigated in detail.

2.1.2 The Structure and Chemistry of $Os_3Pt(\mu\text{-}H)_2(CO)_{10}(PR_3)$, 19.

The heterometallic triosmium platinum cluster 19 contains a *closo*-tetrahedral metal framework,[147] as shown for 19a in Figure 27. As previously discussed, Pt containing clusters are often formally electron deficient. However, if the hydride bridged Pt-Os bond is ignored, the coordination geometry about Pt in 19a approximates to trigonal bipyramidal, and the Pt atom may be considered as contributing all ten of its valence electrons. Application of various electron counting schemes[54,55,57,75] leads to the conclusion that 19 contains 58 valence electrons and is, therefore, unsaturated.

The Os-Os bond lengths observed in 19a are all shorter than those in the saturated $Os_3(CO)_{12}$,(1), where the average Os-Os distance is 2.877(3) Å.[87] In particular, the hydride bridged Os(2)-Os(3) separation of 2.789(1) Å is significantly shorter than expected. Typical Os(μ-H)Os metal-metal separations in MOs_3 systems,

Table 17 : Syntheses of Osmium - Platinum Clusters.

Cluster	Preparation	Ref
$OsPt_2(CO)_5(PPh_3)_3$	$OsH_2(CO)_4+Pt(C_2H_4)(PPh_3)_2$	243
$Os_2Pt(CO)_7(PMePh_2)_3$	$OsH_2(CO)_4+Pt(PMePh_2)_4$	243
$Os_2Pt_2(\mu\text{-}H)_2(CO)_8(PPh_3)_2$	i) $OsH_2(CO)_4+Pt(C_2H_4)(PPh_3)_2$	243
	ii) $OsH_2(CO)_4+Pt(C_2H_4)_2(PPh_3)$	244
$Os_3Pt(\mu\text{-}H)_2(CO)_{10}(PR_3)$	$\underline{4}+Pt(C_2H_4)_2(PR_3)$	147
$Os_3Pt(\mu\text{-}H)_2(CO)_{10}(PR_3)_2$	$\underline{4}+Pt(C_2H_4)(PR_3)_2$	148
$Os_3Pt(\mu\text{-}H)_2(\mu_4\text{-}C)(CO)_{10}(PCy_3)$	$Os_3(\mu\text{-}H)(\mu_3\text{-}CH)(CO)_{10}+Pt(C_2H_4)_2(PCy_3)$	250
$Os_3Pt(\mu\text{-}H)_2(\mu\text{-}CH_2)(cod)(CO)_9$	$\underline{4}+Pt(cod)(CH_3)_2$	255
$Os_3Pt(\mu\text{-}CH_2)(CO)_{11}(PPh_3)_2$	$Os_3(\mu\text{-}CH_2)(\mu\text{-}CO)(CO)_{10}+Pt(C_2H_4)(PPh_3)_2$	254
$Os_3Pt(\mu_3\text{-}S)(CO)_{10}(PMe_2Ph)_2$	$Os_3(\mu_3\text{-}S)(CO)_{10}+Pt(PMe_2Ph)_4$	245
$Os_3Pt(\mu_3\text{-}S)(CO)_9(PMe_2Ph)_3$	" " " "	245
$Os_3Pt(\mu_3\text{-}S)(CO)_9(PMe_2Ph)_2$	" " " "	245
$Os_3Pt(\mu_3\text{-}S)(CO)_8(PMe_2Ph)_3$	" " " "	245
$Os_3Pt(\mu_3\text{-}S)_2(CO)_{10}(PPh_3)$	$Os_3(\mu_3\text{-}S)_2(CO)_9+Pt(C_2H_4)(PPh_3)_2$	249
$Os_3Pt(\mu_3\text{-}S)_2(CO)_9(PPh_3)_2$	" " "	249
$Os_3Pt(\mu_3\text{-}S)_2(CO)_9(PMe_2Ph)_2$	$Os_4(\mu_3\text{-}S)_2(CO)_{12}+Pt(PMe_2Ph)_4$	253
$Os_3Pt_2(\mu\text{-}H)_2(\mu\text{-}CO)(\mu_5\text{-}C)(CO)_9(PCy_3)_2$	$Os_3(\mu\text{-}H)(\mu_3\text{-}CH)(CO)_{10}+Pt(C_2H_4)_2(PCy_3)$	250
$Os_3Pt_2(\mu\text{-}H)(\mu\text{-}CO)(\mu\text{-}COMe)(\mu_5\text{-}C)(CO)_9(PCy_3)_2$	: $Os_3(\mu\text{-}H)(\mu\text{-}COMe)(CO)_{10}+Pt\text{-}(C_2H_4)_2(PCy_3)$	250
$Os_4Pt(\mu\text{-}H)_2(CO)_{12}(dppe)$	$Os_4(\mu\text{-}H)_4(CO)_{12}+PtR_2(dppe)$ R = Me, Ph	251
$Os_4Pt(\mu_4\text{-}S)(CO)_{13}(PPh_3)$	$Os_5(\mu_4\text{-}S)(CO)_{15}+Pt(C_2H_4)(PPh_3)_2$	252
$Os_4Pt(\mu_3\text{-}S)_2(CO)_{11}(PMe_2Ph)_2$	$Os_4(\mu_3\text{-}S)_2(CO)_{12}+Pt(PMe_2Ph)_4$	253
$Os_4Pt_2(CO)_{18}$	$\underline{4}+Pt(CO)_2(Me)_2$	256
$Os_5Pt(\mu_4\text{-}S)(CO)_{15}(PPh_3)$	$Os_5(\mu_4\text{-}S)(CO)_{15}+Pt(C_2H_4)(PPh_3)_2$	252
$Os_5Pt(\mu_4\text{-}S)(CO)_{15}(PPh_3)_2$	" " "	252
$Os_6Pt(\mu_3\text{-}NCMe)(cod)(CO)_{17}$	$Os_6(CO)_{17}(MeCN)+Pt(cod)_2$	247
$Os_6Pt_2(cod)_2(CO)_{16}$	$Os_6(CO)_{16}(MeCN)_2+Pt(cod)_2$	229
$Os_6Pt_2(cod)_2(CO)_{17}$	i) $Os_6(CO)_{20}+Pt(cod)_2$	246
	ii) $Os_6(CO)_{17}(MeCN)+Pt(cod)_2$	229
$Os_6Pt_2(\mu\text{-}C_8H_{10})(cod)H_2(CO)_{16}$	$Os_6(CO)_{16}(MeCN)_2+Pt(cod)_2$	248

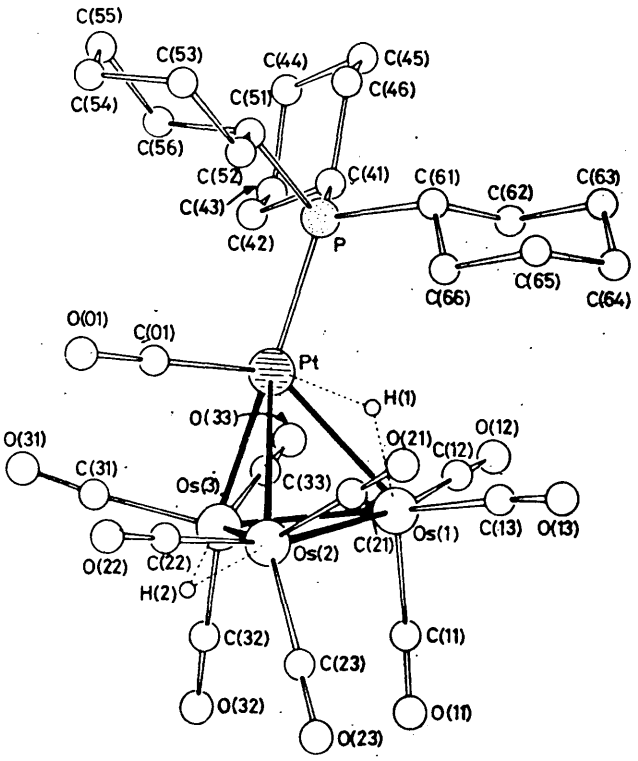

M-M bond length	(Å)
Os(1)-Os(2)	2.777(1)
Os(1)-Os(3)	2.741(1)
Os(2)-Os(3)	2.789(1)
Pt-Os(1)	2.863(1)
Pt-Os(2)	2.791(1)
Pt-Os(3)	2.832(1)

Figure 27 : Molecular structure and inter-metal bond lengths of $Os_3Pt(\mu\text{-}H)_2(CO)_{10}(PCy_3)$.

listed in Table 18, lie in the range 2.870(1)-2.940 Å. This suggests that unsaturation in 19 may be localised at the Os(μ-H)Os unit.[147]

Table 18. Hydride bridged Os-Os distances in MOs_3 clusters.

Cluster.	Bond length (Å)	Ref.
$Os_3Pt(\mu\text{-}H)_2(CO)_{10}(PCy_3)$	2.789(1)	147
$Os_3W(\mu\text{-}H)(Cp)(CO)_{12}$	2.932(2)	257
$FeOs_3(\mu\text{-}H)_2(CO)_{13}$	2.934(1), 2.937(1)	136
$CoOs_3(\mu\text{-}H)_3(CO)_{12}$	2.893(1)-2.909(1)	139
$CoOs_3(\mu\text{-}H)_2(\mu\text{-}CO)(Cp)(CO)_9$	2.870(1), 2.940(1)	140

In keeping with the proposed unsaturation of 19, an EHMO investigation by Hoffmann and Schilling,[175] using the $[Fe_3Pt(CO)_{10}(PH_3)]^{2-}$ dianion as a model for 19, indicated that the complex has a low lying LUMO. A more detailed MO description of 19 will be presented in Section 2.2.(i).

The chemistry of unsaturated clusters, described in Chapter 1, is typified by reactions that relieve their unsaturation, e.g. electrochemical reduction and nucleophilic addition. The reactivity of 19, is, likewise, expected to be dominated by reactions yielding saturated cluster products.

Electrochemical studies reveal that 19a undergoes a chemically reversible two electron reduction.[148] However, the attempted reduction of 19a by sodium amalgum failed to yield the expected saturated dianion $[Os_3Pt(\mu\text{-}H)_2(CO)_{10}(PCy_3)]^{2-}$ as an isolable product.[148] However 19a reacts readily with two electron donors, L, to form the 60 electron adducts $Os_3Pt(\mu\text{-}H)_2(CO)_{10}(PCy_3)(L)$, as depicted in Scheme 11.

19a rapidly adds CO to yield $Os_3Pt(\mu\text{-}H)_2(CO)_{11}(PCy_3)$, 20.[148] In the absence of a CO atmosphere this adduct is unstable in solution and readily undergoes decarbonylation to regenerate 19a. The cluster has a butterfly core geometry shown in Figure 28(i), with wing tip $Pt(PCy_3)(CO)$ and $Os(CO)_4$ groups. The hydride ligands span the hinge Os-Os bond and the Os-Pt vector cis to the PCy_3 function.

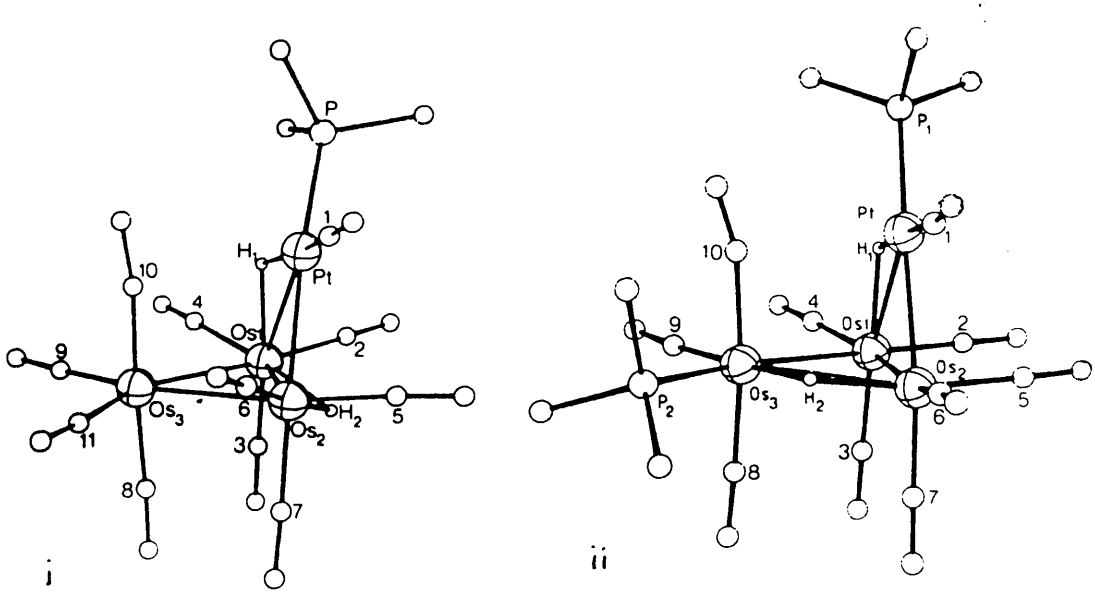

Figure 28. The solid state structures of (i)$Os_3Pt(\mu\text{-}H)_2(CO)_{11}(PCy_3)$ * and (ii)$Os_3Pt(\mu\text{-}H)_2(CO)_{10}(PPh_3)_2$ *

*Only the contact carbon atoms of (i)PCy_3 and (ii)PPh_3 functions are included for clarity.

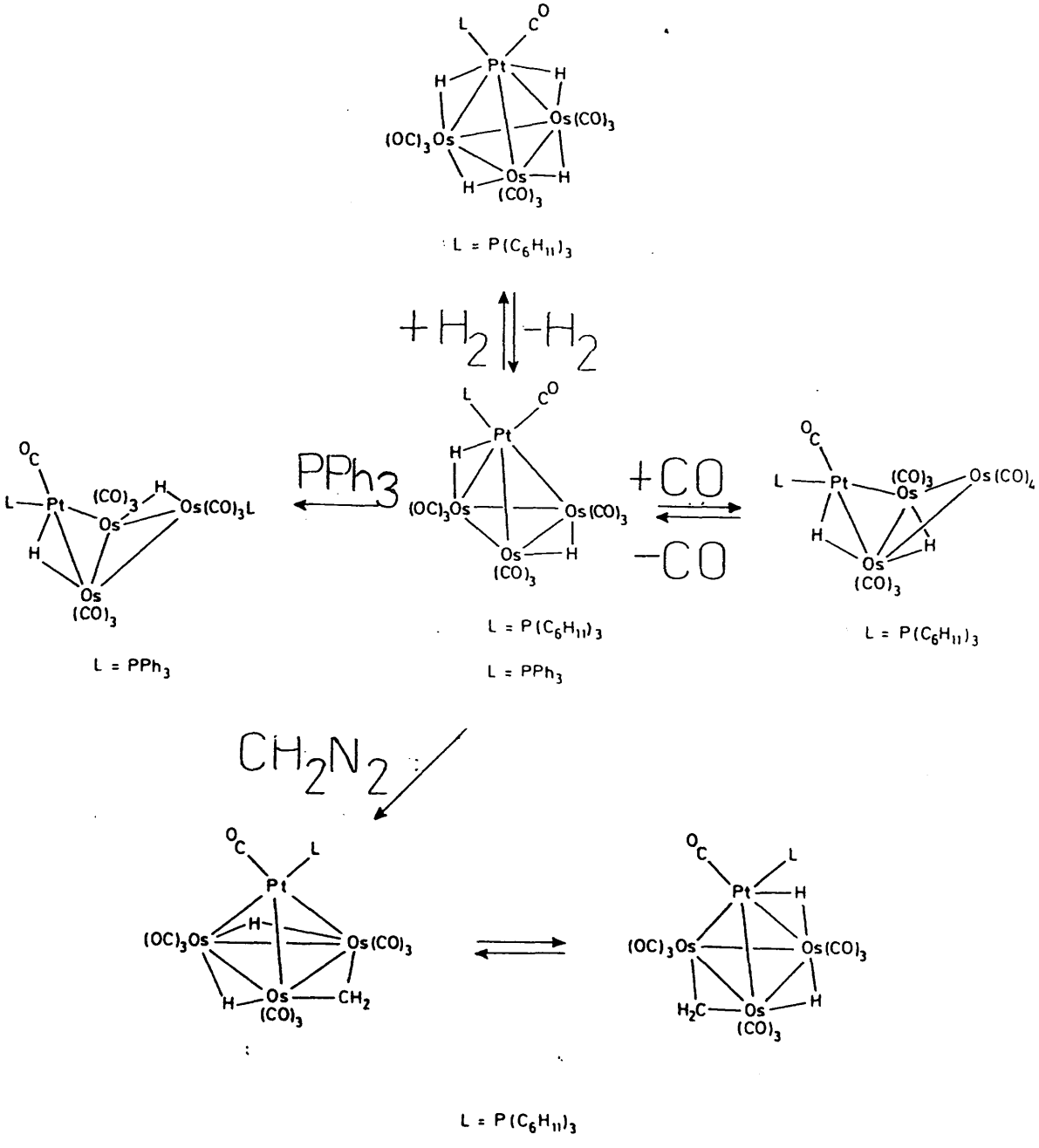

Scheme 11 : The reactions of $Os_3Pt(\mu\text{-}H)_2(CO)_{10}(PR_3)$, 19, with two electron donor ligands.

Treatment of $Os_3Pt(\mu\text{-}H)_2(CO)_{10}(PPh_3)$, 19b, with PPh_3 yields $Os_3Pt(\mu\text{-}H)_2(CO)_{10}(PPh_3)_2$,[148] 21, depicted in Figure 28(ii) which has a similar structure to that of 20. The incoming PPh_3 function ligates at an equatorial position on the wing tip Os atom. The hydride ligands in 21 occupy the Os-Os and Os-Pt edges cis to the two phosphine groups.

Both 20 and 21 are 60 electron butterfly species. Electron counting rules[54,55,57,75] predict a 62 electron count for this framework geometry. One might expect, therefore, that, like the parent 19, 20 and 21 are also unsaturated. However the M-M bond lengths, listed in Table 19, are in accord with those observed in saturated species and these complexes are unreactive to further ligand addition.[148]

Table 19 : Comparison of M-M bond distances in 20 and 21.

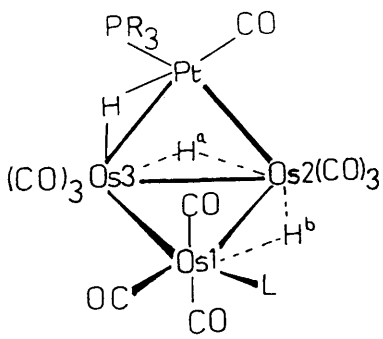

a) L=CO R=Cy; b) L=PPh_3 R=Ph

20	Bond length(Å)	21	Bond length(Å)
Os(1)-Os(2)	2.877(1)	Os(1)-Os(2)	3.043(1)
Os(1)-Os(3)	2.882(1)	Os(1)-Os(3)	2.914(1)
Os(2)-Os(3)	2.869(1)	Os(2)-Os(3)	2.773(1)
Pt-Os(2)	2.729(1)	Pt-Os(2)	2.717(1)
Pt-Os(3)	2.914(1)	Pt-Os(3)	2.848(1)
Pt---Os(1)	3.775(1)	Pt---Os(1)	3.530(1)
L = CO, R = Cy		L = PPh_3, R = Ph	

The anomalous electron count can be attributed to the presence of Pt in the core. Disregarding the hydride bridged Pt-Os vector, the coordination about Pt is pseudo-square planar and therefore the Pt atom can be considered to donate only 8 electrons to the valence electron count as opposed to the 10 it contributes to 19. This accounts for the apparent formal electron deficiency of 20 and 21.

Under H_2 pressure 19a reacts reversibly with dihydrogen to yield $Os_3Pt(\mu\text{-}H)_4(CO)_{10}(PCy_3)$, 22.[258] The crystal structure of 22,[258] shown in Figure 29, reveals that the metal core retains the *closo*-tetrahedral geometry of 19. Furthermore, two Os-Os and two Os-Pt edges are spanned by bridging hydride ligands. 22 is a 60 electron tetrahedral cluster, in keeping with electron counting rules, prediction,[54,55,54,75] and the core M-M separations, listed in Table 20, reveal no unusually short M-M vectors.

Table 20 : M-M distances in 22,23 and 24.

Cluster	Length of M-M separation (Å)				
	Os-Os	Os(μ-H)Os	Os-Pt	Os(μ-H)Pt	Os(μ-CH_2)Os
22[a]	2.866	2.987	2.716	2.971	-
23	-	2.947	2.730(1) 2.820[b]	-	2.826(1)
24[c]	2.808	2.974	2.777 2.853[b]	2.867	2.865

a) Bond distances averaged over all bonds in molecule and over 2 independent molecules.

b) Mean of Os-Pt vectors sharing $PtOs_2$ face with CH_2

c) Bond lengths averaged over 2 independent molecules.

Treatment of 19a with diazomethane yields $Os_3Pt(\mu\text{-}H)_2(\mu\text{-}CH_2)(CO)_{10}(PCy_3)$ as a mixture of two isomeric products.[258] ^1H n.m.r spectroscopy indicates that the initially formed C_s isomer, 23, has both hydrides spanning Os-Os edges, whereas in the latter C_1 isomer, 24,

the hydrides bridge one Pt-Os and one Os-Os vector. The solid state structures of both 23 and 24 are presented in Figure 29.

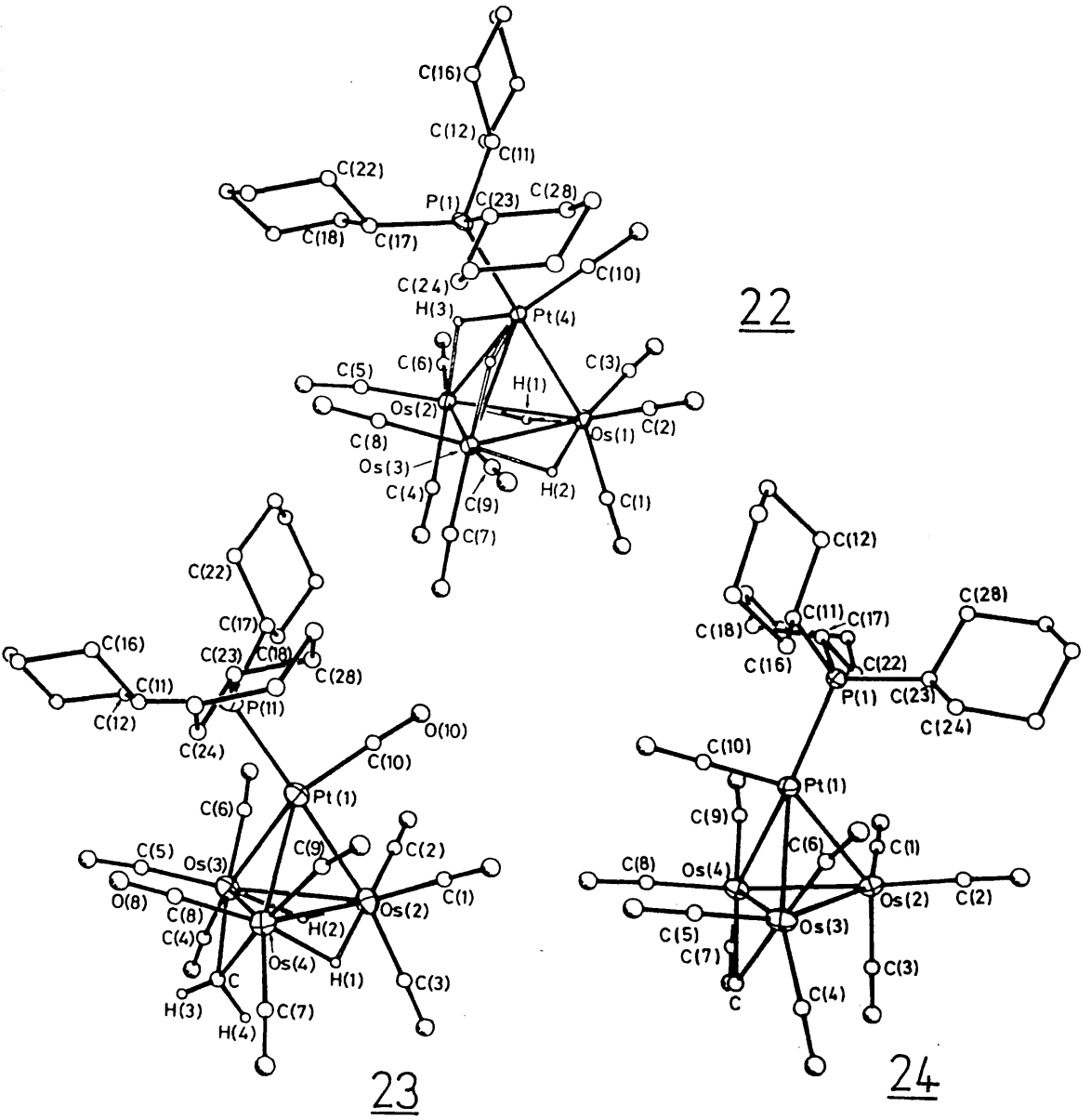

Figure 29 : The molecular structures of 22, 23 and 24.

The metal framework geometry of 23 and 24 is *closo*-tetrahedral, and in both isomers the methylene function bridges an Os-Os edge in the expected[105] μ_2-coordination mode. The metal-metal separations for the 60 electron species 23 and 24 are listed in Table 20 and are in accord with the electronic saturation of these complexes. An interesting structural difference between 23 and 24 is that in 23 the $Pt(CO)(PCy_3)$ moiety is disposed above the Os_3 triangle such that

the phosphine ligand lies cisoid to the methylene function, whereas in 24 it is transoid to the CH_2 group.

Unlike $Os_3(\mu\text{-}H)_2(CO)_{10}$, $Os_3Pt(\mu\text{-}H)_2(CO)_{10}(PR_3)$ does not react with ethylene at ambient temperatures,[148] however extensive thermolytic treatment of 19b with excess but-2-yne[148] results in the formation of several products, shown in Figure 30, none of which retain the Os_3Pt core of 19b.

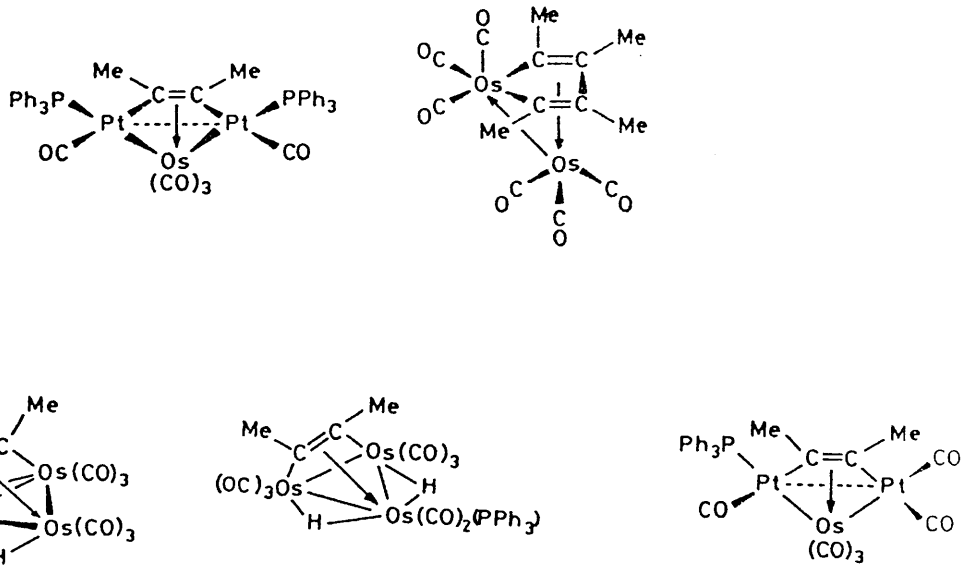

Figure 30 : Products of thermolysis of 19b with MeC≡CMe.

The reactivity of unsaturated clusters and heterometallic complexes are of current interest in cluster chemistry, for reasons outlined previously. Pertinently, 19 provides an example of a heterometallic unsaturated cluster. The chemical behaviour of 19 reveals some intriguing facets of cluster reactivity. 19 can bind H_2 [258] and CO [148] reversibly, which makes it an interesting model for

Fischer-Tropsch catalysis. Furthermore, the 60-electron adducts of 19 display both *closo*-tetrahedral and butterfly geometries, the latter resulting from facile Pt-Os bond cleavage. The reaction of 19b with $CH_3C{\equiv}CCH_3$ [148] shows that, with ligands capable of donating more than two electrons, 19 can undergo degradation producing novel Os-Pt clusters. In view of these interesting features, further studies on the chemistry of 19 were deemed desirable in particular to elucidate the factors influencing the contrasting skeletal geometries adopted by the adducts of $Os_3Pt(\mu\text{-}H)_2(CO)_{10}(PR_3)$.

2.2 Reactivity of $Os_3Pt(\mu\text{-}H)_2(CO)_{10}(PCy_3)$ towards CO and CH_2 analogues.

2.2.1 Extended Hückel Calculations on the Model Complex $[Ru_3Pt(CO)_{10}(PH_3)]^{2-}$ and the corresponding *closo* tetrahedral CO and CH_2 adducts.

Hoffmann and co-workers have developed a conceptually simple, qualitative approach to the complex problem of understanding the electronic structure of cluster complexes.[108] This involves the build up of the cluster framework from discrete ML_n fragments of known orbital constitution, the so called fragment formalism. The semi-empirical Extended Hückel[259] method allows rapid calculation of the eigenvalues and eigenvectors arising from orbital interactions of these component ML_n fragments. This technique has enabled molecular orbital analyses of many cluster systems (see for example, ref. 108 and references therein).

Before embarking on a description of the new Os_3Pt chemistry developed in the course of this work, it is informative to examine the bonding in 19 and related systems using the EHMO approach.

Schilling and Hoffmann[175] have presented an EHMO analysis of 19 using the model dianion $[Fe_3Pt(CO)_{10}(PH_3)]^{2-}$ which indicated that the complex has a low lying LUMO, in keeping with the unsaturation of 19.

However this work did not describe the symmetry or localisation of the cluster frontier orbitals, which are important in defining its reactivity towards uncharged nucleophiles. Therefore, a re-examination of the bonding in 19 was undertaken. In addition, cluster orbital interactions with CH_2 and CO were studied to establish whether the framework geometry differences between these adducts of 19 could be rationalised by molecular orbital considerations.

In the present analysis, the unsaturated cluster 19 is modelled by the hypothetical dianion $[Ru_3Pt(CO)_{10}(PH_3)]^{2-}$, Z, shown in Figure 31. Ru is used to model Os since satisfactory orbital exponents and H_{ii} terms for Os were not available. Furthermore, the $Ru_3(CO)_9$ framework has idealised C_s symmetry, modelling the approximate mirror symmetry observed for 19.[147] The $Fe_3(CO)_9$ framework in the Hoffmann and Schilling study had C_{3v} symmetry. The hydrides in 19 are modelled by negative charges and the PR_3, (R = Ph, Cy) function is replaced by PH_3 to simplify the calculations.

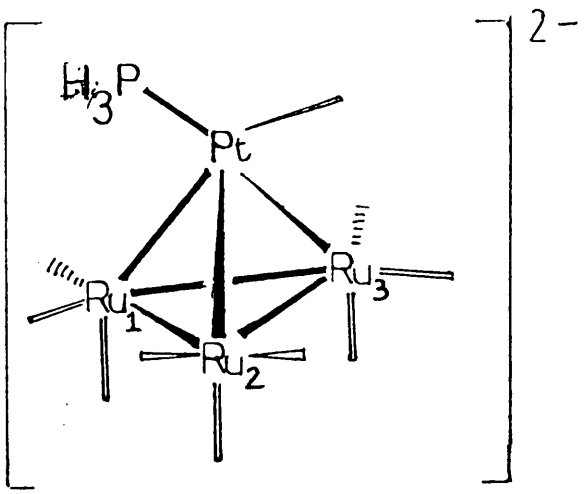

Figure 31 : The Hypothetical Dianion $[Ru_3Pt(CO)_{10}(PH_3)]^{2-}$

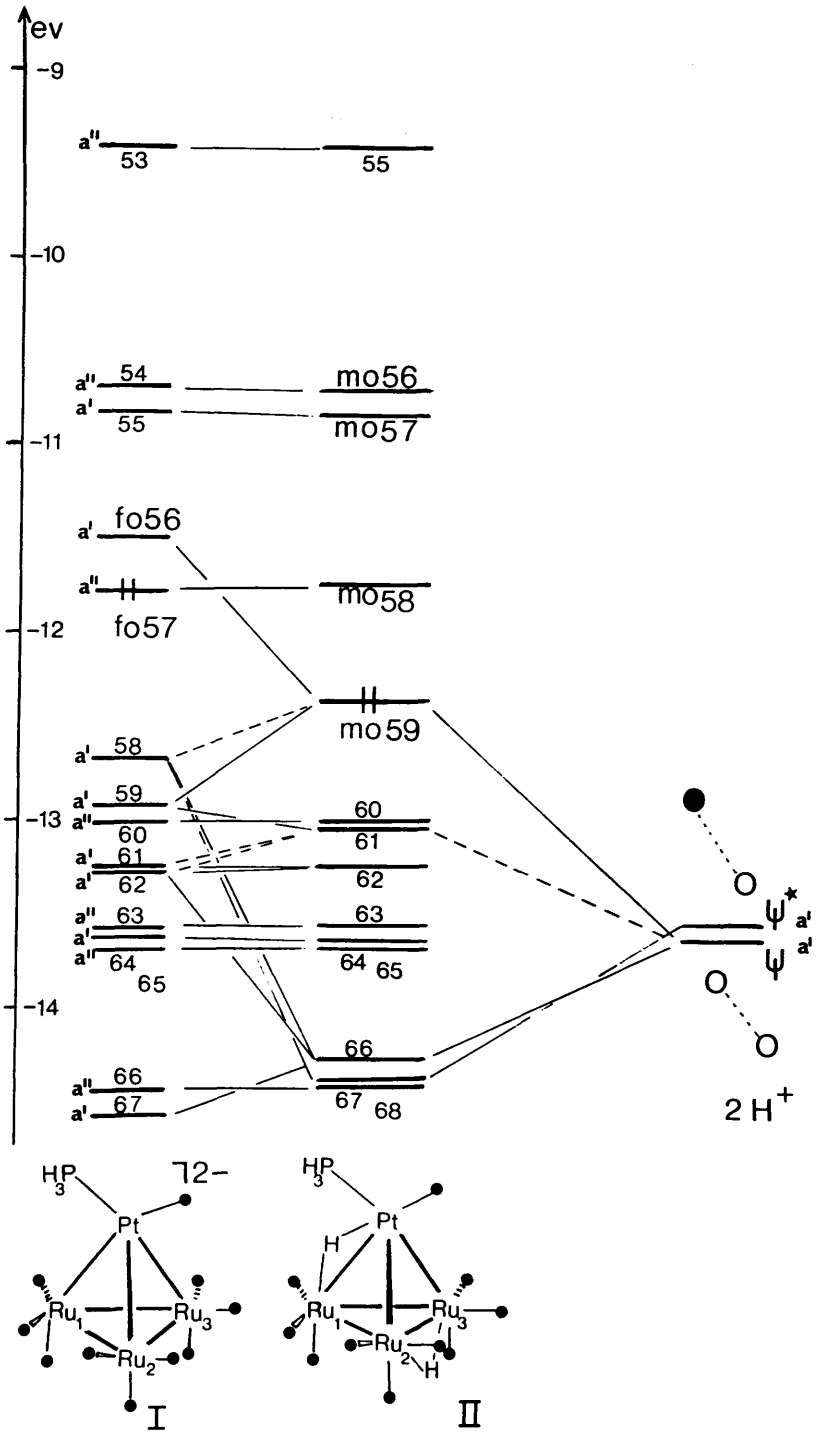

Figure 32 : MO energy level diagram for Z, and the interaction of Z with two protons yielding Y.

(a) MO analysis of $[Ru_3Pt(CO)_{10}(PH_3)]^{2-}$, Z.

The molecular orbitals of Z can be generated by considering the interactions between the $M_3(CO)_9^{2-}$ and PtL_2 fragments. These interactions have been previously reported by Hoffmann and Schilling for M = Fe.[175] The MO energy level diagram derived for Z is shown in Figure 32. The HOMO-LUMO gap is small (0.28eV), consistent with the unsaturation of this species.

Contour plots of the HOMO and LUMO in the $PtRu_{2,3}$ and $Ru_{1,2,3}$ planes are presented in Figure 33. The LUMO (a') is symmetric with respect to the molecular mirror plane, and is delocalised over the four metal centres. It is σ-bonding between $Pt/Ru_{2,3}$ and along the $Ru_{2,3}$ edge, but antibonding between the $Ru_1/Ru_{2,3}$ centres. The HOMO (a'') is localised on $Ru_{2,3}$, is strongly antibonding between these metal centres, and is antisymmetric with respect to the molecular mirror plane.

The interaction of this model dianion with two protons, yielding $Ru_3Pt(\mu\text{-}H)_2(CO)_{10}(PH_3)$, Y, has been investigated[260] and the corresponding orbital interaction diagram is presented in Figure 32. Since the two H atoms lie on the molecular mirror plane, the symmetry designation of both the in-phase and out-of-phase H 1s combinations is a'. Hence, all orbitals of Z of a'' designation are unaffected by protonation. The principal effect of protonation is the reversal of the relative stabilities of the HOMO and LUMO in Z, though some lower lying orbitals are also stabilised. Thus the LUMO in Y (i.e. the HOMO in Z) is heavily localised along the $Ru_{2,3}$ vector, supporting the proposal that unsaturation is localised at the corresponding $Os(\mu\text{-}H)Os$ unit in $Os_3Pt(\mu\text{-}H)_2(CO)_{10}(PR_3)$.[147]

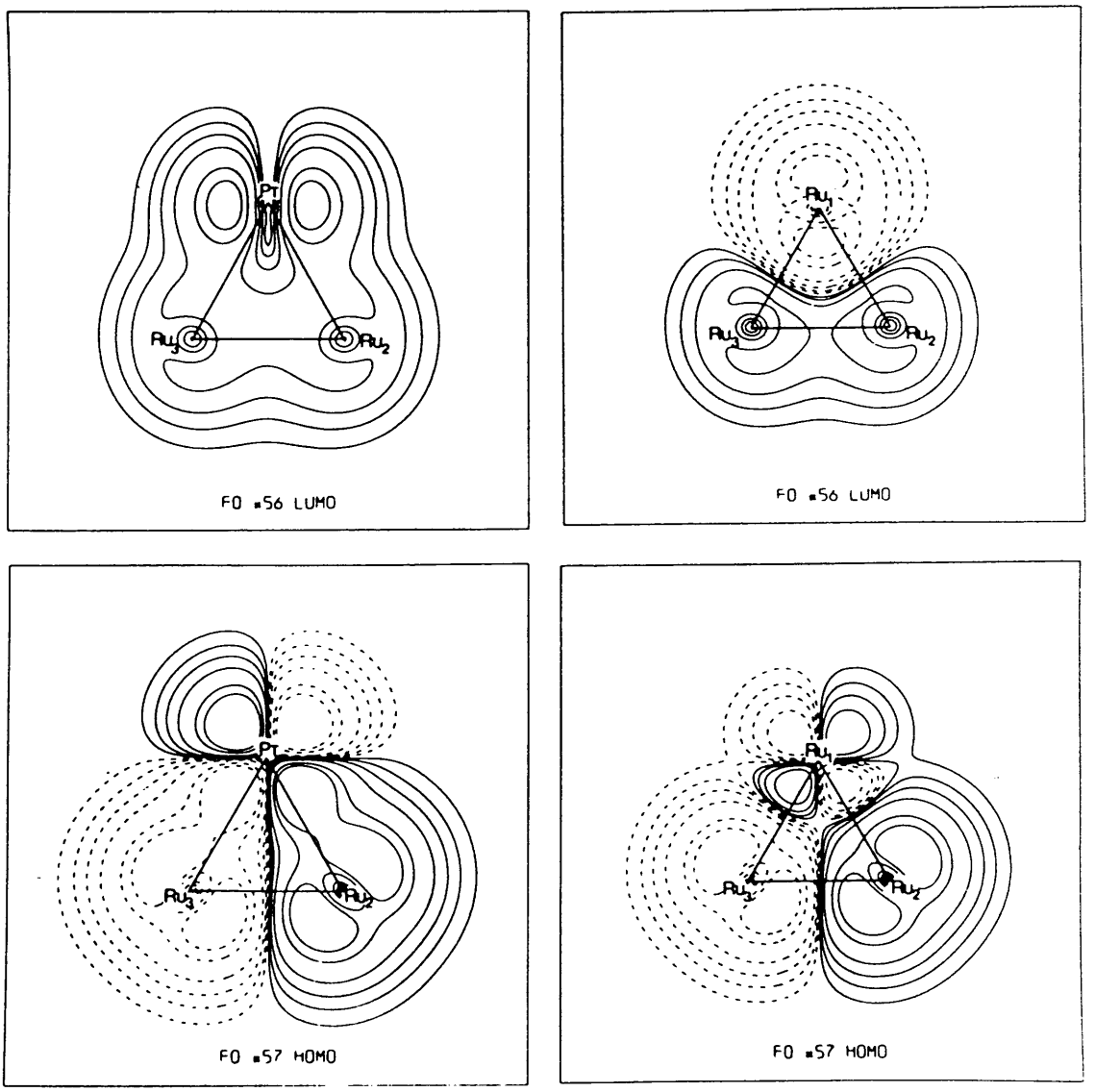

Figure 33 : Contour plots of the HOMO and LUMO of $[Ru_3Pt(CO)_{10}(PH_3)]^{2-}$ in the $PtRu_{2,3}$ and $Ru_{1,2,3}$ planes.

(b) MO Analysis of Nucleophilic Addition to $[Ru_3Pt(CO)_{10}(PH_3)]^{2-}$, Z

Nucleophilic attack at an electron deficient cluster occurs, in general, at the site of localised unsaturation.[85-91,156-165] Therefore it seems reasonable to presume that the best model for nucleophilic addition at Z will involve interaction of the nucleophile with the cluster at the $Ru_{2,3}$ site. If Y is used as the cluster prototype the hydride spanning the $Ru_{2,3}$ vector must migrate to make way for the incoming ligand. In order to remove this complication, Z was chosen as the model cluster for the present study. This is not too unrealistic since the high mobility of the hydride ligands in these systems has been established[147,265] As Z and Y have the same number of valence electrons, and their frontier orbitals are very similar, the analysis will not depend critically on the relative stabilities of the HOMO and LUMO.

The nucleophiles considered were CH_2 and CO, being representative of two electron donors yielding *closo*-tetrahedral and butterfly adducts with 19 respectively.[258]

The least sterically demanding approach for an incoming nucleophile to the $Ru_{2,3}$ bond is shown in Figure 34, and the Z/Nu (Nu = CH_2, CO) interactions are calculated with Nu held in this position. It should be noted that, in this analysis, no allowance has been made for carbonyl reorientation on complexation of Nu, which could lower the total energies of the adducts appreciably.[261]

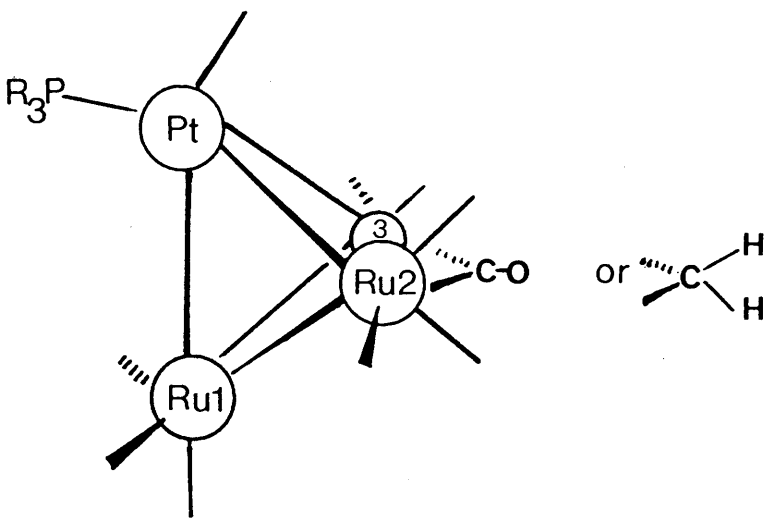

Figure 34 : Coordination of Nu to Cluster Framework (Nu = CH_2, CO).

(c) Interaction of Z with CH_2 to give $[Ru_3Pt(\mu\text{-}CH_2)(CO)_{10}(PH_3)]^{2-}$, X.

The orbital interaction diagram for Z and CH_2, generating X, the methylene adduct, is presented in Figure 35.

The frontier orbitals of the methylene fragment consist of a σ-donor, a', and a π-acceptor, a'', orbital.[286] These match well with the HOMO and LUMO of Z, which are of π-donor and σ-acceptor character along the $Ru_{2,3}$ edge (see Figure 33). MO 61 is derived from the in-phase combination of the a'' methylene orbital and FO57, the HOMO of Z, with a small contribution from mixing with FO60. The overlap between the a'' orbital of CH_2 and FO57 is maximised if the methylene coordinates with the H-C-H plane perpendicular to the $Ru_{2,3}$ vector. This geometry is found in the crystal structure of 23, where the methylene protons were located crystallographically.[258] The out-of-phase interaction of the $CH_2\pi_x^*$ orbital with FO57 generates MO59, the LUMO of $[Ru_3Pt(\mu\text{-}CH_2)(CO)_{10}(PH_3)]^{2-}$.

The σ-donor CH_2 orbital mixes with low-lying cluster orbitals and interacts slightly with FO56 (the LUMO of Z) and FO58, to form MO60, the adduct HOMO. The HOMO-LUMO gap in X is calculated to be 0.66 eV (cf. 0.28 eV for Z), which is relatively large, in keeping with the saturated nature of $[Ru_3Pt(\mu\text{-}CH_2)(CO)_{10}(PH_3)]^{2-}$, X.

The interactions described above are responsible for over 60% of the total overlap population between Z and CH_2 and, therefore, contribute significantly to the bonding between these fragments. The component fragments of X are calculated to be 320 kJ mol^{-1} less stable than X, which indicates that formation of X should be exothermic.

(d) Interaction of $[Ru_3Pt(CO)_{10}(PH_3)]^{2-}$ with CO

A σ-donor and two degenerate, orthogonal π-acceptor orbitals form the HOMO and LUMO's respectively of the CO fragment. The MO energy level diagram arising from the interaction of these CO frontier orbitals with those of Z, to generate $[Ru_3Pt(\mu\text{-}CO)(CO)_{10}(PH_3)]^{2-}$, W, is presented in Figure 35.

Several features distinguish the MO interactions leading to W and X. Firstly the σ-donor orbital in CO is of lower energy than that of CH_2, thus the interaction of the nucleophile's σ-donor orbital with FO56 is smaller in W than in X. In addition, the CO π* orbitals lie at higher energy than the π-acceptor orbital of CH_2. Hence MO61, generated by in-phase mixing of π_x^* with FO57 is relatively destabilised in W compared with the corresponding π_x^* /FO57 derived MO61 in X. More significantly, the interaction of the π_z^* orbital of CO with the frontier orbitals of Z is minimal, and, consequently, MO56 of W is principally derived from the CO π_z^* contribution (having 44% CO character).

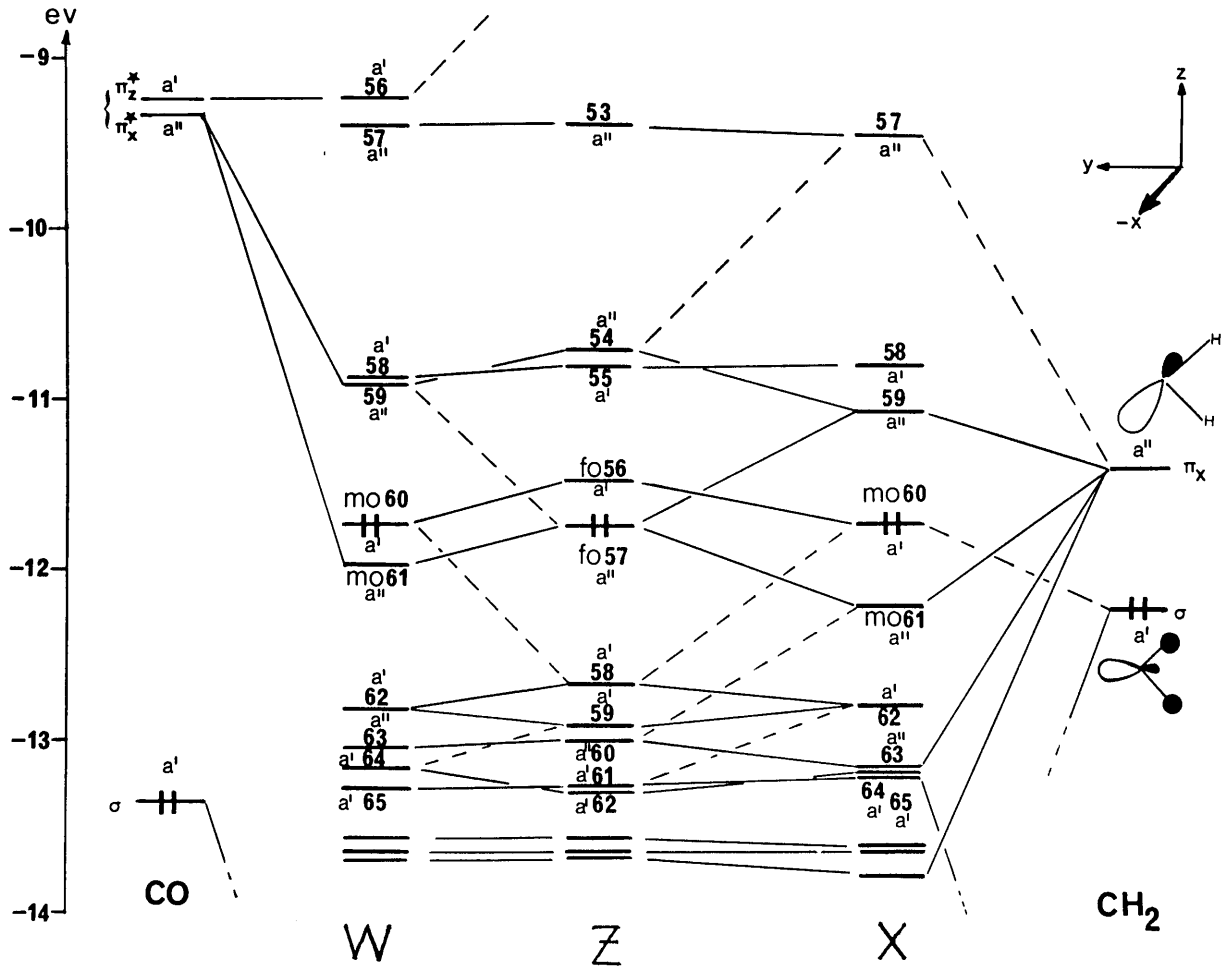

Figure 35. The interaction diagrams for $[Ru_3Pt(CO)_{10}(PH_3)]^{2-}$ with CH_2 and CO.

W is calculated to be 223 kJ mol^{-1} more stable than the component fragments and has a sizeable HOMO-LUMO gap. Both these factors indicate that W could be an energetically favoured configuration. Nevertheless, the CO adduct of 19 has a butterfly metal geometry.[258] The present study suggests that the inability of W to stabilise both CO π* orbitals effectively may be the determining factor in deciding the metal framework geometry adopted in the adduct. For the butterfly geometry, each Os centre exhibits pseudo-octahedral coordination geometry, which allows efficient stabilisation of both CO π* orbitals through back-bonding to the "t_{2g}" orbitals of the metal centres.

From the preceding considerations it may be expected that, where adducts of 19 form under frontier orbital control, isolobal[108] nucleophiles should react to yield adduct complexes with the same metal core geometry. Thus carbene analogues are anticipated to yield *closo*-tetrahedral adducts of 19, while nucleophiles isolobal with CO are predicted to give rise to butterfly adducts. Therefore the study of reactions of 19 with CNR (isolobal with CO), and the inorganic carbenes SO_2 and $SnCl_2$ was undertaken in order to assess the predictive utility of this qualitative MO analysis.

2.2.2(i) The Reaction of $Os_3Pt(\mu\text{-}H)_2(CO)_{10}(PCy_3)$, 19a, with CNR (R=t-Bu, Cy), an isolobal analogue of CO.

The chemistry of 19 bears some similarity to that of 4 - both add CO reversibly,[85,86,148] and form CH_2[101-104,258] and PR_3[85,86,148] adducts. In addition, 19 and 4 contain hydride ligands that can potentially transfer to cluster-bound moieties. There are many examples of this behaviour known in the adduct chemistry of 4.[33,94]

For example treatment of 4 with RNC, (R = Ph,Me, t-Bu) yields the expected adduct $Os_3(\mu\text{-H})(CO)_{10}(H)(RNC)$.[89] In the presence of a donor solvent (THF) or base, transfer of a hydride ligand to the N site of the isocyanide function is effected, affording the iminyl complexes $Os_3(\mu\text{-H})(\mu\text{-}\eta^1\text{-C=N(H)R})(CO)_{10}$.[262] In contrast, thermolysis of the isocyanide adduct in refluxing octane (in the absence of base) yields the substituted RNC derivative of 4 [89] and, subsequently the formimidoyl complexes $Os_3(\mu\text{-H})(\mu\text{-}\eta^2\text{-HC=NR})(CO)_{10}$ and $Os_3(\mu\text{-H})(\mu_3\text{-}\eta^2\text{-HC=NR})(CO)_9$, (R = Me,Ph).[89] These transformations are summarised in Scheme 12.

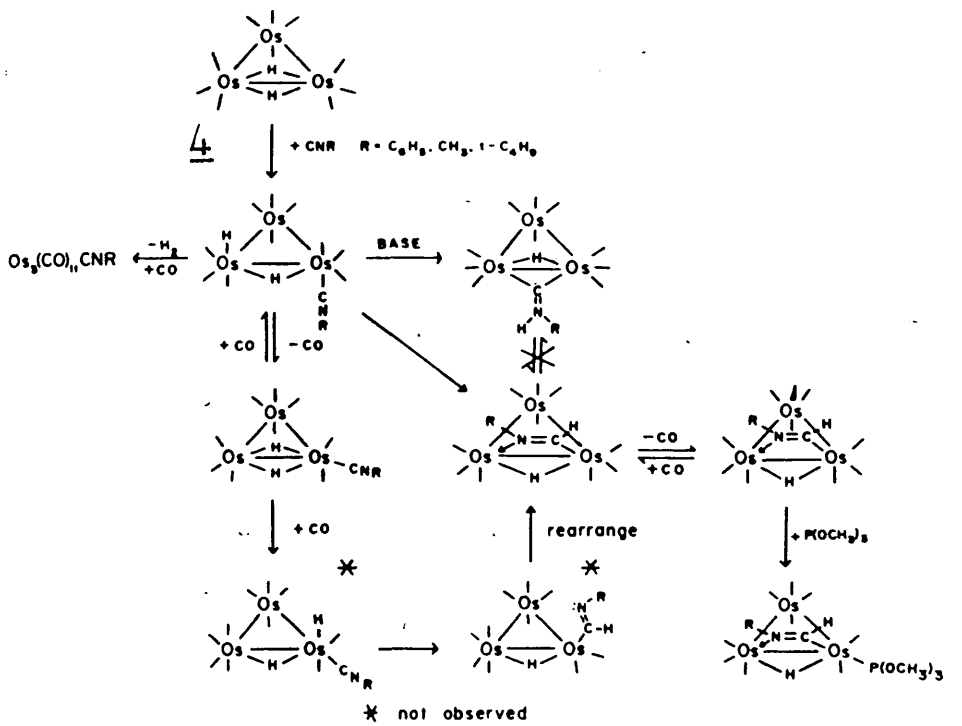

Scheme 12. RNC ligand transformations on an Os_3 framework.

In view of this interesting chemistry, and the potential similarities in reactivity between 19 and 4, coupled with the desire

to investigate the chemistry of 19 with CO analogue molecules, the reaction of 19 with RNC was studied. The orbital similarities between CO and CNR have been described previously.[269]

On treating solutions of 19a with one equivalent of RNC, (R = t-Bu, Cy), the dark green colour of 19a rapidly gives way to the yellow of the isocyanide adducts $Os_3Pt(\mu\text{-}H)_2(CO)_{10}(PCy_3)(RNC)$, (25a, R = t-Bu; 25b, R = Cy). ^1H n.m.r studies suggest that several isomers of 25 are formed and that the relative proportions of each depend upon the reaction temperature. The formation of predominantly one species, A, is observed for the addition of RNC at 195K. The hydride region of the ^1H n.m.r spectrum of the reaction mixture formed on addition of CyNC at 195K is depicted in Figure 36(a). Species A displays resonances attributed to Os(μ-H)Pt and Os(μ-H)Os hydrides at -9.78 and -17.63 p.p.m. respectively. The Os(μ-H)Pt proton resonance is clearly distinguishable by its large coupling (565Hz) to ^{195}Pt. The chemical shift of the Os(μ-H)Os proton in 19a is -6.84 p.p.m,[147] and the displacement to high field of the corresponding resonance in A is observed in all known saturated adducts of 19 [148,258] suggesting that A is likewise, saturated. In addition to resonances due to A, low intensity signals attributed to species B and D are also observed.

Three principal products arise from the addition of CyNC at 273K, species A, B and C (Figure 36(b)). Both species B and C show resonances due to Os(μ-H)Pt and Os(μ-H)Os protons [for B; Os(μ-H)Pt -11.59 p.p.m., J(Pt-H) = 503, J(P-H)=11Hz; Os(μ-H)Os -17.56 p.p.m., J(Pt-H) = 26, J(P-H) = 1.5Hz; for C; Os(μ-H)Pt -9.70 p.p.m., J(Pt-H) = 570, J(P-H) = 15Hz; Os(μ-H)Os -18.94 p.p.m., J(Pt-H) = 16Hz]. On standing at ambient temperatures for one hour, this solution gives rise to the spectrum shown in Figure 36(c), in which the most intense

resonances arise from A, signals due to B have decreased significantly in intensity and those of C are unobserved. A similar spectrum is obtained by warming a sample prepared at 195K to room temperature. It therefore seems plausible that species A,B and C are isomers in thermodynamic equilibrium. Resonances due to C disappear rapidly (ca. 5 minutes at 298K), while the equilibrium between A and B is established more slowly.

Low intensity signals due to species D are present in all spectra recorded from reaction mixtures of 19a and RNC, and the intensities of these signals are apparently invariant with time, suggesting that D is not involved in the proposed equilibrium between A, B and C.

The carbonyl region of the variable temperature ^{13}C n.m.r spectrum of isomer A of 25b is depicted in Figure 37, and a listing of relevant n.m.r parameters is presented in Table 21. At 218K, isomer A displays ten signals due to terminally ligated carbonyl moieties. The large ^{195}Pt coupling to resonance f is indicative that this signal arises from a carbonyl directly bound to Pt. From the magnitude of ^{195}Pt coupling in the ^{31}P and ^{1}H n.m.r spectra of isomer A (see Table 21) it is evident that one hydride and the PCy_3 group remain bonded to Pt. Furthermore, the observation of ^{31}P and ^{195}Pt couplings to signals due to the Os-bound carbonyls, confirms that the Pt remains bound to the Os_3 unit. The isocyanide must, therefore, be coordinated to an Os centre, and a broad resonance, with no detectable ^{195}Pt satellites, due to the contact carbon of the isocyanide ligand is observed in the ^{13}C nmr spectrum at 110.8 p.p.m. This RNC function is terminally ligated, as evidenced by the broad stretch at 2175 cm^{-1} in the solid state i.r. spectrum of isomer A of species 25a.

Figure 36 : Highfield region of ^{1}H n.m.r spectra recorded at 233K of 25b

(a) immediately after addition of 1:1 equimolar stoichiometric amounts of CyNC to $Os_3Pt(\mu\text{-}H)_2(CO)_{10}(PCy_3)$ at 195K.

(b) same as (a) for addition at 273K.

(c) same sample as (b) after warming to room temperature for ca. 1 hour.

* denotes signals from $Os_3Pt(\mu\text{-}H)_2(CO)_9(CyNC)(PCy_3)$.

X - denotes uncharacterised species.

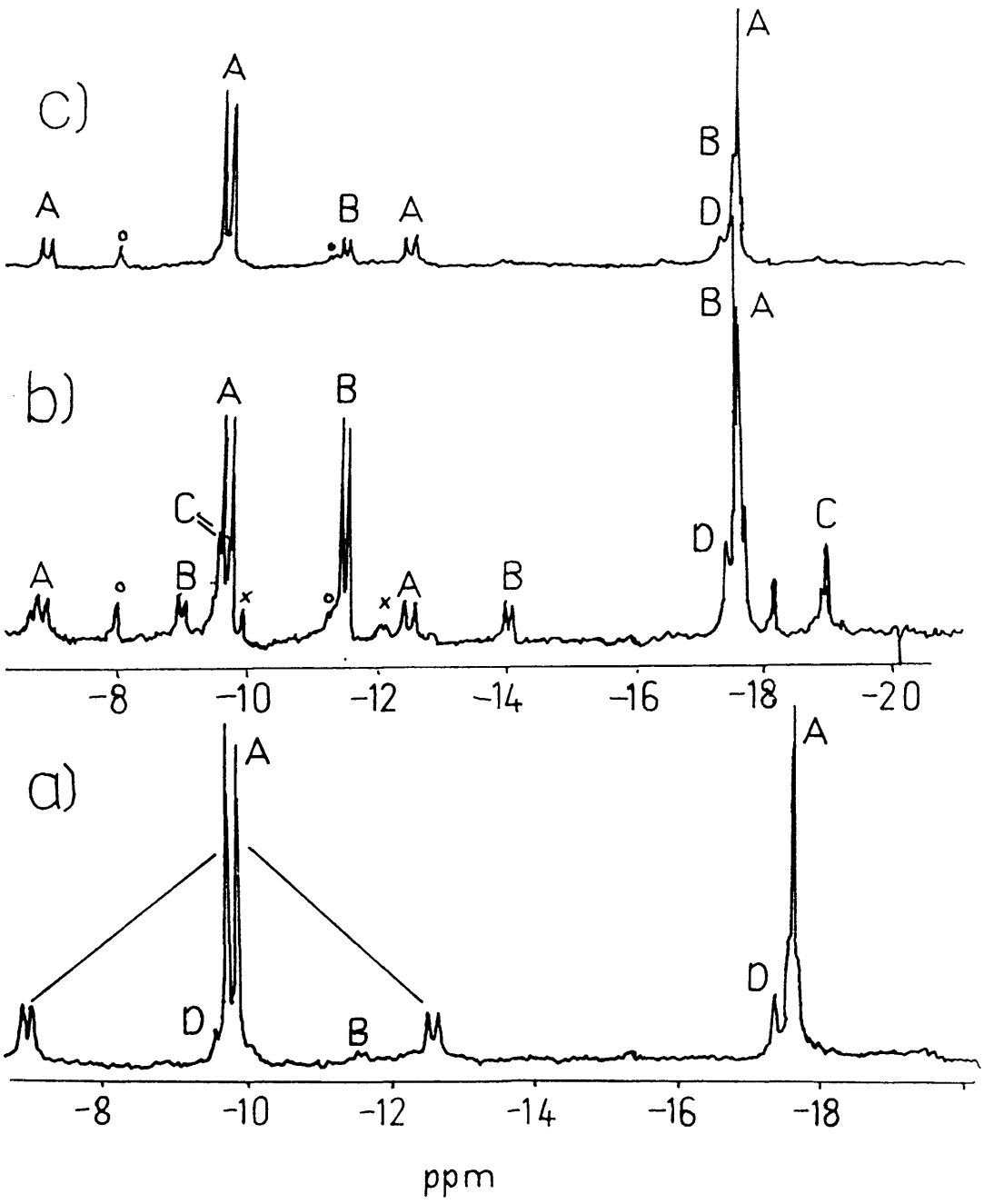

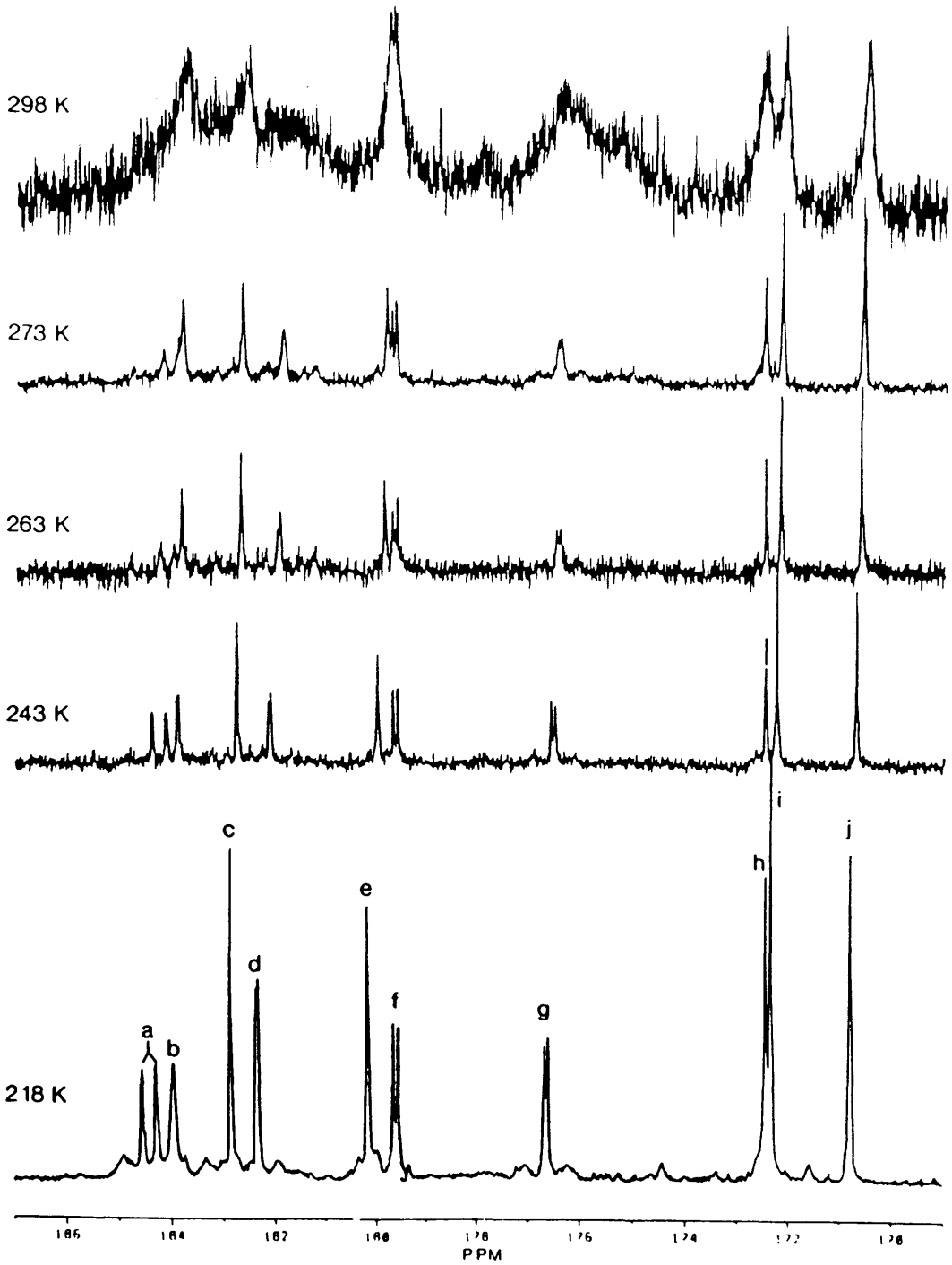

Figure 37 : Variable temperature $^{13}C\{^{1}H\}$ n.m.r spectrum of ^{13}CO enriched $Os_3Pt(\mu\text{-}H)_2(CO)_{10}(PCy_3)(CyNC)$, 25b, isomer A.

Table 21 : N.m.r parameters for $Os_3Pt(\mu\text{-}H)_2(CO)_{10}(PCy_3)(CyNC)$, 25b, isomer A.

^{13}C data [a]

Resonance[b]	p.p.m.	Mult.[c]	Assignment[g]	J/Hz[d]			
				Pt-C	P-C	H1-C	H2-C
a	184.4	d	C6	-	13.3	-	w
b	184.0	s	C3	-	-	10.4	-
c	182.9	s	C2/C4	-	-	3.9	-
d	182.3	d	C7	-	1.2	-	4.3
e	180.2	s	C2/C4	18	-	2.3	-
f	179.6	d	C1	1784	4.6	28.7	-
g	176.7	d	C5	42	3.2	-	6.7
h	172.5	s	C10/C8	-	-	-	-
i	172.4	s	C9	-	-	-	8.8
j	170.8	s	C10/C8	-	-	-	3.4
	110.8	s	CyNC	-	-	-	-

^{1}H data [e]

-9.78 (d,Os(μ-H)Pt, J(Pt-H) = 565, J(P-H) = 14.2Hz).

-17.63 (d, Os(μ-H)Os, J(Pt-H) = 32, J(P-H) = 1.2Hz).

^{31}P data [f]

51.6 (s, Pt-P, J(Pt-P) = 2520Hz).

a) 218K, CD_2Cl_2/CH_2Cl_2 1:1; b) Figure 37; c) multiplicities based on $^{13}C\text{-}\{^{1}H\}$ spectra; d) w indicates small unresolved coupling e) 233K, $CDCl_3$, p.p.m. rel. to TMS; f) 233K, $CDCl_3$ p.p.m. rel. to ext. H_3PO_4; g) Figure 38.

The spectroscopic data indicate that A has twelve terminally bound ligands : 10 CO's, the RNC function and the PCy_3 group. By analogy with 20 and 21, which similarly have twelve terminal functions, the metal framework of isomer A, can be assumed to have a butterfly geometry. (In the *closo* adducts, 22, 23 and 24, the incoming functions are located at bridging sites.[258])

By consideration of selectively ^1H decoupled ^{13}C spectra it is clear that the hydrides do not span adjacent M-M edges, since no carbonyl signal shows coupling to both hydrides.

Two factors indicate that the isocyanide function is ligated to the wing tip Os. Firstly, three Os-bound carbonyl resonances b, c, and e, show coupling to the hydride spanning an Os-Pt edge, indicating that the RNC group cannot be ligated to the Os centre of the Os(μ-H)Pt unit. In addition, of the remaining six signals, three resonances a, d and g show coupling to both the Os-Os edge bridging hydride, and the ^{31}P nucleus of the PCy_3 group, suggesting that these signals correspond to carbonyls ligated to a butterfly hinge Os centre. In support of this, the resonances a,d and g broaden more rapidly than the rest on heating the sample above 218K, indicative of an $Os(CO)_3$ group undergoing tripodal rotation. Thus the resonances h,i and j may be assigned to carbonyls on the wing tip Os site, where the isocyanide function must also be bound.

It is apparent from Figure 37 that further carbonyl exchange processes are operative at 298K, however the inherent instability of isomer A precluded a detailed investigation of this fluxional behaviour.

A possible structure for isomer A consistent with the spectroscopic data is shown in Figure 38 and the assignments of carbonyl resonances are listed in Table 21. Assignments within $Os(CO)_3$ groups are made on the basis of ^1H

selective decoupling experiments where it is assumed that the magnitude of trans $^{2}J(H-C)$ coupling is greater than that of cis couplings, (in keeping with previously reported spectral analyses of hydrido osmium clusters[263,264] and by comparison with n.m.r data obtained from the related systems $Os_3Pt(\mu-H)_2(CO)_{10}(PCy_3)(L)$ (L = CO, PCy_3)[148,265]

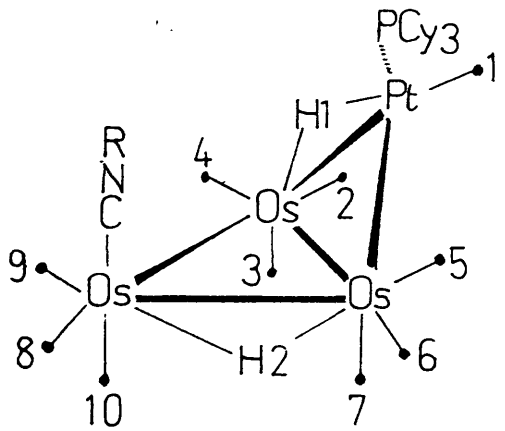

Figure 38 : Proposed structure of isomer A of 25.

The axial coordination of the RNC group shown in Figure 38 is in accord with the observed axial ligation of isocyanide in $Os_3(CO)_{11}(RNC)$[47] and $Os_3(\mu-H)(CO)_{10}(H)(t-BuNC)$[91] However the t-BuNC function in $Os_3(\mu-H)_2(CO)_9(t-BuNC)$[91] occupies an equatorial site and n.m.r evidence for an equatorial/axial isomerisation process in $Os_3(CO)_{11}(t-BuNC)$ has been reported.[47] Therefore, the precise site of isocyanide coordination in isomer A is not unambiguously defined.

Tentative structures for isomers B and C are presented in Figure 39, based on consideration of ^{1}H n.m.r data. The chemical shifts and coupling constants of the hydride resonances due to B bear a close resemblance to those observed in 20,[148] suggesting that B has a

similar structure with hydrides spanning adjacent Pt-Os and Os-Os bonds. Isomer C may have the structure shown for which rotation of the $Os(CO)_3(RNC)$ group effects conversion to A; this could account for the facile formation of A from C. Species D may involve ligation of the isocyanide function at another metal site. Unfortunately crystals of a suitable quality for X-ray diffraction could not be obtained, despite many efforts.

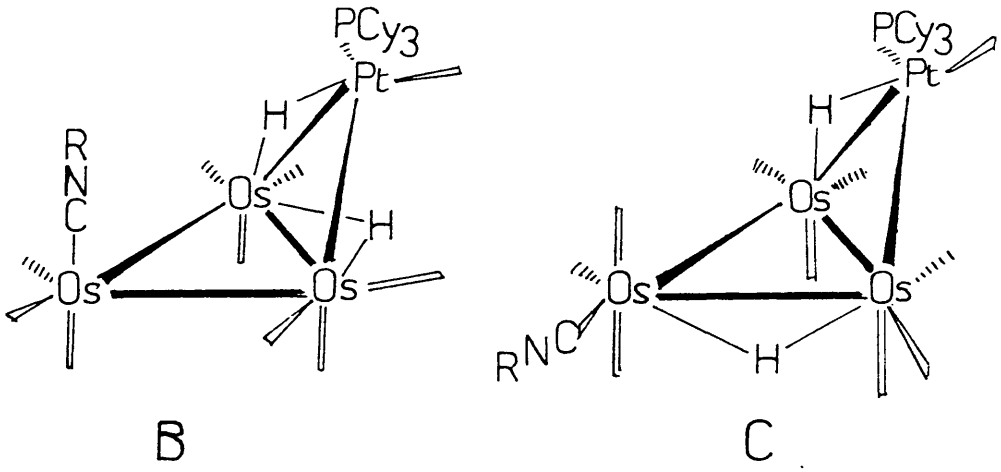

Figure 39. Proposed structures for B and C.

ii)Formation of $Os_3Pt(\mu\text{-}H)_2(CO)_9(PCy_3)(RNC)$, R = t-Bu, Cy.

In refluxing hexane, under a dinitrogen purge, solutions of 25a,b undergo a colour change from yellow to dark green. Concentration of the resulting solution affords high yields of dark green crystals characterised as the 58 electron cluster $Os_3Pt(\mu\text{-}H)_2(CO)_9(PCy_3)(RNC)$, 26, (26a, R = t-Bu, 26b, R = Cy). Solution i.r. spectra of 26 indicate that the RNC and CO ligands are terminally bound. ^1H and ^{13}C n.m.r spectroscopic data suggest that 26 is related in structure to the parent cluster 19, with the Pt-bound carbonyl group being substituted by RNC. This was confirmed by an X-ray diffraction study on $Os_3Pt(\mu\text{-}H)_2(CO)_9(PCy_3)(CyNC)$, (see below).

The hydride resonances in the ^{1}H n.m.r spectrum of 26b, indicate the presence of Os(μ-H)Os and Os(μ-H)Pt units, with chemical shifts of -8.01 and -11.35 p.p.m., (J(Pt-H) = 544, J(P-H)= 9.1Hz). The shift to low field of the Os(μ-H)Os resonance in 26b, compared with that of isomer A, of 25b (-17.63 p.p.m) is suggestive that 26 is an unsaturated complex (vide supra).

In order to delineate the structure of 26b, a single crystal X-ray diffraction experiment was carried out by Dr. L.J. Farrugia.

The molecular structure is presented in Figure 40 along with the atomic labelling scheme used. Important metrical parameters are listed in Table 22. 26b has a *closo*-tetrahedral metal framework and the overall structure is very similar to that of 19a,[147] with the distinction that, in 26b, a near linear (C(10)-N-C(141) = $166(3)^{o}$) CNCy moiety is terminally bound to Pt, lying over the PtOs(2)Os(3) face, replacing a CO group in 19a. The metal-metal bond distances in 26b differ from those in 19a,[147] by only 0.02-0.05 $\overset{o}{A}$ and a listing of corresponding M-M separations in 19a is given in Table 22 for ease of comparison. The hydride ligand sites were not directly located in electron density difference maps, but were determined by potential energy minimisation calculations.[271] In accord with ^{1}H n.m.r evidence, these calculations position the hydrides at Os(μ-H)Os and Os(μ-H)Pt sites. The hydride bridged Os(2)-Os(3) separation in 26b of 2.752(1) $\overset{o}{A}$ is significantly shorter than is expected (vide supra) and parallels the short Os(μ-H)Os distance in 19a,[147] suggesting that unsaturation is localised at this unit. The crystal structure of 26b shows that the molecule has a pseudo mirror plane passing through Os(1),Pt,P,C(3),C(10) and the two hydride ligands

The carbonyl region of the variable temperature (v.t) ^{13}C n.m.r spectrum of 26b is presented in Figure 41, and the corresponding

Figure 40 : The molecular structure of $Os_3Pt(\mu\text{-}H)_2(CO)_9(PCy_3)(CyNC)$, 26b

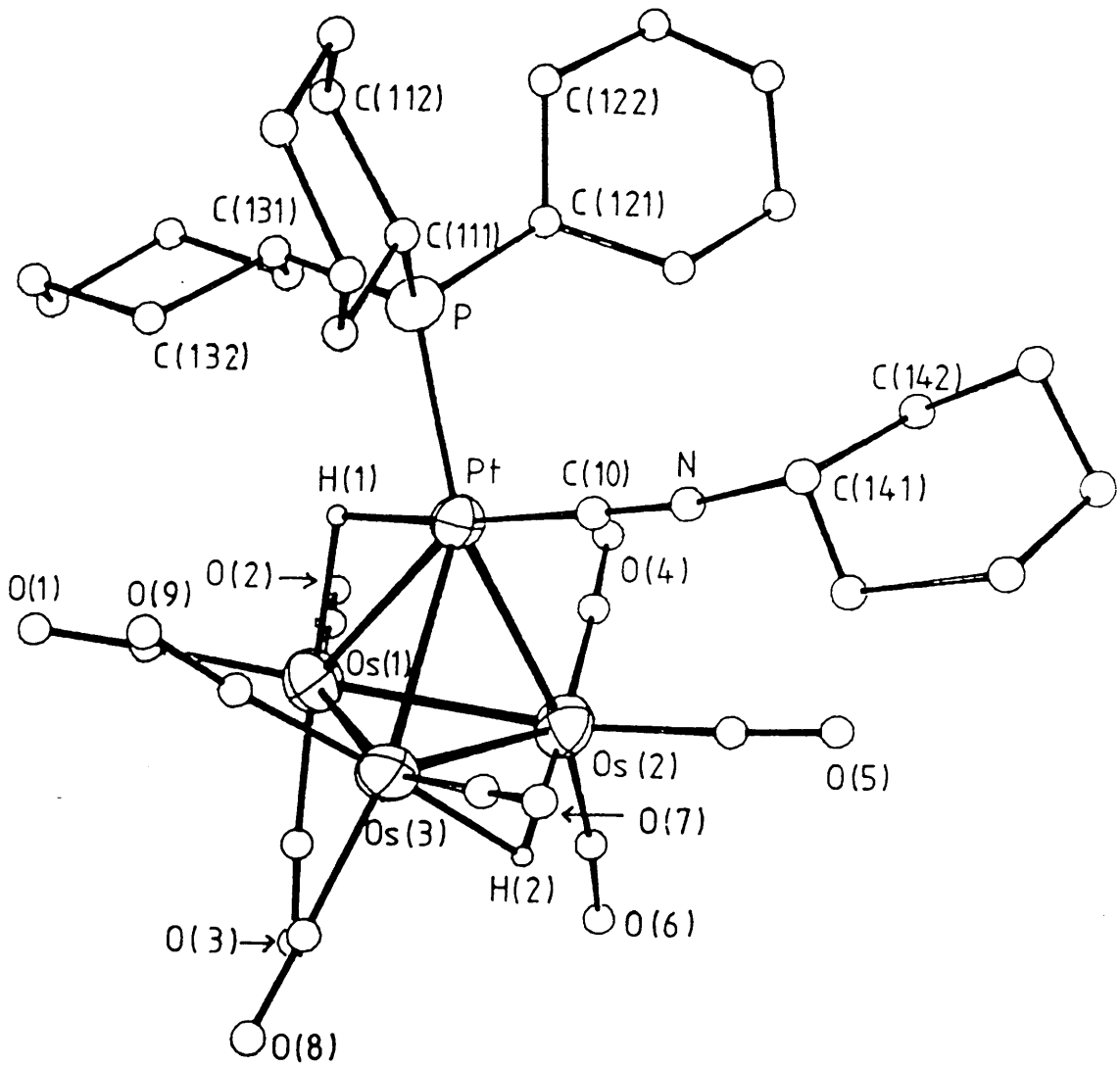

Table 22 : Important bond lengths (Å) and bond angles (deg) for the complex $Os_3Pt(\mu\text{-}H)_2(CO)_9(PCy_3)(CyNC)$ (26b).

Bonds.

Os(1)-Os(2)	2.745(1) [2.777(1)]*	Os(1)-C(3)	1.87(3)
Os(1)-Os(3)	2.742(1) [2.741(1)]	Os(2)-C(4)	1.89(3)
Os(2)-Os(3)	2.752(1) [2.789(1)]	Os(2)-C(5)	1.89(3)
Pt -Os(1)	2.844(1) [2.863(1)]	Os(2)-C(6)	1.85(3)
Pt -Os(2)	2 773(1) [2.791(1)]	Os(3)-C(7)	1.87(3)
Pt -Os(3)	2.781(1) [2.832(1)]	Os(3)-C(8)	1.86(3)
Pt -P	2.346(6)	Os(3)-C(9)	1.84(3)
Pt -C(10)	1.85(3)	P -C(111)	1.84(3)
Os(1)-C(1)	1.83(3)	P -C(121)	1.82(3)
Os(1)-C(2)	1.84(3)	P -C(131)	1.80(3)
C(10)-N	1.14(4)		

C-O(carbonyl) mean 1.16[1]

Angles

Os(1)-Pt -Os(2)	58.5(1)	Pt -Os(2)-Os(1)	62.1(1)
Os(1)-Pt -Os(3)	58.3(1)	Pt -Os(2)-Os(3)	60.4(1)
Os(2)-Pt -Os(3)	59.4(1)	Os(1)-Os(2)-Os(3)	59.8(1)
Pt -Os(1)-Os(2)	59.4(1)	Pt -Os(3)-Os(1)	62.0(1)
Pt -Os(1)-Os(3)	59.7(1)	Pt -Os(3)-Os(2)	60.1(1)
Os(2)-Os(1)-Os(3)	60.2(1)	Os(1)-Os(3)-Os(2)	59.9(1)
C(10)-Pt -P	93.5(7)	P -Pt -H(1)	82.2(2)
Pt -C(10)-N	175(2)	C(10)-N -C(141)	166(3)

Os-C-O mean 176[1]

* Values in square parentheses are those corresponding distances $Os_3Pt(\mu\text{-}H)_2(CO)_{10}(PCy_3)$, 19a (ref. 147)

parameters are listed in Table 23. At 213K, 5 signals, due to nine carbonyls, of intensities 2:2:2:1:2 are observed, consistent with the pseudo mirror plane of 26b. Significantly, while no carbonyl resonance shows a large ^{195}Pt coupling, the CyNC resonance at ambient temperatures is a broad signal at 117.0 p.p.m. with a ^{195}Pt coupling of 1468Hz, corresponding to a Pt bound CyNC function.

Data from ^{1}H selective decoupling experiments are in accord with the solid state structure of 26b. It is clear that resonances a and d, of intensity 2 and 1 respectively, (Figure 41) are coupled to the Os(μ-H)Pt proton; the coupling to d is larger than that to a, and, therefore d can be assigned to C3, trans to the hydride, while resonance a is attributed to C1,2. Similarly the double intensity signals b,c and e, are coupled to the Os(μ-H)Os proton, and the magnitude of $^{2}J(H-C)$ coupling to c indicates that this resonance corresponds to C4,9 situated trans to this hydride; resonances b and e are assigned to C5,7 and C6,8 respectively, by comparison with the reported spectrum of $Os_3Pt(\mu-H)_2(CO)_{10}(PCy_3)$, 19a.[265]

The fluxional behaviour of the carbonyl ligands in 26b closely resembles that observed in 19a.[265] The lowest energy process in 26b exchanges resonances b,c and e, due to the localised rotation of the $Os(CO)_3$ groups containing C4/5/6 and C7/8/9. A second higher energy process permutes all nine Os-ligated carbonyls. The Pt-bound carbonyl in 19a does not exchange with the carbonyls ligated to Os centres up to 293K,[265] and, similarly, the magnitude of $^{195}Pt-C$ coupling to CyNC at 298K suggests there is no significant CyNC/CO exchange in 26b. The $^{1}J(Pt-C)$ coupling to CyNC in 26b of 1468Hz compares with the 1936Hz $^{1}J(Pt-C)$ coupling to terminal t-BuNC carbons in $Pt_3(\mu-t-BuNC)_3(t-BuNC)_3$.[270]

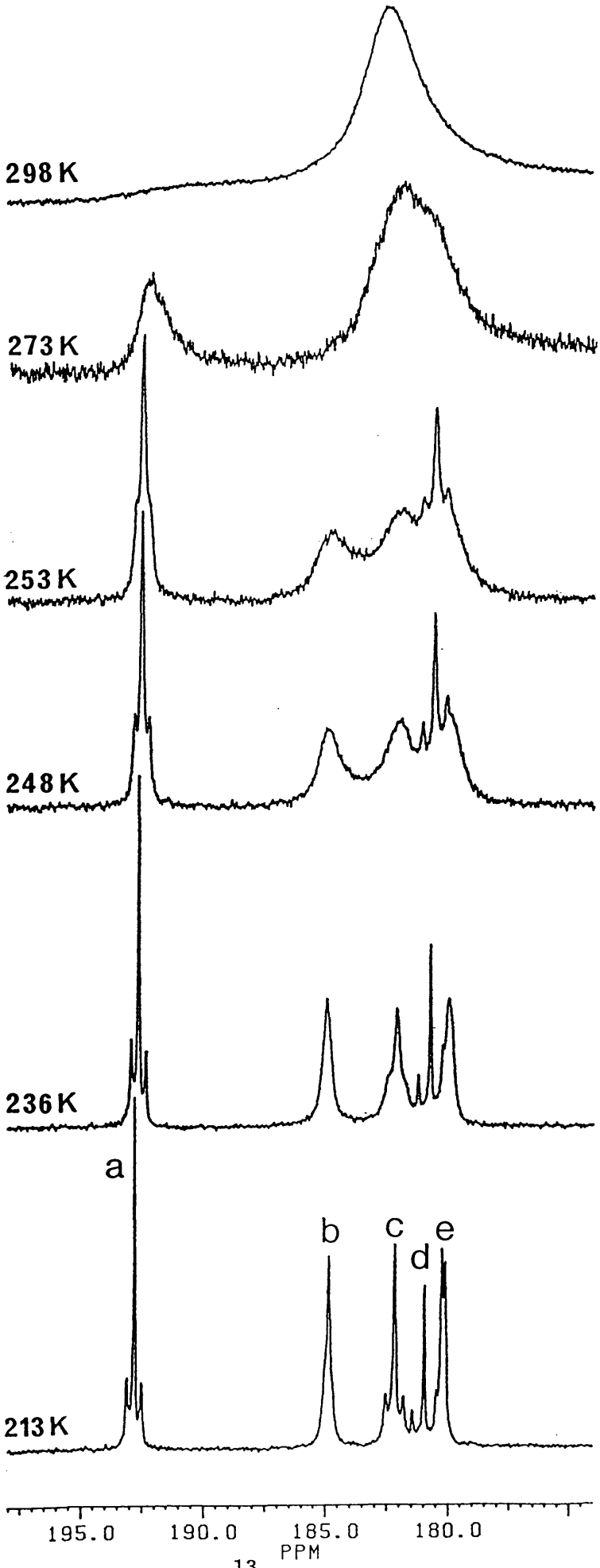

Figure 41 : Variable Temperature ^{13}C n.m.r spectrum of $Os_3Pt(\mu\text{-}H)_2(CO)_9(CyNC)(PCy_3)$, 26b.

Table 23 : N.M.R Parameters for $Os_3Pt(\mu\text{-}H)_2(CO)_9(PCy_3)(CyNC)$

	^{13}C Data [a]							
					J/Hz [d]			
Resonance [b]	Chem. Shift p.p.m.	Mult. [c]	Int.	Assign. [g]	Pt-C	P-C	H1-C [g]	H2-C [g]
a	192.8	s	2	C1,C2	30	-	2.3	-
b	184.8	s	2	C5,C7	16	w	-	w
c	182.1	s	2	C4,C9	36	w	-	11.6
d	180.9	s	1	C3	50	-	7.2	-
e	180.2	d	2	C6,C8	-	7.0	-	w
	117.0	s	1	CyNC	1468 [e]			

^1H Data [f]

H2: -8.01 (s, Os(μ-H)Os)

H1: -11.35 (d,Os(μ-H)Pt, J(Pt-H) = 544, J(P-H) = 9.1Hz).

a) 213K, CD_2Cl_2:CH_2Cl_2 b) Figure 41 c) Multiplicities based on ^1H decoupled spectra d) w indicates small unresolved coupling e) ^{195}Pt coupling observed in spectrum recorded at ambient temperature f) 233K, $CDCl_3$, ppm relative to TMS. g) Numbering scheme for C and H is consistent with that used in Figure 40 for the X-ray structure of 26b.

Hydride Fluxionality in $Os_3Pt(\mu\text{-}H)_2(CO)_9(CyNC)(PCy_3)$, 26b.

Interestingly, a MO analysis by Hoffmann and Schilling,[175] using the model complex $[Fe_3Pt(CO)_{10}(PH_3)]^{2-}$ suggested that the barrier to rotation of the PtL_2 unit about the $M_3(CO)_9$ framework is low in 19 although the presence of bridging hydrides was expected to raise this barrier. The rotation of $Pt(H)L_2$ above the Os_3 framework may be detected in 19 and 26 from consideration of the temperature dependence of the magnitude of $^1J(^{187}Os\text{-}H)$ coupling to the hydride signals. This was possible for 26b as, unlike 19,[147] the Os(μ-H)Os and Os(μ-H)Pt hydrides do not exchange rapidly on the n.m.r timescale and, hence, the ^{187}Os-H coupling was observable.

The I = ½ ^{187}Os isotope has a natural abundance of 1.64% and, thus, we need only consider isotopomers containing one ^{187}Os atom. For a static structure there are three possible isotopomers of 26b, shown in Figure 42. (a) and (b) are enantiomers related by a molecular mirror plane. In the static structure, the $^1J(^{187}Os\text{-}H)$ coupling to H1, the Os(μ-H)Pt proton, is expected to be ca. 17-40Hz.[266-268] However if the $PtL_2(H)$ unit undergoes rapid rotation, an averaged ^{187}Os-H splitting of 1/3 $[^1J(Os_1\text{-}H) + 2(^2J(Os_{2,3}\text{-}H)]$ is anticipated - assuming a degenerate exchange. Furthermore, the ^{187}Os satellites in

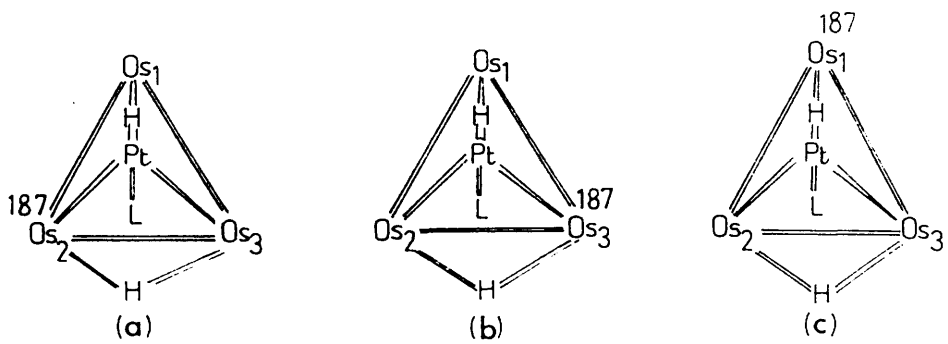

Figure 42 : The ^{187}Os isotopomers of 26b, (L = CyNC).

this fast exchange regime should be three times as intense as the corresponding peaks in the spectrum of the static structure.

The observed ^{1}H n.m.r spectrum at 238K shows $^{1}J(Os-H1)$ coupling of 31.4Hz (Figure 43a), in keeping with a static structure. Significantly, at 298K, the magnitude of $^{187}Os-H1$ splitting is 9.7Hz (Figure 43a). Substitution of this value for the average $^{187}Os-H1$ coupling into the above equation allows calculation of $^{2}J(Os-H1)$ viz:

$(3x9.7) - 31.4 = 2[^{2}J(Os-H1)]$, hence $^{2}J(Os-H1) = -1.6Hz$

which is in close agreement with previously observed $^{2}J(Os-H)$ couplings.[266] These results are compatible with a rapid rotation of the $Pt(H)(CNCy)(PCy_3)$ unit above the Os_3 triangle. The expected increase in intensity of the ^{187}Os satellites was not detected since the low temperature spectrum required line narrowing in order to resolve the broad satellite peaks (broadness may be due to coupling to the quadrupolar ^{14}N nucleus of the CyNC function, trans to this hydride). Nevertheless, these results show unambiguously that at 298K, the Pt-ligated hydride visits all three Os sites.

Similarly, at 238K, the $^{1}J(Os-H)$ coupling to H2, the $Os(\mu-H)Os$ proton, is 41.8Hz, while at 298K the average $^{187}Os-H$ coupling is 27.3Hz (see Figure 43b). This average coupling can be represented by the expression:

$$J_{AVE}(Os-H) = {}^{2}/3[^{1}J(Os-H)] + {}^{1}/3[^{2}J(Os-H)]$$

Substitution of $J_{AVE}(Os-H)$ and $^{1}J(Os-H)$ allows calculation of $^{2}J(Os-H) = -1.7Hz$, which agrees well with known values of $^{2}J(Os-H)$ coupling.[266] These results indicate that this hydride is non-fluxional at 238K, while at 298K it undergoes rapid migration about the Os_3 framework.

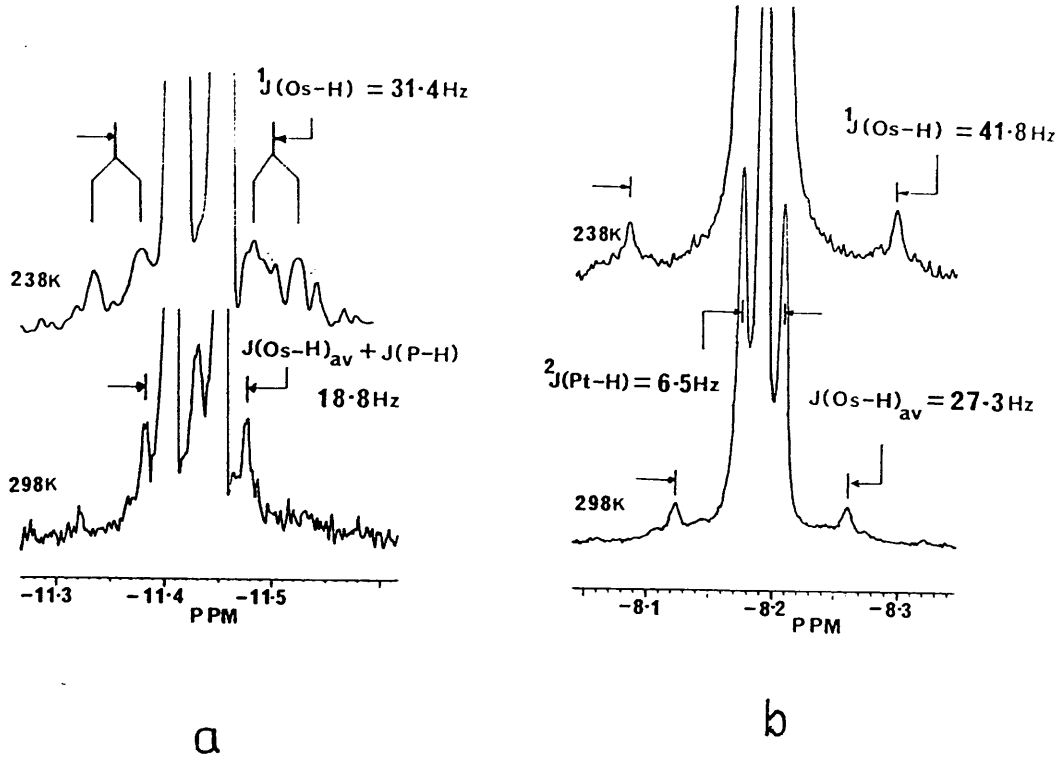

Figure 43 : ^{187}Os satellites of (a) Os(μ-H)Pt and (b) Os(μ-H)Os hydride resonances in the ^1H nmr spectrum of 26b.

The concerted migration of H1 and H2 about the Os_3 triangle as shown in Figure 44, in tandem with the low energy tripodal rotation of equivalent $Os(CO)_3$ groups provides a plausible mechanism for the permutation of all nine Os-ligated carbonyls in 26b, as observed in the ^{13}C n.m.r spectrum at 298K.

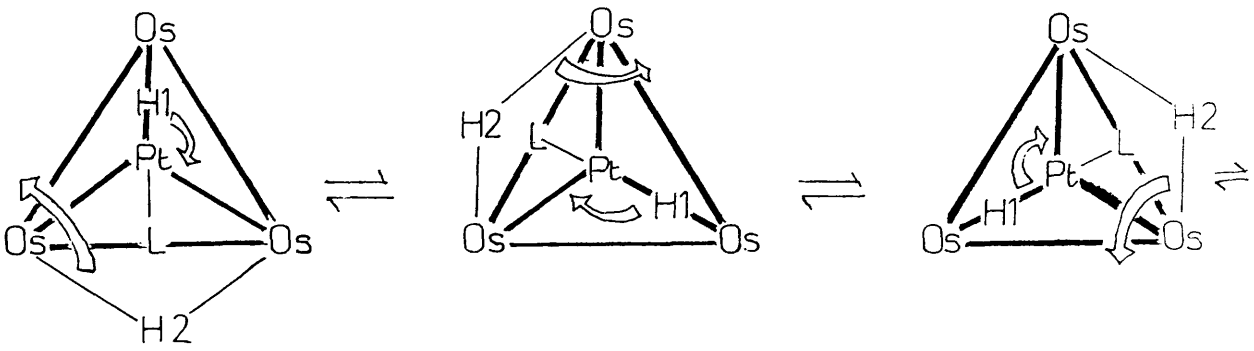

Figure 44 : Proposed mechanism for hydride migration in 26b.

The rotation of a $Pt(H)(PR_3)(L)$ unit has been observed previously in the complex $[PtRh_2(\mu\text{-}H)(\mu\text{-}CO)_2(Cp^*)_2(CO)(PPh_3)]^+BF_4^-$.[306]

One common feature of all known substituted derivatives of 4 is that substitution occurs at the $Os(\mu\text{-}H)_2Os$ unit, where unsaturation is localised.[91,112,113,115-118] It is, therefore, of interest that in 26 the site of substitution is at the Pt centre and not the Os atoms of the Os(μ-H)Os group, the proposed site of unsaturation in 19.

The investigation of the reactivity of 19 towards RNC did not produce evidence for hydride transfer to the isocyanide function, in contrast to the reaction of RNC with 4.[89,91,262] Nevertheless, the syntheses of 26a and 26b, the first carbonyl substituted derivatives of 19, have been effected via formation of the saturated intermediates $Os_3Pt(\mu\text{-}H)_2(CO)_{10}(PCy_3)(RNC)$, R = t-Bu, Cy. As described in Chapter 1, the preparation of substituted analogues from parent unsaturated clusters via decarbonylation of saturated adducts is a feature of

electron deficient cluster chemistry.[12,89,192]

The reactivity of ligand substituted unsaturated clusters can be distinct to that of the parent unsaturated system for reasons outlined previously. In order to investigate the differences in reactivity between 19 and 26, the reactions of 26 towards a) CO and b) CH_2N_2 were examined.

iii)a) Reaction of $Os_3Pt(\mu\text{-}H)_2(CO)_9(PCy_3)(RNC)$, 26, with CO.

Treatment of 26a,b with CO at 195K and at ambient temperatures resulted in the green colour of 26 rapidly giving way to yellow. The ^1H n.m.r spectra of these solutions immediately after CO addition revealed that the only hydride containing product formed displayed resonances identical to those of isomer A of 25a,b. On standing at ambient temperatures, signals due to isomer B are observed, in keeping with the proposed equilibrium between A and B. The addition of CO to 26 therefore effects a facile transfer of RNC from Pt to Os centres in tandem with the opening of the cluster framework from a *closo*-tetrahedron to a butterfly. That isomer A is the unique initial product formed from CO addition to 26 is suggestive that no isomers of 25a,b contain Pt-bound isocyanide functions, as these would be expected to be the first observed products.

Addition of CO to 19a similarly produces the butterfly adduct 20. It is noteworthy that in 20 a very low energy fluxional process exchanges carbonyls between Os and Pt sites.[265] This process permutes six carbonyls and is believed to follow the mechanism shown in Scheme 13, where formation of a *closo* or semi-*closo* tetrahedral intermediate is proposed. A similar fluxional process does not appear to be operative in isomer A of 25 (See Figure 37). Nevertheless, if such an exchange was occurring the involvement of the isocyanide would render the

process non-degenerate. Therefore, the stabilities and, hence, the populations of various intermediates need not be equal. Ejection of CO from a semi-*closo* transition state of 25a,b provides a possible mechanism for the closure of the metal framework in the formation of 26a,b.

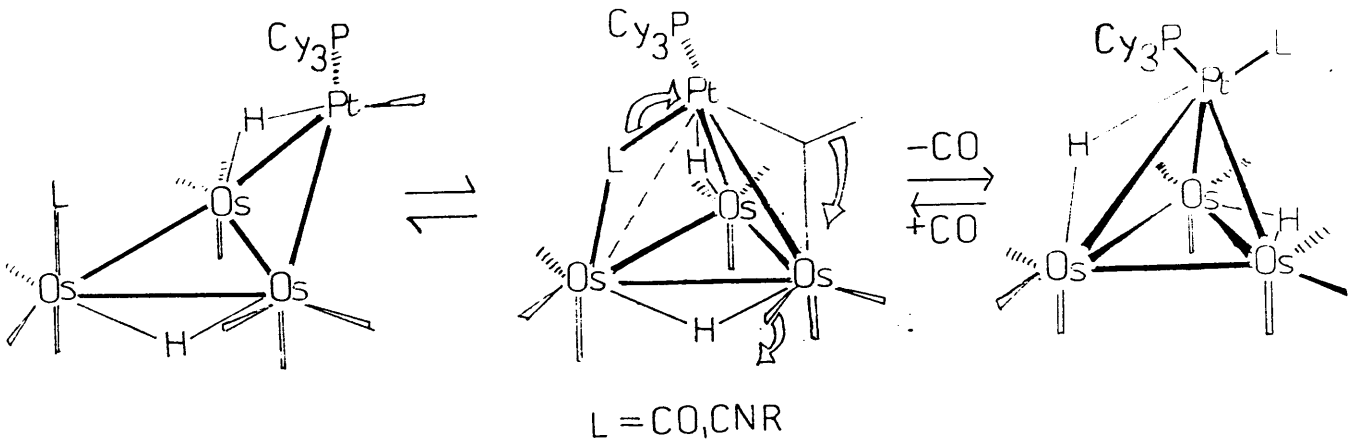

Scheme 13 : Proposed mechanism for formation of 25 from 26.

The facile formation of isomer A of 25a,b on CO addition to 26a,b, coupled with the fluxional behaviour of 20 indicate that, in certain Os_3Pt systems, ligand transfer between Pt and Os sites can be a low energy process. Nevertheless, the dynamic behaviour of 19a,[265] and 26b suggests that such exchange is not facile in *closo*-tetrahedral Os_3Pt complexes.

iii) Reaction of $Os_3Pt(\mu\text{-}H)_2(CO)_9(PCy_3)(CyNC)$, 26b with CH_2N_2.

Treatment of a solution of 26b in toluene with excess ethereal diazomethane resulted in a colour change from green to orange. On evaporation of this solution and recrystallisation of the residue from diethyl ether, red crystals of a single product, formulated as the 60 electron species $Os_3Pt(\mu\text{-}H)_2(\mu\text{-}CH_2)(CO)_9(CNCy)(PCy_3)$, 27, were isolated in high (>80%) yield. The i.r spectrum of 27 indicates that both the isocyanide and carbonyl ligands are terminally bound to the cluster. The high field region of the ^1H n.m.r spectrum displays two resonances due to Os(μ-H)Pt and Os(μ-H)Os protons at -15.87 (J(Pt-H) = 534, J(P-H) = 7.3Hz) and -21.82 (J(Pt-H) = 22, J(H-H) = 2Hz)ppm respectively. The shift to high field of the Os(μ-H)Os resonance (c.f. -8.01 p. p.m in 26b), is suggestive that 27 is saturated (vide supra). Signals due to two inequivalent methylene protons are observed at 7.02 (multiplet) and 6.61 (J(H-H) = 6.0 and 2.3Hz) p.p.m. A selective ^1H decoupling experiment reveals that the 6.0Hz splitting of the latter signal arises, unsurprisingly, from coupling to the other methylene proton, while coupling to the Os(μ-H)Os is presumably responsible for the smaller splitting of 2.3Hz.

These ^1H n.m.r studies provide no evidence for the formation of an analogue of 23 containing two Os(μ-H)Os hydrides, and, on standing, solutions of 27 show no new signals in the highfield region.

The spectroscopic data suggests that the structure of 27 closely resembles that of 24, and this was confirmed by a single crystal X-ray study by Dr. L.J. Farrugia.

The molecular structure of 27 is depicted in Figure 45. Relevant bond distances and angles are listed in Table 24. A *closo*-tetrahedral Os_3Pt core is maintained, and the increase in M-M separations within this framework, compared with those in 26b; is in keeping with the saturated nature of 27, and parallels the core expansion in 24 c.f. 19a. The CyNC ligand remains terminally bound to Pt, lying over the Pt-Os(2)-Os(3) face. The methylene function spans the Os(2)-Os(3) edge somewhat asymmetrically (Os(2)-C(11) = 2.08(3), Os(3)-C(11) = 2.20(3)Å). Thus the methylene and isocyanide functions share a common $PtOs_2$ face. Interestingly, C(6) and C(9), the two carbonyl moieties trans to C(11), interact weakly with the Pt centre, as evidenced by the comparatively short Pt---C(6) = 2.78(2) and Pt---C(9) = 2.87(2) Å separations and the corresponding Os-C-O angles of 162(2) and 172(2)°, for C6 and C9 respectively.

The M(μ-H)M and CH_2 hydrogen positions were not located experimentally and are included at calculated positions. In the former case, the HYDEX[271] program situates the hydrides at Os-Os and Os-Pt edges, in keeping with the ^1H n.m.r spectroscopic data.

As in 26b, the Pt atom in 27 adopts a pseudo-trigonal bipyramidal geometry and can be considered to donate 10 electrons to the valence electron count, hence 27 is a saturated 60 electron *closo*-tetrahedral complex, in keeping with common electron counting schemes.[54,55,57,75]

Apart from 23,24 and 27, two other methylene containing Os_3Pt clusters have been crystallographically defined, $Os_3Pt(\mu\text{-}H)_2(\mu\text{-}CH_2)(cod)(CO)_9$,[255] and $Os_3Pt(\mu\text{-}CH_2)(CO)_{11}(PPh_3)_2$,[254] shown in Figure 46. The former is structurally similar to 23 with the exception that the $Pt(CO)(PCy_3)$ group of 23 is replaced by a Pt(cod) unit. The latter has a "spiked-triangular" metal framework with the

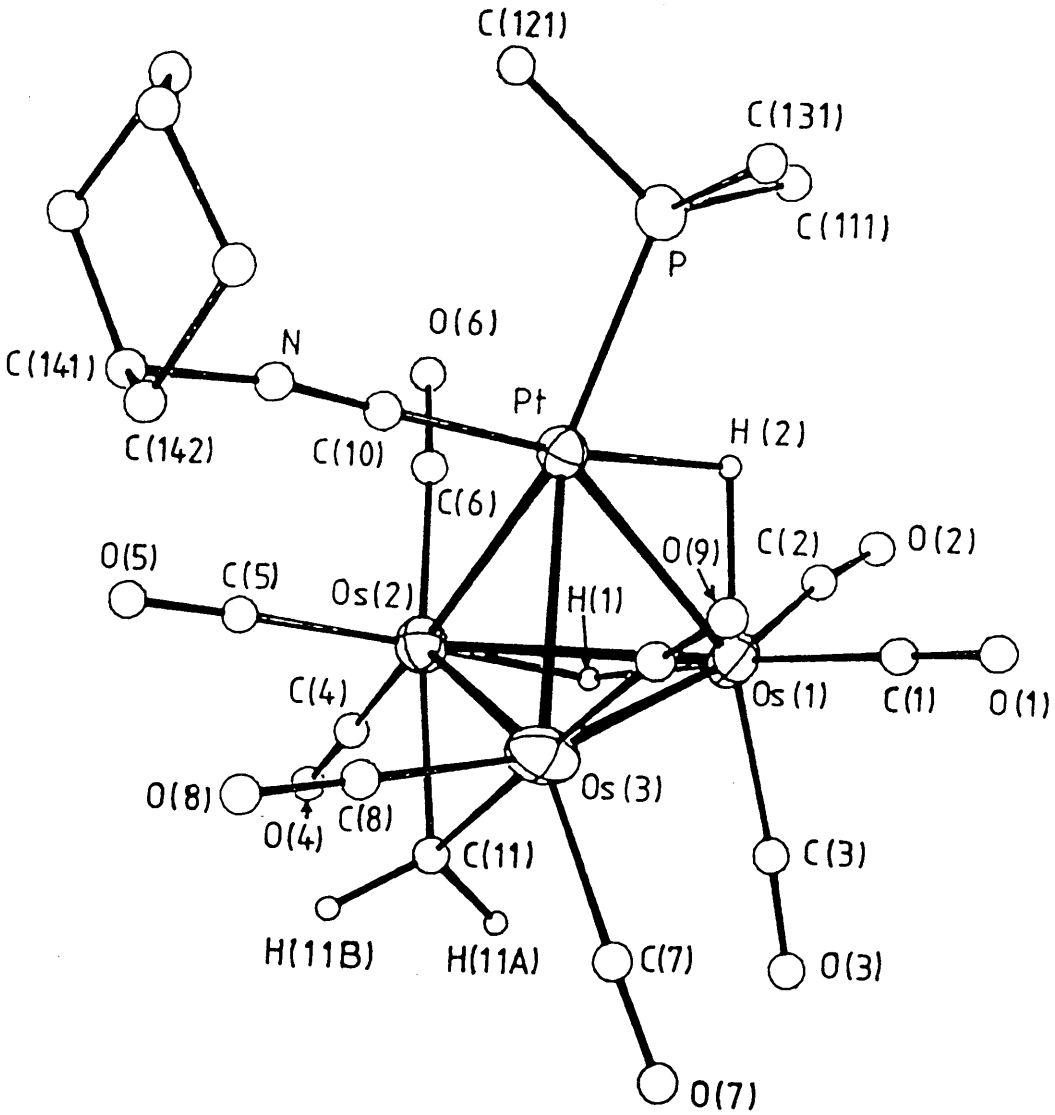

Figure 45 : The molecular structure of $Os_3Pt(\mu\text{-}H)_2(\mu\text{-}CH_2)(CO)_9(PCy_3)$-(CyNC), 27.

Table 24. Important bond lengths (Å) and bond angles (deg) for the complex $Os_3Pt(\mu\text{-}H)_2(\mu\text{-}CH_2)(CO)_9(PCy_3)(CyNC)$, 27

Bonds

Os(1)-Os(2)	2.965(2)	Os(2)-C(4)	1.86(2)
Os(1)-Os(3)	2.796(2)	Os(2)-C(5)	1.86(3)
Os(2)-Os(3)	2.841(2)	Os(2)-C(6)	1.83(3)
Pt -Os(1)	2.865(1)	Os(3)-C(7)	1.92(3)
Pt -Os(2)	2.858(1)	Os(3)-C(8)	1.89(3)
Pt -Os(3)	2.787(2)	Os(3)-C(9)	1.92(3)
Os(1)-C(1)	1.92(2)	Os(2)-C(11)	2.08(3)
Os(1)-C(2)	1.91(3)	Os(3)-C(11)	2.20(3)
Os(1)-C(3)	1.92(3)	Pt -C(10)	1.95(3)
Pt -P	2.322(5)	C(10)-N	1.12(3)
Pt....C(6)	2.78(2)	Pt....C(9)	2.87(2)

C-O (carbonyl) mean 1.14[1]

Angles

Os(1)-Pt -Os(2)	62.4(1)	Pt -Os(2)-Os(1)	58.9(1)
Os(1)-Pt -Os(3)	59.3(1)	Pt -Os(2)-Os(3)	58.6(1)
Os(2)-Pt -Os(3)	60.4(1)	Os(1)-Os(2)-Os(3)	57.5(1)
Pt -Os(1)-Os(2)	58.7(1)	Pt -Os(3)-Os(1)	61.8(1)
Pt -Os(1)-Os(3)	59.0(1)	Pt -Os(3)-Os(2)	61.0(1)
Os(2)-Os(1)-Os(3)	59.0(1)	Os(1)-Os(3)-Os(2)	63.5(1)
C(10)-Pt -P	95.5(6)	P -Pt -H(2)	77.7(2)
Os(2)-C(11)-Os(3)	83.2(8)	C(10)-N -C(141)	171(2)
Os(2)-C(6) -O(6)	162(2)	Os(3)-C(9) -O(9)	172(2)
Pt -C(10)-N	178(2)		

remaining Os-C-O mean 176[1]

methylene function bridging the Os-Pt bond. The 62 electron count of this species is two less than expected[54,55,57,75] and arises from the pseudo-square planar coordination geometry around the Pt centre, rendering it a 16 rather than 18 electron metal.

Hoffmann[108] has argued that the PtL_2 unit can be viewed as an inorganic "methylene" and, hence, this complex can be viewed as substituted derivative of $Os_3(CO)_{12}$, where the substituent is the "inorganic ethylene" $(Ph_3P)_2Pt{=}CH_2$.

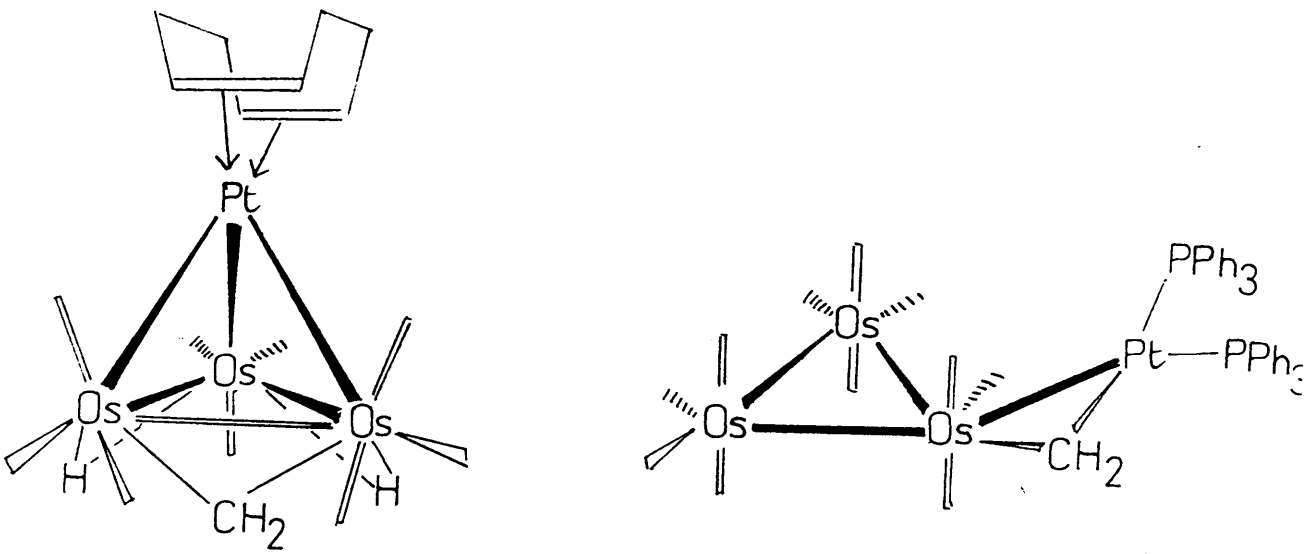

Figure 46. Structures of $Os_3Pt(\mu\text{-}H)_2(\mu\text{-}CH)_2(cod)(CO)_9$ and $Os_3Pt(\mu\text{-}CH_2)(CO)_{11}(PPh_3)_2$.

The carbonyl region of the ^{13}C n.m.r spectrum of a ^{13}CO enriched sample of 27 at 298K is presented in Figure 47, and a listing of relevant parameters is given in Table 25. The ^{13}C n.m.r spectrum displays nine resonances of unit intensity in the range 184.2 - 169.8 p.p.m, typical of terminal carbonyl signals. All resonances except b display ^{195}Pt satellites, and by consideration of the magnitudes of the ^{195}Pt - ^{13}C coupling constants, it is evident that no carbonyl moiety is directly bound to the Pt atom.

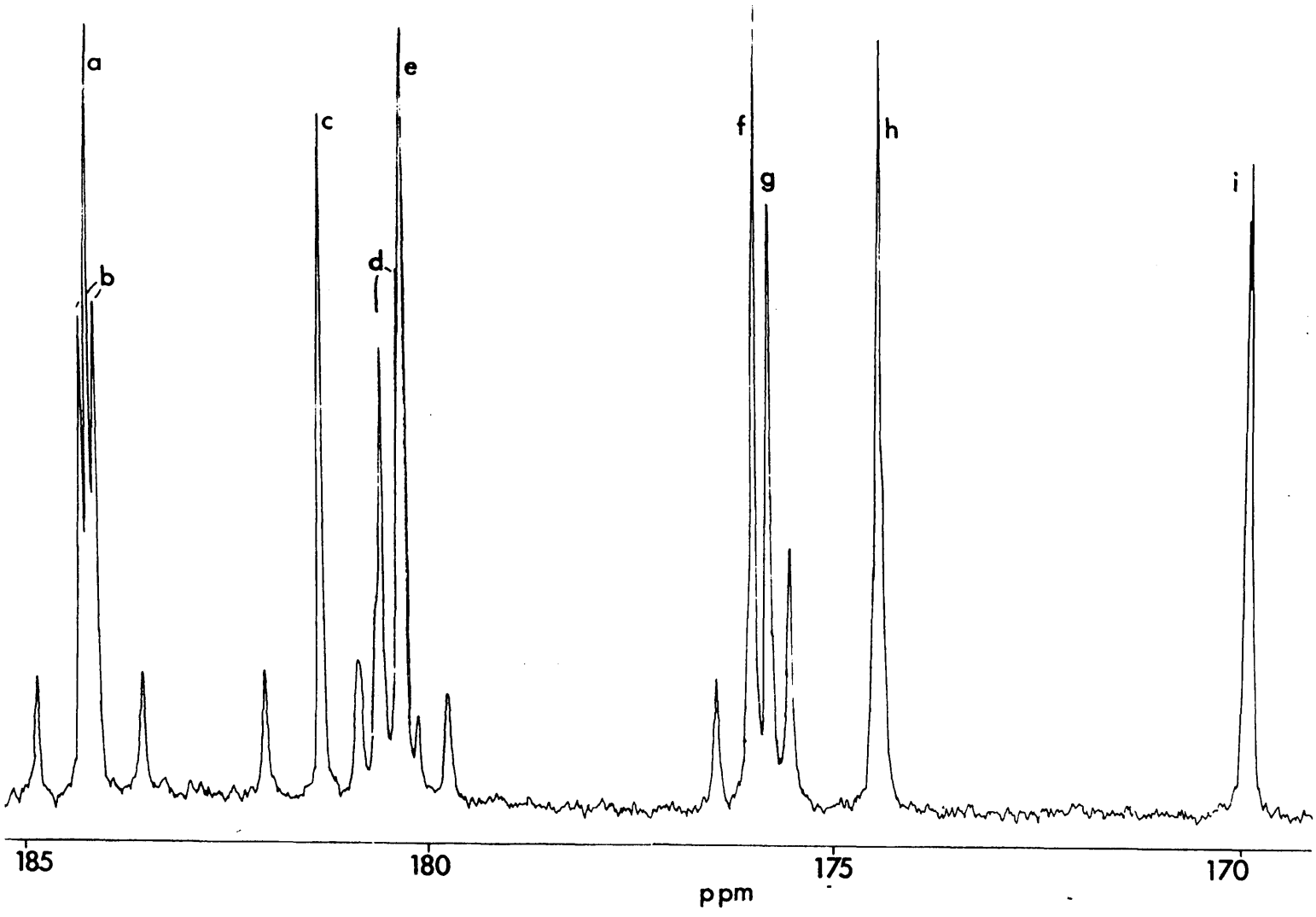

Figure 47: The $^{13}C\{^{1}H\}$ n.m.r spectrum of $Os_3Pt(\mu\text{-}H)_2(\mu\text{-}CH_2)(CO)_9(PCy_3)(CyNC)$, 27 at 298K.

Table 25 : ^{13}C n.m.r parameters for $Os_3Pt(\mu\text{-}H)_2(\mu\text{-}CH_2)(CO)_9(CNCy)(PCy_3)$, 27.

Signal [b]	Chem. Shift p.p.m.	Assignment [d]	J (Hz) [c] Pt-C	P-C	H2[d]-C	H1[d]-C	H11A[d]-C	H11B[d]-C
a	184.2	C9	66	-	-	-	-	-
b	184.2	C7	-	8.8	w	w	-	2
c	182.3	C6	69.7	-	-	3.0	-	-
d	180.5	C4	25.3	10.5	-	3.6	w	w
e	180.3	C3	55.8	-	7.9	2.9	w	w
f	176.0	C2	44.9	-	3.7	4.3	-	-
g	175.8	C8	22.5	-	-	-	3.3	w
h	174.4	C1	5[a]	-	3.1	10.4	-	-
i	169.9	C5	4[a]	1.3	-	11.5	2.0	w

T = 298K, CD_2Cl_2

a - from line narrowed spectrum

b - see Figure 47; c-w indicates small unresolved coupling

d - for labelling scheme see Figure 45.

The results of selective $^{13}C-\{H\}$n.m.r experiments are consistent with the solid state structure being maintained in solution. Three resonances, e,f and h, are coupled to both H1 and H2 indicating that the hydrides bridge adjacent Pt-Os and Os-Os edges. By consideration of the magnitudes of hydride proton coupling to these signals, e, f and h can be assigned to C3,C2 and C1 respectively. The resonances c,d and i are also coupled to H1 and correspond to C4,5 and 6. Assignments within this group are made as follows. The large $^{2}J(H-C)$ splitting of signal i due to H1 assigns i to C5, trans to H1. Signals c and d are assigned by reference to the solid state structure where a carbonyl group ligated to each Os atom of the $Os(\mu-CH_2)Os$ unit interacts weakly with the Pt centre. Due to this interaction, such carbonyls might be expected to have relatively large $^{195}Pt-^{13}C$ coupling constants. Thus, c may be assigned to C6 and d to C4.

The remaining resonances, a,b and g correspond to C7,8 and 9. In the light of the preceding $^{195}Pt-^{13}C$ coupling arguments, a may be attributed to C9; assignments of b to C7 and g to C8 are tentatively made on the basis of observed couplings to the methylene protons. Furthermore these assignments are compatible with the proposed racemisation of 27, (see below) which equivalences b/d and g/i.

The carbonyl ligands in 27 are markedly less fluxional than those in 19a,[265] and 26b which, likewise, contain *closo*-tetrahedral Os_3Pt metal cores. At 298K, ^{13}C n.m.r studies reveal the Os-ligated carbonyls in 19a[265] and 26b are in rapid exchange (vide supra). However, for 27, at the same temperature, the carbonyl resonances are sharp. This indicates that any CO exchange processes must be sufficiently slow on the n.m.r timescale as to produce no line broadening.

The 2D exchange correlation NOESY experiment can detect exchange processes with rates that are orders of magnitude smaller than those which can be observed by exchange broadening.[329] This technique has recently been applied to elucidate the dynamic behaviour in cluster systems[265,330,331] and was used to investigate the fluxionality in complex 27. Correlations between peaks arise from three sources:- a) scalar coupling; b) dipolar coupling, i.e. N.O.E; and c) chemical exchange. At the level of ^{13}CO enrichment in 27 (ca. 10%) contributions from (a) and (b) can be discounted (in addition, the mixing time t_m was varied by ± 15% to reduce contributions from (a)).

At 298K, a symmetrised 2D exchange correlation NOESY ^{13}C n.m.r spectrum (t_m = 0.5s) (Figure 48a) displays off-diagonal peaks relating e, f and h, indicating a slow exchange of C1,C2 and C3, by rotation of the $Os(1)(CO)_3$ group.

The 2D exchange correlation NOESY spectrum at 318K (t_m = 1.0s) is shown in Figure 48(b). Resonances a/b, d/e and f/g are fortuitously coincident at this temperature which confuses analysis of this spectrum. Nevertheless, there is evidence for three separate dynamic processes involving i) rotation of $Os(1)(CO)_3$ and ii)$Os(3)(CO)_3$ groups and iii) cluster racemisation:-

i) The exchange of e,f and h (C3/2/1) is more rapid than at 298K, as indicated by the more intense off-diagonal peaks relating these signals.

ii) The peak relating a/b to f/g is assumed to correspond to the exchange of a,b and g (C9,7,8) resulting from slow tripodal rotation of the $Os(3)(CO)_3$ group. Due to the overlap of a with one peak of the doublet resonance b, this off-diagonal peak should appear as a "doublet" of intensity 3:1, however, as the rate of exchange is slow

Figure 48 : Symmetrised 2D exchange correlation NOESY ^{13}C n.m.r spectrum of ^{13}CO enriched $Os_3Pt(\mu\text{-}H)_2(\mu\text{-}CH_2)(CO)_9(PCy_3)(CyNC)$ a) at 298K, t_m=0.5s; b) at 318K, t_m=1.0s.

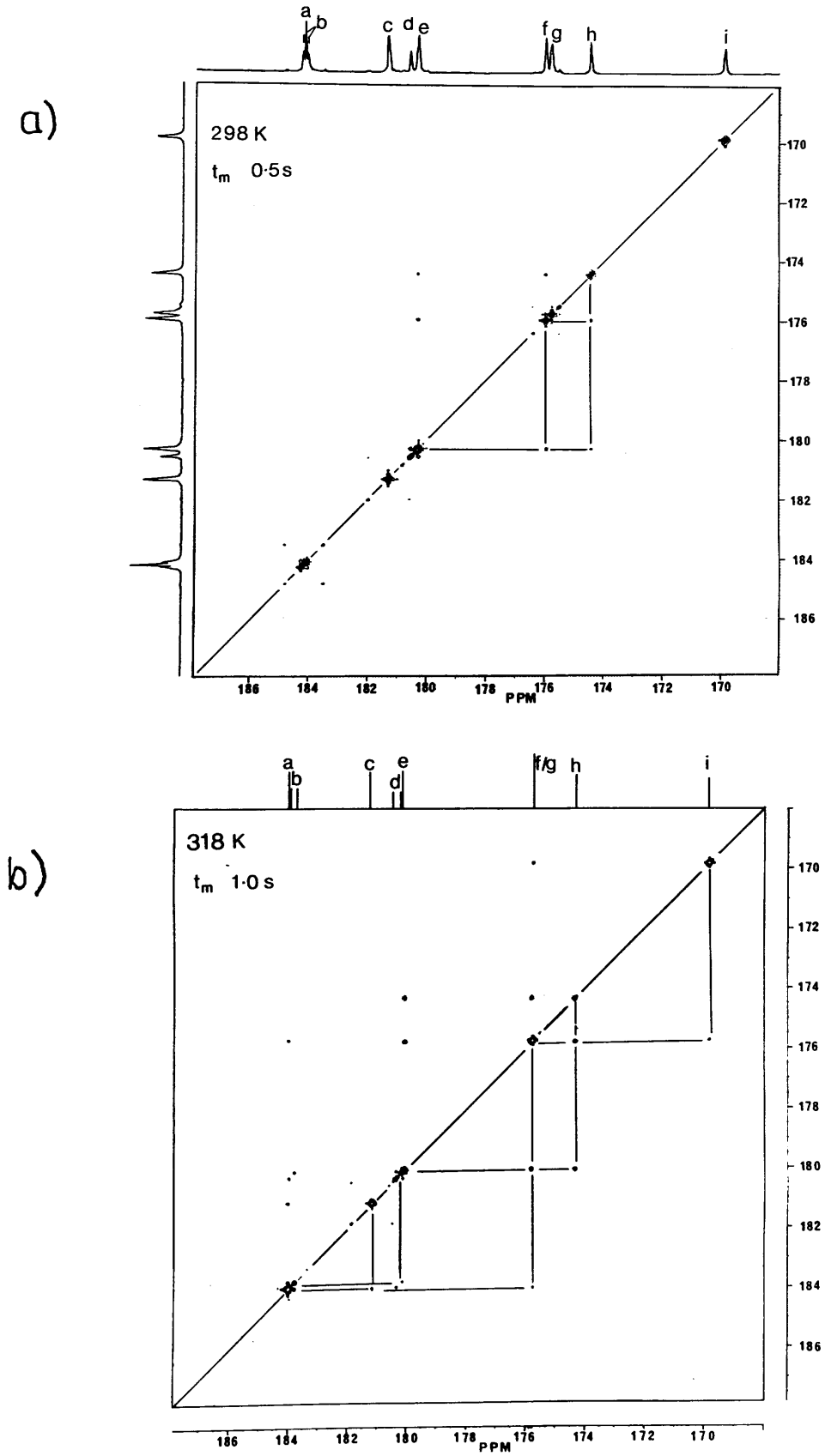

only the more intense signal is observed as a "pseudo" singlet. The off-diagonal peak relating a to b is difficult to observe due to the overlap of these resonances.

iii) The characteristic doublet, parallel to the diagonal, that relates a/b to d/e can be unambiguously assigned to exchange of the doublet resonances b and d (C7/4), while exchange between a and c (C9/6) is shown by an off-diagonal singlet peak. i is in exchange with f or g,i.e. C5 exchanges with C2 or C8. If it is assumed that C5 exchanges with C8 (i.e. i/g), the spectroscopic data is compatible with a slow racemisation process involving formal transfer of the Os(μ-H)Os proton to the unbridged Os-Os edge. Such a process would also exchange f/h i.e. C2/C1, however as the racemisation is slow compared with the tripodal rotation exchanging e, f and h, the expected increased rate of exchange between f/h is difficult to detect. The mechanism proposed in Figure 49 accounts for this racemisation as well as the slow exchange of Os(μ-H)Os and Os(μ-H)Pt hydrides observed by line broadening in the ^{1}H n.m.r spectrum of 27 at higher temperatures.

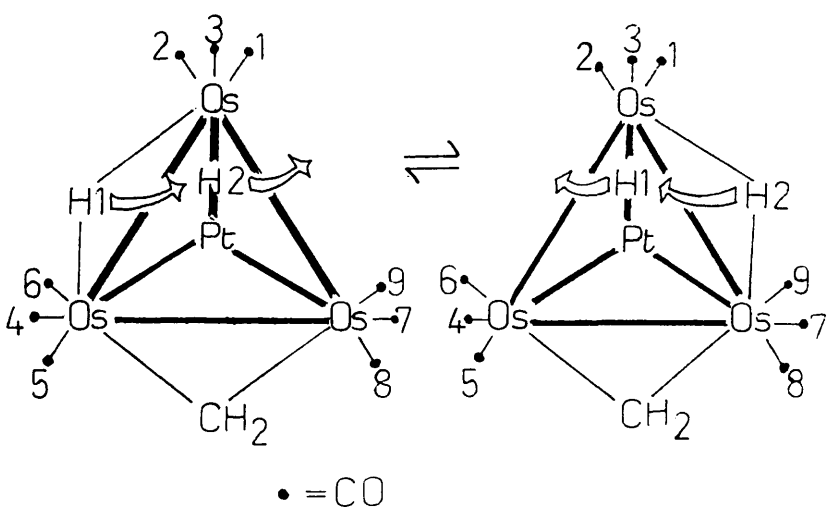

Figure 49 : Proposed mechanism for racemisation of 27 and H1/H2 exchange.

Cluster ligated CH_2 functions are considered to model surface bound methylene species in Fischer-Tropsch syntheses.[272,273] In this context, it is of considerable interest that C-H formation (effected by e.g. insertion of CH_2 into a M-H-M unit[101-104] and protonation of CH_2[226]) and C-C coupling (by coupling with CO[274-276], unsaturated hydrocarbon ligands[275,276] etc.) occur at cluster bound methylene sites.

The CyNC and CH_2 moieties share a common $PtOs_2$ face in 27, and, in view of the reactivity of CH_2 towards insertion, the possibility of inducing methylene-isocyanide coupling in 27 was examined. However thermolysis failed to produce any tractable products, and 27 is unreactive towards CO (50 atm) at ambient temperatures. At higher temperatures, treatment of 27 with CO and, similarly, PPh_3 yield numerous products in very low yield. Any insertion reactions are clearly not facile processes and these reactions were not investigated further.

Several points of interest have been revealed in this investigation of the chemistry of isocyanide substituted Os_3Pt systems. Firstly there is no evidence for the insertion of hydrides into the CNR function in any of the new complexes, in contrast to the observed behaviour of the isocyanide adducts and derivatives of 4.[89,91] Secondly, the first substituted analogue of complexes 19, 26a,b have been prepared and the site of ligand substitution is the Pt centre. The reactivity of 26b towards CH_2N_2 and CO is somewhat different to that of 19 as only one isomer of the methylene adduct, 27, is observed and the disposition of hydrides about the metal framework in isomer A of 25a,b differs from that observed in 20.

2.2.3 Reactions of $Os_3Pt(\mu\text{-}H)_2(CO)_{10}(PCy_3)$ with Inorganic Carbenes.

i.) Reaction of $Os_3Pt(\mu\text{-}H)_2(CO)_{10}(PCy_3)$ with SO_2.

The coordination chemistry of SO_2 has been well researched[277-279] however, the number of cluster compounds containing SO_2 ligands remains comparatively small.[280-282] The majority of these are trimetallic Pd or Pt clusters (see ref. 280) although recently, Rh,[283] Ir,[281] Fe[280] and Os[107] clusters with coordinated SO_2 have been reported. In view of the variety of coordination modes displayed by SO_2 in mononuclear complexes[277-279] it is somewhat surprising that in all but two SO_2 containing clusters, the SO_2 adopts a μ_2-$\underline{S}O_2$ M-M bridging configuration. The exceptions are $Rh_4(\mu\text{-}CO)_4(\mu\text{-}SO_2)(\mu_3\text{-}\eta^2\text{-}SO_2)_2\{P(OPh)_3\}_4$,[283] and $Pd_5(\mu\text{-}SO_2)_2(\mu_3\text{-}\eta^2\text{-}SO_2)_2(PMe_3)_5$,[284] where 4 electron donor μ-η^2-$\underline{S},\underline{O}$ SO_2 moieties are found. Coordination of SO_2 to a heterometallic framework is particularly rare, and only a few *closo*-tetrahedral Pt_3Au complexes of this kind have been reported.[285]

Hoffmann et al[286] have detailed the frontier orbital similarity between SO_2 and CH_2 and, in view of the interest in investigating the reactivity of 19 towards inorganic carbenes, a study of the reaction of SO_2 with 19a was undertaken.

Saturating a CH_2Cl_2 solution of 19a with SO_2 at 298K effected a rapid colour change from dark green to red. Addition of hexanes to this solution and overnight standing at -30^oC yielded $Os_3Pt(\mu\text{-}H)_2(\mu\text{-}SO_2)(CO)_{10}(PCy_3)$, 28, as a red/purple crystalline solid. The solution i.r. spectrum of 28 indicates that the CO ligands are terminally bound (ν_{CO}, 2101-1968 cm^{-1}), while the bands at 1040 and 1195 cm^{-1} observed in the solid state (KBr disc) i.r spectrum are typical of μ-SO_2 coordinated S-O stretching frequencies.[278]

The ^{1}H n.m.r spectrum of 28 recorded immediately following dissolution of a pure, crystalline sample, shows three high field resonances in 1:1:0.34 intensities. The 1:1 signals are at -14.48 (J(P-H) = 7.9, J(Pt-H) = 574Hz) and -20.66 p.p.m (J(P-H) = 1.5, J(Pt-H) = 19Hz). The low intensity signal occurs at -20.20 p.p.m. (J(P-H) = 3.1, J(Pt-H) = 15Hz). A similar ratio of intensities is observed in all recorded spectra of 28, which suggests that 28 exists in solution, as a mixture of two isomers. The major species contains two hydrides that span Pt-Os and Os-Os edges, while for the minor complex the high field signal arises from Os(μ-H)Os hydride coordination.

The ^{1}H n.m.r and i.r spectroscopic data suggest that the major solution species has a similar structure to complex 24, the C_1 isomer of $Os_3Pt(\mu\text{-}H)_2(\mu\text{-}CH_2)(CO)_{10}(PCy_3)$, with $\mu\text{-}SO_2$ replacing $\mu\text{-}CH_2$. This was confirmed by an X-ray diffraction experiment.

Crystal Structure of 28.

An X-ray diffraction study of 28 was undertaken by Dr. L.J. Farrugia. The structure is depicted in Figure 50, while important bond lengths and angles are given in Table 26. The metal core of 28 retains the *closo*-tetrahedral framework of 19 while the overall cluster geometry closely resembles that of 24,[258] with the $\mu\text{-}SO_2$ group replacing $\mu\text{-}CH_2$. The hydride locations in 28 were not directly observed and are included at Os-Os and Os-Pt edge bridging positions, as calculated by the program HYDEX.[271] These positions are consistent with the high field ^{1}H resonances due to the major isomer.

28 is a saturated 60 electron species and, as expected, there are no unusually short M-M bonds. With the exception of the SO_2 bridged Os(1)-Os(3) vector, the metal-metal bond distances are very similar to those of 24, with corresponding bond lengths differing by

Figure 50 : Crystal structure of $Os_3Pt(\mu\text{-}H)_2(\mu\text{-}SO_2)(CO)_{10}(PCy_3)$, 28.

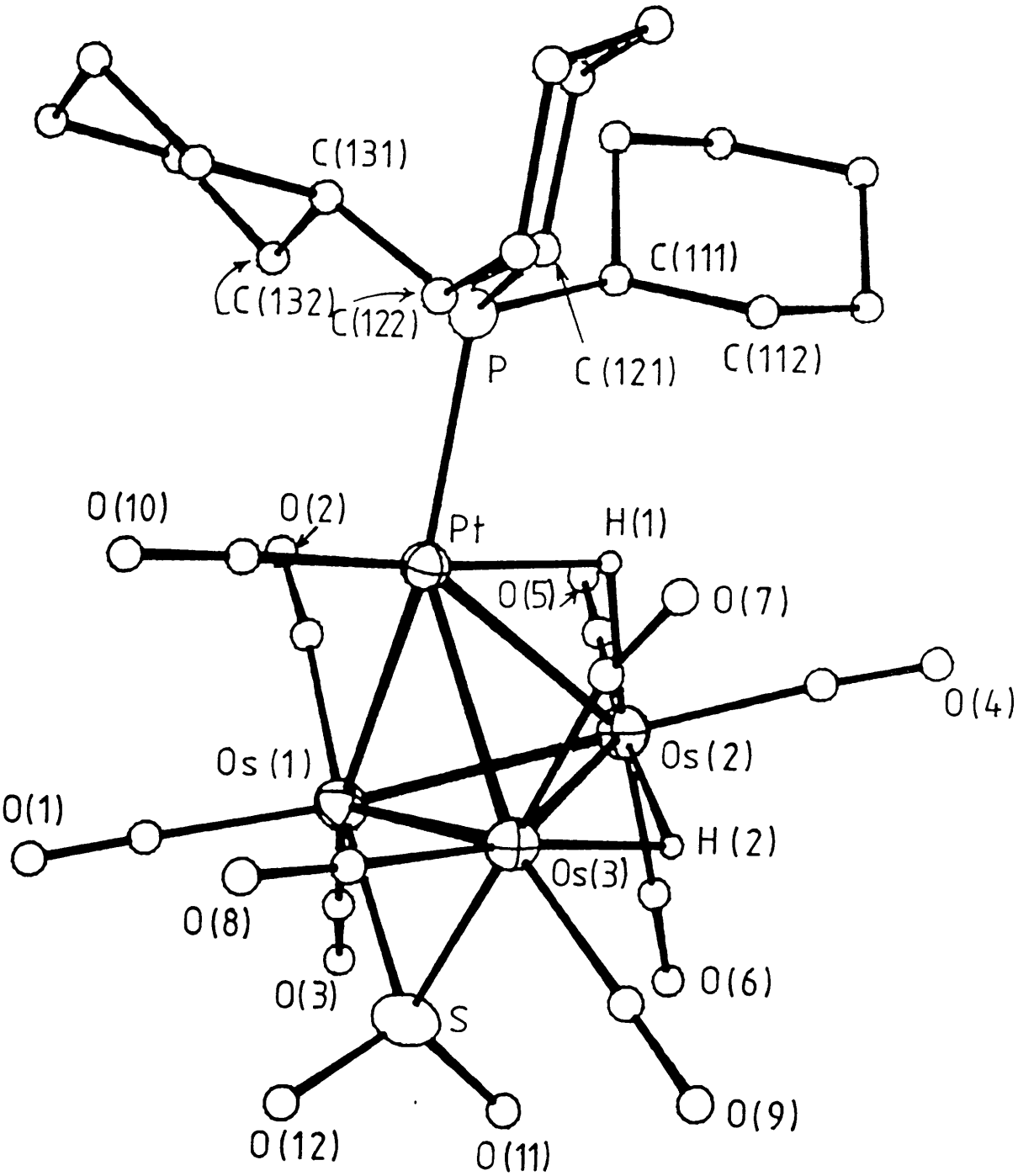

Table 26 : Selected Bond Lengths (Å) and Bond Angles (deg) for

$Os_3Pt(\mu\text{-}H_2)(\mu\text{-}SO_2)(CO)_{10}(PCy_3)$, 28

Bond Lengths

Os(1) - Os(2)	2.795(1)	Os(1) - Os(3)	2.988(1)
Os(1) - Pt	2.792(1)	Os(1) - S	2.367(3)
Os(1) - C(1)	1.943(12)	Os(1) - C(2)	1.923(10)
Os(1) - C(3)	1.899(11)	Os(2) - Os(3)	2.976(1)
Os(2) - Pt	2.906(1)	Os(2) - C(4)	1.945(11)
Os(2) - C(5)	1.912(12)	Os(2) - C(6)	1.934(10)
Os(3) - Pt	2.821(1)	Os(3) - S	2.346(3)
Os(3) - C(7)	1.964(9)	Os(3) - C(8)	1.876(11)
Os(3) - C(9)	1.903(10)	Pt - P	2.359(3)
Pt - C(10)	1.847(11)	S - O(11)	1.444(7)
S - O(12)	1.475(8)	Pt-----C(2)	2.785(9)
		Pt-----C(7)	2.748(9)

mean C-O = 1.130

Bond Angles.

Os(2) - Os(1) - Pt	62.7(1)	Os(2) - Os(1) - S	87.4(1)
Os(3) - Os(1) - S	50.4(1)	Os(3) - Os(1) - Pt	58.3(1)
Pt - Os(1) - S	108.5(1)	Os(3) - Os(1) - C(1)	103.4(4)
S - Os(1) - C(1)	89.0(4)	Pt - Os(1) - C(1)	102.9(4)
S - Os(1) - C(3)	88.3(4)	S - Os(1) - C(2)	175.5(3)
Os(1) - Os(2) - Os(3)	62.3(1)	Os(1) - Os(2) - Pt	58.6(1)
Os(1) - Os(3) - Pt	57.4(1)	Os(3) - Os(2) - Pt	57.3(1)
Os(2) - Os(3) - S	83.6(1)	Os(1) - Os(3) - Os(2)	55.9(1)
Pt - Os(3) - S	108.1(1)	Os(1) - Os(3) - S	51.0(1)
S - Os(3) - C(7)	175.0(3)	Os(2) - Os(3) - Pt	60.1(1)
Os(1) - Pt - Os(2)	58.7(1)	Os(1) - Pt - Os(3)	64.3(1)
Os(1) - Pt - P	150.6(1)	Os(2) - Pt - P	116.0(1)
Os(2) - Pt - Os(3)	62.6(1)	Os(3) - Pt - P	142.6(1)
Os(1) - S - Os(3)	78.7(1)	P - Pt - C(10)	95.5(4)
Os(1) - S - O(12)	113.4(4)	Os(1) - S - O(11)	118.2(4)
Os(3) - S - O(12)	112.3(4)	Os(3) - S - O(11)	116.3(3)
Os(3) - C(7) - O(7)	165.7(8)	O(11) - S - O(12)	113.5(5)
		Os(1) - C(2) - O(2)	169.6(9)

Remaining M-C-O mean = 177.7

0.003 - 0.033 Å.

Os(1)-Os(3) is 0.123 Å longer than the methylene bridged Os-Os separation in 24. This elongation can be attributed to the increased steric requirements of μ-SO_2 over μ-CH_2. A similar effect has been commented on by Jarvinen and Ryan[107] in their comparative structural analysis of $Os_3(\mu\text{-}H)_2(\mu\text{-}CH_2)(CO)_{10}$ and $Os_3(\mu\text{-}H)_2(\mu\text{-}SO_2)(CO)_{10}$ The SO_2 ligand spans the Os(1)-Os(3) vector slightly asymmetrically, with Os(1)-S = 2.367(3), and Os(3)-S = 2.346(3) Å. These Os-S distances are in close agreement with those observed in $Os_3(\mu\text{-}H)_2(\mu\text{-}SO_2)(CO)_{10}$,[107] (of 2.360(2), and 2.358(2) Å), while the Os-S-Os angles in both clusters [78.7(1)° in 28; 75.7(6)° in $Os_3(\mu\text{-}H)_2(SO)_2(CO)_{10}$] are also similar.

The Os bound carbonyl ligands trans to the bridging SO_2 function, C(2)-O(2) and C(7)-O(7) form weak bonding interactions with the Pt centre, as evidenced by Os-C-O angles of 169.6(9) and 165.7(8)° and Pt---C separations of 2.785(9) and 2.748(9) Å respectively. Similar weak interactions were observed in the solid state structures of 24[258] and 27 (vide supra). Finally, the S atom is almost coplanar with the PtOs(1)Os(3) triangle with a Pt-Os(1)-Os(3)-S dihedral angle of 174.2°.

N.m.r studies of the addition of SO_2 to $Os_3Pt(\mu\text{-}H)_2(CO)_{10}(PCy_3)$

The course of the reaction of SO_2 with 19a in solution was followed using multinuclear n.m.r spectroscopy. This investigation showed that the reaction is very complex, with three hydride containing species formed on SO_2 addition to 19a at 195K and, on warming such a solution to ambient temperatures, these give way to five new hydrido-cluster products. Addition of SO_2 to 19a at 298K yields the same five species. Furthermore the relative proportion of each species formed is dependent on time, temperature and concentration of excess

SO_2 in solution.

i) Addition at 195K.

Addition of excess SO_2 to a green solution of 19a in CD_2Cl_2 at 195K gave a dark yellow solution. The ^1H n.m.r spectrum of the reaction mixture in the hydride region is shown in Figure 51(a). One major product, complex A, is formed in ~80% yield. Important ^1H, ^{31}P and ^{13}C n.m.r parameters for A are listed in Table 27.

The high field ^1H resonance at -13.92 p.p.m is assigned to an Os(μ-H)Pt hydride, H1, on the basis of the large ^{195}Pt coupling (J(Pt-H) = 802Hz), while the signal at -18.94 p.p.m is attributed to an Os(μ-H)Os hydride, H2. Selective decoupling experiments show that the two hydride resonances are mutually coupled (J(H-H) = 2Hz), which suggests they span adjacent M-M edges. The ^{31}P n.m.r spectrum of species A displays a singlet resonance at 69.9 p.p.m. with a large ^{195}Pt coupling of 4505Hz indicating that the phosphine function remains bound to the Pt centre. The ^{13}C n.m.r spectrum of a ^{13}CO enriched sample of A recorded at 218K (Figure 51b) shows ten distinct carbonyl resonances in the terminal CO range. Interestingly, no carbonyl signal shows a large coupling to ^{195}Pt which is clear evidence that there is no Pt ligated carbonyl. For other Os_3Pt clusters with direct Pt-CO bonds reported in this Thesis and elsewhere[265], $^1J(^{195}Pt-C)$ couplings normally range between 1500-1800Hz. Therefore, it seems likely that species A has a SO_2 function ligated to Pt.

The spectroscopic data for A do not unambiguously define the structure, nevertheless certain structural features can be deduced. The ten ^{13}C carbonyl resonances indicate A has low symmetry. Furthermore, selective ^1H decoupling experiments show that seven carbonyl resonances couple to H2, suggesting that the Os(μ-H)Os

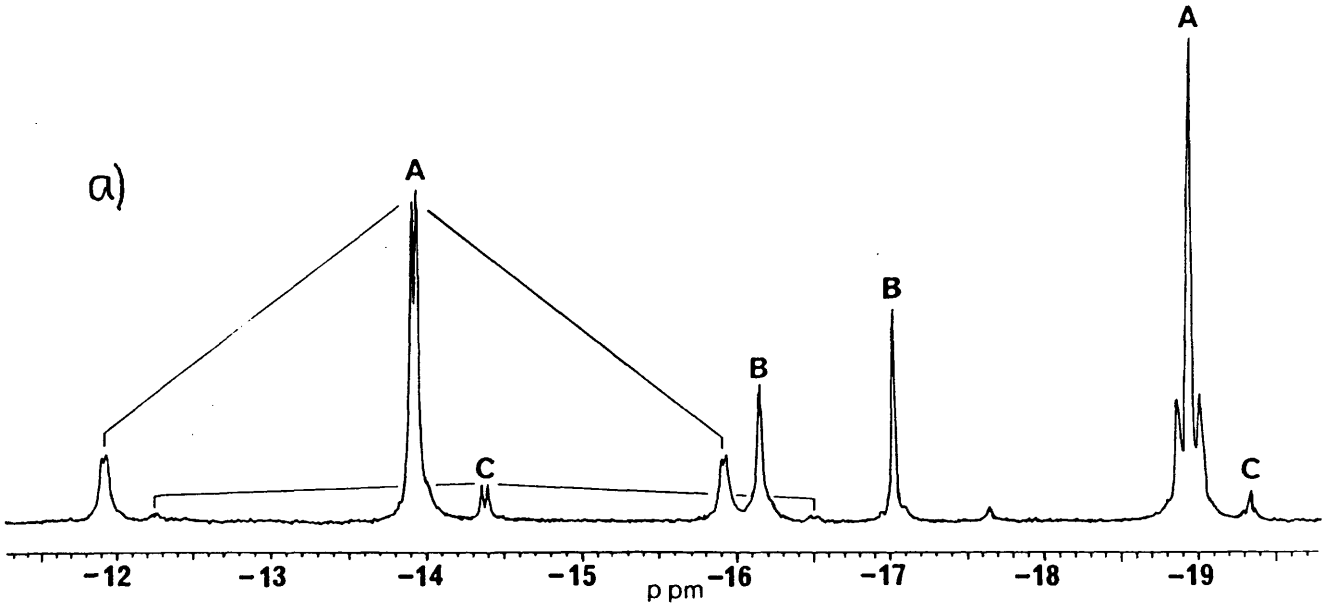

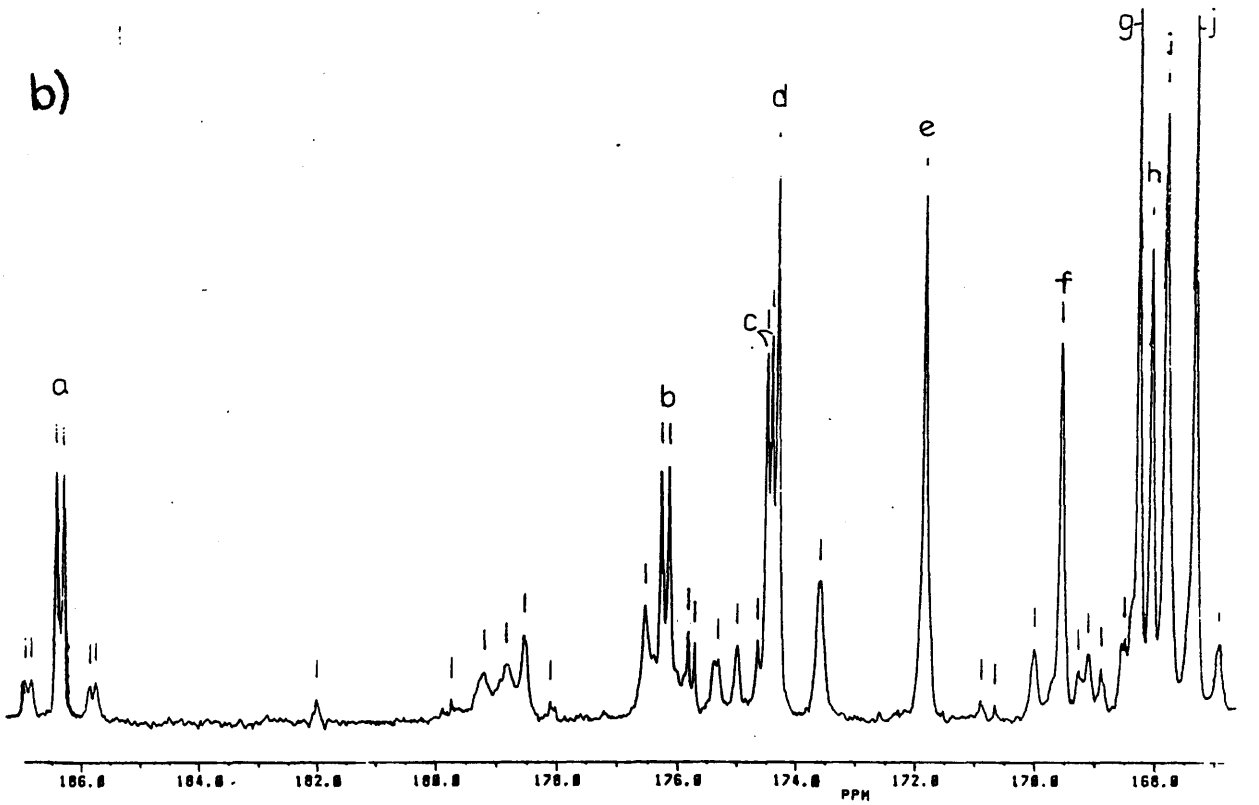

Figure 51(a)-^{1}H and (b)-^{13}C n.m.r spectra of reaction mixture following SO_2 addition at 195K.

Table 27. NMR Parameters for Species A.

reson [a]	chem shift/δ ppm	mult [b]	assgnt [c]	J/Hz ^{31}P	J/Hz ^{195}Pt	J/Hz H1	J/Hz H2
		^{13}C Data					
a	186.3	d	4/5/6	6.0	55	-	-
b	176.2	d	4/5/6	6.4	*	-	-
c	174.5	d	1	4.3	-	5	3.6
d	174.3	s	3	-	-	14.0	2.0
e	171.8	s	4/5/6	-	-	-	-
f	169.6	s	7/9/10	-	45	-	2.0
g	168.3	s	7/9/10	-	-	-	2.9
h	168.1	s	2	-	*	2.8	8.4
i	167.8	s	7/9/10	-	-	-	2.8
j	167.3	s	8	-	-	-	8.4
		^{1}H Data					
H1	-13.92	dd	Os(μ-H)Pt	7	802		2
H2	-18.94	t	Os(μ-H)Os	2	30	2	
		^{31}P Data					
	69.90	s			4505		

218K, CD_2Cl_2 (a) - see Figure 51(b); (b) multiplicities for ^{13}C and ^{31}P based on ^{1}H decoupled spectra; (c) assignments refer to Figure 52. (*) indicates a small resolved ^{195}Pt coupling was expected based on signal intensity, but was obscured by overlapping resonances.

hydride spans a vector between an $Os(CO)_3$ and $Os(CO)_4$ group. As three of these carbonyl resonances show coupling to H1, it seems likely that the Os(μ-H)Pt hydride bridges from the Pt centre to the same $Os(CO)_3$ site. Thus H1 and H2 span proximate M-M vectors, as suggested by the observed H-H coupling between the hydride signals. Three carbonyl resonances show no coupling to H1 or H2 and are attributed to an $Os(CO)_3$ unit remote from the hydrides. A suggested structure for A is shown in Figure 52 but this is by no means the only structural possibility consistent with the n.m.r data. Due to the inherent instability of A, it has not proved possible to obtain i.r data which would be useful in determining the coordination of SO_2 to the cluster framework.[278] Due to lack of microanalytical data and the excess SO_2 used in these experiments the number of SO_2 ligands in A is not certain.

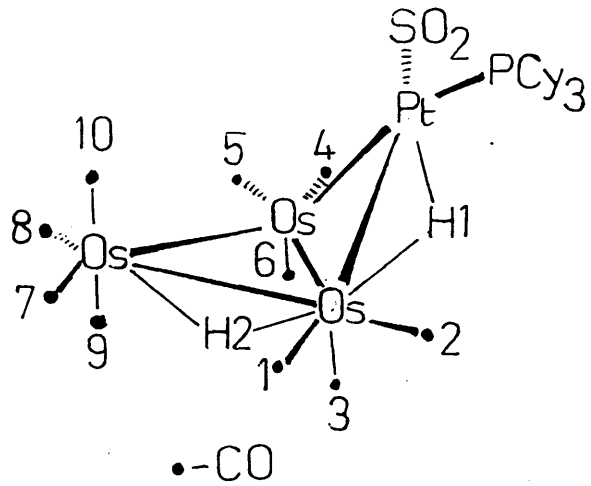

Figure 52 : Proposed structure for A.

Low intensity signals due to two other species, B and C are also observed in the ^{1}H and ^{31}P n.m.r spectra of the reaction mixture formed at 195K (Figure 51a). B shows two distinct Os(μ-H)Os proton resonances at -16.15 and -17.03 p.p.m.; these signals are mutually coupled (J(H-H) = 1.6Hz) suggesting adjacent hydrides. Smaller quantities of C are formed which have Os(μ-H)Os and Os(μ-H)Pt hydrides. In both B and C the phosphine functions are bound to the Pt atom, from ^{31}P n.m.r evidence. ^{1}H and ^{31}P n.m.r parameters for complexes B and C are cited in Table 28. It is noteworthy that the parameters for C resemble those of A. Structures that are consistent with the spectroscopic data are shown in Figure 53.

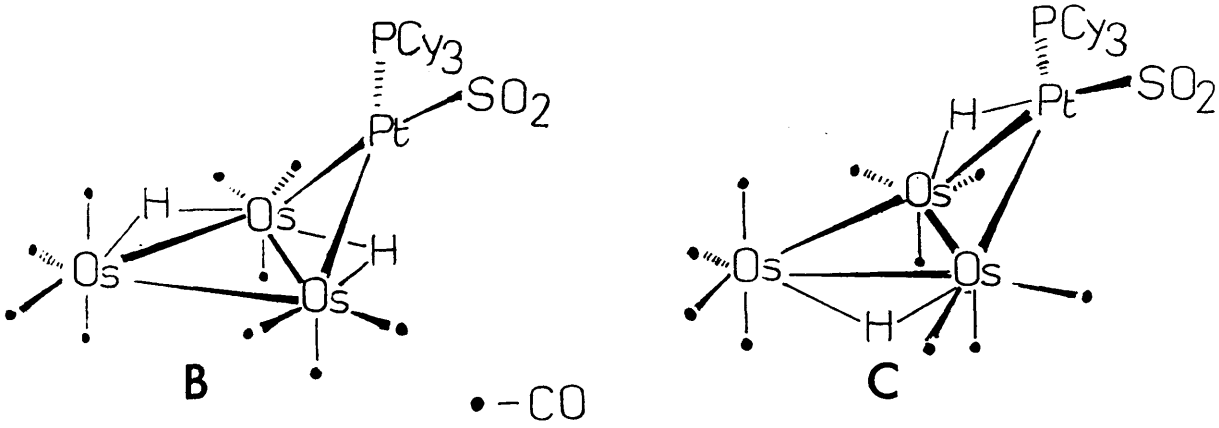

Figure 53: Proposed structures for species B and C.

Table 28. ^{1}H and ^{31}P Data for Species B - G.

Species B [a]

^{1}H ppm -16.15 (t, J(P-H) = 1.7, J(H-H) = 1.6, J(Pt-H) = 14 Hz)

-17.03 (d, J(H-H) = 1.6 Hz)

^{31}P ppm 56.6 (s, J(Pt-P) = 1892 Hz)

Species C [a]

^{1}H ppm -14.35 (d, J(P-H) = 8.5, J(Pt-H) = 851 Hz)

-19.35 (d, J(P-H) = 2.0, J(Pt-H) = 18 Hz)

^{31}P ppm 69.93 (s, J(Pt-P) = 4396 Hz)

Species D [b]

^{1}H ppm -14.48 (d, J(P-H) = 7.9, J(Pt-H) = 574 Hz)

-20.66 (d, J(P-H) = 1.5, J(Pt-H) = 19 Hz)

^{31}P ppm 73.0 (s, J(Pt-P) = 2617 Hz)

Species E [b]

^{1}H ppm -20.20 (d, J(P-H) = 3.1, J(Pt-H) = 15 Hz)

^{31}P ppm 9.3 (s, J(Pt-P) = 2402 Hz)

Species F [c]

^{1}H ppm -15.02 (s)

-18.15 (s, J(Pt-H) = 28 Hz)

^{31}P ppm 46.2 (s, J(Pt-P) = 2222 Hz)

Species G [b]

^{1}H ppm -17.57 (t, J(Pt-H) = 15, J(P-H) = J(H-H) = 1.6 Hz)

ppm -18.22 (t, J(Pt-H) = 12, J(P-H) = J(H-H) = 1.6 Hz)

CD_2Cl_2 [a] 218 K [b] 298 K [c] 233 K

ii) N.m.r Studies at 298K.

Spectra obtained during the warming of a solution containing A-C (prepared at 195K) to 298K indicate that A rapidly converts to B which, in turn, decomposes to yield a mixture of five new products D-H. ^{1}H and ^{31}P n.m.r parameters for each of these complexes are listed in Table 28. The ^{1}H n.m.r spectra of the resultant solution are essentially identical to those recorded after addition of SO_2 to 19a at 298K. The hydride region of the ^{1}H n.m.r spectrum of the initially formed species at 298K is presented in Figure 54(a). The predominant species is D, attributed to the isolated complex 28. The relative concentrations of D-H vary with time, temperature and concentration of free SO_2. The spectrum recorded 12 hours after reaction at 298K in the presence of excess SO_2 is shown in Figure 54(b). Signals due to F and G lose intensity with time, while the relative concentration of H increases. If the excess SO_2 is removed under vacuum, the intensity of the resonance attributed to H increases more rapidly and, after 12 hours, H is the major hydrido species present in solution. Resonances due to 20, the CO adduct of 19a, are also observed in the ^{1}H and ^{31}P n.m.r spectra of samples in which excess SO_2 has been removed.

On dissolution of a pure sample of complex 28 in SO_2 saturated CD_2Cl_2, a similar spectrum to that depicted in Figure 54(b) is obtained after 12 hours. However, after a similar period of time if no excess SO_2 is present, signals due to significant quantities of 20, as well as those attributed to D-H, are observed, and the relative concentration of D decreases. This indicates that D is stabilised in solution by the presence of excess SO_2.

Attempts to separate this mixture by column chromatography failed and complexes E-H have only been characterised by ^{1}H, ^{31}P and

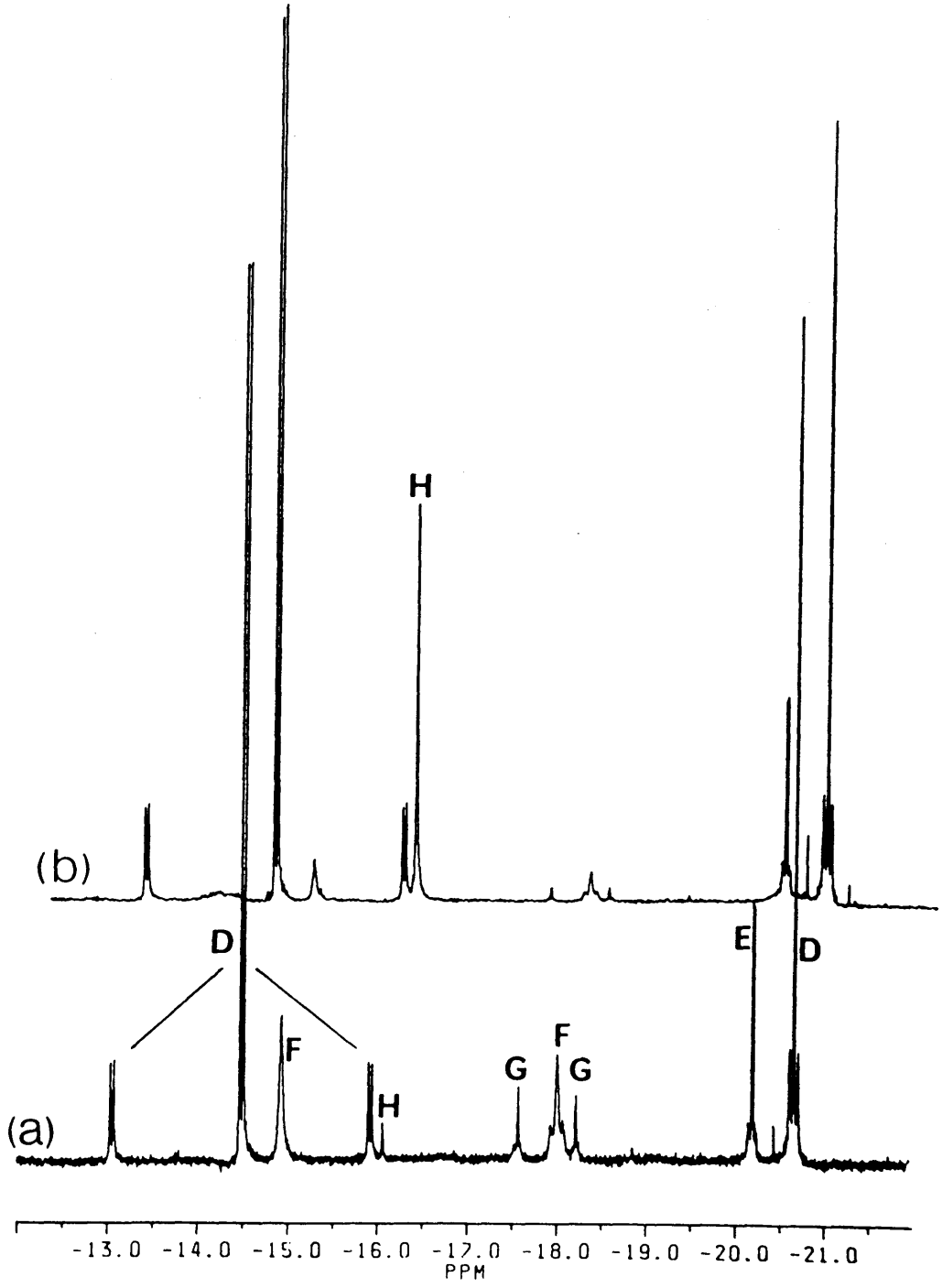

Figure 54: High field region of the ^{1}H n.m.r spectrum recorded (a) immediately after and (b) 12 hours after addition of SO_2 to 19a at 298K.

(for H) ^{13}C n.m.r data obtained from reaction mixtures. The correlations between ^{1}H and ^{31}P resonances in specific complexes were determined by selective decoupling and saturation transfer experiments, together with consideration of the time dependency of relative intensities of signals in ^{1}H and ^{31}P n.m.r spectra. It should be noted that the chemical shifts in these spectra depend upon the concentration of SO_2 dissolved in the deuterated solvent.

Dynamic Behaviour of $Os_3Pt(\mu\text{-}H)_2(\mu\text{-}SO_2)(CO)_{10}(PCy_3)$, 28, (species D).

At 298K the ^{13}C n.m.r spectrum of a mixture containing predominantly D displays ten sharp CO resonances in the range 179.4 - 159.3 p.p.m. Assignments of particular resonances in D did not prove possible, with the exception of the peak at 159.3 p.p.m, which can be assigned to the Pt-bound carbonyl C(10) on the basis of the large ^{195}Pt coupling (J(Pt-C) = 1560Hz) to this signal. These resonances are sharp, which suggests that the carbonyls are non-fluxional at 298K. Complex 27, which is structurally related to 28 by replacement of $\mu\text{-}SO_2$ with $\mu\text{-}CH_2$, and the Pt-bound CO with CyNC, displays a similar carbonyl rigidity at 298K, where slow rotation of an $Os(CO)_3$ group, observed in a 2D exchange correlation NOESY ^{13}C n.m.r experiment, was the only fluxional process operative (vide supra). Furthermore, as shown in Figure 55, J(^{187}Os-H) couplings to the hydride signals in the ^{1}H n.m.r spectrum of D are in accord with a static structure. Two inequivalent Os atoms, Os(2) and Os(3), are coupled to the Os(μ-H)Os proton ($^{1}J(^{187}Os\text{-}H)$ = 40.7, 32.0Hz) while the Os(μ-H)Pt hydride couples to one Os centre ($^{1}J(^{187}Os\text{-}H)$ = 28.1Hz). The magnitudes of these couplings are typical of $^{1}J(^{187}Os\text{-}H)$ values observed in non-fluxional hydrido-osmium clusters.[266-268] Nevertheless, both hydride and phosphorous resonances due to D broaden at 168K, in

keeping with the "freezing out" of a fluxional process. The nature of this dynamic process is, at present, undetermined. However, it may involve a polytopal rotation of the $HPt(CO)(PCy_3)$ fragment about the triangular Os_3 frame, similar to the fluxional behaviour observed in 26. If such a process is operative in D, it would result in the exchange of the rotomers I,II and III shown in Figure 56.

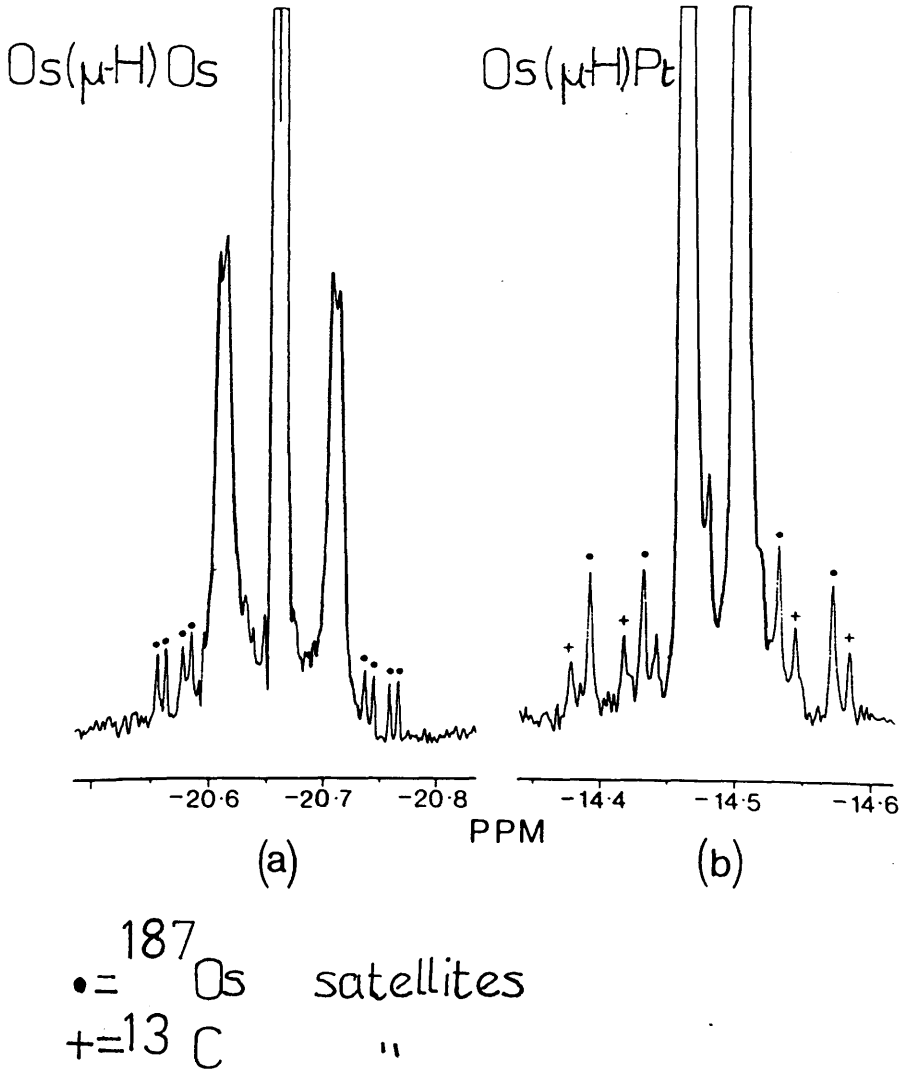

Figure 55. ^{187}**Os-H satellites of hydride signals in** ^{1}**H n.m.r spectrum of** D.

The magnitudes of ^{187}Os couplings observed at 298K are in accord with such a process if and only if it is assumed that one rotomer is thermodynamically favoured over the other two. Rotation of $HPt(CO)(PCy_3)$ exchanges three non-degenerate rotomers and, hence, the observed chemical shifts and couplings for n.m.r resonances at fast exchange would be population weighted.

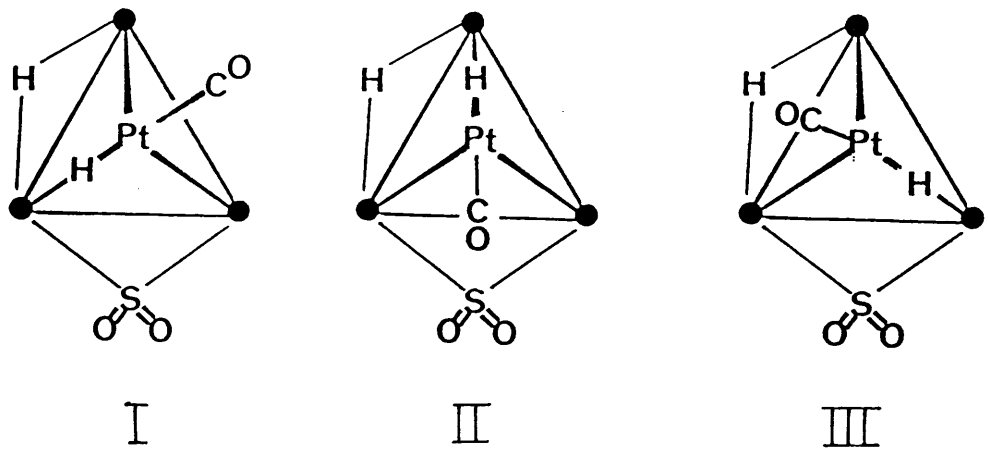

Figure 56. Rotomers I,II and III.

The ^{1}H and ^{31}P n.m.r parameters for E (Table 28) are similar to those observed for 23,[258] an isomeric form of the methylene adduct of 19. Like 23, one hydride resonance is observed in the ^{1}H n.m.r spectrum of E, possibly corresponding to two equivalent Os(μ-H)Os protons. The phosphine resonance in the ^{31}P n.m.r of 23 comes at 10.8 p.p.m [258] (c.f 50-80 ppm normally observed in $Os_3Pt\text{-}PCy_3$ systems) [147,148,258] Species E also has a highfield ^{31}P resonance (9.3 p.p.m) which may indicate some structural similarity between E and 23. Furthermore, with the PPh_3 substituted analogue of 19a, the isomer corresponding to E is the major species formed at room temperature[287]

and a ^{13}C n.m.r spectrum of this complex shows carbonyl resonances which can be assigned and are consistent with the structure shown in Figure 57.

In solution, the isomeric forms of the methylene adduct are in equilibrium with each other and a similar equilibrium between D and E is suggested by the observation that, in solution, pure samples of D (i.e. complex 28) rapidly convert to mixtures of D and E.

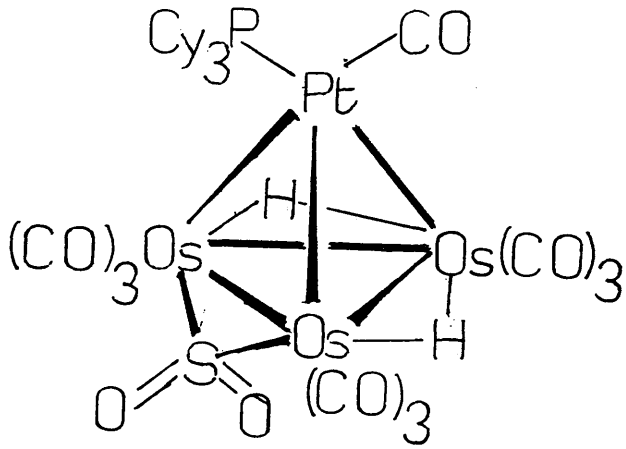

Figure 57. Proposed structure of E.

Species F and G both contain two inequivalent Os(μ-H)Os hydrides. The corresponding high field resonances in the ^{1}H n.m.r spectrum, with the exception of the -15.02 p.p.m. signal of F, show ^{195}Pt satellites indicating that these complexes retain a Pt-Os core. Furthermore, the corresponding ^{31}P resonances show large couplings to ^{195}Pt indicating the Pt-PCy_3 unit is maintained in both complexes. The amount of free SO_2 in solution does not appear to affect the production of F and G, though, under a CO atmosphere, their formation is suppressed. It is possible that these complexes result from a

loss of CO from D or E to give the species shown in Figure 58.

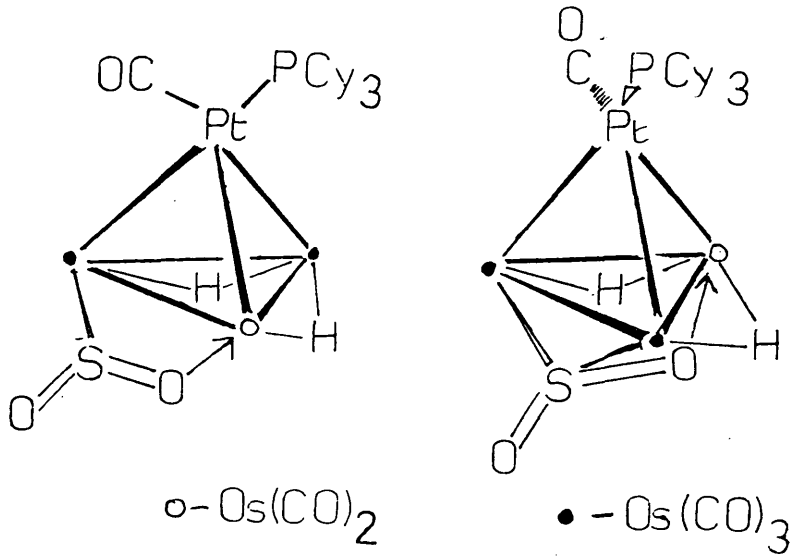

Figure 58 : Proposed structures for F and G.

As mentioned previously, on removal of excess SO_2 from reaction mixtures, H becomes the major hydride containing species. In the ^1H n.m.r spectrum, the single resonance attributed to H at -16.06 p.p.m at ambient temperatures gives rise to two doublets at -16.05 and -16.14 p.p.m. (J(H-H) = 1.4Hz) on cooling to 213K. Hence H contains two inequivalent Os(μ-H)Os hydrides which undergo exchange at 298K. The ^{13}C n.m.r spectrum at 198K of a reaction mixture containing ~50% of H shows nine sharp carbonyl resonances of equal intensity between 158.1 and 176.4 p.p.m. These signals may be unambiguously assigned to H on the basis of selective ^1H decoupling experiments. Significantly none of these signals show ^{31}P or ^{195}Pt couplings, indicating that there is no $PtPCy_3$ fragment in H. The number, and coordination mode of SO_2 ligand(s) in H could be deduced from microanalytical and i.r spectroscopic data. However such analyses were precluded as H could not be isolated as a pure solid. The n.m.r spectroscopic evidence is compatible with a formulation $Os_3(\mu\text{-}H)_2(CO)_9(SO_2)_n$, n = 1,2.

Possible structures for H are shown in Figure 59, however, these are by no means unique.

In their report of the synthesis of $Os_3(\mu\text{-}H)_2(\mu\text{-}SO_2)(CO)_{10}$ from 4 and SO_2, Jarvinen and Ryan[107] state that a variety of other (unspecified) products are formed in this reaction. In the hope of obtaining evidence that one of these unidentified products was H, the reaction of SO_2 with 4 was re-examined by ^1H n.m.r spectroscopy. However no resonances attributable to H were observed.

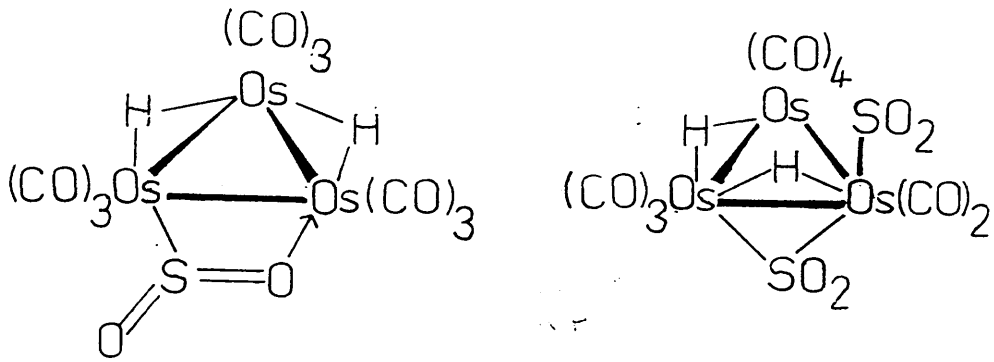

Figure 59 : Possible structures for H.

The fate of the $Pt\text{-}PCy_3$ fragments was not precisely established. However, solutions in which H is present in significant quantities display a ^{31}P resonance at 68.5 p.p.m which is coupled to two distinct ^{195}Pt nuclei (J(Pt-P) = 4056, 330; J(P-P) = 34Hz). This splitting pattern is typical of complexes containing two equivalent $PtPR_3$ units [148,250,288] and could arise from a dinuclear Pt_2 species or a mixed Pt_2Os_n cluster. Small amounts of the previously known complex $Pt_3(\mu\text{-}SO_2)_2(\mu\text{-}CO)(PCy_3)_3$ [289] were isolated from these reaction mixtures and characterised by X-ray diffraction by Dr. L.J. Farrugia.

The reaction of 19a with SO_2 yields a complex mixture of products. The predominant initial product formed at ambient temperatures, complex 28 (i.e. species D), is structurally related to 24, the methylene adduct of 19a. This emphasises the similarity in bonding capability of the CH_2 and SO_2 fragments. Nevertheless, unlike 23 and 24, 28 is unstable in solution and undergoes cluster degradation in the presence and absence of excess SO_2. Degradation is accelerated by the removal of free SO_2 from solution.

2.2.3 (ii) Reaction of $Os_3Pt(\mu\text{-}H)_2(CO)_{10}(PCy_3)$ with $SnCl_2$.

In furtherance of the investigation into the reactivity of 19 with inorganic carbene analogues, a study of the reaction of 19a with $SnCl_2$ was undertaken.

Treatment of a dichloromethane solution of 19a with a 2:1 molar excess of anhydrous $SnCl_2$ in THF resulted in a rapid colour change from the green of 19a to orange. On careful addition of a layer of diethyl ether to the top of this solution, orange crystals formulated as $Os_3PtSn(\mu\text{-}H)_2(Cl)(CO)_{10}(OEt_2)(PCy_3)(SnCl_3)$, 29 were isolated in over 80% yield. When equimolar quantities of 19a and $SnCl_2$ were used, 29 was formed in much reduced yields, while substantial amounts of 19a remained unreacted.

In the solution i.r. spectrum, 29 shows CO stretching bands in the range 2103 - 1987 cm^{-1}, indicating that the carbonyl ligands are terminally ligated. The highfield region of the ^1H n.m.r spectrum of 29 at ambient temperature displays two signals at -10.49 and -20.01 p.p.m. The magnitude of ^{195}Pt coupling to these resonances indicates that the former arises from an Os(μ-H)Pt proton, while the latter is due to an Os(μ-H)Os hydride. Furthermore, two sets of low

intensity satellites (J = 58, 40Hz) are observed for the -10.49 p.p.m., resonance, due to coupling to ^{117}Sn and ^{119}Sn nuclei, for which I = ½. The magnitude of coupling to Sn -117 and -119 isotopes is expected to differ by 4.6%, according to γ_o considerations (γ_o for ^{117}Sn = -9.578 whereas for ^{119}Sn, γ_o = -10.021; the magnitude of coupling between two nuclei varies with γ_o, hence the $\frac{\gamma_o{}^{117}Sn}{\gamma_o{}^{119}Sn}$ ratio gives a difference of 4.6%).

However, as the Sn couplings to the ^{1}H and ^{13}C n.m.r resonances reported herein for 29 are small, the satellites due to distinct Sn nuclei are not resolved and are, instead, reported as averaged $^{117/119}Sn$ couplings. The observation of two distinct sets of $^{117/119}Sn$ satellites is, therefore, indicative of two chemically inequivalent Sn centres in 29. The Os(μ-H)Os proton is also coupled to $^{117/119}Sn$ (J = 70Hz). The small values of $^{117/119}Sn$ couplings to these high field ^{1}H n.m.r resonances suggests there is no M(μ-H)Sn unit in 29 (c.f. $Os_3Sn(\mu\text{-}H)_2(CO)_{10}[CH(SiMe_3)_2]_2$, where a $^{117/119}Sn$-H coupling of ∿ 290Hz is observed for the Os(μ-H)Sn proton resonance[106]).

In the light of crystallographic studies of 29, (vide infra) the broad triplet and quartet resonances at 1.29 and 2.50 p.p.m respectively are attributed to Sn bound OEt_2 protons. In the solid state structure of 29, the methyl groups and each methylene proton are in chemically distinct environments. Unhindered rotation about the Sn-OEt_2 bond will equivalence the methyl protons, but not the diastereotopic CH_2 protons of individual methylene groups. The broadness of these signals, which increases as the sample is cooled, may be due to a combination of restricted rotation about the Sn-OEt_2 bond and unresolved couplings to these protons.

The ^{31}P n.m.r spectrum of 29 displays one singlet resonance at

54.0 p.p.m. with a large ^{195}Pt coupling of 2473Hz, indicating that the PCy_3 moiety remains bound to Pt.

Figure 60 shows the ^{13}C n.m.r spectrum of 29 recorded at 248K, and the relevant n.m.r data are listed in Table 29. Ten discrete resonances are observed in the terminal carbonyl region. These signals remain sharp at ambient temperatures, indicating that carbonyl exchange in 29 is not a low energy process. Assignments of these resonances have been made with reference to the solid state structure of 29 (see below, Figure 61), which is presumed to be maintained in solution. Four resonances, a,b,c and i show no coupling to either H1 or H2 and are attributed to the $Os(CO)_4$ carbons, which are remote from the hydrides. d is clearly due to C10, from the large ^{195}Pt and H1 coupling to this signal. C6 and C9 give rise to peaks g and j respectively, by consideration of their relatively large coupling to H2; similarly e can be assigned to C8 on the strength of the large H1 coupling to this resonance. The remaining resonances f and h can, therefore, be attributed to C5 and C7.

It is obvious, from the spectral data, that the reaction of $SnCl_2$ with 19a does not yield the expected carbene-like adduct. Therefore an X-ray crystallographic analysis of 29 was performed to fully delineate the molecular structure. The diffraction data was kindly collected by Dr. A.J. Welch at Edinburgh University and the structure was solved by Dr. L.J. Farrugia.

The crystal structure of 29 is presented in Figure 61, while important metrical parameters are given in Table 30. The metal framework of 29 can be described as having a tetrahedral PtOs(2)Os(3)Sn(1) core with the Os(2)-Sn(1) edge bridged by Os(1). The hydride ligands were not observed crystallographically, and are included at calculated positions (using the HYDEX[271] program). In

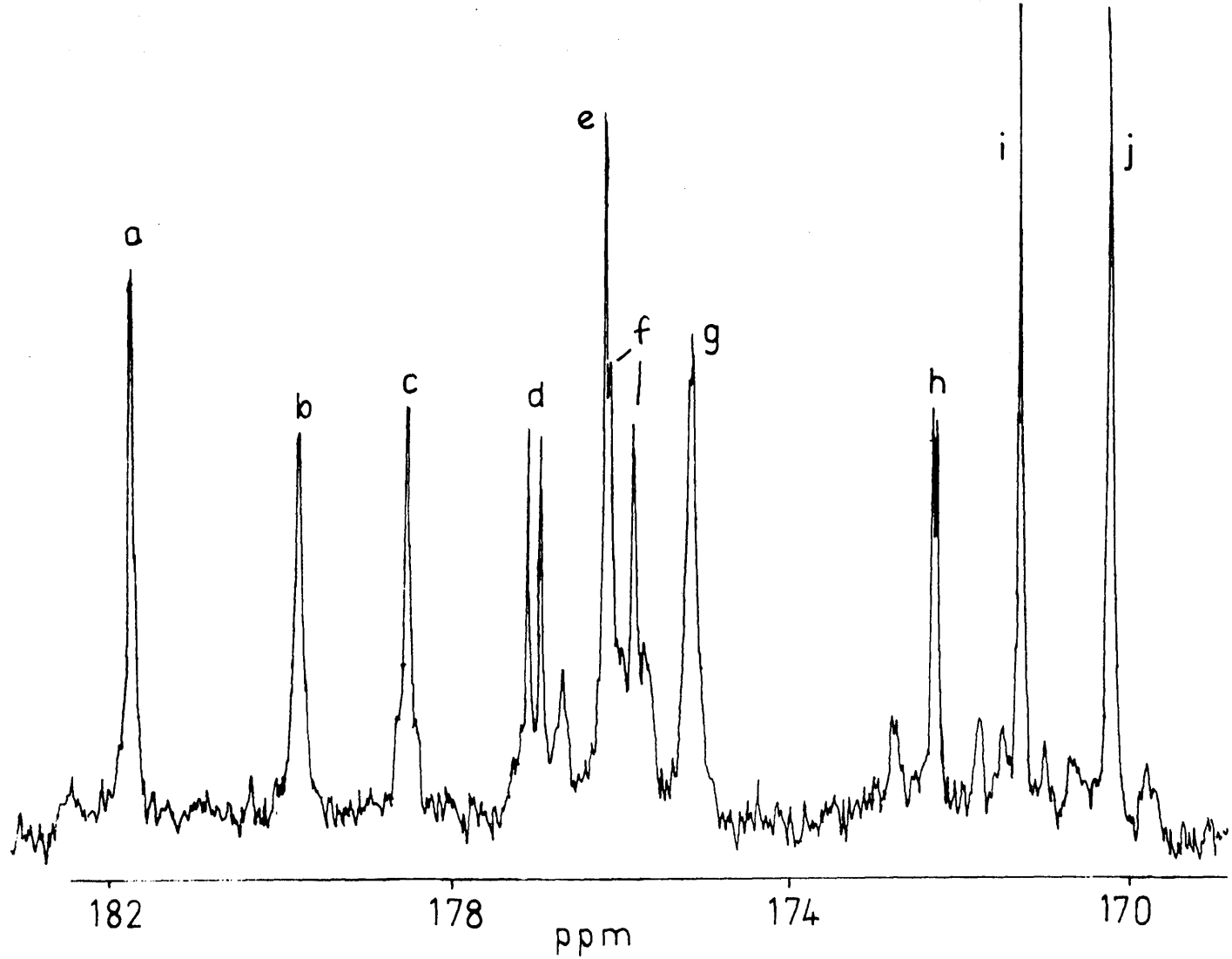

Figure 60 : Carbonyl region of ^{13}C n.m.r spectrum of $Os_3PtSn(\mu\text{-}H)_2(Cl)(CO)_{10}(OEt_2)(PCy_3)(SnCl_3)$ at 248K.

Table 29 : N.m.r parameters for $Os_3PtSn(\mu\text{-}H)_2(CO)_{10}(Cl)(OEt_2)(PCy_3)(SnCl_3)$, 29.

^{13}C Data [a]

Reson.[b]	p.p.m.	Mult.[c]	Assgnmt.[e]	J/Hz.[d] P-C	Pt-C	Sn-C	H1-C	H2-C
a	181.7	s	C1-C4	-	-	68,30	-	-
b	179.7	d	C1-C4	2.0	5	*	-	-
c	178.5	s	C1-C4	-	11	*	-	-
d	177.0	d	C10	7.7	1734	5	29.2	-
e	176.1	s	C8	-	52	5	7.0	w
f	175.9	d	C5/C7	12.9	12	-	w	4.0
g	175.1	d	C6	1.8	5	-	-	9.2
h	172.2	d	C5/C7	2.4	50	64,20	-	3.7
i	171.2	s	C1-C4	-	4	23	-	-
j	170.2	s	C9	-	4	48,38	3.7	6.2

^{1}H Data [a]

H1[e] -10.49 [d,Os(μ-H)Pt,J(Pt-H) = 582, J(P-H) = 8.8, J($^{117/119}$Sn-H) = 58,40Hz].

H2[e] -20.01 [d,Os(μ-H)Os, J(Pt-H) = 19, J(P-H) = 2.2, J($^{117/119}$Sn-H) = 79Hz].

^{31}P Data [f]

54.0 (s,PtP, J(Pt-P) = 2473Hz).

a) 248K, CD_2Cl_2, p.p.m. rel to TMS; b) see Figure 60 ; c) multiplicities based on $^{13}C\{^{1}H\}$spectra

d) ^{117}Sn and ^{119}Sn couplings are unresolved, w indicates weak, unresolved coupling, *indicates $^{117/119}$Sn couplings partially obscured by noise. e) assignments refer to Figure 61;

f) 298K, $CDCl_3$, p.p.m. rel to ext 85% H_3PO_4

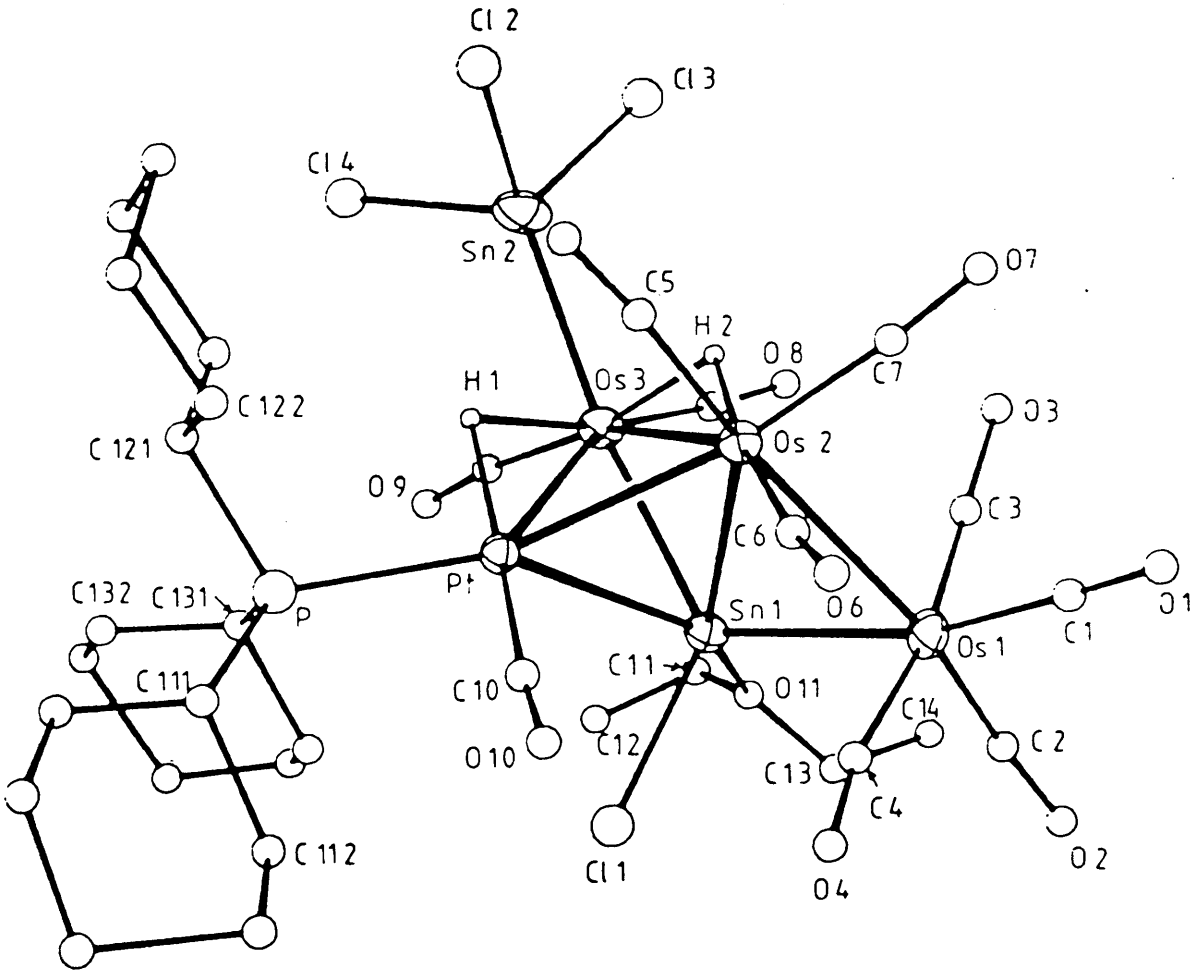

Figure 61 : The molecular structure of $Os_3PtSn(\mu\text{-}H)_2(Cl)(CO)_{10}(OEt_2)$-
$(PCy_3)(SnCl_3)$, 29.

Table 30 : Selected Bond Lengths (Å) and Bond Angles (deg) for the complex $Os_3PtSn(\mu\text{-}H)_2(CO)_{10}(Cl)(OEt_2)(PCy_3)(SnCl_3)$, 29

Bonds

Os(1)-Os(2)	3.003(3)	Os(1)-Sn(1)	2.645(5)
Os(2)-Os(3)	3.092(3)	Os(2)-Pt	2.782(3)
Os(2)-Sn(1)	3.058(5)	Os(3)-Pt	2.865(3)
Os(3)-Sn(1)	2.608(4)	Os(3)-Sn(2)	2.612(5)
Pt -Sn(1)	2.975(5)	Pt -P	2.388(14)
Os(1)-C(1)	1.95(6)	Os(1)-C(2)	1.87(5)
Os(1)-C(3)	1.73(6)	Os(1)-C(4)	1.90(4)
Os(2)-C(5)	1.93(5)	Os(2)-C(6)	1.95(7)
Os(2)-C(7)	1.87(7)	Os(3)-C(8)	1.86(6)
Os(3)-C(9)	1.91(6)	Pt -C(10)	2.04(17)
Sn(1)-Cl(1)	2.400(15)	Sn(1)-O(11)	2.49(4)
Sn(2)-Cl(2)	2.36(2)	Sn(2)-Cl(3)	2.375(18)
Sn(2)-Cl(4)	2.36(3)	C-O(carbonyl) mean	1.16

Angles

Os(2)-Os(1)-Sn(1)	65.2(1)	Os(2)-Os(1)-C(4)	88.1(12)
Os(2)-Os(1)-C(3)	81.9(19)	Os(2)-Os(1)-C(1)	94.3(15)
Os(2)-Os(1)-C(2)	162.7(15)	Sn(1)-Os(1)-C(1)	159.2(15)
Sn(1)-Os(1)-C(2)	98.0(15)	Sn(1)-Os(1)-C(3)	87.9(20)
Sn(1)-Os(1)-C(4)	84.9(13)	C(1) -Os(1)-C(2)	102.7(21)
C(1) -Os(1)-C(3)	92.9(26)	C(1) -Os(1)-C(4)	91.2(20)
C(2) -Os(1)-C(3)	93.7(24)	C(2) -Os(1)-C(4)	94.9(19)
C(3) -Os(1)-C(4)	169.5(23)	Os(1)-Os(2)-Os(3)	95.2(1)
Os(1)-Os(2)-Pt	105.3(1)	Os(1)-Os(2)-Sn(1)	51.7(1)
Os(3)-Os(2)-Pt	58.1(1)	Os(3)-Os(2)-Sn(1)	50.2(1)
Pt -Os(2)-Sn(1)	61.0(1)	C(5) -Os(2)-C(6)	90.1(23)
C(5) -Os(2)-C(7)	90.4(23)	C(6) -Os(2)-C(7)	88.2(28)
Os(2)-Os(3)-Pt	55.5(1)	Os(2)-Os(3)-Sn(1)	64.2(2)
Os(2)-Os(3)-Sn(2)	105.4(2)	C(8) -Os(3)-C(9)	89.3(24)
Os(2)-Pt -Os(3)	66.4(1)	Os(2)-Pt -Sn(1)	64.1(1)
Os(3)-Pt -Sn(1)	53.0(1)	Os(2)-Pt -P	163.0(4)
Os(3)-Pt -P	114.4(4)	Sn(1)-Pt -P	131.1(4)
P -Pt -C(10)	93.2(44)	Os(1)-Sn(1)-Os(2)	63.1(1)
Os(1)-Sn(1)-Os(3)	117.8(2)	Os(1)-Sn(1)-Pt	109.8(2)
Os(1)-Sn(1)-Cl(1)	109.1(4)	Os(1)-Sn(1)-O(11)	105.4(9)
Os(2)-Sn(1)-Os(3)	65.6(1)	Os(2)-Sn(1)-Pt	54.9(1)
Os(2)-Sn(1)-Cl(1)	124.7(4)	Os(2)-Sn(1)-O(11)	150.9(9)
Os(3)-Sn(1)-Pt	61.3(1)	Os(3)-Sn(1)-Cl(1)	128.3(4)
Os(3)-Sn(1)-O(11)	102.7(9)	Pt -Sn(1)-Cl(1)	83.9(4)
Pt -Sn(1)-O(11)	144.8(9)	Os(3)-Sn(2)-Cl(2)	126.2(5)
Os(3)-Sn(2)-Cl(3)	114.5(6)	Os(3)-Sn(2)-Cl(4)	115.3(6)
Sn(1)-O(11)-C(11)	134.3(46)	Sn(1)-O(11)-C(13)	122.7(48)

keeping with the ^{1}H n.m.r data, these hydrides span the Pt-Os(3) and Os(2)-Os(3) vectors.

The Os(1)-Os(2) and Os(2)-Os(3) separations of 3.003(3) and 3.092(3) Å respectively, are longer than the average Os-Os distance of 2.877(3) Å in 1.[87] Nevertheless, similar Os-Os bond lengths (2.985(2) and 3.057(1) Å) are reported for $Os_3Sn(\mu\text{-}CH_2)(Cl)_2(CO)_{11}$[290] which, like 29, has an open Os_3 framework spanned by a Sn centre. Furthermore, Adams and co-workers have reported Os-Os bond lengths of over 3.00 Å in electron-rich (e.g. $Os_4(\mu_3\text{-}S)_2(CO)_{12}$,[291] Os-Os = 3.002(1) and 3.091(1) Å) and electron-precise (e.g. $Os_4Pt(\mu_3\text{-}S)_2(CO)_{11}(PMe_2Ph)_2$,[253] Os-Os = 3.106(2) Å) Os clusters with main group (sulphido-) atoms incorporated into the polyhedral cage.

There is considerable asymmetry in the Os-Sn(1) separations with Os(1)-Sn(1) = 2.645(5), Os(2)-Sn(1) = 3.058(5), and Os(3)-Sn(1) = 2.608(4) Å. In previously reported structures with mixed Os-Sn metal cores,[106,128,214,290,292] the Os-Sn bonding distances vary from 2.641(2) (in $Os_3Sn(\mu\text{-}CH_2)(Cl)_2(CO)_{11}$[290]) to 2.873(3) Å (in $Os_3Sn_2(dppm)(CO)_8[CH(SiMe_3)_2]_4$,[128]). The Os(2)-Sn(1) separation in 29 is substantially longer than these distances and is indicative of a weak bonding interaction.

Pt-Sn distances reported in the literature normally range from 2.5 - 2.6 Å,[293] however in $Pt_3(cod)_3(\mu_3\text{-}SnCl_3)_2$,[294] the mean Pt-Sn distance is 2.80(1) Å. The Pt-Sn(1) separation in 29 of 2.975(5) Å is, by comparison, very long. The elongated Os(2)-Sn(1) and Pt-Sn(1) vectors could result from a weak, delocalised bonding interaction over the three metal centres. All other bond lengths fall within the expected ranges.

By ignoring the hydride bridged M-M and the long Os(2)-Sn(1) vectors the coordination about each Os atom is pseudo-octahedral, while

that of Pt is approximately square planar, if the elongated Pt-Sn(1) distance is considered non-bonding. Sn(1) adopts an almost tetrahedral coordination geometry if the Os(2)-Sn(1) and Pt-Sn(1) vectors are discounted.

The transition metal framework geometry is spiked triangular, with a triangular PtOs(2)Os(3) unit axially ligated at Os(2) by Os(1). Similar frameworks are observed in $Os_3Pt(\mu_3\text{-}S)_2(CO)_{10}(PPh_3)$ [249] and $Os_3Pt(\mu_3\text{-}S)_2(CO)_9(PPh_3)_2$.[249]

However the overall cluster geometry in 29 bears more resemblance to that observed in the 62 electron species $Os_3Pt(\mu\text{-}H)_2(\mu_4\text{-}C)(CO)_{10}(PCy_3)$,[250] which has a *closo*-tetrahedral Os_3C core with one Os-C bond bridged by Pt.

If the $SnCl(OEt_2)$ group is considered a three electron donor, 29 has 62 valence electrons, in accord with the E.A.N rule[54] prediction for a spiked triangular geometry with a 16 electron Pt centre. Alternatively, if Sn(1) is regarded as part of the polyhedral framework, the P.S.E.P.T.[55,57] predicts that 29 has 66 valence electrons and 8 skeletal pairs, corresponding to an *arachno*-pentagonal bipyramid. This geometry can be derived with Sn(1) and Os(2) as the axial vertices if the vector between these centres is considered non-bonding.

The addition of $SnCl_2$ to 19 effects the formal transfer of Cl^- between Sn centres yielding $SnCl_3^-$ and $SnCl(OEt_2)^+$ fragments. The diethyl ether unit in this latter fragment is a Sn-coordinated solvent molecule. The reaction of $SnCl_2$ with $Os_3(\mu\text{-}CH_2)(\mu\text{-}CO)(CO)_{10}$ did not result in halide transfer between tin centres and the $SnCl_2$ moiety inserted into an Os-Os bond intact.[290]

Finally, Pt/Sn clusters have been used as precursors to a variety of supported mixed-metal heterogeneous catalysts.[295,296]

Furthermore, heterometallic OsM[130-133] systems have proved useful as sources of catalytically active mixed-metal systems. 29 provides the first cluster in which Os, Pt and Sn are composite metals, and has potential as a useful catalyst precursor complex. The activity of the catalyst systems derived from 29 is currently under investigation.[297]

2.2.4 Concluding Remarks.

In the light of these investigations, it is pertinent to reassess the EHMO analysis of the framework geometries adopted in adducts of 19.

Schemes 14 and 15 summarise the chemistry of 19 with the nucleophiles CNR and SO_2,$SnCl_2$ respectively. The framework transformations observed on reaction of 19 with CO and the isolobal analogue, CNR are very similar. In both cases, the initially formed adducts 20 and 25 have butterfly geometries and undergo facile decarbonylation to yield *closo*-tetrahedral unsaturated complexes 19 and 26 respectively. The reactivity of 26 towards CO and CH_2 is similar to that of 19, yielding adducts with butterfly and *closo*-tetrahedral metal cores respectively. This suggests that the substitution of the Pt-bound CO in 19 for CNR in 26 does not grossly perturb the cluster's frontier orbitals.

The addition of the inorganic carbene, SO_2, to 19 yields a complex mixture of products. However, at ambient temperatures, the predominant species initially formed is 28, the expected *closo*-tetrahedral μ-SO_2 adduct. This is structurally analogous to 24, one isomeric form of the CH_2 adduct of 19.[258] In solution 28 isomerises rapidly to give a mixture of 28 and another species, believed to resemble 23, the other isomeric form of $Os_3Pt(\mu\text{-}H)_2(\mu\text{-}CH_2)(CO)_{10}(PCy_3)$.[258]

This isomerisation in solution is also observed for 23 and 24.[258] Unlike the methylene adduct analogue, 28 decomposes slowly in solution and this process is promoted by the removal of excess SO_2. Nevertheless the chemical reactivity of 19 towards CH_2 and SO_2 is similar and is compatible with the preceding EHMO analysis.

In the reaction of 19a with $SnCl_2$, it is clear that formation of a μ_2-carbene-like adduct does not occur and a fundamental change of the cluster core is observed, with incorporation of a $Sn(Cl)(OEt_2)$ unit into the polyhedral cage. Furthermore, the integrity of the $SnCl_2$ unit is not maintained. Hence, despite the proposed isolobal relationship between $SnCl_2$ and CH_2, frontier orbital effects may not be the main factor determining the course of reaction. Other considerations that may influence product formation include:- (a) relative steric requirements of CH_2 versus $SnCl_2$; (b) the availability of low energy inter-tin halide transfer pathways for $SnCl_2$ is not paralleled by inter-carbon hydrogen migration in CH_2; (c) the electronic charge distribution on $SnCl_2$ is not likely to be the same as CH_2 (Sn likely to have more positive charge character than C due to high electronegativity of Cl).

It may be that dialkyl tin complexes would yield μ_2-carbene type adducts of 19, however such reactions were not investigated.

Thus the frontier orbitals of two electron donor fragments are important in defining the framework geometry adopted in adducts of 19. For the majority of reactions investigated, the products formed can be rationalised in terms of the EHMO analysis presented in Section 2.2(i) i.e. carbene and carbene-like nucleophiles add to 19 yielding *closo*-tetrahedral complexes, while CO and isolobal analogues of CO give butterfly adducts with 19, 26.

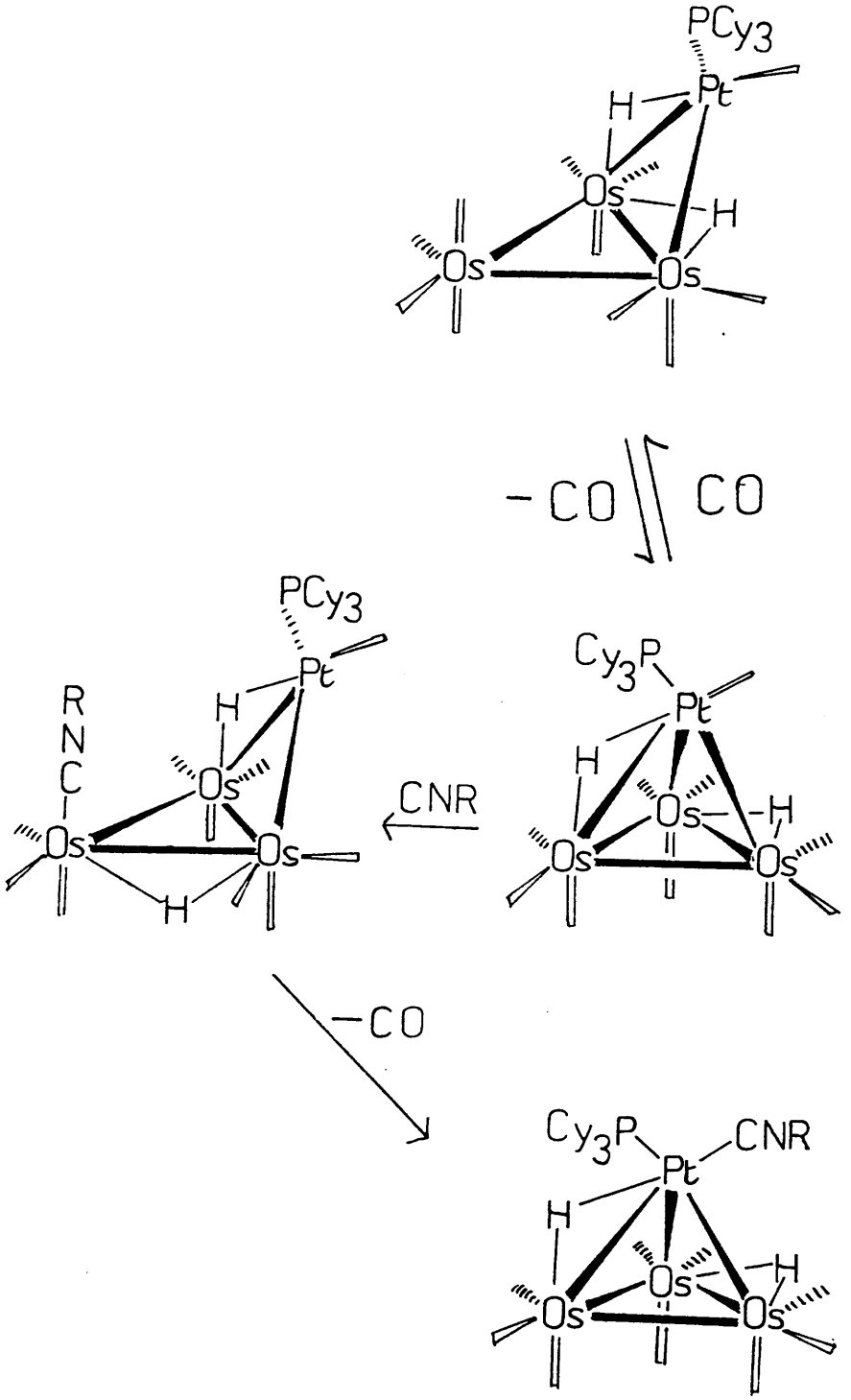

Scheme 14 : The reactions of $Os_3Pt(\mu\text{-}H)_2(CO)_{10}(PCy_3)$, 19a, with CO and CNR.

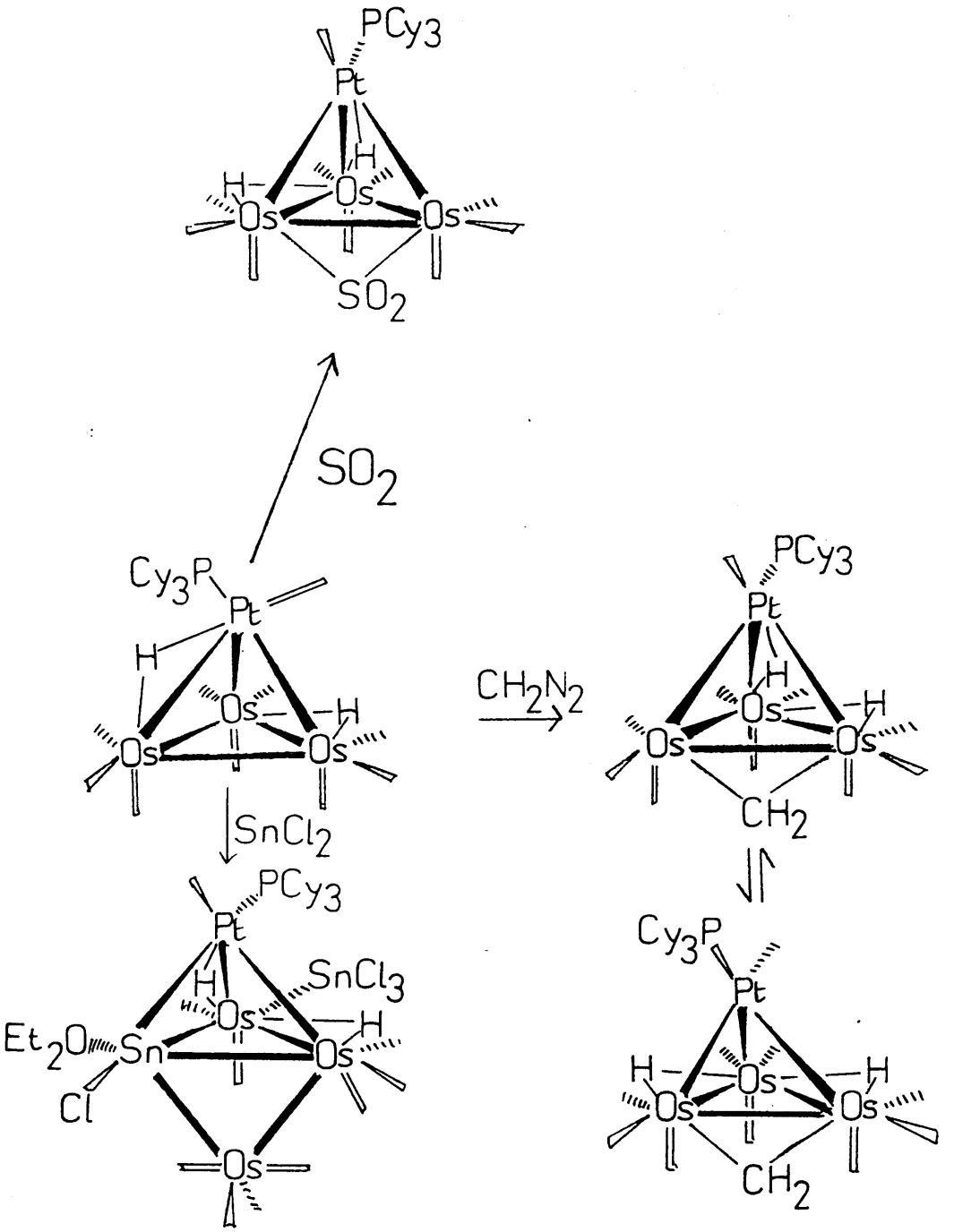

Scheme 15 : The reactions of $Os_3Pt(\mu\text{-}H)_2(CO)_{10}(PCy_3)$, 19a with CH_2N_2, SO_2 and $SnCl_2$.

Finally, it should be noted that the complex $Os_3Pt(\mu\text{-}H)_2(\mu\text{-}CO)$-$(cod)(CO)_9$ [closely related to the butterfly adducts 20 and 25 by formal replacement of $Pt(PCy_3)(L)$, (L = CO,CNR) with Pt(cod)] has a *closo*-tetrahedral geometry with a μ-CO ligand (see Chapter 3). Thus ligand substitution can influence the framework adopted in these adduct complexes.

2.3 Protonation of several Os_3Pt systems.

There are various methods of obtaining M-H bonds in cluster chemistry including cluster hydrogenolysis,[79,114,125,126] hydrogen transfer from cluster-bound functions,[96,101,110] H^- treatment,[92] and protonation by strong acids. This latter method has provided several examples of Os(μ-H)Os formation in electron precise clusters.[298-302] It is, perhaps, somewhat surprising that the electron deficient clusters 4 [301] and $Os_3(\mu\text{-}H)_2(CO)_9(PEt_3)$ [301] are also susceptible to electrophilic attack by H^+, and protonate at Os-Os sites.

The *closo*-tetrahedral Os_3Pt clusters 19, 26 and 27 have both Os-Os and Os-Pt edges and the reaction of these clusters with H^+ was investigated to define the site of protonation.

2.3.1 Protonation of $Os_3Pt(\mu\text{-}H)_2(CO)_{10}(PCy_3)$

A CH_2Cl_2 solution of 19a, when treated with excess $HBF_4.Et_2O$, yielded the trihydrido species $[Os_3Pt(\mu\text{-}H)_3(CO)_{10}(PCy_3)]^+ BF_4^-$, 30, in very high isolable yield (>90%). The ^1H n.m.r spectrum of 30 at 213K (Figure 62a) shows three highfield signals at -10.58 (J(Pt-H) = 603, J(P-H) = 8.0Hz), -12.37 (J(Os-H) = 46.0, J(P-H) = 1.1, J(H-H) = 1.7Hz), and -12.86 p.p.m. (J(Pt-H) = 21.5, J(P-H) = 1.7, J(H-H) = 1.7Hz). From the magnitude of ^{195}Pt-H couplings to these resonances,

Figure 62 : ^{1}H NOE difference spectra for $[Os_3Pt(\mu\text{-}H)_3(CO)_{10}(PCy_3)]^+BF_4^-$, 30, in hydride region:

a) off-resonance irradiation; b)irradiation at -10.58 p.p.m; c) irradiation at -12.37 p.p.m; d) irradiation at -12.86 p.p.m.

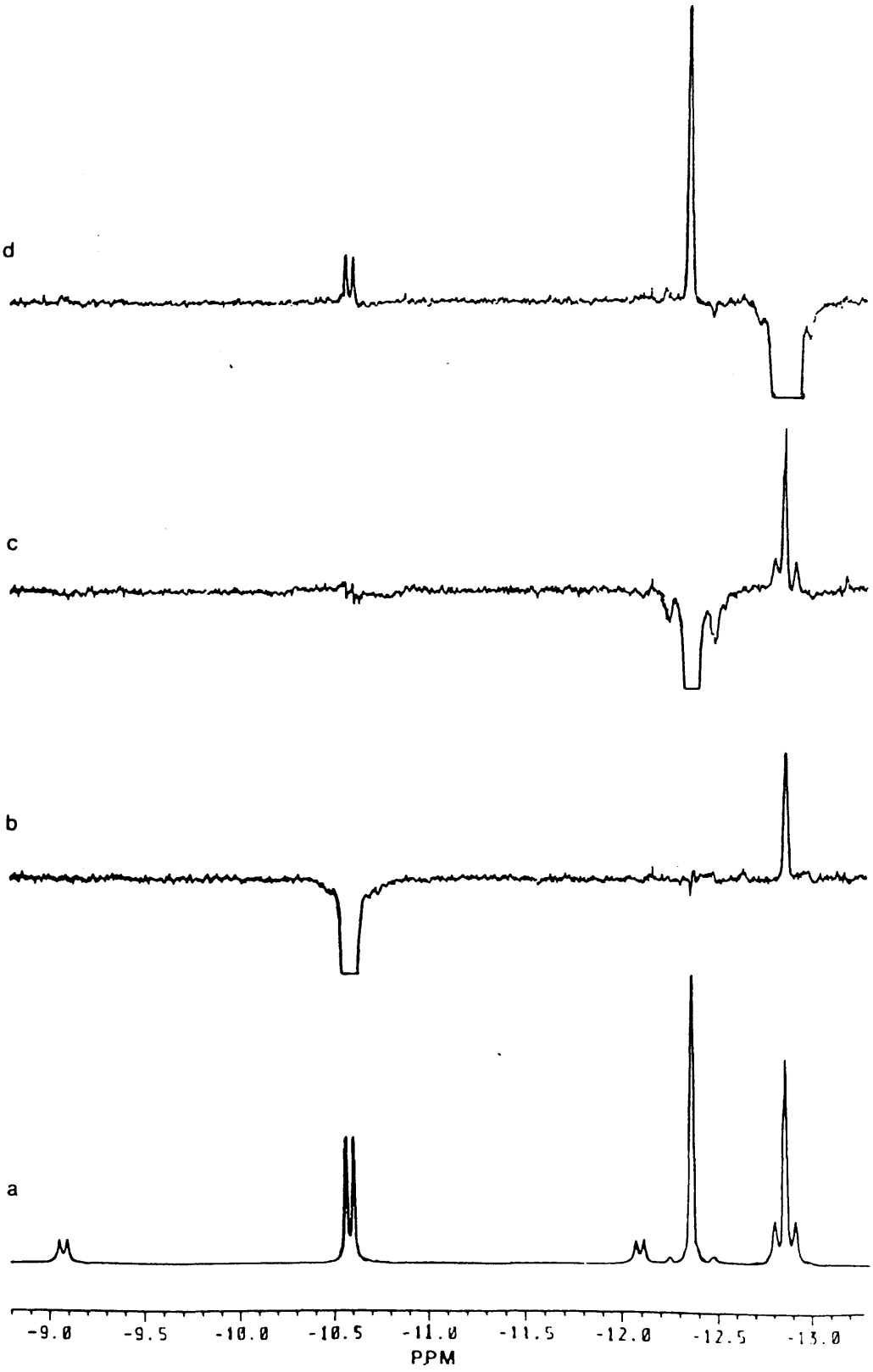

it is clear that the former signal arises from an Os(μ-H)Pt proton, while the two latter signals are due to inequivalent Os(μ-H)Os hydrides. Thus 19a protonates at an Os-Os edge. The i.r. data for 30 is compatible with the cluster having terminally bound carbonyl groups (ν_{CO} 2124 -2004 cm^{-1}).

A crystallographic analysis of 30 was undertaken by Dr. L.J. Farrugia in order to assess the structural alterations imposed by protonation of 19a. The solid state molecular structure of 30, together with the atomic labelling scheme employed are shown in Figure 63.

Important metrical parameters are listed in Table 31. Consideration of electron density difference maps did not facilitate direct location of the metal hydrides, and these are included at HYDEX[271] calculated positions, which agree with the ^1H n.m.r spectroscopic data. The structure of 30 is very similar to that of 19a, with both clusters having *closo* tetrahedral frameworks and corresponding core M-M distances are listed in Table 31 for ease of comparison. With the exception of the Os(1)—Os(3) vector, these separations differ by only 0.02 - 0.04 Å. The elongation of the Os(1)-Os(3) vector in 30 (2.891(1) Å c.f. 2.741 Å in 19a [147]) is consistent with the coordination of a μ-H ligand at this edge.[87,303] The CO functions on Os(1) and Os(3) are disposed slightly differently in 30, compared with 19a, in order to accommodate this bridging hydride.

The pseudo mirror plane of 19a is destroyed by protonation of an Os-Os edge. No evidence of disordered hydride occupation of the Os(2)-Os(3) edge was observed in this analysis.

The trihydride cation is a 58 electron species and is, therefore, unsaturated. 30 contains two Os(μ-H)Os units with quite different bond lengths; (Os(1)-Os(2) = 2.747(1), Os(1)-Os(3) =2.891(1)Å).

Figure 63 : Crystal structure of $[Os_3Pt(\mu\text{-}H)_3(CO)_{10}(PCy_3)]^+$

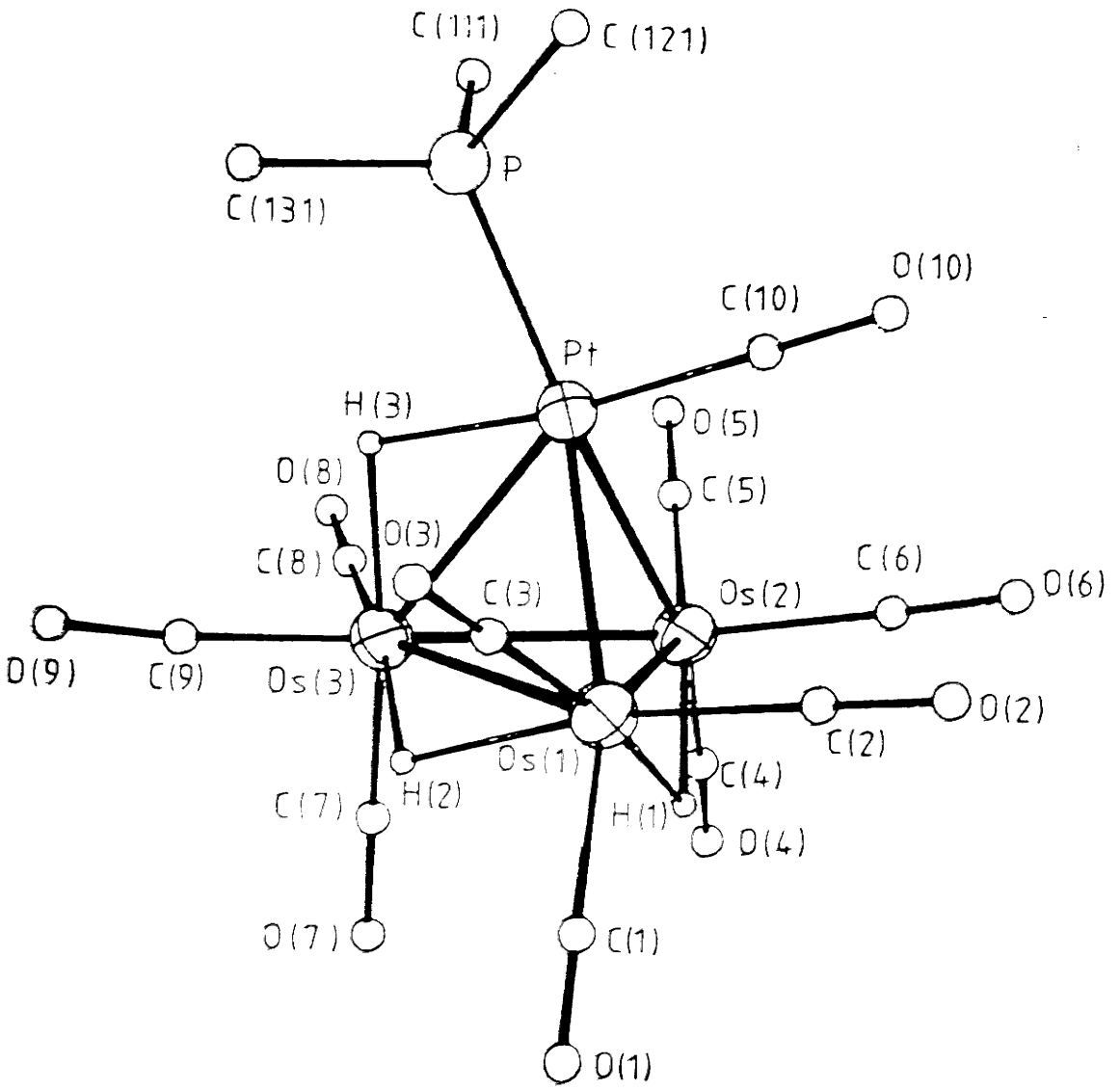

Cy Rings Omitted for Clarity

Table 31. Important bond lengths (Å) and bond angles (deg) for the complex $[Os_3Pt(\mu\text{-}H)_3(CO)_{10}(PCy_3)]^+BF_4^-$, **30**.

Bonds

Os(1)-Os(2)	2.747(1)	[2.789(1)]*	Os(1)-C(3)	1.89(2)	
Os(1)-Os(3)	2.891(1)	[2.741(1)]	Os(2)-C(4)	1.87(2)	
Os(2)-Os(3)	2.790(1)	[2.777(1)]	Os(2)-C(5)	1.90(2)	
Pt -Os(1)	2.812(1)	[2.832(1)]	Os(2)-C(6)	1.90(2)	
Pt -Os(2)	2.819(1)	[2.791(1)]	Os(3)-C(7)	1.85(3)	
Pt -Os(3)	2.845(1)	[2.863(1)]	Os(3)-C(8)	1.87(3)	
Pt -P	2.366(4)		Os(3)-C(9)	1.89(3)	
Pt -C(10)	1.85(1)		P -C(111)	1.83(1)	
Os(1)-C(1)	1.93(2)		P -C(121)	1.87(2)	
Os(1)-C(2)	1.93(2)		P -C(131)	1.85(1)	

C-O(carbonyl) mean 1.15[1]

Angles

Os(1)-Pt -Os(2)	58.4(1)		Pt -Os(2)-Os(1)	60.7(1)	
Os(1)-Pt -Os(3)	61.5(1)		Pt -Os(2)-Os(3)	60.9(1)	
Os(2)-Pt -Os(3)	59.0(1)		Os(1)-Os(2)-Os(3)	62.9(1)	
Pt -Os(1)-Os(2)	60.9(1)		Pt -Os(3)-Os(1)	58.7(1)	
Pt -Os(1)-Os(3)	59.8(1)		Pt -Os(3)-Os(2)	60.0(1)	
Os(2)-Os(1)-Os(3)	59.3(1)		Os(1)-Os(3)-Os(2)	57.8(1)	
Os(2)-Os(3)-C(8)	90.8(7)		Os(3)-Os(2)-C(5)	95.8(6)	
P -Pt -C(10)	95.1(5)		Pt -H(3) -Os(3)	101	
P -Pt -H(3)	78		Os(1)-H(1) -Os(2)	96	
H(3) -Pt -C(10)	173		Os(1)-H(2) -Os(3)	103	
Pt -C(10)-O(10)	178(2)		H(1) -Os(1)-C(3)	172	
Os(2)-Os(3)-C(9)	167.8(8)		H(1) -Os(2)-C(5)	170	
H(3) -Os(3)-C(7)	170		Os(3)-Os(2)-C(6)	158.6(6)	
H(2) -Os(3)-C(8)	168		H(2) -Os(1)-C(2)	169	

Os-C-O mean 176.7[1]

* Values in square parentheses are those corresponding distances in complex **19a** (ref. 147).

While this latter separation is close to previously observed Os(μ-H)Os distances in MOs_3 tetrahedral systems (see Table 18, 2.1.2), the Os(1)-Os(2) bond is certainly short, and is comparable with the Os(μ-H)Os vector in 19a of 2.789(1) Å.[147] It has been proposed that unsaturation in 19 may be localised at the corresponding Os(μ-H)Os edge,[147] and EHMO calculations presented in this Thesis (section 2.2(i)) support this interpretation. That two distinct Os(μ-H)Os bond lengths are observed in 30 lends further credence to this argument.

Unambiguous Assignment of Hydride Resonances in 30.

The three hydride resonances in the 213K ^{1}H n.m.r spectrum of 30 at -10.58, -12.37 and -12.86 p.p.m can be attributed to H(3), H(1) and H(2) respectively (using the atomic labelling scheme from Figure 63). The former assignment was made on the basis of the large ^{195}Pt-H coupling to the signal at -10.58 p.p.m. which clearly arises from a Os(μ-H)Pt proton, H(3). The two Os(μ-H)Os resonances were assigned by consideration of NOE difference spectra shown in Figure 62b-d.

In the n.m.r experiment, electromagnetic radiation of an appropriate frequency transfers spin population of the excited nucleus from one energy level to another. The return to equilibrium (i.e spin-lattice relaxation) is effected by interaction with magnetic fields of suitable frequency which, for protons in diamagnetic molecules, are generally due to magnetic moments of other protons in the same molecule.[329] This is dipole-dipole relaxation and its efficiency depends upon r^{-6}, where r is the internuclear separation between relevant ^{1}H nuclei. Due to the dipole-dipole relaxation mechanism, a process that alters the spin population distribution of a

particular nucleus (e.g. spin saturation) will, consequently, affect the intensity of signals due to protons which relax the excited nucleus. This is Nuclear Overhauser Enhancement (NOE) and, on irradiation of a particular resonance, the rate at which this enhancement develops at other signals also depends on r^{-6}.[329] Hence the NOE experiment can give information about inter-proton distances.

For 30, the calculated[271] internuclear separations of the hydride ligands are H(1)-H(2) = 2.67, H(1)-H(3) = 4.27, H(2)-H(3) = 2.98 Å.* In view of the inter-hydride separations, irradiation of resonances due to H(1) and H(3) is expected to give a relatively large NOE at the H(2) signal, while irradiation of the H(2) resonance is anticipated to result in significant NOE's at signals due to H(1) and H(3), with the former signal showing the larger enhancement (as H(1)-H(2) is shorter than H(2)-H(3)). Irradiation of the H(3) resonance at -10.58 p.p.m gives rise to an enhancement of 2.8% at -12.86 p.p.m. (Figure 62b) while irradiation at -12.37 p.p.m results in a 3.4% enhancement at -12.86 p.p.m (Figure 62c). Moreover, irradiation at -12.86 p.p.m leads to enhancements of 1.4 and 5.0% at -10.58 and -12.37 p.p.m respectively (Figure 62d). These results unambiguously assign the peaks at -12.37 and -12.86 p.p.m to H(1) and H(2) respectively.

* For 36 neutron diffraction determined cluster structures, the HYDEX[271] calculated hydride sites are subject to an average positional error of ± 0.05 Å. The X-ray coordinates used for 30 are likely to increase this margin. Nevertheless, minor errors in the H-H separations do not influence the qualitative interpretation of NOE results.

The signal due to H(1) displays satellites due to ^{187}Os-H coupling with a splitting of 46Hz, indicating that the magnitudes of $^{1}J(^{187}Os-H)$ to the inequivalent Os(1) and Os(2) centres are approximately equal. The size of this coupling constant is similar to that observed for 4 (48Hz),[267] and the larger ^{187}Os-H coupling in $Os_3Pt(\mu-H)_2(CO)_9(PCy_3)(CyNC)$, (41.8Hz).

H(1) is approximately coplanar with H(3) Pt,C(10) and P, and has no resolvable ^{195}Pt coupling, while H(2), lying off this plane shows a larger J(Pt-H) of 21.5Hz. A similar trend is found for other *tetrahedro*-Os_3Pt systems (see Table 32) and, therefore, consideration of the magnitude of ^{2}J(Pt-H) couplings may aid the spectroscopic identification of Os(μ-H)Os hydride locations in related clusters.

Table 32 : Magnitudes of ^{195}Pt couplings to Os(μ-H)Os protons in *closo*-tetrahedral Os_3Pt clusters.

	^{2}J(Pt-H) (Hz)		
Cluster.	Coplanar with PtLL'(H)	Noncoplanar	Ref.
19	6.5	-	147
23	-	18	258
24	-	20	258
26a	unresolved	-	this work
26b	5.7	-	this work
27	-	22	this work
28	-	19	this work
isomer E of 28*	-	15	this work
30	unresolved	21.5	this work

* structure not crystallographically defined.

Dynamic Behaviour of 30.

The two Os(μ-H)Os resonances broaden on warming above 213K, while the Os(μ-H)Pt signal remains sharp. (Variable temperature ^{1}H n.m.r spectrum is shown in Figure 64). A value of $\Delta G^{\ddagger}_{293}$ = 62.7(5) kJ mol^{-1} was determined for this two site exchange by line-shape analysis. Exchange of the two Os(μ-H)Os hydrides can occur in ways that either maintain the chirality of 30 or lead to racemisation. These processes are shown as I, II and IV in Scheme 16. A further process, III, invisible in the ^{1}H, but not the ^{13}C n.m.r spectrum, could also racemise the cluster by H(2) migration.

The variable temperature ^{13}C n.m.r spectrum of a ^{13}CO enriched sample of 30 is shown in Figure 65. At 228K ten distinct resonances of equal intensity are observed for the inequivalent carbonyls. These resonances have been assigned on the basis of couplings to the hydrides, and a full listing of these assignments and the n.m.r parameters for 30 is given in Table 33. The only signals that were not unambiguously assigned by J(H-C) coupling considerations are d and f, however magnetisation transfer experiments confirmed that these resonances are due to C(4) and C(6) respectively (vide infra). The $^{1}J(^{187}Os-C)$ couplings observed for 30 range from 98-114Hz and are similar to those reported for 19a[265] and other osmium carbonyl clusters.[266,304]

On warming the sample to 273K, (Figure 65) all resonances except e and g broaden, suggesting that 30 is racemising rapidly on the n.m.r timescale, and, consequently, acquiring a time-averaged mirror plane. This is consistent with processes II and III and IV of Scheme 16. At 296K, it is clear that the Pt-bound carbonyl is the only non-exchanging CO.

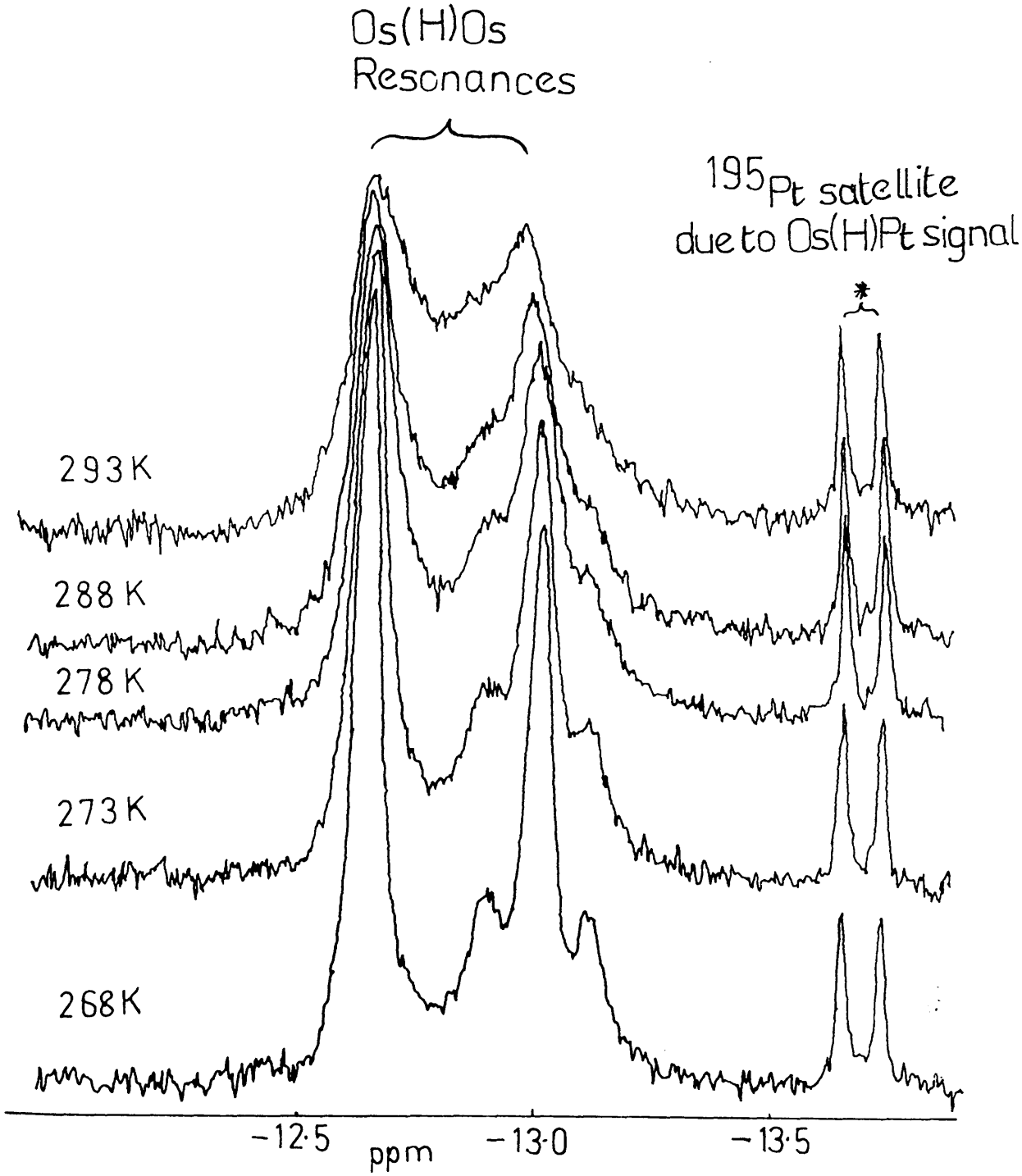

Figure 64 : Variable temperature ^{1}H n.m.r spectrum of $[Os_3Pt(\mu\text{-}H)_3(CO)_{10}(PCy_3)]^+BF_4^-$.

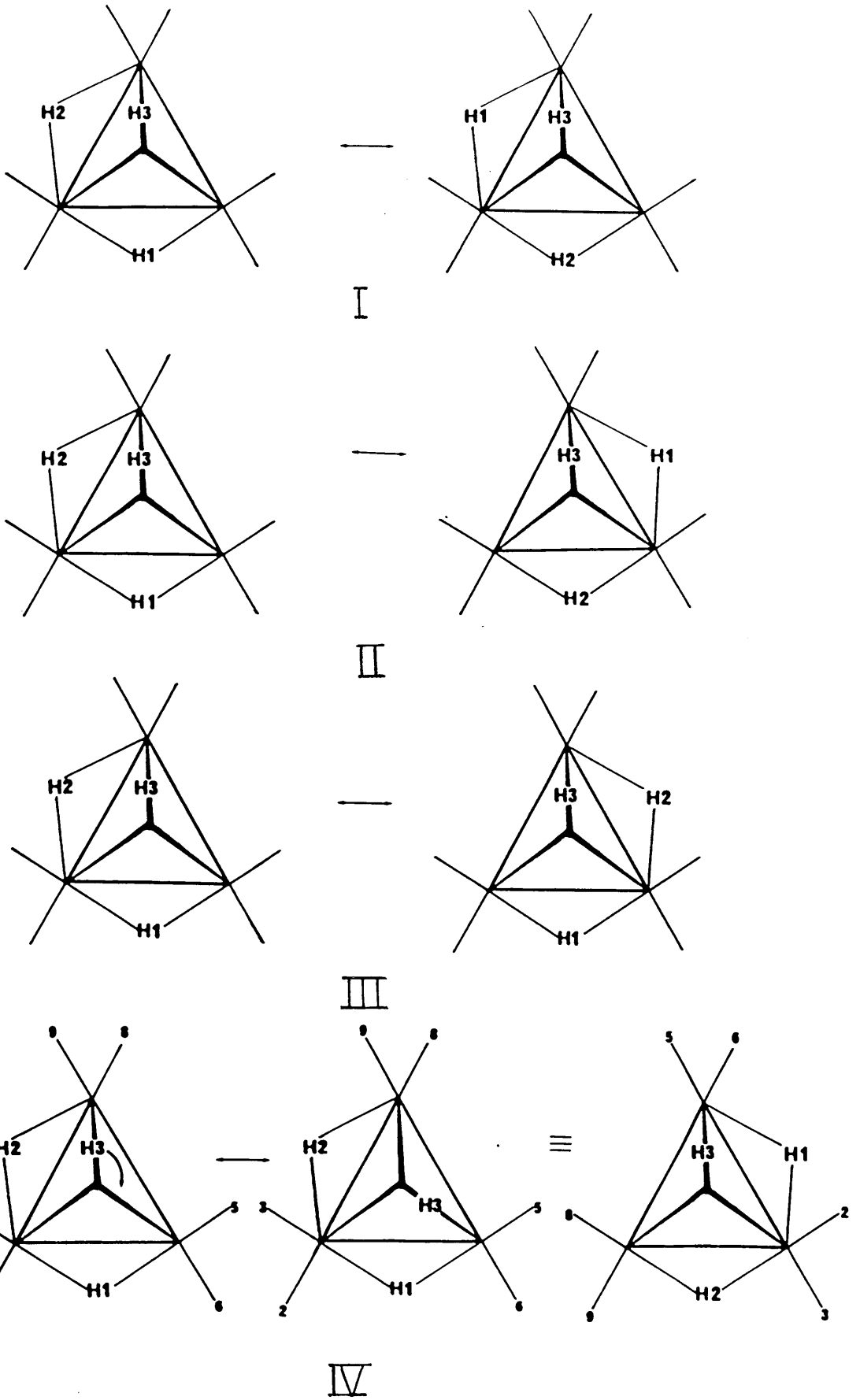

Scheme 16 : Possible mechanisms for Os(μ-H)Os hydride exchange in 30.

Selective excitation of resonances using the DANTE[305] pulse sequence allows further elucidation of the carbonyl fluxionality in 30. At 253K, inversion of signal a [due to C(5)] leads to exclusive saturation transfer to h [C(3)]. No transfer to C(4),(6) or C(1),(2) is observed indicating that tripodal rotation of the $Os(CO)_3$ groups at Os(1), Os(2) centres is not occuring at a significant rate. This contrasts with the carbonyl fluxionality in 19a[265] and 26b (Section 2.2(ii)), where such a process is already operative at 218K for 19a, and 236K for 26b. As exclusive saturation transfer is observed between j/f, and d/i the resonances d and f are assigned to C(4) and C(6) respectively. Due to the small difference in chemical shift between signals b and c it did not prove possible to demonstrate saturation transfer between C(8) and C(9). Thus, the ^{13}C n.m.r evidence suggests that 30 is racemising at 253K. Process II of Scheme 16 accounts for both the hydride and carbonyl fluxionality observed here. However contributions from I and III cannot be excluded in the absence of rate data showing that the rate of hydride exchange is equal to the rate of cluster racemisation. It is evident, finally, that process IV cannot be the sole fluxional process operative since this results in pairwise exchange of C2/3, C9/6, C8/5 and C7/4, which is not observed in the ^{13}C n.m.r spectrum.

At 263K, similar DANTE experiments indicated that, on irradiation of a, saturation is transferred to b,c,f and j, in addition to h. d, e and i remain unaffected. This is indicative of a further dynamic process which exchanges the six pseudo-equatorial carbonyls C(2), C(3), C(5), C(6), C(8) and C(9) and leaves the axial carbonyls C(1), C(4) and C(7) distinct. This is compatible with a mechanism involving polytopal rotation of the $PtH(CO)(PCy_3)$ fragment about the Os_3 framework in tandem with hydride migration.

Figure 65 : Carbonyl region of V.T. ^{13}C n.m.r spectrum of $[Os_3Pt(\mu\text{-}H)_3(CO)_{10}(PCy_3)]^+$

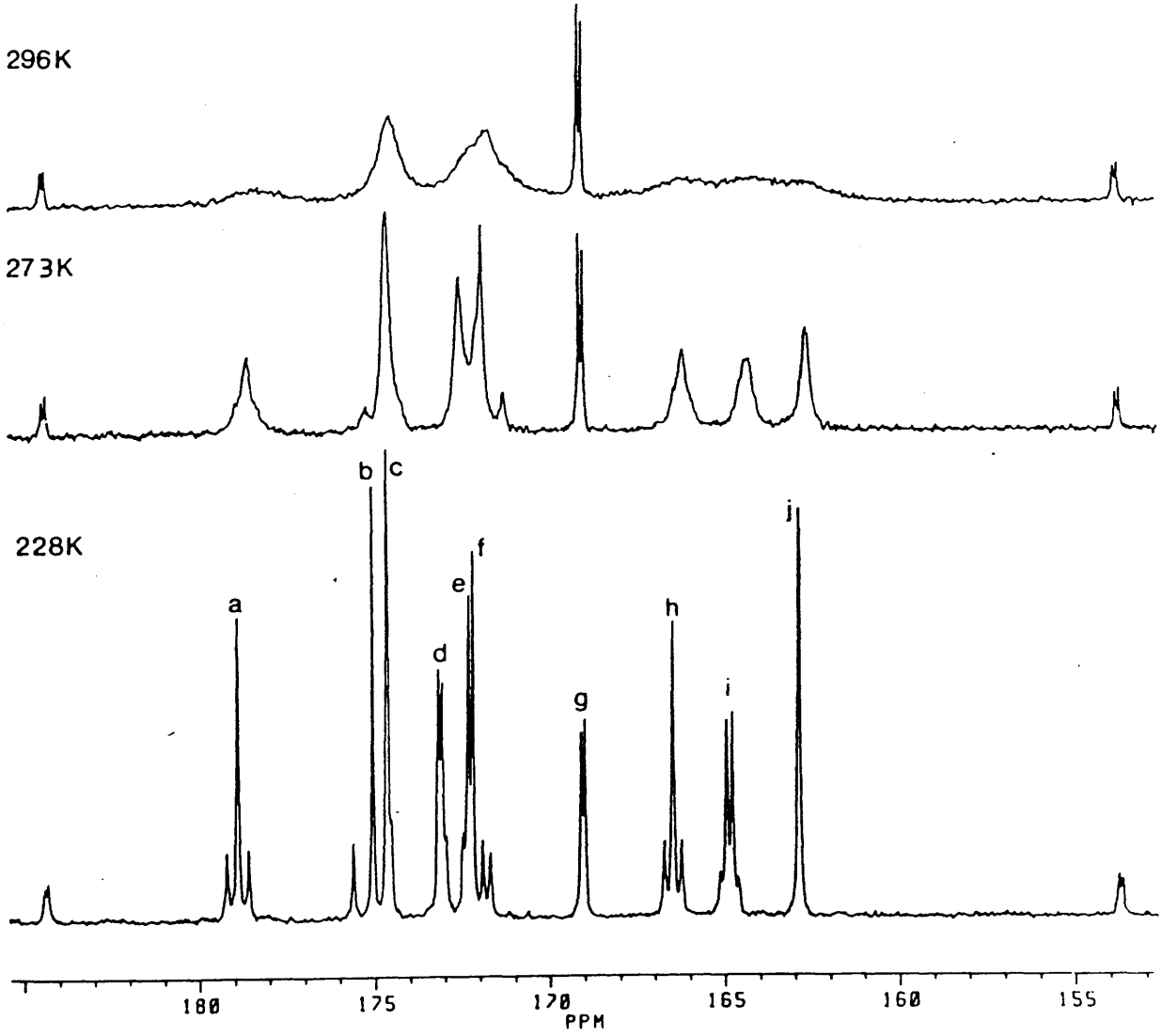

Table 33 : NMR Parameters for $[Os_3Pt(\mu\text{-}H)_3(CO)_{10}(PCy_3)]^+BF_4^-$, 30.

^{13}C Data [a]

Reson.[b]	ppm	Mult.[c]	Assgnmt.[e]	J/Hz[d]					
				P-C	Pt-C	Os-C	H1-C	H2-C	H3-C
a	178.3	s	C(5)	-	31	103	10.4	-	-
b	174.5	s	C(9)	-	54	105	-	w	w
c	174.0	s	C(8)	-	-	-	-	6.7	w
d	172.6	d	C(4)	5.4	-	-	w	-	-
e	171.8	s	C(7)	-	64	114	-	w	6.7
f	171.5	s	C(6)	-	29	104	w	-	-
g	168.3	d	C(10)	5.1	1543	-	-	-	34.0
h	165.9	s	C(3)	-	25	98	12.7	w	-
i	164.3	d	C(1)	8.4	17	-	w	w	-
j	162.2	s	C(2)	-	-	108	w	12.1	w

^{1}H Data [f]

-10.58 (d, Os(μ-H)Pt, J(Pt-H) = 603, J(P-H) = 8.0)
-12.37 (dd,Os(μ-H)Os, J(Os-H) = 46, J(P-H) = 1.1
J(H-H) = 1.7)
-12.86 (dd,Os(μ-H)Os, J(P-H) = 1.7, J(H-H) = 1.7
J(Pt-H) = 21.5)

(a) 213K, CD_2Cl_2,CH_2Cl_2 1:1; b) Figure 65; c) Refers to C-{H}spectra
d) w indicates small unresolved couplings; e) Figure 63;
f) 213K, CD_2Cl_2, ppm rel. to TMS.

Furthermore, rotation of the $PtH(CO)(PR_3)$ unit with retention of stereochemical rigidity has been previously observed in the fluxional behaviour of $[PtRh_2(\mu\text{-}H)(\mu\text{-}CO)_2(Cp^*)_2(CO)(PPh_3)]^+BF_4^-$,[306] while rotation of a $PtH(CNCy)(PCy_3)$ unit is observed in 26b. A planar "merry-go-round"[307] exchange of the six equatorial carbonyl ligands about the Os_3 triangle is also consistent with the experimental data, however, such a process involves the formation of CO bridges, which is considered to be unfavourable as two Os-Os edges are already spanned by hydride ligands.

2.3.2 Protonation of $Os_3Pt(\mu\text{-}H)_2(CNCy)(CO)_9(PCy_3)$, 26b.

Addition of excess $HBF_4.Et_2O$ to CH_2Cl_2 solutions of 26b, effected a rapid colour change from green to dark purple, yielding $[Os_3Pt(\mu\text{-}H)_3(CNCy)(CO)_9(PCy_3)]^+BF_4^-$, 31. 31 has been identified spectroscopically. The i.r. spectrum of 31 shows a band due to a terminally ligated isocyanide (ν_{CN} 2202 cm^{-1}) and several bands in the terminal CO region (ν_{CO} 2111-1990 cm^{-1}). The highfield region of the ^1H n.m.r spectrum shows three resonances at -13.13, -13.29 (J(Pt-H) = 547, J(P-H) = 7.2Hz) and -13.47 p.p.m., (J(Pt-H) = 21Hz).

The signal at -13.29 p.p.m is attributed to an Os(μ-H)Pt proton, on the basis of the large ^{195}Pt coupling, while two inequivalent Os(μ-H)Os hydrides give rise to the resonances at -13.13 and -13.47 p.p.m. The fluxional behaviour of the hydrides in 31 closely resembles that observed in 30, with the two Os(μ-H)Os resonances broadening on heating and coalescing at ca. 330K, while the Os(μ-H)Pt proton is not involved in this exchange. The proposed structure of 31 is shown in Figure 66a. The Os(μ-H)Os resonances at -13.13 and -13.47 p.p.m can be assigned to H2 and H3 respectively

on the basis of the magnitudes of $^{2}J(^{195}Pt\text{-}H)$ coupling to these signals (see Table 32). The ^{31}P n.m.r spectrum shows the PCy_3 function remains ligated to the Pt.

2.3.3 Protonation of $Os_3Pt(\mu\text{-}H)_2(\mu\text{-}CH_2)(CNCy)(CO)_9(PCy_3)$, 27.

27 was protonated with CF_3CO_2H, yielding $[Os_3Pt(\mu\text{-}H)_3(\mu\text{-}CH_2)(CNCy)(CO)_9(PCy_3)]^+CF_3CO_2^-$, 32 which was identified spectroscopically. Two hydride signals are observed for 32 at -17.73 (J(Pt-H) = 490Hz) and -21.67 p.p.m (J(Pt-H) = 11Hz) in the ratio 1:2, suggestive of a structure with one Os(μ-H)Pt and two equivalent Os(μ-H)Os protons, such as that shown in Figure 66b.

It is noticeable that for the hydrido clusters reported above, the chemical shifts of the hydride signals move to highfield (with the exception of the Os(μ-H)Os resonance in 32) on protonation c.f. the chemical shifts of the unprotonated parent clusters.

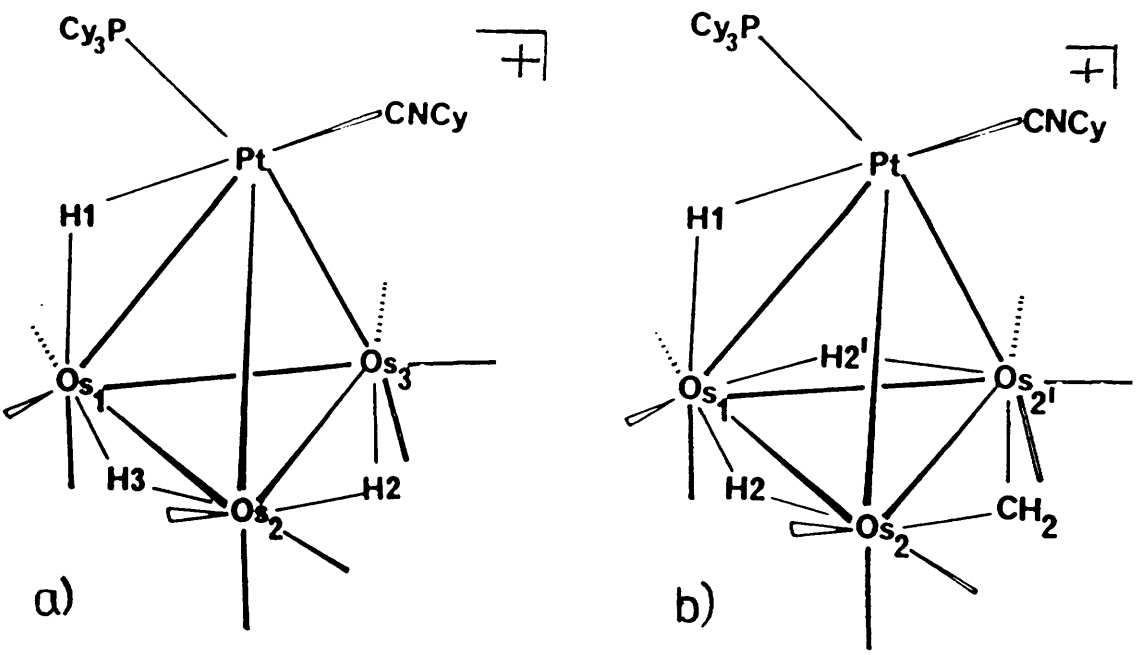

Figure 66 : Proposed structures for (a) $[Os_3Pt(\mu\text{-}H)_3(CNCy)(CO)_9(PCy_3)]^+$ and (b) $[Os_3Pt(\mu\text{-}H)_3(\mu\text{-}CH_2)(CNCy)(CO)_9(PCy_3)]^+$.

Thus, 19a, 26b and 27 all protonate at Os-Os edges. For 26b protonation does not affect the CNCy function. It is noteworthy that the CN^- adduct of 4 undergoes successive protonation at the N site of the cyanide function to yield CNH and μ-CNH_2 moieties.[93] The crystal structure of complex 30 shows the Os(μ-H)Os separations very considerably in length. This is in keeping with the proposed localisation of unsaturation at an Os(μ-H)Os unit of 19 and 26b.

2.4 Reactions of $Os_3Pt(\mu\text{-}H)_2(CO)_{10}(PCy_3)$ with Heteroatomic Unsaturated Species.

The study of the reactions of heteroatomic unsaturated species with Os clusters has provided synthetic routes to a variety of interesting cluster-bound ligands.[33,94] These complexes are of importance in the elaboration of cluster reactivity trends (since, in the incoming ligand, there is a choice of potential cluster binding sites) and with respect to the elucidation of catalytic processes involving transformations of heteroatomic functions.[308]

The unsaturated complex, 4, has proved a particularly versatile synthon in the preparation of functionalised Os_3 clusters (see Chapter 1.3.2). One noteworthy feature of these reactions is that, in many cases, the transfer of a hydride from the cluster to the unsaturated ligand is effected.[89,109,111,101-104,120]

In view of our interest in investigating the chemistry of 19, which, like 4, is an unsaturated hydrido-cluster, a study of the reactions of 19 with several heteroatomic unsaturated species was undertaken. The reactions of CH_2N_2,[258] and CO[148] with 19a have been reported previously, while the reactivity of 19a towards RNC (R = t-Bu, Cy) and SO_2 is detailed in sections 2.2 (ii) and 2.2 (iii) of this Chapter.

2.4.1 Reaction of $Os_3Pt(\mu\text{-}H)_2(CO)_{10}(PCy_3)$, 19, with a thioketene.

The heteroallene species $R_2C{=}C{=}S$, have been shown to be reactive towards mononuclear,[312,314] binuclear[313,316] and cluster[315] complexes. A summary of some of these reactions is presented in Scheme 17. A number of coordination modes can be adopted by thioketene functions bound to metal sites, and in Scheme 17 $\mu_2\text{-}\eta^1\text{-}S$, $\eta^2\text{-}C\text{-}S$ and $\mu_2\text{-}\eta^2\text{-}C\text{-}S$ bonding modes are illustrated. Transfer of a metal hydride to the thioketene function is observed in the reaction of $R_2C{=}C{=}S$ with $NbH_3(Cp)_2$.[312]

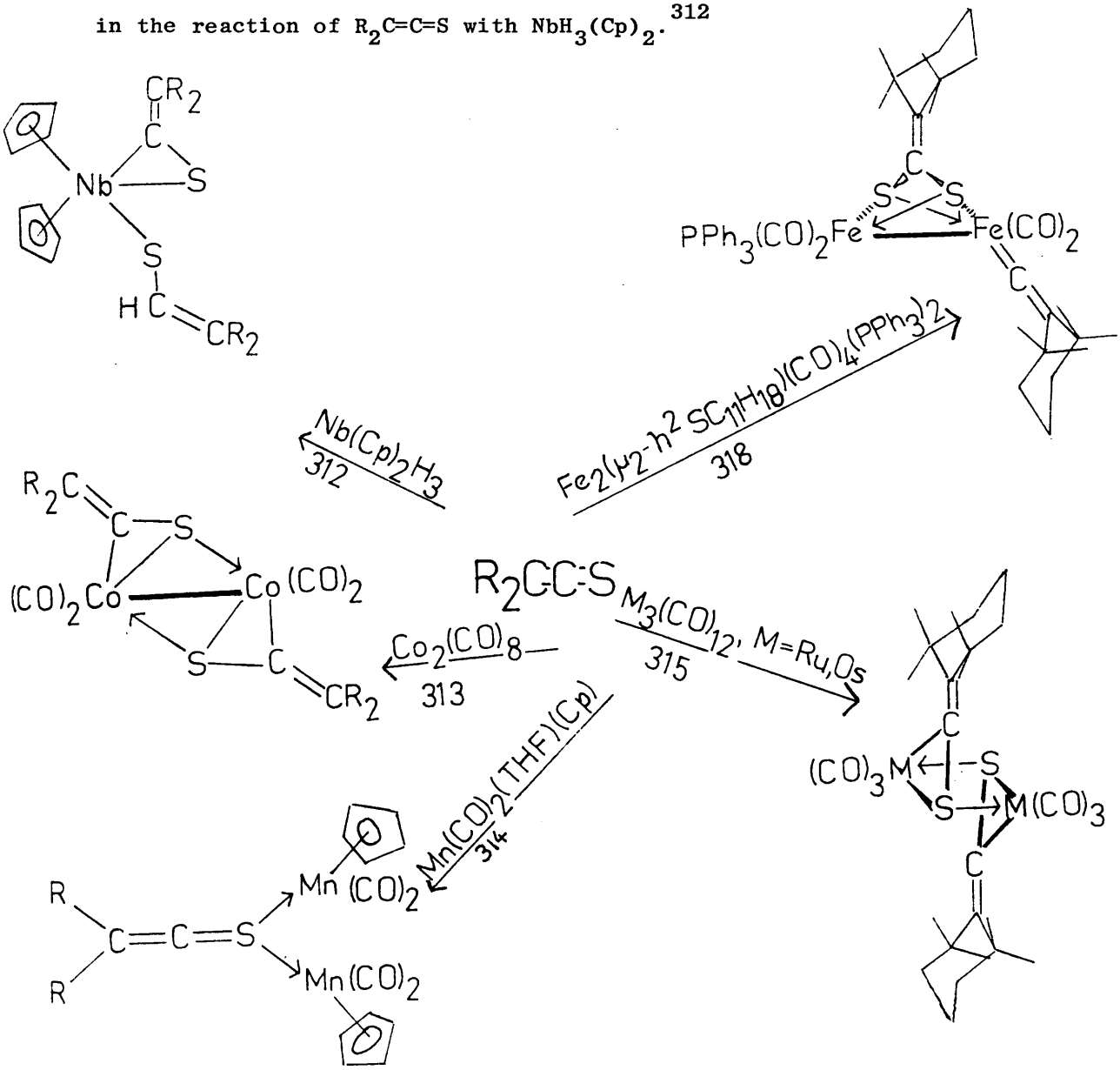

Scheme 17 : Some Reactions of $R_2C{=}C{=}S$ with transition metal complexes.

In view of the interesting organometallic chemistry associated with $R_2C=C=S$ functions, the reaction of 19a with the thioketene 1-thiocarbonyl, 2,2,6,6-tetramethylcyclohexane (cyclohexylthioketene) was studied. A sample of this thioketene was kindly supplied by Dr. U. Behrens, Hamburg University.

Extensive thermolysis (90°C, 22h) of a toluene solution of 19a and excess 1-thiocarbonyl,2,2,6,6 tetramethyl cyclohexane under reduced pressure resulted in the green colour of 19 giving way to brown. Column chromatography of the hexane soluble products effected the elution of fourteen separate bands. The major product obtained was isolated from the second band as red crystals in 6% yield and is formulated as $Os_3Pt(\mu_3\text{-}S)_2[\eta^1\text{-}C=(C_{10}H_{18})](CO)_9(PCy_3)$, 33

The ^{31}P n.m.r spectrum of 33 shows a single resonance at 36.1 p.p.m (J(Pt-H) = 2771 Hz), consistent with a Pt-bound PCy_3 function. No highfield resonances are observed in the ^1H n.m.r spectrum of 33, indicating that the complex has no metal hydride ligands. Signals arising from CH_3 and CH_2 protons are observed in the expected range 2.36 - 0.84 p.p.m. The i.r. spectrum of 33 shows terminally bound CO stretches that range from 2069 - 1946 cm^{-1}.

The spectroscopic data obtained for 33 is consistent with many possible structures. Therefore an X-ray diffraction experiment was undertaken by Dr. L.J. Farrugia in order to determine the solid state structure of 33.

The crystal structure of 33 is shown in Figure 67, while relevant metrical parameters are listed in Table 34. From consideration of the intermetallic distances, it is clear that all M-M vectors apart from the Pt---Os(1) (3.656(1)Å and Os(1)---Os(3) (3.618(1)Å), separations are bonding. Thus, the metal core of 33 has a spiked triangular geometry with a PtOs(2)Os(3) triangle being

Figure 67 : Molecular structure of $Os_3Pt(\mu_3\text{-}S)_2[\mu_1\text{-}C{=}(C_{10}H_{18})]\text{-}(CO)_9(PCy_3)$, 33.

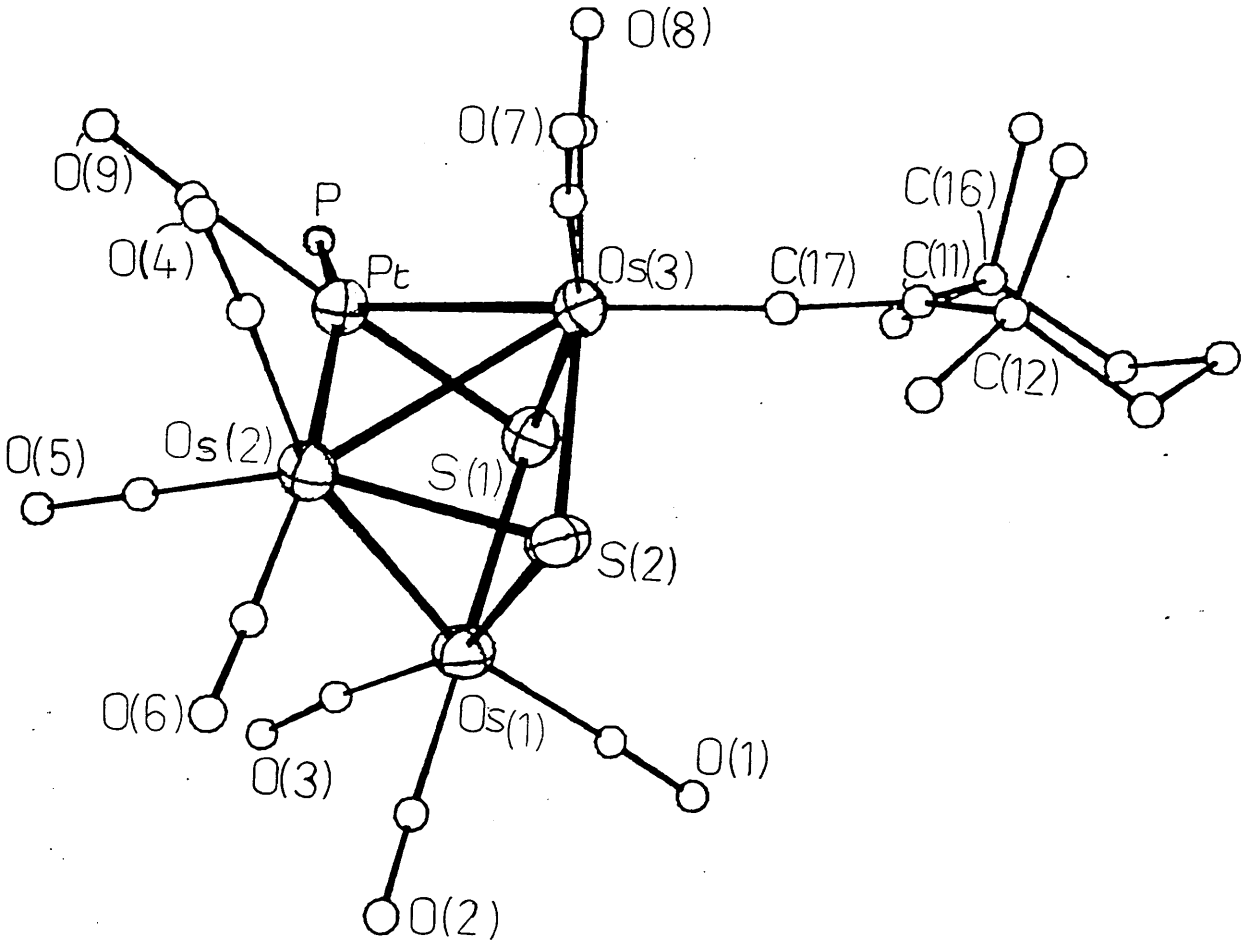

Table 34 : Selected Bond Lengths (Å) and Bond Angles (deg) for the complex $Os_3Pt(\mu_3\text{-}S)_2[\eta^1\text{-}C{=}(C_{10}H_{18})](CO)_9(PCy_3)$, 33

Bonds

Pt-Os(2)	2.848(1)	Pt-Os(3)	2.862(1)
Pt-S(1)	2.325(3)	Os(1)-Os(2)	2.810(1)
Os(1)-S(1)	2.464(3)	Os(1)-S(2)	2.387(3)
Os(2)-Os(3)	3.030(1)	Os(2)-S(2)	2.400(3)
Os(3)-S(1)	2.450(4)	Os(3)-S(2)	2.384(3)
Os(1)-C(1)	1.916(16)	Pt-P	2.350(4)
Os(1)-C(2)	1.885(15)	Pt-C(9)	1.867(16)
Os(1)-C(3)	1.912(17)	Os(2)-C(4)	1.870(12)
Os(2)-C(5)	1.859(12)	Os(2)-C(6)	1.899(13)
Os(3)-C(7)	1.895(15)	Os(3)-C(8)	1.908(13)
Os(3)-C(17)	1.898(13)	C(11)-C(17)	1.286(17)
C(11)-C(12)	1.56(2)	C(11)-C(16)	1.51(2)

mean C-O = 1.138

Angles

Os(2)-Pt-Os(3)	64.1(1)	Os(2)-Pt-P	161.6(1)
Os(2)-Pt-S(1)	84.0(1)	Os(3)-Pt-S(1)	55.2(1)
Os(3)-Pt-P	131.2(1)	P-Pt-S(1)	97.3(2)
P-Pt-C(9)	93.6(5)	S(1)-Pt-C(9)	168.1(5)
Os(2)-Os(1)-S(1)	82.4(1)	Os(2)-Os(1)-S(2)	54.3(1)
Pt-Os(2)-Os(3)	58.2(1)	S(1)-Os(1)-S(2)	82.0(1)
Os(1)-Os(2)-S(2)	53.8(1)	Pt-Os(2)-Os(1)	80.5(1)
Os(3)-Os(2)-S(2)	50.5(1)	Pt-Os(2)-S(2)	100.0(1)
Pt-Os(3)-Os(2)	57.7(1)	Os(1)-Os(2)-Os(3)	76.5(1)
Pt-Os(3)-S(2)	100.0(1)	Pt-Os(3)-S(1)	51.2(1)
Os(2)-Os(3)-S(1)	78.1(1)	Os(2)-Os(3)-S(2)	50.9(1)
Pt-S(1)-Os(1)	99.5(1)	S(1)-Os(3)-S(2)	82.3(1)
Os(1)-S(1)-Os(3)	94.8(2)	Pt-S(1)-Os(3)	73.6(1)
Os(1)-S(2)-Os(3)	98.7(2)	Os(1)-S(2)-Os(2)	71.9(1)
Os(3)-C(17)-C(11)	175.6(14)	Os(2)-S(2)-Os(3)	78.6(1)
C(12)-C(11)-C(17)	119.4(13)	C(12)-C(11)-C(16)	120.6(11)
		C(16)-C(11)-C(17)	120.0(14)

mean M-C-O = 176.6

axially ligated at Os(2) by Os(1). Two triply bridging sulphido ligands span PtOs(1)Os(3) and Os(1)Os(2)Os(3) sites. The transition metal framework of 33 is similar to that of 29, however the overall cluster geometry more closely resembles that in the $Os_3Pt(\mu_3\text{-}S)_2(CO)_{11-n}(L)_n$, (n = 1,2 L = PPh_3,[249]; n = 2, L = PMe_2Ph,[253]) systems, where the η^1-vinylidene function of 33 is replaced by a terminal CO ligand.

The distorted trigonal bipyramidal geometry about Pt renders it an 18 electron metal centre. Hence the 64 valence electron count of 33 is in keeping with the E.A.N.[53] predictions for a spiked triangular metal framework. This structure is however, incompatible with the P.S.E.P.T.[55,57] (incorporation of sulphido ligands into the cluster framework gives 8 SEP's for which a *nido* pentagonal bipyramid is predicted; this is not found as the Pt---Os(1) separation is non-bonding).

The M-M bond lengths and the Pt-S, and Os-S distances (Table 34) are in accord with similar separations observed in other $OsPt(\mu_3\text{-}S)$ systems.[249,252,253] The M-C metal-carbonyl bond lengths fall within the expected range, and the carbonyl functions are approximately linear throughout (M-C-O varies between 173(1)-178(1)°).

The most unusual feature of this structure is the near linear (Os(3)-C(17)-C(11) = 176(1)°) η^1-coordinated vinylidene function ligated to Os(3). Cluster bound vinylidenes are normally observed in multi-site bonding modes[34-36] and it is unprecedented for η^1-coordination to be adopted in a cluster system. The Os(3)-C(17) bond length of 1.898(13) Å is very similar to the corresponding vinylidene α-carbon-Os separation of 1.90(1) Å observed in $Os[\eta^1\text{-}C{=}\overline{C.C(H){=}C(H).C(H)(CH_3).C(H){=}C}(H)](CO)_2(PPh_3)_2$[317]. Furthermore the bond angles about C(11), (119(1)-120(1)°) and the C(17)-C(11) distance of 1.29(2) Å are both indicative of a C(11)-C(17) double bond.

The vinylidene ligates trans to the Pt-Os(3) vector and its axial coordination is presumably enforced by the steric bulk of the ligand.

It has been proposed [253] that the structurally similar complex $Os_3Pt(\mu_3\text{-}S)_2(CO)_9(PMe_2Ph)_2$ undergoes a facile dynamic framework rearrangement involving transfer of the $Pt(PMe_2Ph)_2$ unit from one Os-Os edge to the other (see Scheme 18).

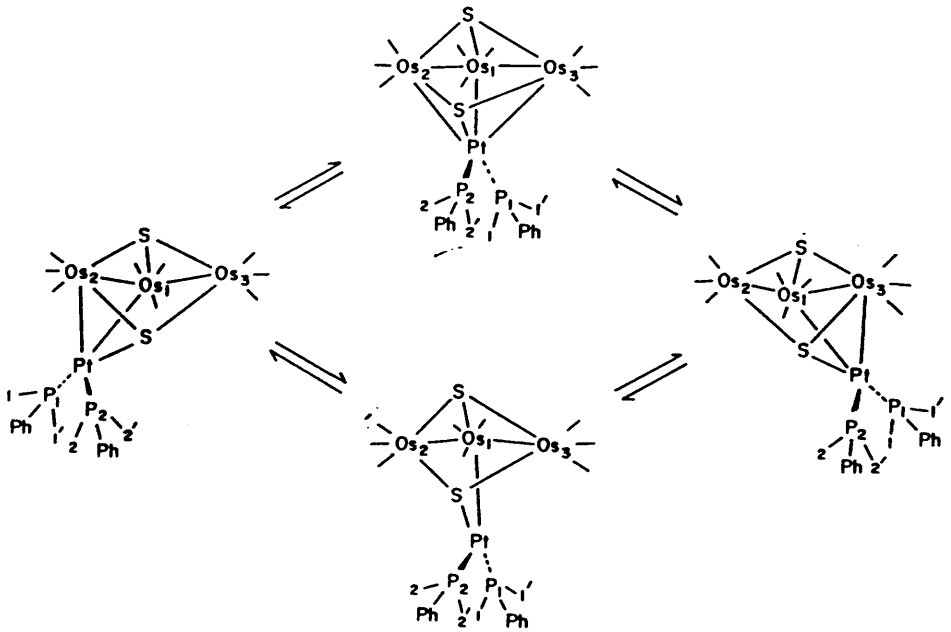

Scheme 18 : Proposed skeletal fluxionality in $Os_3Pt(\mu_3\text{-}S)_2(CO)_9(PMe_2Ph)_2$

A similar process operative in 33 would transfer the $Pt(CO)(PCy_3)$ unit from the Os(2)-Os(3) edge to span Os(1)-Os(2). As Os(3) and Os(1) are chemically inequivalent, such an exchange would be a non-degenerate process and would lead to averaging of two distinct phosphine resonances in the ^{31}P n.m.r spectrum. However, the variable temperature ^{31}P n.m.r spectrum of 33 shows only one, sharp signal in the temperature range 213K - 313K.

This suggests that a similar exchange process is not operative in 33; or the fluxionality is not "frozen out" at 213K; or, as the

migration of the $Pt(CO)(PCy_3)$ unit is a non-degenerate process in 33, one structural isomer dominates at equilibrium and signals due to the other isomer are difficult to detect. An examination of the variable temperature ^{13}C n.m.r spectrum of 33 over a wider temperature range would further elucidate any framework fluxionality. Such a study was precluded by the very low recoverable yields of 33.

The reaction of 19 with cyclohexyl thioketene has resulted in C=S bond cleavage to yield two μ_3-sulphido ligands and an unusual η^1-vinylidene moiety. The fate of the second $C_{11}H_{18}$ unit and the two metal hydride functions of 19 is unknown, although it is possible that the hydrides transfer to this organic fragment to yield 2,2,4,4-tetramethylmethylene cyclohexane. Interestingly, the dinuclear complex $Fe_2[\mu\text{-}\eta^2\text{-}SC\overline{C\cdot C(CH_3)_2\cdot CH_2\cdot CH_2\cdot CH_2\cdot C(CH_3)_2}](CO)_4(PPh_3)_2$ on treatment with cyclohexyl thioketene also inserts a metal into the C=S bond of the thioketene function yielding $Fe_2(\mu\text{-}\eta^2\text{-}S_2C{=}R)(\eta^1\text{-}C{=}R)(CO)_4(PPh_3)$ [318] $R = \overline{C\cdot C(CH_3)_2\cdot CH_2\cdot CH_2\cdot CH_2\cdot C(CH_3)_2}$, which like 33, has an η^1-bound vinylidene ligand. In contrast the reactions of 1 and 2 with cyclohexyl thioketene [315] result in cluster degradation and the formation of the dinuclear species $[M(C_{11}H_{18}S)(CO)_3]_2$, (M = Ru, Os), (shown in Scheme 17) where the thioketene functions have not cleaved.

It is noteworthy that the series of similar $Os_3Pt(\mu_3\text{-}S)_2$ complexes synthesised by Adams[249,253] have all been prepared by reaction of $Os_3(\mu_3\text{-}S)_2(CO)_9$ with mononuclear Pt species. It is possible that, under the somewhat forcing thermal condition necessary for the reaction of 19a with cyclohexyl thioketene cluster degradation occurs to give Os_3 sulphido-species which subsequently add a Pt fragment at a sulphido site. A mechanism involving cluster degradation of 19 would account for the low yields of 33, and the large number of other species produced in this reaction.

Finally, reactions of various stoichiometric ratios of 19a and cyclohexyl thioketene were investigated and the yield of 33 is optimised when a 3:1 ratio of

cyclohexyl thioketene to 19a is used, although the dependence of yield on reactant stoichiometry is slight. In all reactions studied, 33 was the major product.

2.42 The Reaction of $Os_3Pt(\mu\text{-}H)_2(CO)_{10}(PCy_3)$, 19, with [PPN]SCN.

There is considerable interest, at present, in the reactivity of cluster complexes towards anionic nucleophiles. It has been demonstrated that nucleophilic attack of an anion at a coordinatively saturated cluster can promote CO substitution.[241] This has led to the development of catalytic cluster activation by anions as a synthetic strategy as described in Chapter 1. Furthermore anions can provide a useful route for the introduction of new functionality to clusters and, once bound to a cluster, anions containing multiple bonds can undergo various transformations to yield novel products. For example, cluster ligated N_3 functions, derived from N_3^-, are known to add CO and convert to NCO, with loss of N_2,[319,224] while the CN^-adduct of 4 protonates at the N site to yield successively CNH and $\mu\text{-}CNH_2$ functions.[93]

In the context of establishing the reactivity of 19 towards heteronuclear unsaturated species, the reaction of 19 with [PPN] SCN was studied.

On treatment with a CH_2Cl_2 solution of excess [PPN] SCN , a green solution of 19a in methylene chloride rapidly changed colour to yellow. The ^1H n.m.r spectrum of the resulting reaction mixture showed two major signals in the highfield region, at -9.62 (J(P-H) = 15.3, J(Pt-H) = 564Hz) and -14.7 p.p.m. due to Os(μ-H)Pt and Os(μ-H)Os

protons respectively. Highfield resonances due to minor products occur at -11.65 (J(P-H)= 11Hz), -14.41, -14.62, -17.59, -20.98 and -21.28 p.p.m. Peaks due to ligated SCN (ν_{CN}: 2121 cm^{-1}) and terminally bound CO ligands (ν_{CO}: 2055 - 1915 cm^{-1}) are observed in the i.r spectrum of the reaction mixture. Unfortunately the ν_{CN} frequency does not unambiguously determine whether the SCN function binds through the S or the N site.[320]

Analysis of the ^{13}C n.m.r spectrum of the reaction mixture at ambient temperatures proved uninformative due to the number of products present, and the fluxionality of the carbonyls in these systems at room temperature. Nevertheless, three sharp signals are observed at 156.9, 162.6 and 169.1 (J(P-C) = 6, J(Pt-C) = 1542Hz). This latter resonance is clearly due to a Pt-bound CO, although whether this signal arises from the main hydrido-cluster product is not determined.

All attempts to isolate pure samples of any product of this reaction failed. The reaction of stoichiometric quantities of 19 and [PPN] SCN left large amounts of 19 unreacted, as shown by ^{1}H n.m.r spectroscopy. Protonation of reaction mixtures,in an attempt to isolate neutral products, resulted in reformation of 19 in small amounts as the major isolable species, as did treatment of 30 with [PPN] SCN .

The preference of SCN^- to ligate at the sulphur site with heavy transition metals is in accord with soft Lewis acid/base arguments and has been commented on previously.[321] This has been demonstrated in an Os_3 cluster system, where $Os_3(\mu\text{-}AuPPh_3)(\mu\text{-}SCN)(CO)_{10}$[112] has a 3 electron donor S-bound thiocyanate function. Furthermore, recently reported tetra-[309] and hexanuclear[310] iridium clusters have thiocyanate functions ligated at the S site. Hence it is thought

that SCN^- adducts of 19 will bind through the sulphur. A possible structure for such species, that is consistent with the spectroscopic data, is shown in Figure 68.

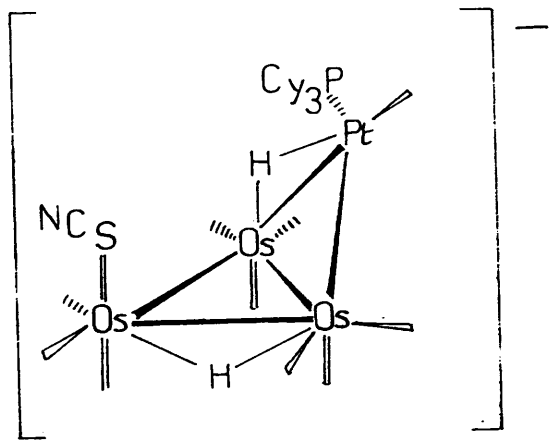

Figure 68 : Possible structure of SCN^- adduct of 19.

Several other reactions of this type were investigated. 19 was unreactive towards Me_3SiN_3, MeNCS and SeO_2, while on treatment with CS_2 and NO_2^- numerous products were observed in very low yields. Finally reaction of 19 with O_3 (formally analogous to SO_2) and the reactive heterocumulene O=C=C=C=O (carbon suboxide) resulted in extensive cluster degradation. None of these reactions were studied further.

2.5 Reaction of $Os_3Pt(\mu\text{-}H)_2(CO)_{10}(PCy_3)$, 19, with LiC≡CPh.

In view of the proposed cluster-surface analogy,[2-4] and the catalytic potential that clusters themselves show,[9-17] there is great interest in the elucidation of cluster reactivity towards unsaturated hydrocarbons. The reactivity of alkyne and acetylide moieties[34-37]

with cluster systems has provided a particularly rich chemistry. These functions display a wide range of cluster coordination modes; illustrative examples are shown in Scheme 19.

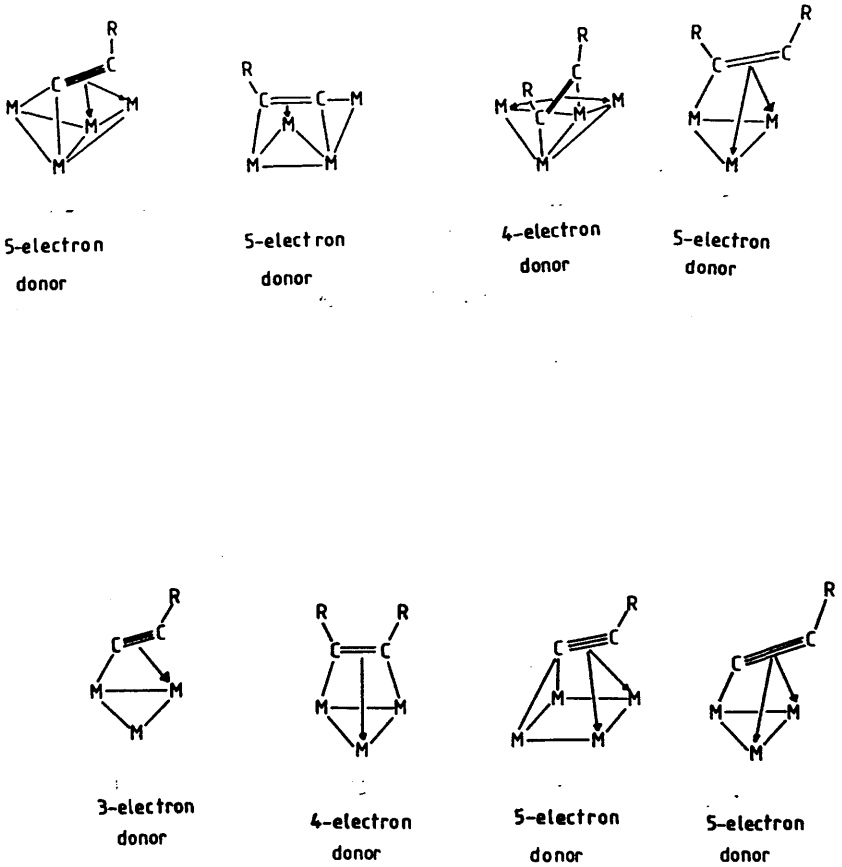

Scheme 19 : Possible bonding modes of cluster-bound C≡CR and RC≡CR' functions.

Furthermore many observed transformations of cluster-ligated alkynes and acetylides are of potential mechanistic importance in catalytic processes. For example, alkyne scission[178,179,322,323] and alkylidyne coupling yielding alkyne functions,[322,324,325] alkyne coupling[98,99] and alkyne-methylene coupling[275,276] have all been

observed on a cluster framework.

The reaction of 19 with $CH_3C{\equiv}CCH_3$ has been investigated previously[148] and it was found that extensive thermolytic treatment resulted in cluster degradation. In an effort to investigate the reactivity of 19 under conditions that will retain the integrity of the Os_3Pt core, the reaction of 19 with the nucleophilic acetylide $^-C{\equiv}CPh$ was studied.

Addition of a 1:1 stoichiometric quantity of $PhC{\equiv}C^-Li^+$ in diethyl ether to an ethereal solution of 19 at -20^oC effected a rapid colour change from green to orange. In an effort to establish the nature of the initial, presumably anionic, cluster species formed in this reaction, a slight excess of [PPN] Cl in CH_2Cl_2 was added to the reaction mixture. This resulted in the formation of a fine white precipitate, assumed to be LiCl, which was removed from solution by "flash" filtration through a small Celite pad. The carbonyl region of the i.r. spectrum of the resulting solution indicated that a mixture of products had formed. Despite many unsuccessful attempts, it was not possible to isolate a pure compound from the resulting mixture.

However, addition of $PhC{\equiv}C^-Li^+$ to 19 in an analogous manner followed by treatment of the resulting solution with excess CF_3CO_2H yielded $Os_3Pt(\mu\text{-}H)(\mu_4\text{-}\eta^2\text{-}C{\equiv}CPh)(CO)_{10}(PCy_3)$, 34, as a yellow crystalline solid in ca. 10% yield. The i.r. spectrum of 34 shows bands in the terminal CO stretching region (ν_{CO}:2086 - 1964 cm^{-1}), while in the ^1H n.m.r spectrum signals at 7.39 - 7.03 (C_6H_5,5H), 1.75 - 0.88 (C_6H_{11},33H), and -20.42 p.p.m. (Os(μ-H)Os, 1H) are observed. One singlet resonance is displayed in the ^{31}P n.m.r spectrum of 34 at 49.2 p.p.m. (J(Pt-P) = 3987Hz) which is attributed to a Pt-bound PCy_3 function.

Another, red compound was isolated in this reaction however, the very small quantities of this complex obtained precluded its

characterisation.

In order to fully delineate the structure of 34, an X-ray diffraction experiment was undertaken by the author of this Thesis. The experimental details and full discussion of this structural investigation will be presented in Chapter 4.

The molecular structure of 34 is shown in Figure 69 and important metrical parameters are cited in Table 35. The metal framework adopts a spiked triangular geometry, in which a near equilateral Os_3 triangle is axially ligated at Os(1) by the Pt centre. The hydride is included at a calculated position[271] which agrees with the ^1H n.m.r spectroscopic data insofar as it spans an Os-Os vector.

The phenyl acetylide function is coordinated in a μ_4-η^2 fashion which is rarely observed in spiked triangular clusters,[326-328] although μ_4-η^2 acetylide ligation is known in systems with butterfly[332] or square-faced cluster[333] frameworks.

Assuming the μ_4-η^2-C≡CPh function to be a five electron donor gives a 62 electron count for 34, c.f the 64 c.v.e's predicted by the E.A.N rule.[54] This is consistent with the spiked triangular framework because the pseudo-square planar coordination about Pt renders it a 16 electron centre. A similar electron count is observed for $Os_3Pt(\mu\text{-}H)_2(\mu_4\text{-}C)(CO)_{10}(PCy_3)$,[250] $Os_3Pt(\mu\text{-}CH_2)(CO)_{11}(PPh_3)_2$,[254] and 29, which, like 34, have spiked-triangular metal cores incorporating a 16 electron Pt centre.

The acetylide coordinates to the metal framework such that the C(11)-C(12) vector makes an angle of 80.0° with the Os(2)-Os(3) edge. Consequently the C(11)-Os(2) separation of 2.59(1) Å is ca. 0.2 Å longer than the C(11)-Os(3) distance and can be considered non-bonding. In contrast, for clusters containing the μ_3-C≡CR functionality, a symmetric, perpendicular η^2-(⊥) bonding mode is more common[34-36,178]

Figure 69 : Molecular structure of $Os_3Pt(\mu\text{-}H)(\mu_4\text{-}\eta^2\text{-}C{\equiv}CPh)(CO)_{10}(PCy_3)$, 34.

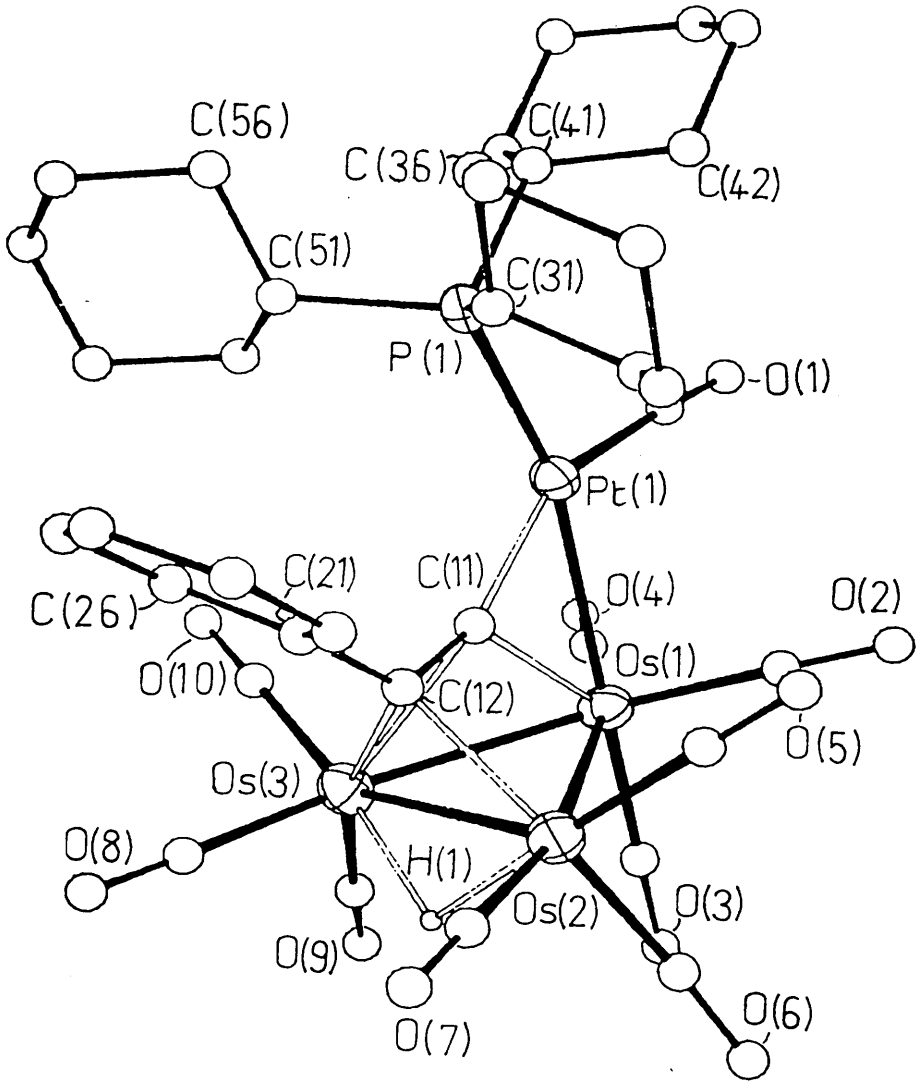

Table 35 : Selected bond lengths and angles for $Os_3Pt(\mu\text{-}H)_2(\mu_4\text{-}\eta^2\text{-}C{\equiv}CPh)(CO)_{10}(PCy_3)$, 34

Bonds (Å)

Pt(1)-Os(1)	2.712(1)	Os(1)-Os(2)	2.845(1)
Os(1)-Os(3)	2.824(1)	Os(2)-Os(3)	2.838(1)
Pt(1) -C(11)	2.002(10)	Os(1)-C(11)	2.146(10)
Os(3)-C(11)	2.397(10)	Os(2)-C(12)	2.149(10)
Os(3)-C(12)	2.227(11)	Pt(1)-C(1)	1.893(11)
Pt(1)-P(1)	2.328(3)	C(11)-C(12)	1.335(14)
C(12)-C(21)	1.486(14)		

Os-CO Mean = 1.901

C-O Mean = 1.141

Phenyl C-C Mean = 1.379

Angles

Os(2)-Os(1)-Os(3)	60.1(1)	Os(1)-Pt(1)-C(1)	100.8(3)
Os(2)-Os(1)-Pt(1)	101.6(1)	Os(1)-Pt(1)-C(11)	51.5(3)
Os(2)-Os(1)-Pt(1)	94.6(1)	P(1)-Pt(1)-C(1)	101.2(3)
Os(1)-Os(2)-Os(3)	59.6(1)	P(1)-Pt(1)-C(11)	106.5(3)
Os(1)-Os(3)-Os(2)	60.3(1)	Os(1)-C(11)-C(12)	124.4(7)
Os(3)-C(11)-C(12)	66.3(6)	Pt(1)-C(11)-C(12)	152.7(8)
Os(2)-C(12)-C(11)	93.2(6)	Os(3)-C(12)-C(11)	80.4(6)
Os(2)-C(12)-C(21)	130.6(7)	Os(3)-C(12)-C(21)	125.8(8)
C(11)-C(12)-C(21)	128.6(9)	Pt(1)-C(1)-O(1)	174.4(1)

Os-C-O Mean = 177

Phenyl C-C-C Mean = 120

Similarly, in $Fe_2Ni_2(\mu\text{-}PPh_2)(\mu_4\text{-}\eta^2\text{-}C{\equiv}CPh)(Cp)_2(CO)_5$, [326] the $\mu_4\text{-}\eta^2$-C≡CPh ligand makes an angle of 89.5° with the Fe(2)-Ni(2) vector (see Table 36).

Table 36 : Angle between CC (acetylide) and the M-M bond spanned by CCR in spiked triangular systems.

Cluster.	Angle, between C≡C vector and M_1-M_2 edge.	Ref.
$Fe_2Ni_2(\mu\text{-}PPh_2)(CCPh)(Cp)_2(CO)_5$	89.5°	326
34	80°	This work
$Co_2FeRu(CCPh)(Cp)(CO)_{10}$	69°	327
$Co_2RuW(CCPh)(Cp)(CO)_{11}$	80°	327
$Co_2NiRu(CCMe)(Cp)(CO)_8(PPh_3)$	87°	328
$CoMo_2Ru(CCMe)(Cp)_2(CO)_9$	73°	328

Finally, it is interesting to note the isolobal relationship between PtL_2 and CH_2 [108] allows the $PtL_2C{=}CPh$ fragment to be considered a $\mu_3\text{-}\eta^3$ platina-allenyl function. In the cluster systems $Ru_3(\mu\text{-}H)[\mu_3\text{-}\eta^3\text{-}CH(Me){=}C{=}C(Et)](CO)_{10}$ [334] and $Ru_3(\mu\text{-}PPh_2)[\mu_3\text{-}\eta^3\text{-}CH_2{=}C{=}C\text{-}(Pr^i)](CO)_8$, [276] the central carbon of the allenyl moiety binds to only two metal centres. Similarly in 34, C(11) appears to bond only to Os(1) and Os(2) of the Os_3 unit.

There is an interesting flexibility in coordination of the $\mu_4\text{-}\eta^2$CCR ligand in spiked triangular clusters, evidenced by the variance in angle that the acetylide C-C vector makes with the bridged M_1M_2 vector (see Table 36). However only a few systems incorporating

this acetylide bonding mode are known.[326-328] Therefore, in an effort to extend the preparative routes to such complexes and further elucidate the flexibility of alkynyl-cluster bonding in these systems, a study of the synthesis and structure of analogues of 34 was undertaken. The results are presented in Chapter 3.

CHAPTER THREE.

CHAPTER 3.

Preparation and Reactivity of some Triruthenium-Platinum Clusters.

In the last section of Chapter 2 the structure and low yield synthesis of $Os_3Pt(\mu\text{-}H)(\mu_4\text{-}\eta^2\text{-}C{\equiv}CPh)(CO)_{10}(PCy_3)$, 34, was described. The acetylide moiety in this spiked triangular cluster displays an interesting twisted $\mu_4\text{-}\eta^2\text{-}C{\equiv}CR$ coordination. In view of this, an investigation into the preparation of related complexes was undertaken. In this Chapter, the synthesis and reactivities of some Ru_3Pt analogues of 34 are described.

Formally 34 can be considered to arise from the addition of a PtL_2 unit[L=(CO),(PCy_3)] to $Os_3(\mu\text{-}H)(\mu_3\text{-}\eta^2\text{-}C{\equiv}CPh)(CO)_9$. Therefore, the complex $Ru_3(\mu\text{-}H)(\mu_3\text{-}\eta^2\text{-}C{\equiv}Ct\text{-}Bu)(CO)_9$,[337] 35, was considered as a precursor to Ru_3Pt analogues of 34. The structure of 35 has been determined by neutron diffraction[338] and is shown in Figure 70.

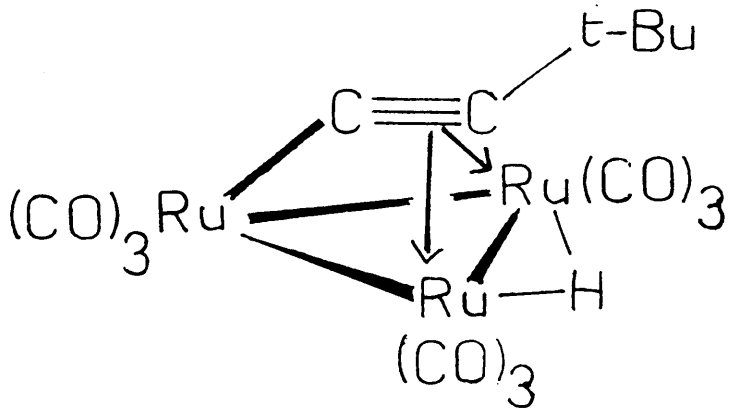

Figure 70 : Structure of $Ru_3(\mu\text{-}H)(\mu_3\text{-}\eta^2\text{-}C{\equiv}Ct\text{-}Bu)(CO)_9$.

Theoretical calculations on the related system $Ru_3(\mu\text{-}H)(\mu_3\text{-}\eta^2\text{-}C{\equiv}CMe)(CO)_9$ [339] suggest that the α-carbon of the acetylide unit is slightly positively charged, rendering it susceptible to nucleophilic

attack in a charge controlled reaction. (The HOMO and LUMO are localised on the metal sites and, hence, under orbital control, nucleophilic attack is more likely to occur at Ru centres).[339] In keeping with this analysis, nucleophilic attack at the α-carbon site has been observed in several $M_3(\mu\text{-H})(\mu_3\text{-}\eta^2\text{-C}\equiv\text{CR})(CO)_9$, (M=Ru,Os) systems.[340-343] However, Deeming et al[341,342] have demonstrated that nucleophilic attack at the Cβ site of similar acetylides is also possible.

Carty and coworkers[276] have recently reported that reaction of CH_2N_2 with $\mu_3\text{-}\eta^2$ acetylides bound to Ru_3 frameworks leads to formation of $\mu_3\text{-}\eta^3$ allenyl functions. Bearing in mind the isolobal analogy between CH_2 and PtL_2 [108] and the propensity for $\mu_3\text{-}\eta^2$ acetylides to undergo addition at C_α, the reaction of 35 with $Pt(cod)_2$[347] was investigated with a view to the synthesis of a Ru_3Pt analogue of complex 34.

3.1 The Reaction of $Ru_3(\mu\text{-H})(\mu_3\text{-}\eta^2\text{-C}\equiv\text{Ct-Bu})(CO)_9$, 35, with $Pt(cod)_2$

Addition of a toluene solution of $Pt(cod)_2$ to an equimolar quantity of complex 35 in toluene at 0^oC resulted in the yellow colour of 35 giving way to dark brown. After work-up, the resulting solution affords reasonable yields (50-60%) of $Ru_3Pt(\mu\text{-H})(\mu_4\text{-}\eta^2\text{-C}\equiv\text{Ct-Bu})(cod)(CO)_9$, 36, as bright orange crystals, which are stable indefinitely if stored under a N_2 atmosphere. Solutions of 36 are more air sensitive and under N_2 decompose slowly in the absence of trace amounts of free cod. The major product of decomposition has recently been identified as $Pt\{Ru_3(\mu\text{-H})(\mu_4\text{-}\eta^2\text{-C}\equiv\text{Ct-Bu})(CO)_9\}_2$ [344] by a single crystal X-ray study. The i.r. spectrum of 36 indicates that the carbonyl ligands are terminally bound (ν_{CO} ranges 2080-1953 cm^{-1}). The ^1H n.m.r spectrum at 233K shows resonances due to methyl protons (1.30 p.p.m), cod methylene hydrogens (broad signal at 1.62 p.p.m.), olefinic protons (6.02, 5.28 p.p.m., J(Pt-H) = 49, 71Hz respectively), and a Ru(μ-H)Ru

hydride (-19.25 p.p.m., J(Pt-H) = 6.4Hz). The magnitude of ^{195}Pt coupling to the olefinic protons indicates that the cod moiety remains bound to Pt. The resonances due to these olefinic protons broaden at ambient temperature, compatible with "ring-whizzing" of the cod ligand. At 233K, the two sets of signals due to inequivalent olefinic protons show quite different ^{195}Pt couplings, and can be assigned by reference to the crystal structure of complex 36 (see below, Figure 71). The resonance at 5.28 p.p.m. with the larger ^{195}Pt coupling is attributed to the protons on C(20) and C(21) on the basis of the shorter Pt-C distances to this olefinic bond, while the resonance at 6.02 p.p.m. is assigned to the protons bound to C(24) and C(25).

Further discussion of the spectroscopic data is deferred until the solid state structure of 36 has been described.

An X-ray analysis of this complex was carried out by the author of this Thesis. A full discussion of the structure determination is presented in Chapter 4.

The molecular structure of complex 36 is presented in Figure 71, while relevent bond lengths and angles are given in Table 37. The metal framework of 36 has a spiked triangular geometry. An approximately equilateral Ru_3 triangle (Ru-Ru distances vary between 2.791(1)-2.815(1)Å) is axially ligated at Ru(2) by Pt (the Pt-Ru(2) vector is inclined at 10.9° to the normal to the Ru_3 plane). If the μ_4-η^2 acetylide function is assumed to be a five electron donor, the valence electron count associated with 36 is 62, which is consistent with a spiked triangular geometry incorporating a 16 electron Pt centre (c.f. $Os_3Pt(\mu\text{-}H)_2(\mu_4\text{-}C)(CO)_{10}(PCy)_3$,[250] $Os_3Pt(\mu\text{-}CH_2)(CO)_{11}(PPh_3)_2$,[254] $Os_3Pt(\mu\text{-}H)(\mu_4\text{-}\eta^2\text{-}C{\equiv}CPh)(CO)_{10}(PCy_3)$, 34). Although the Pt-Ru(2) distance in complex 36 of 2.645(1)Å is shorter than any previously reported Pt-Ru separation

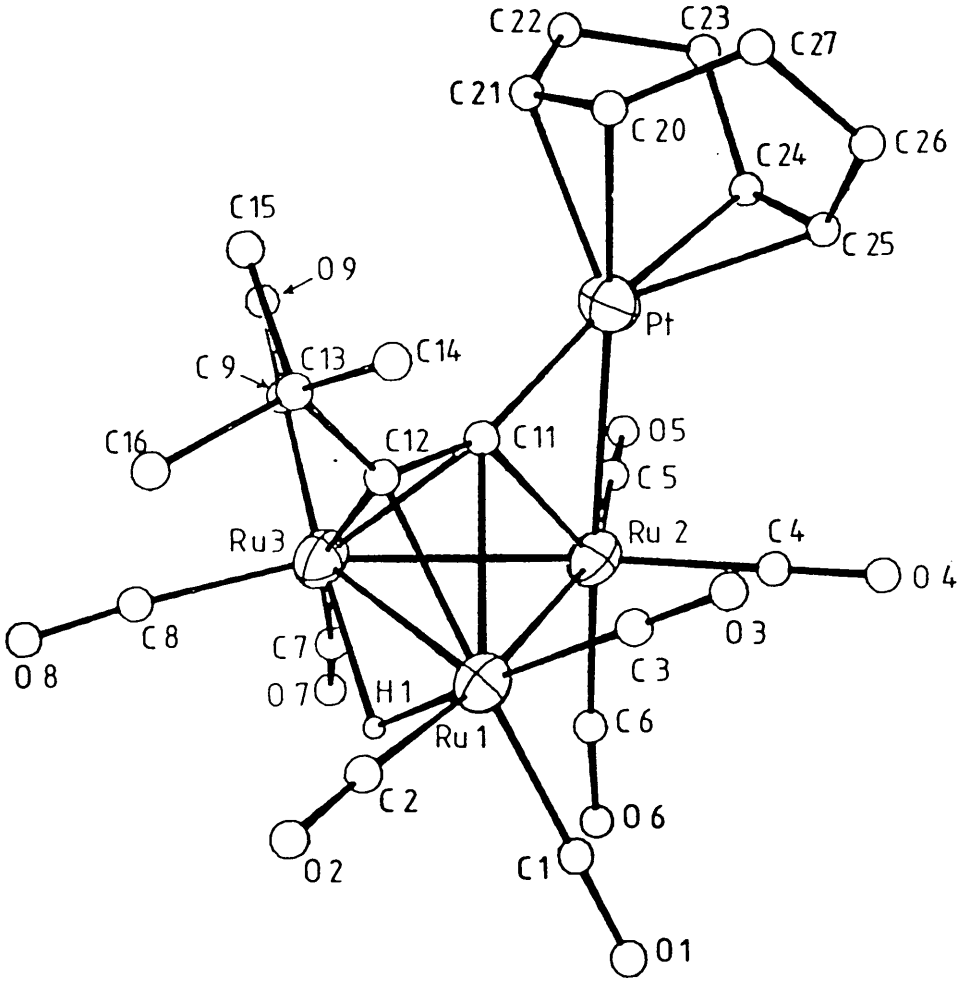

Figure 71 : The crystal structure of $Ru_3Pt(\mu\text{-}H)(\mu_4\text{-}\eta^2\text{-}C{\equiv}Ct\text{-}Bu)(cod)(CO)_9$, 36.

Table 37 : Selected Bond Lengths (Å) and Bond Angles (deg) for $Ru_3Pt(\mu\text{-}H)(\mu_4\text{-}\eta^2\text{-}C{\equiv}Ct\text{-}Bu)(cod)(CO)_9$, 36.

Bonds.

Pt-Ru(2)	2.645(1)	Ru(1)-Ru(2)	2.810(1)
Ru(1)-Ru(3)	2.815(1)	Ru(2)-Ru(3)	2.791(1)
Pt-C(11)	1.969(6)	Pt-C(20)	2.202(7)
Pt-C(21)	2.221(8)	Pt-C(24)	2.358(8)
Pt-C(25)	2.317(8)	Ru(1)-C(11)	2.488(5)
Ru(1)-C(12)	2.154(6)	Ru(1)-H(1)	1.62(6)
Ru(2)-C(11)	2.164(5)	Ru(3)-C(11)	2.291(5)
Ru(3)-C(12)	2.198(5)	Ru(3)-H(1)	1.91(6)
C(11)-C(12)	1.332(7)	C(12)-C(13)	1.548(8)

mean Ru - CO = 1.906

mean C - O = 1.138

Angles

Ru(2)-Pt-C(11)	53.5(2)	Ru(2)-Ru(1)-Ru(3)	59.5(1)
Ru(2)-Ru(1)-C(11)	47.7(2)	Ru(2)-Ru(1)-C(12)	78.3(2)
Ru(2)-Ru(1)-H(1)	74.9(19)	Ru(3)-Ru(1)-C(11)	50.7(2)
Ru(3)-Ru(1)-C(12)	50.4(2)	Ru(3)-Ru(1)-H(1)	40.7(19)
C(11)-Ru(1)-C(12)	32.3(2)	Pt-Ru(2)-Ru(1)	100.0(1)
Pt-Ru(2)-Ru(3)	91.1(1)	Ru(1)-Ru(2)-Ru(3)	60.3(1)
Ru(1)-Ru(3)-Ru(2)	60.2(1)	Pt-C(11)-Ru(2)	79.4(2)
Pt-C(11)-C(12)	151.1(4)	Ru(2)-C(11)-C(12)	129.0(4)
C(11)-C(12)-C(13)	131.1(5)		

(these range 2.707-2.858Å,[335,336,345]), all known Pt-Ru bonds are bridged by at least one ligand, which complicates direct comparisons of bond lengths.

The acetylide C(11)-C(12) bond in 36 is inclined at 98.5° to the Ru(1)-Ru(3) vector and, consequently, the Ru(1)-C(11) distance of 2.488(5)Å is significantly longer than the Ru(3)-C(11) separation of 2.291(5)Å. This twisted μ_4-η^2-C≡CR coordination is reminiscent of that observed in $Os_3Pt(\mu\text{-}H)(\mu_4\text{-}\eta^2\text{-}C{\equiv}CPh)(CO)_{10}(PCy_3)$, complex 34, and serves as further evidence of the versatile bonding capabilities of the μ_4-η^2-C≡CR ligand in spiked triangular clusters.

The hydride ligand, spanning the Ru(1)-Ru(3) edge, was observed directly in an electron density difference map and agrees with the calculated [271] position.

The Pt-C(olefin) bond distances in the Pt(cod) unit show a marked asymmetry; the Pt-C(20) and Pt-C(21) separations (2.202(7) and 2.221(8)Å respectively) are distinctly shorter than the Pt-C(24) and Pt-C(25) lengths (2.358(8) and 2.317(8)Å respectively). The origin of this asymmetry may be the differing trans influences of the Pt-C and Pt-Ru bonds.

The carbonyl region of the ^{13}C n.m.r spectrum of 36 is shown in Figure 72, while relevant parameters are listed in Table 38. At 200K, (Figure 72a), five signals are observed in the intensity ratio 1:2:2:2:2. This is indicative that in solution 36 acquires a mirror plane. Assignments of these signals are based on the fluxional behaviour of 36 and selective ^1H decoupling experiments. The unique signal of unit intensity, a, can be assigned to C(6) as this is the only carbonyl carbon lying on the molecular pseudo-mirror plane. Furthermore, on warming the sample to 220K

Figure 72 : CO region of VT ^{13}C NMR spectrum of $Ru_3Pt(\mu\text{-}H)(\mu_4\text{-}\eta^2\text{-}C{\equiv}Ct\text{-}Bu)(cod)(CO)_9$

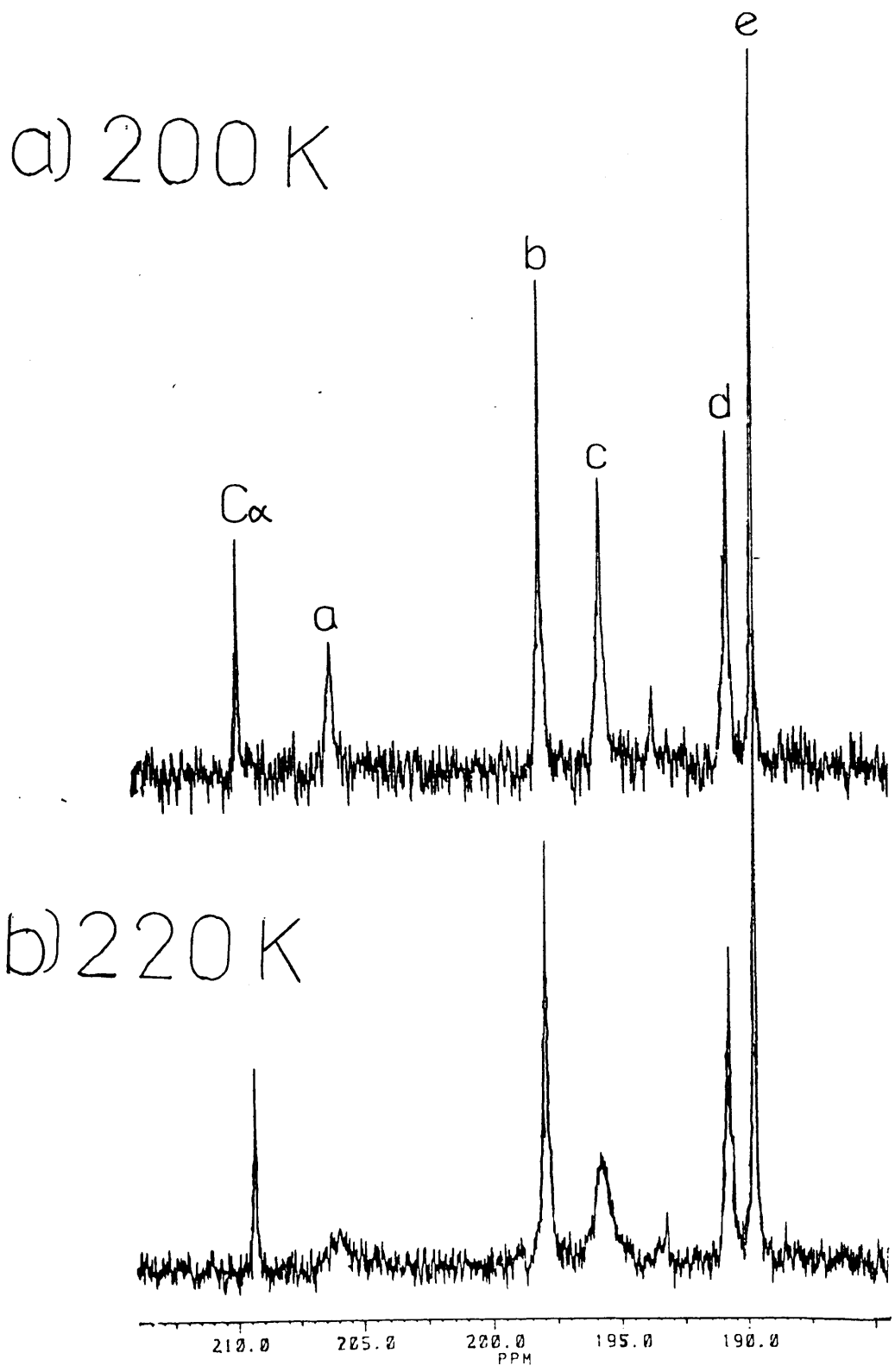

Table 38 : N.m.r. Parameters for 36.

	^{13}C Data [a]				
Resonance [b]	p.p.m.	Rel. Int.	Assign. [c]	J/Hz. Pt-C	H-C
a	205.8	1	C6	-	-
b	197.7	2		12	-
c	195.4	2	C4/C5	-	-
d	190.4	2	C3/C9	16	13
e	189.4	2		-	-
	209.4	1	C(11)	1621	-
	121.9	1	C(12)	224	

a) CD_2Cl_2, 220 K;

b) Figure 72;

c) Figure 71.

(Figure 72b), resonances a and c broaden considerably, consistent with a tripodal rotation of the unique $Ru(CO)_3$ unit; hence c is attributed to C(4)/C(5). The remaining signals, b,d, and e, are assigned to the equivalent pairs of CO units on Ru(1) and Ru(3). Due to the large coupling (13Hz) to the Ru($^{\mu}$-H)Ru proton, resonance d is attributed to C(3)/C(9), trans to the hydride. Resonances b and e are due to C(1)/C(7) and C(2)/C(8), but cannot be unambiguously assigned. At ambient temperatures one broad signal at ca. 195 p.p.m. is observed, consistent with complete carbonyl scrambling.

The solid-state structure of complex 36 is asymmetric, with a twisted μ_4-η^2 acetylide moiety ligated to the Ru_3Pt framework. However the ^{13}C n.m.r spectrum of 36 at 200K reveals that, in solution the molecule acquires a mirror plane. This observation is compatible with either a rapid exchange of two enantiomeric forms of 36, as shown in Figure 73, or a static structure with symmetric μ_4-η^2 acetylide coordination.

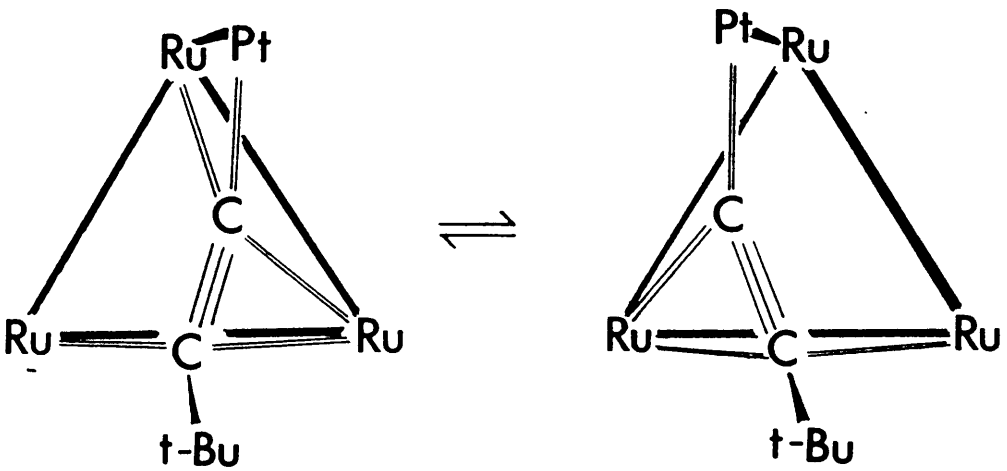

Figure 73 : Possible dynamic behaviour giving rise to time-averaged mirror plane in complex 36.

Resonances due to the C_α and C_β carbons of the acetylide ligand appear at 209.4 (J(Pt-C) = 1621Hz) and 121.9 p.p.m. (J(Pt-C) = 224Hz) respectively. Assignments are unambiguously obtained from the magnitudes of ^{195}Pt-couplings. Moreover, these chemical shifts compare well with those observed for similar cluster bound acetylides.[346]

By similar consideration of the magnitude of ^{195}Pt couplings, the olefinic carbon resonances at 105.2 (J(Pt-C) = 60Hz) and 92.4 p.p.m. (J(Pt-C) = 134Hz) can be assigned to C(24)/C(25) and C(20)/C(21) respectively.

Signals due to the two pairs of inequivalent methylene groups on the cod function are coalesced (at 29.6 p.p.m) at ambient temperatures whereas, at 220K, two separate resonances (at 30.3, 29.0 p.p.m) are observed. This provides further evidence for the "ring-whizzing" of the cod ligand at ambient temperatures.

In conclusion, the reaction of $Ru_3(\mu\text{-H})(\mu_3\text{-}\eta^2\text{-C}\equiv\text{Ct-Bu})(CO)_9$ with $Pt(cod)_2$ results in the formation of the first triruthenium-platinum complex, $Ru_3Pt(\mu\text{-H})(\mu_4\text{-}\eta^2\text{-C}\equiv\text{Ct-Bu})(cod)(CO)_9$, 36.

It has been shown that Pt-ligated cod can readily be displaced by a variety of ligands.[229,247,248,347,348] Thus, complex 36 may be expected to undergo similar cod displacement and, with this in mind, the reactivity of 36 was investigated.

3.2 The Reaction of $Ru_3Pt(\mu\text{-H})(\mu_4\text{-}\eta^2\text{-C}\equiv\text{Ct-Bu})(cod)(CO)_9$ with bis(diphenylphosphino)ethane, dppe.

Addition of an ethereal solution of dppe to equimolar amounts of complex 36 in Et_2O resulted in the formation of two species formulated as the acetylide complex $Ru_3Pt(\mu\text{-H})(\mu_4\text{-}\eta^2\text{-C}\equiv\text{Ct-Bu})(dppe)(CO)_9$, 37, and the isomeric vinylidene cluster $Ru_3Pt(\mu_4\text{-}\eta^2\text{-C=C(H)t-Bu})(dppe)(CO)_9$, 38. These products have been characterised by spectroscopic and crystallo-

graphic analyses. Complexes 37 and 38 are separable by column chromatography. However after separation and crystallisation, orange samples of 37 are frequently contaminated with small quantities of dark red crystals of 38.

The course of this reaction has been followed using ^1H n.m.r spectroscopy, which indicated that the initially formed species is 37 and this undergoes subsequent isomerisation to yield 38. The formation of 38 from 37 seems to be promoted by column chromatography.

This isomerisation is reversible as solutions of pure 38 soon show signals due to 37 in the ^1H n.m.r spectrum. A kinetic study of the conversion of 37 to 38 at 296K was undertaken. A plot of $\ell n(a_e/a_e-x)$ versus time (where a_e = equilibrium concentration of 38, x = concentration of 38 at time t) gives a straight line showing that this isomerisation process obeys first order kinetics (see Figure 74, line a).

The overall rate constant k (i.e. k_1+k_{-1}) for the process

$$\underline{37} \underset{k_{-1}}{\overset{k_1}{\rightleftharpoons}} \underline{38}$$

of $1.8(\pm0.2)\times 10^{-3}$ min^{-1} is given by the gradient of line (a) of Figure 74. Identical values for k (within experimental error) were obtained for the isomerisation process in the absence of base and in the presence of either NEt_3 (line (b), Figure 74; $k = 2.1(\pm0.2)\times 10^{-3}$ min^{-1}) or pyridine (line (c), Figure 74, $k = 2.1(\pm0.2)\times 10^{-3}$ min^{-1}). The transformation of 37 to 38 involves the formal transfer of a hydrogen atom from a Ru-Ru edge to the C_β site of the acetylide function. As the presence of added base does not affect the rate of isomerisation, a mechanism with a rate determining step involving either protonation or deprotonation of the cluster is clearly not the major reaction pathway.

Figure 74 : Kinetic plot of the conversion of 37 to 38 in CD_2Cl_2 at 296 K. (a) pure 37; (b) 37 with added NEt_3 (1:1.1 molar ratio); (c) 37 in presence of pyridine (1:2.75 molar ratio). For clarity, plot for (c) is displaced by 0.1 unit along the ordinate.

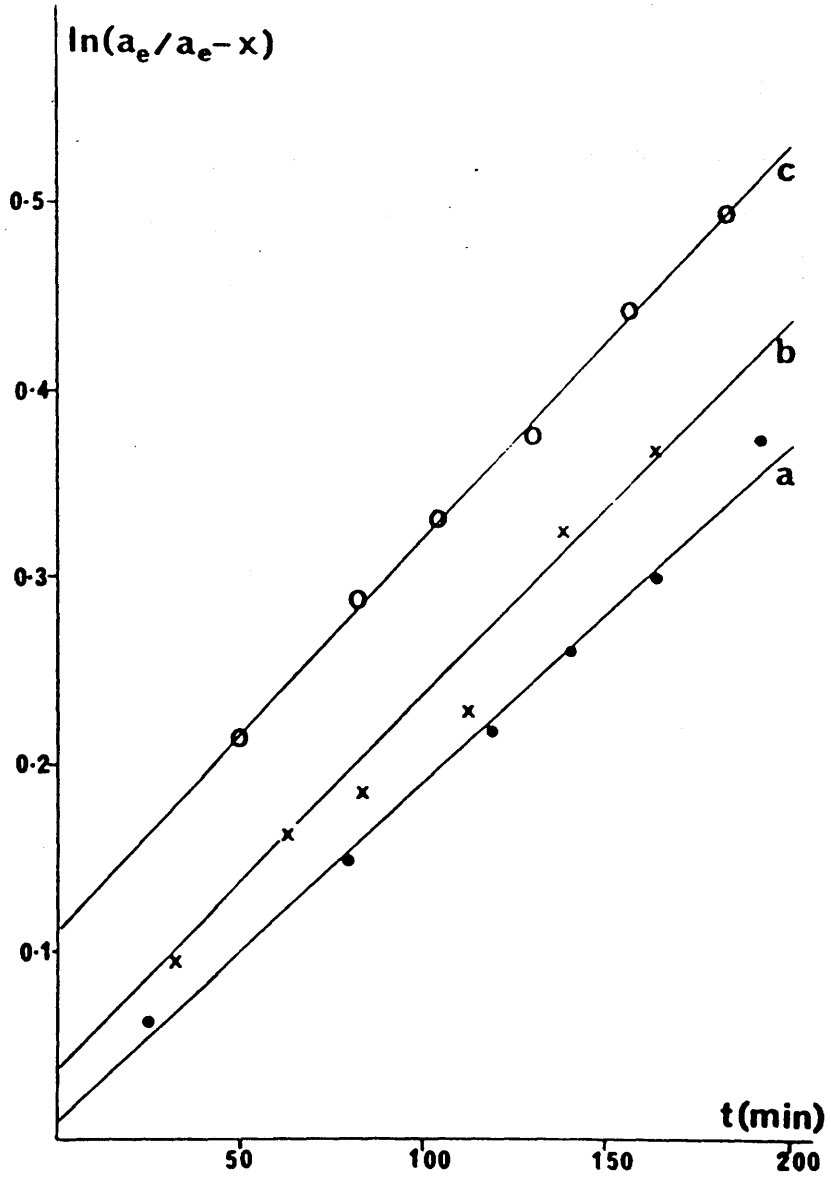

The kinetic data are compatible with an intramolecular migration of the hydrogen atom. The vinylidene complex, 38, is the thermodynamically favoured product ($K_{eq} = k_1/k_{-1} = 12$ (±1) at 298 K).

Molecular Structure of Complex 37

In order to determine the solid-state structure of 37, a single crystal X-ray diffraction experiment was undertaken by Dr. L.J. Farrugia.

The molecular structure of 37 is depicted in Figure 75 while important metrical parameters are listed in Table 39. The structure of 37 is very similar to that of 36, with the major difference arising from the replacement of the cod ligand in 36 by the bidentate dppe moiety. The Pt-P distances in 37 vary in a similar fashion to the Pt-C (olefin) separations in 36. Thus, the Pt-P(1) vector (2.267(2)Å), trans to the Pt-Ru(3) bond is significantly shorter than Pt-P(2) (2.304(2)Å), which lies trans to the Pt-C(11) separation.

The C(11) -C(12) vector is inclined at 91.3° to the Ru(1)-Ru(2) bond, hence the acetylide unit adopts a nearly symmetric ($\perp$)μ_4-η^2-C≡CR coordination mode. Consequently, the C(11)-Ru(1), C(11)-Ru(2) bond lengths are approximately equal (2.396(6), 2.427(6)Å respectively).

The spiked trangular metal framework in 37 bears a close resemblance to that of 36, with corresponding bond lengths differing by 0.001-0.036 Å. The hydride is included at a calculated position[271] spanning the Ru(1)-Ru(2) edge.

Finally, the configuration of the dppe ligand disrupts the approximate mirror symmetry of the core as shown in Figure 76.

Figure 75 : The molecular structure of $Ru_3Pt(\mu\text{-}H)(\mu_4\text{-}\eta^2\text{-}C{\equiv}Ct\text{-}Bu)(dppe)(CO)_9$, 37.

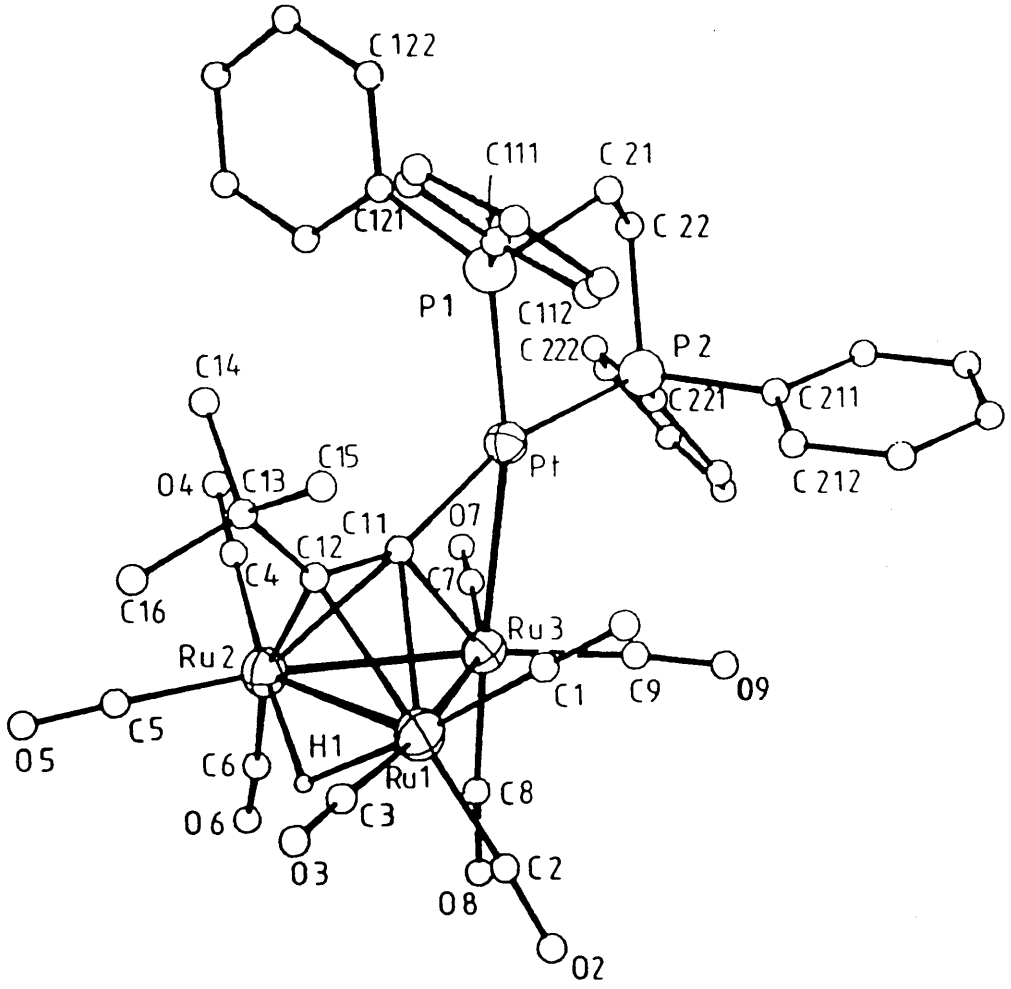

Figure 76 : Stereoview of cluster core geometry of 37.

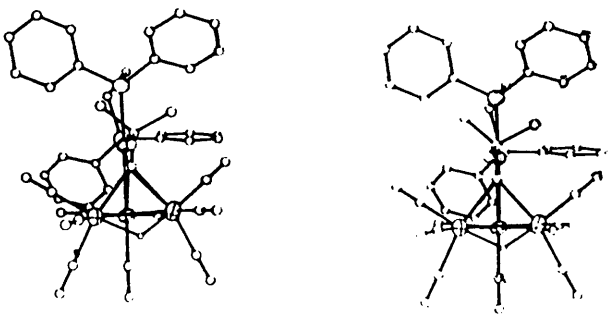

Table 39 : Selected Bond lengths (Å) and angles (deg) for

$Ru_3Pt(\mu\text{-}H)(\mu_4\text{-}\eta^2\text{-}C{\equiv}Ct\text{-}Bu)(dppe)(CO)_9$, 37.

Bond lengths.

Pt-Ru(3)	2.681(1)	Ru(1)-Ru(2)	2.824(1)
Ru(1)-Ru(3)	2.792(1)	Ru(2)-Ru(3)	2.796(1)
Pt-P(1)	2.267(2)	Pt-P(2)	2.304(2)
Pt-C(11)	1.985(6)	Ru(1)-C(11)	2.396(6)
Ru(1)-C(12)	2.213(6)	Ru(1)-H(1)	1.686(1)
Ru(2)-C(11)	2.427(6)	Ru(2)-C(12)	2.209(6)
Ru(2)-H(1)	1.857(1)	Ru(3)-C(11)	2.202(6)
C(11)-C(12)	1.332(8)	C(12)-C(13)	1.521(8)

mean Ru-CO = 1.902

mean C-O = 1.134

Bond angles

Ru(3)-Pt-P(1)	166.7(1)	Ru(3)-Pt-P(2)	108.2(1)
P(1)-Pt-P(2)	85.0(1)	Ru(3)-Pt-C(11)	53.8(2)
P(1)-Pt-C(11)	113.0(2)	Ru(2)-Ru(1)-Ru(3)	59.7(1)
Ru(1)-Ru(2)-Ru(3)	59.6(1)	Ru(1)-Ru(3)-Ru(2)	60.7(1)
Pt-Ru(3)-Ru(1)	94.4(1)	Pt-Ru(3)-Ru(2)	97.0(1)
Pt-Ru(3)-C(11)	46.7(2)	Pt-C(11)-Ru(3)	79.5(3)
Pt-C(11)-C(12)	151.2(5)	Ru(3)-C(11)-C(12)	129.4(5)
C(11)-C(12)-C(13)	135.2(6)	Ru(1)-C(12)-C(11)	80.9(4)
Ru(1)-C(12)-C(13)	128.6(5)	Ru(2)-C(12)-C(11)	82.5(4)
Ru(2)-C(12)-C(13)	130.2(4)	Ru(1)-H(1)-Ru(2)	105.6(1)

Mean Ru-C-O = 176.8

N.m.r. Spectroscopic Data for $Ru_3Pt(\mu\text{-}H)(\mu_4\text{-}\eta^2\text{-}C{\equiv}Ct\text{-}Bu)(dppe)(CO)_9$, 37.

The ^1H nmr spectrum of 37 displays the anticipated resonances for the dppe and t-Bu functions. In addition, a highfield resonance at -19.12 p.p.m. is observed, due to the Ru(μ-H)Ru proton. Two doublet signals at 51.8 (J(Pt-P)=2643, J(P-P)=17.3Hz) and 46.5 p.p.m. (J(Pt-P)=4152, J(P-P)=17.3Hz) are observed in the ^{31}P-{H} n.m.r spectrum at 233 K, arising from the two inequivalent P atoms. Within series of complexes that are similar to each other the magnitude of $^1J(Pt\text{-}P)$ coupling generally increases as the Pt-P separation decreases[349]. On this basis, the ^{31}P signals for 37 at 51.8 and 46.5 p.p.m. can be attributed to P(2) and P(1) respectively. The resonances broaden on warming the sample to ambient temperatures, while sharp signals due to small quantities of 38 are also observed in this spectrum. As the signals attributed to 38 are sharp, it is clear that the broadening of the resonances due to 37 arises from intramolecular exchange rather than slow isomerisation of 37 to 38. The Pt(dppe) unit is presumably rotating in an analogous process to that observed for the cod ligand in 36. A line shape analysis gives $\Delta G^{\neq}_{295} = 63.2(5)kJmol^{-1}$ for this exchange.

The carbonyl region of the ^{13}C n.m.r spectrum of 37 is shown in Figure 77, while relevant n.m.r parameters are cited in Table 40. At 233K, the spectrum is very similar to that of 36, with five carbonyl resonances in the intensity ratio 1:2:2:2:2. Hence the molecule assumes effective C_s symmetry in solution, which implies a rapid "flipping" of the Pt-bound dppe ligand. At 263K, the double intensity peaks b,d and e broaden markedly, while a and c remain sharp. This suggests the two equivalent $Ru(CO)_3$ groups have a lower barrier to tripodal rotation than the unique $Ru(CO)_3$

Figure 77 : CO region of VT ^{13}C NMR spectrum of $Ru_3Pt(\mu\text{-}H)(\mu_4\text{-}\eta^2\text{-}C{\equiv}Ct\text{-}Bu)(dppe)(CO)_9$

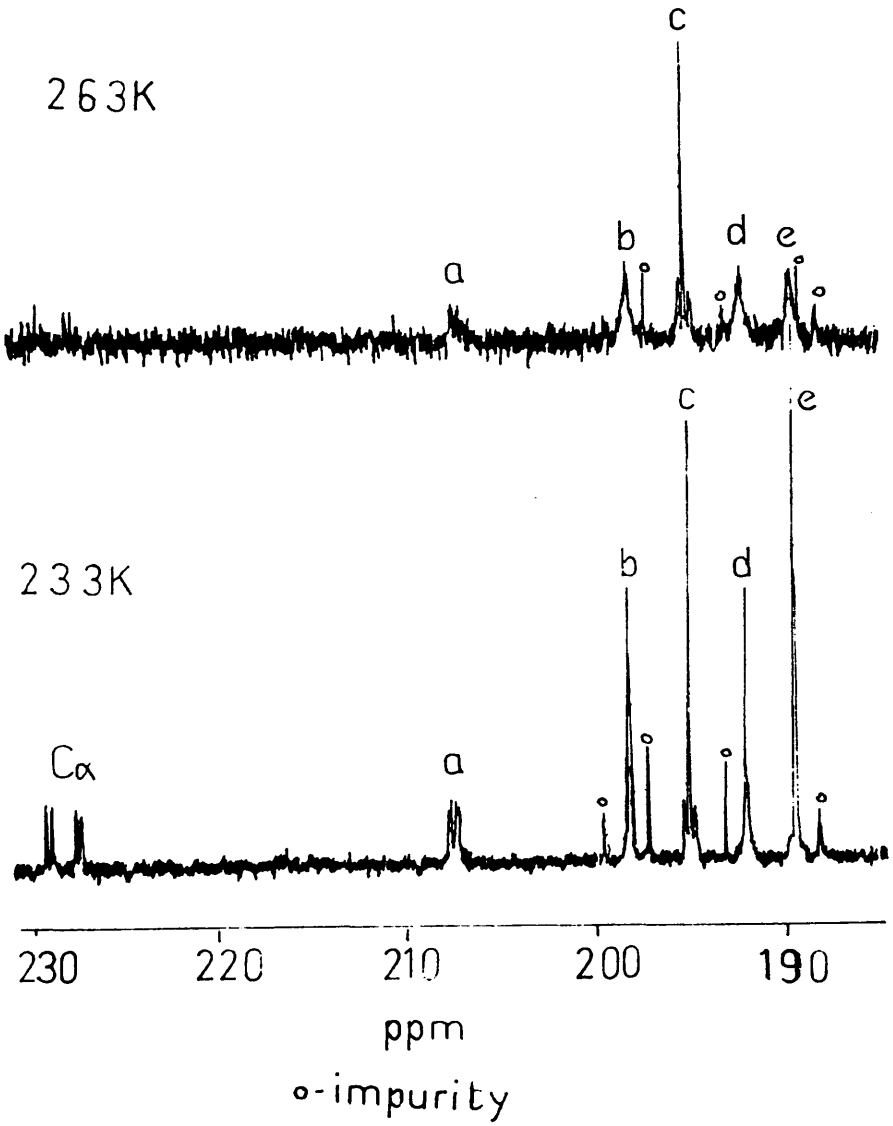

Table 40. ^{13}C N.m.r. parameters for $Ru_3Pt(\mu\text{-}H)(\mu_4\text{-}\eta^2\text{-}C{\equiv}Ct\text{-}Bu)(dppe)(CO)_9$

Resonance [a]	δ	Rel.Int.	Mult. [b]	Assign. [c]	J(Hz) P-C	J(Hz) Pt-C	J(Hz) H1-C
a	207.7	1	dd	C(8)	4,15	-	-
b	198.5	2	s				
c	195.3	2	s	C(7)/C(9)		27	
d	192.4	2	s	C(1)/C(4)			13
e	189.9	2	s				
	228.3	1	dd	C(11)	15,75		
	123.7	1	d	C(12)	5	178	

CD_2Cl_2, 233 K.

a - see Figure 77;

b - refer to $^{13}C\text{-}\{H\}$ spectrum

c - see Figure 75.

unit. This is the reverse of the situation observed for 36. A selective decoupling experiment indicated that d is coupled to H(1) (J(H-C) = 13Hz) and, hence, is attributed to C(1)/C(4), while a (relative intensity 1), and c(relative intensity 2) are assigned to C(8) and C(7)/C(9) respectively of the unique $Ru(CO)_3$ centre. Resonances due to the C_α and C_β atoms of the acetylide unit are observed at 228.3 (J(P-C)= 15,75Hz) and 123.7 p.p.m. (J(P-C)=5, J(Pt-C)= 178Hz) respectively. The ^{195}Pt coupling to the C_α carbon was anticipated to be large however ^{195}Pt satellites were not observed, possibly due to the multiplicity of the signal and the spectrum's poor signal to noise ratio. These C_α and C_β signals have chemical shifts similar to those observed for 36 and, likewise, are consistent with previously reported values.[346]

Molecular Structure of $Ru_3Pt(\mu_4\text{-}\eta^2\text{-}C{=}C(H)t\text{-}Bu)(dppe)(CO)_9$, 38.

The solid state structure of 38 was determined by a single crystal X-ray analysis performed by Dr. L.J. Farrugia. The structure is shown in Figure 78 and important bond lengths and angles are given in Table 41. The metal core of 38 has a butterfly geometry with a wingtip Pt(dppe)unit. Assuming the $\mu_4\text{-}\eta^2$ vinylidene ligand acts as a four electron donor, the valence electron count for 38 is 60, which is consistent with a butterfly structure containing a 16 electron Pt centre.[148,258]

The Pt-Ru(1) and Pt-Ru(2) distances in 38 (2.730(1) and 2.792(1) Å respectively) are significantly different from each other and are certainly larger than the Pt-Ru separations in 36 and 37. The hinge Ru(1)-Ru(2) separation (2.708(1) Å) is markedly shorter than the other Ru-Ru vectors. Moreover, the wingtip Ru(3)-Ru(1), Ru(3)-Ru(2) separations (2.799(1) and 2.823(2)Å) are unequal. The elongation of the Ru(2)-Pt and Ru(2)-Ru(3) distances c.f. Pt-Ru(1) and

Figure 78 : The molecular structure of $Ru_3Pt(\mu_4\text{-}\eta^2\text{-}C{=}C(H)t\text{-}Bu)(dppe)(CO)_9$, 38.

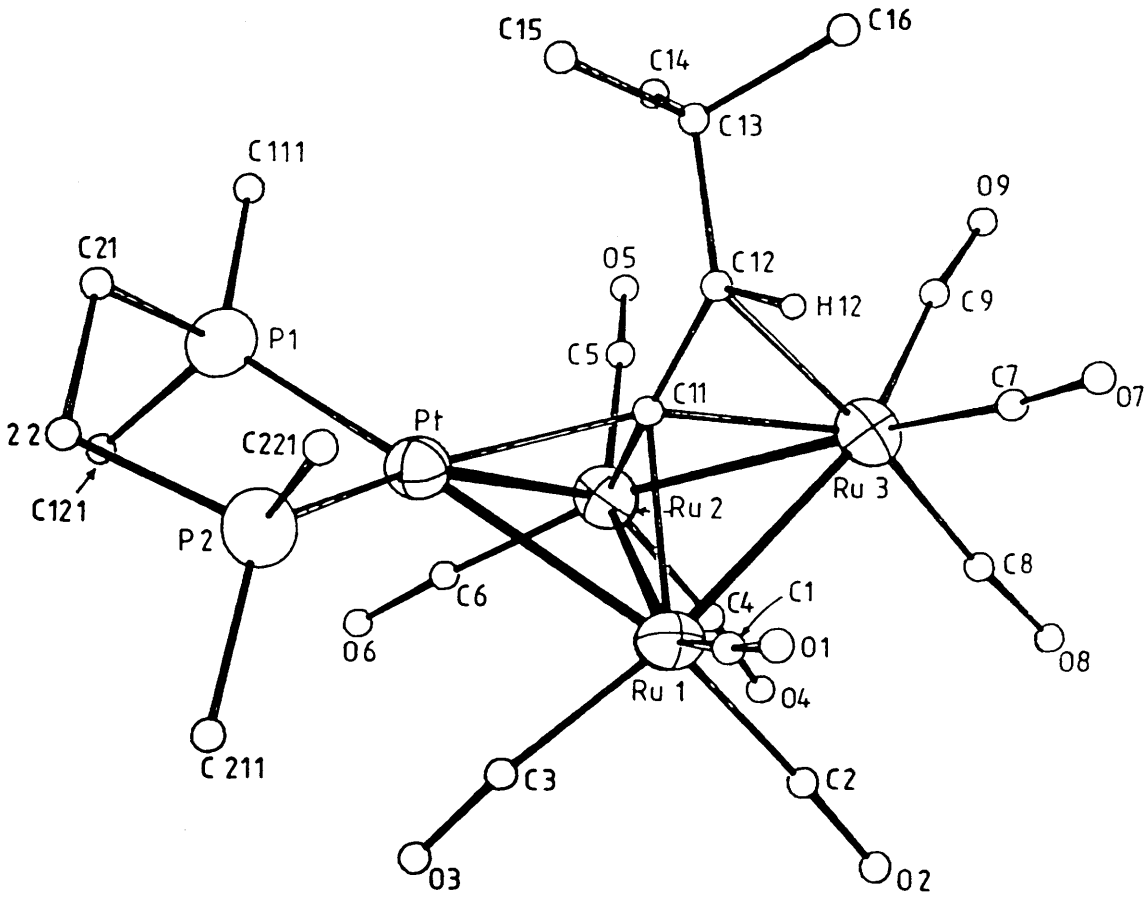

Table 41 : Selected Bond lengths and Angles for

$Ru_3Pt(\mu_4\text{-}\eta^2\text{-}C{=}C(H)t\text{-}Bu)(dppe)(CO)_9$, 38

Bonds.

Pt-Ru(1)	2.730(1)	Pt-Ru(2)	2.792(1)
Pt-P(1)	2.260(4)	Pt-P(2)	2.276(4)
Pt-C(11)	2.120(10)	Ru(1)-Ru(2)	2.708(2)
Ru(1)-Ru(3)	2.799(2)	Ru(1)-C(11)	2.123(12)
Ru(2)-Ru(3)	2.823(2)	Ru(2)-C(11)	2.142(12)
Ru(3)-C(11)	2.123(10)	Ru(3)-C(12)	2.297(11)
C(11)-C(12)	1.391(16)	C(12)-C(13)	1.535(18)

mean Ru-CO = 1.901

mean C-O = 1.121

Angles

Ru(1)-Pt-P(2)	106.0(1)	Ru(1)-Pt-C(11)	50.0(4)
Ru(2)-Pt-P(1)	108.6(1)	Ru(2)-Pt-C(11)	49.4(3)
P(1)-Pt-P(2)	84.9(2)	P(1)-Pt-C(11)	128.4(4)
P(2)-Pt-C(11)	131.7(4)	Pt-Ru(1)-Ru(2)	61.8(1)
Pt-Ru(1)-Ru(3)	97.9(1)	Pt-Ru(2)-Ru(1)	59.5(1)
Ru(2)-Ru(1)-Ru(3)	61.7(1)	Ru(2)-Ru(3)-C(11)	48.8(4)
Pt-Ru(2)-Ru(3)	95.9(1)	C(11)-Ru(3)-C(12)	36.4(5)
Ru(1)-Ru(3)-Ru(2)	57.6(1)	Pt-C(11)-C(12)	122.3(8)
Ru(1)-Ru(3)-C(12)	77.5(3)	Ru(3)-C(11)-C(12)	78.6(7)
Ru(2)-Ru(3)-C(12)	80.8(3)	C(11)-C(12)-C(13)	130.4(12)
Ru(1)-C(11)-C(12)	131.0(9)	C(13)-C(12)-H(12)	114.7(11)
Ru(2)-C(11)-C(12)	141.3(9)		
Ru(3)-C(12)-C(13)	122.7(9)		
C(11)-C(12)-H(12)	115.0(12)		

mean Ru-C-O = 174.2

Ru(1)-Ru(3) lengths may arise from steric interactions with the bulky t-Bu group, which lies over the Pt-Ru(2) and Ru(2)-Ru(3) edges of the butterfly framework.

The vinylidene function binds to the cluster core in a μ_4-η^2 fashion. The α-carbon, C(11), is approximately equidistant from all four metal sites (M-C(11) = 2.120(10)-2.142(12)Å), while the C=C bond is formally π-bound to the wingtip Ru(3) atom. Similar vinylidene coordination has been previously observed in other butterfly complexes such as $M_3Ni(\mu\text{-}H)(\mu_4\text{-}\eta^2\text{-}C{=}C(H)R)(Cp)(CO)_9$, [M = Ru, R = t-Bu,[350]* i-Pr[351]; M = Os, R = t-Bu[352]] $Co_3Fe(\mu\text{-}CO)_2(\mu_4\text{-}\eta^2\text{-}C{=}CH_2)(Cp)(CO)_7$,[353] and $Ru_4(\mu\text{-}OR)(\mu\text{-}PPh_2)(\mu_4\text{-}\eta^2\text{-}C{=}C(H)i\text{-}Pr)(CO)_{10}$, (R=H,Et)[354]

The C_α-C_β bond length in 38 (1.391(16)Å) is somewhat longer than that observed in 36 (1.332(7)Å) and 37 (1.332(8)Å in keeping with the reduction in formal C-C bond order on formation of a vinylidene moiety from an acetylide ligand.

N.m.r spectroscopic data for complex 38.

The ^1H n.m.r spectrum of 38 displays a pseudo-triplet resonance at 5.75 p.p.m (J(P-H)= 4.5, 5.0Hz) due to the vinylidene proton in addition to the expected t-Bu and dppe proton signals. No highfield resonance is observed in this spectrum, confirming that 38 has no metal hydride ligand. Two doublets [55.5 (J(Pt-P)=3452, J(P-P)=19Hz) and 52.7 p.p.m. (J(Pt-P)=3600, J(P-P)=19Hz] in an AB pattern are observed in the ^{31}P-{^1H} n.m.r spectrum of 38 at 243 K. These signals do not broaden significantly up to 348 K, indicating that there is no detectable

*This complex is incorrectly formulated in the original paper - see ref. 351.

exchange of phosphorus sites in this temperature range.

The carbonyl region of the variable temperature ^{13}C n.m.r spectrum of a ^{13}CO enriched sample of 38 is shown in Figure 79. Relevant ^{13}C n.m.r parameters are listed in Table 42. At 171 K, nine distinct CO resonances are observed, in keeping with the low symmetry of 38. Three signals, b, e and f are broad, indicating that they are due to carbonyls undergoing exchange. These signals coalesce above 248 K giving a broad resonance with an averaged ^{31}P - ^{13}C coupling of ca. 5.5Hz. Resonances a,d and g broaden above 206 K and, at 273 K, give rise to a coalesced peak that is fortuitously coincident with the coalesced resonance of signals b, e and f. The exchanges of b,e,f and a,d,g are attributed to separate tripodal rotations of discrete $Ru(CO)_3$ units and, from line-shape analyses, values for $\Delta G^{\neq}$ of 43(1) and 48(1)kJmol^{-1} for these respective processes have been derived. Resonances c,h and i also broaden at 273 K, however h and i broaden faster than c and, hence, this fluxionality cannot be solely attributed to tripodal $Ru(CO)_3$ exchange and other processes, e.g. inter-Ru CO exchange must also be operative.

The variable temperature ^{13}C nmr spectrum clearly suggests that the three groups of signals a,d,g; b,e,f and c,h,i can be attributed to three $Ru(CO)_3$ groups. Assignments of these signals to specific $Ru(CO)_3$ units are based on the approximate mirror symmetry of complex 38 (lifted principally by the differing substituents on the vinylidene function). It may be expected that ^{31}P coupling to the hinge $Ru(CO)_3$ resonances will be similar. The coalesced peak due to signals b,e,f shows a ^{31}P - ^{13}C coupling of ca. 5.5Hz, while the average of the ^{31}P couplings to signals a,d,g is 4.9Hz, whereas the mean ^{31}P coupling to resonances c,h,i is 2.0Hz. Thus b,e,f and a,d,g are

Figure 79 : CO region of VT ^{13}C NMR spectrum of $Ru_3Pt(\mu_4\text{-}\eta^2\text{-}C{=}C(H)t\text{-}Bu)(dppe)(CO)_9$.

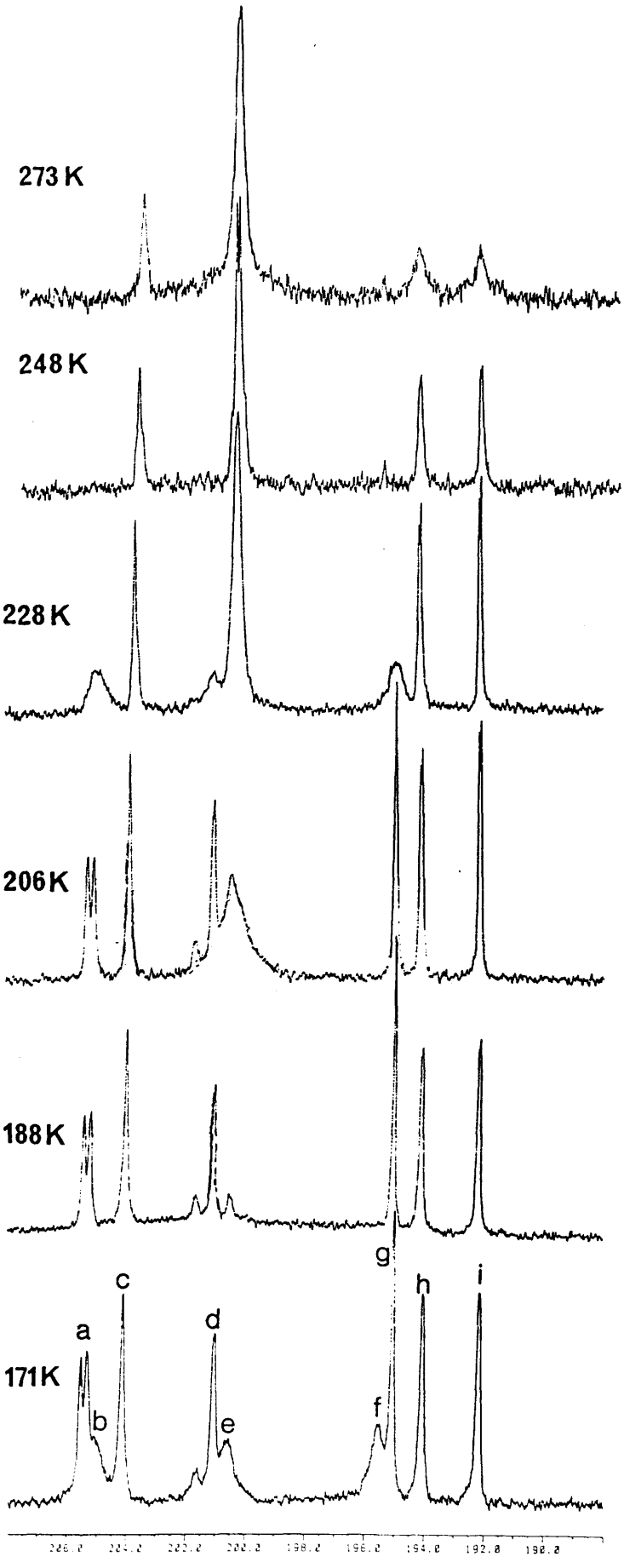

Table 42 : N.m.r. parameters for 38.

^{13}C Data [a]					
				J(Hz)	
Resonance [b]	δ	Multiplicity	Assignment [c]	P-C	Pt-C
a	205.4	d	C4/C5/C6	11.1	
b [d]	205.2	br	C1/C2/C3		
c	204.2	s	C8		
d	201.1	d	C4/C5/C6	3.6	56
e [d]	200.6	br	C1/C2/C3		
f [d]	195.6	br	C1/C2/C3		
g	195.1	s	C4/C5/C6		
h	194.1	d	C7/C9	2.9	
i	192.2	d	C7/C9	3.2	
	319.7 [e]	t	C11	27	
	100.3 [e]	s	C12		73

a- CD_2Cl_2, 171 K

b- refers to Figure 79

c- see Figure 78

d- resonances broad at 171 K, hence multiplicities and ^{31}P and ^{195}Pt couplings to these peaks undetermined.

e- from spectrum at 298 K.

assigned to the two hinge $Ru(CO)_3$ groups. Moreover, c has no ^{31}P coupling, whereas h and i show small ^{31}P splittings. Hence, h, i are attributed to C(7)/C(9), while c is assigned to C(8). Finally, the tripodal rotation of the $Ru(CO)_3$ group giving rise to signals a,d,g is a higher energy process than the b,e,f exchange. a,d,g are tentatively assigned to the carbonyls on Ru(2) on the basis that the steric interactions with the bulky t-Bu group may raise the barrier to rotation of the proximate $Ru(2)(CO)_3$ group. The above assignments are also consistent with the n.m.r data obtained for $[Ru_3Pt(\mu\text{-}H)(\mu_4\text{-}\eta^2\text{-}C{=}C(H)t\text{-}Bu)(dppe)(CO)_9]^+BF_4^-$, the protonated analogue of 38 (see below).

The C_α and C_β carbons of the vinylidene moiety give rise to resonances at 319.7(J(P-C)=27Hz) and 100.3 p.p.m. (J(Pt-C)=73Hz) respectively. The former signal appears as a pseudo-triplet due to equal coupling to the inequivalent ^{31}P nuclei. As in 37, the expected large ^{195}Pt coupling to the C_α resonance was not observed, presumably due to the signals multiplicity and the poor S/N ratio. These chemical shifts compare reasonably well with those reported for the C_α,C_β carbons (δ 304.3 and δ63.0 respectively) in $Co_3Fe(\mu\text{-}CO)_2(\mu_4\text{-}\eta^2\text{-}C{=}CH_2)(Cp)(CO)_7$ which has a similarly coordinated $\mu_4\text{-}\eta^2$ vinylidene ligand.[353]

The hydrido-acetylide/vinylidene exchange.

Transition metal ligated vinylidene moieties can be derived from complexed or free terminal alkynes.[355] This reaction formally represents a 1,2-hydrogen shift and, in certain systems, is believed to proceed through the formation of an intermediate hydrido-acetylide species.[355-357] Hoffmann and Silvestre[358] have considered the alkyne/vinylidene transformation from a theoretical viewpoint and conclude that pathways involving intermediate hydrido-acetylide species are favoured for bi- and trinuclear clusters. In contrast, for mononuclear systems a mechanism involving a "slipped" η^1-coordinated alkyne intermediate,

formed prior to 1,2-hydrogen shift, is considered to be energetically favoured.[358] However, although thermal rearrangement of hydrido-acetylide complexes to vinylidene species has been demonstrated in a few Ir and Rh mononuclear systems,[359-361] such a transformation is not known for hydrido-($\mu_{3,4}$-η^2-C≡CR) clusters. This observation can be rationalised by simple electron counting considerations. The $\mu_{3,4}$-η^2-C≡CR moiety is a 5 electron donor, whereas, the vinylidene function formally donates 4 (or 2) electrons in the $\mu_{3,4}$-η^2 (or μ_2) coordination modes respectively. Hence, the transformation of a hydrido-$\mu_{3,4}$-η^2 - acetylide to a vinylidene involves a formal reduction in the cluster valence electron count of 2 (or 4) electrons. In order to conform to common electron counting schemes[54,55,57,75] this rearrangement must be accompanied by the formation of 1 (or 2) new metal-metal bonds or the generation of an unsaturated cluster; or the addition of 1 (or 2) 2-electron donor ligands.

The tautomerisation exhibited by 37 and 38 is consistent with electron counting rules[54,55,57,75] as the hydrido-acetylide transformation to vinylidene is coupled with the formation of a new Ru-Pt bond. This process involves the first reported reversible cluster bound hydrido-acetylide/vinylidene conversion. A possible mechanism for this tautomeric exchange is depicted in Scheme 20. It is proposed that the initial a→b stage involves the twisting of the acetylide function on the Ru_3Pt framework, in a similar manner to the observed acetylide coordination in the solid state structures of the related species 34 and 36. This mechanism involves intramolecular hydride transfer, which is consistent with the kinetic data obtained for this interconversion. However, this is not the only possible pathway for the tautomeric exchange, and a mechanism involving the intermediacy

Scheme 20 : Proposed Mechanism for the transformation of 37 to 38.

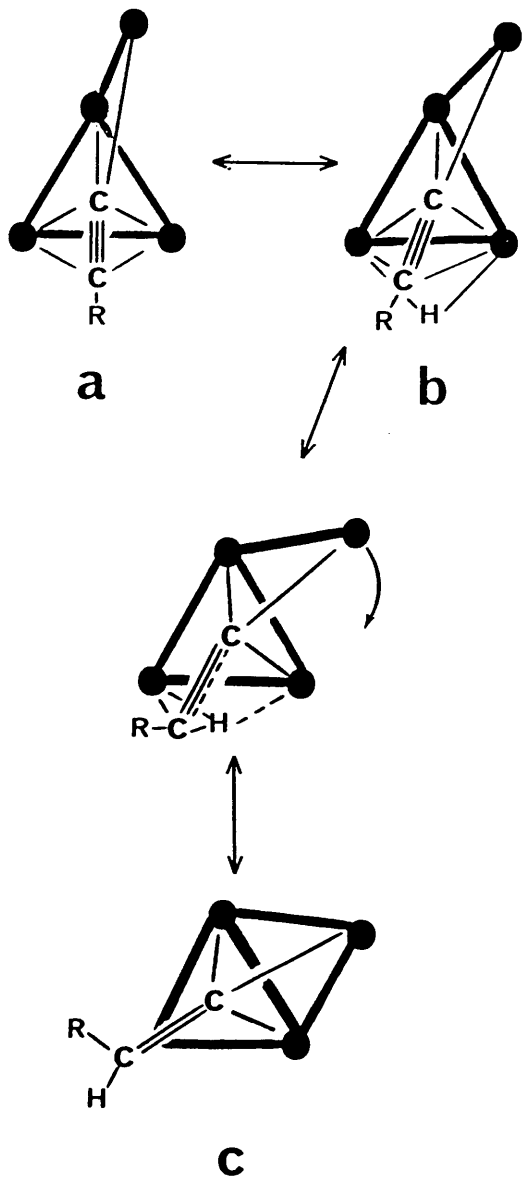

of a μ_4 alkyne or alkynyl ligand is also feasible (several butterfly clusters are known with such coordination; see ref 36 for examples). The reversible migration of the M(μ-H)M hydride to a C atom site is an infrequently observed process in cluster systems, although Shapley and co-workers[101-104,362-365] have reported such transformations occur as fluxional processes in several hydrido-Os_3 species.

Finally, vinylidene clusters are of interest as molecular models for surface-bound vinylidene fragments. These have been proposed as intermediates in the formation of alkylidyne moieties from alkenes and alkynes in heterogeneous catalytic processes.[5, 367] Moreover, Weinberg et al[368] have recently reported the spectroscopic identification of a surface μ_3-η^2-vinylidene species observed in the decomposition of adsorbed ethylidyne. In view of the cluster-surface analogy,[2-4] it is interesting to consider the μ_4-η^2 vinylidene coordination in 38 as a model for surface vinylidene bound at a step-defect metal surface.[352] The spiked-triangular metal framework bound μ_4-η^2-C≡Ct-Bu in 37 can be envisaged as a model for an acetylide fragment coordinated to a related step-defect surface location. Hence, the metal skeletal rearrangement that occurs in tandem with the hydrido-acetylide/vinylidene tautomerisation between 37 and 38 may represent a molecular model for metal surface restructuring during heterogeneous catalytic reactions.[369]

3.3 Protonation of $Ru_3Pt(\mu_4$-η^2-C=C(H)t-Bu)(dppe)$(CO)_9$, 38.

In an effort to induce reduction of the cluster bound vinylidene in complex 38 to yield an alkylidyne species, the reaction of 38 with dihydrogen in refluxing cyclohexane was investigated. However, i.r.

monitoring indicated that over a 3 hour period 38 remained the dominant carbonyl containing species. As mentioned in Chapter 2, protonation can effect the reduction of cluster-bound ligands and, hence, the protonation of 38 was studied.

Treatment of a solution of 38 in CH_2Cl_2 with $HBF_4.Et_2O$ resulted in a colour change from dark red to orange/yellow. Careful addition of diethyl ether to the resulting solution afforded orange crystals of $[Ru_3Pt(\mu\text{-}H)(\mu_4\text{-}\eta^2\text{-}C{=}C(H)t\text{-}Bu)(dppe)(CO)_9]^+BF_4^-$, 39, in good yield. The ^1H n.m.r spectrum of 39 shows a pseudo-triplet signal due to the vinylidene proton at 5.72 p.p.m. (J(P-H)=4.7Hz) and a highfield pseudo-triplet resonance attributed to a Ru(μ-H)Ru hydride at -20.34 p.p.m. (J(Pt-H)=13,J(P-H)=2.9Hz). This indicates that protonation has been effected at a Ru-Ru edge. The expected signals due to the dppe and t-Bu functions are also observed. Two sets of doublet resonances at 55.1 (J(Pt-P)=3345, J(P-P)=19Hz) and 53.2 p.p.m. (J(Pt-P)=3448, J(P-P) = 19Hz) are observed as an AB quartet in the ^{31}P n.m.r spectrum of 39. The ^{13}C n.m.r spectroscopic data closely resembles that of 38, with resonances attributed to C_α and C_β at 303.5 (J(P-C)=28, 33Hz) and 100.2 p.p.m. (J(Pt-C)=73Hz) respectively, in addition to the signals arising from CO, dppe and t-Bu moieties. The multinuclear n.m.r evidence suggests that 39 has a similar structure to 38. However the location of the metal hydride cannot be unambiguously determined from these data. Therefore a single crystal X-ray analysis of 39 was undertaken by the author of this Thesis in order to fully delineate the solid state structure of 39. A detailed description of the structural determination is presented in Chapter 4.

The crystal structure of 39 is depicted in Figure 80, and relevant bond lengths and angles are cited in Table 43. The overall

Figure 80 : The crystal structure of $[Ru_3Pt(\mu\text{-}H)(\mu_4\text{-}\eta^2\text{-}C{=}C(H)t\text{-}Bu)(dppe)(CO)_9]^+$

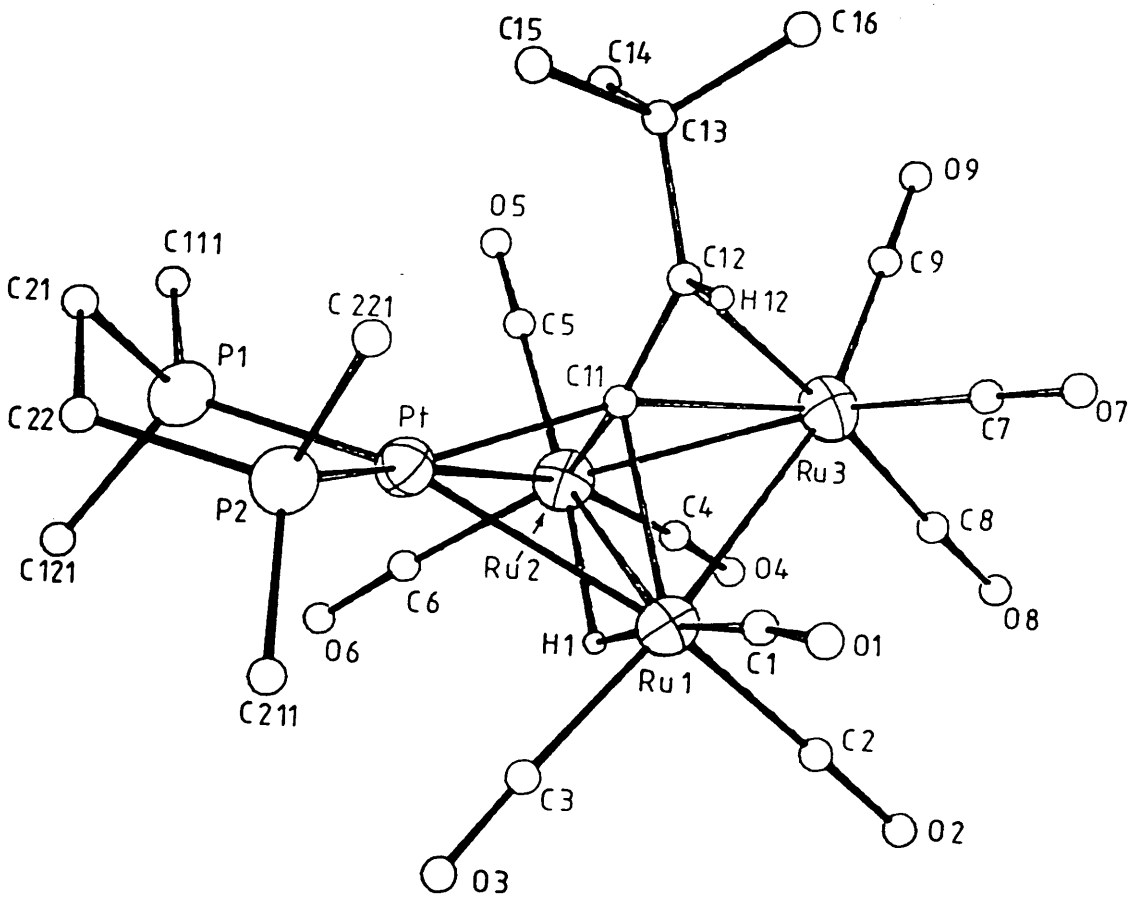

Table 43 : Selected Bond lengths (Å) and Angles (deg) for

$[Ru_3Pt(\mu\text{-}H)(\mu_4\text{-}\eta^2\text{-}C{=}C(H)t\text{-}Bu)(dppe)(CO)_9]^+BF_4^-$, 39

Bonds.

Pt-Ru(1)	2.784(1)	Pt-Ru(2)	2.782(1)
Pt-P(1)	2.269(2)	Pt-P(2)	2.286(2)
Pt-C(11)	2.092(6)	Ru(1)-Ru(2)	2.835(1)
Ru(1)-Ru(3)	2.774(1)	Ru(1)-C(11)	2.155(7)
Ru(1)-H(1)	1.648	Ru(2)-Ru(3)	2.830(1)
Ru(2)-C(11)	2.112(7)	Ru(2)-H(1)	1.793
Ru(3)-C(11)	2.089(6)	Ru(3)-C(12)	2.278(7)
C(11)-C(12)	1.40(1)	C(12)-C(13)	1.51(1)

mean Ru-CO = 1.912

mean C-O = 1.131

mean B-F = 1.324

Angles

Ru(1)-Pt-Ru(2)	61.2(1)	Ru(1)-Pt-P(2)	109.4(1)
Ru(2)-Pt-P(1)	104.8(1)	P(1)-Pt-P(2)	84.1(1)
Pt-Ru(1)-Ru(2)	59.3(1)	Pt-Ru(1)-Ru(3)	95.6(1)
Ru(2)-Ru(1)-Ru(3)	60.6(1)	Pt-Ru(2)-Ru(1)	59.4(1)
Pt-Ru(2)-Ru(3)	94.4(1)	Ru(1)-Ru(2)-Ru(3)	58.6(1)
Ru(1)-Ru(3)-Ru(2)	60.8(1)	Ru(3)-C(11)-C(12)	78.8(4)
Pt-C(11)-C(12)	119.9(5)	C(11)-C(12)-C(13)	134.4(7)
Ru(1)-C(11)-C(12)	127.0(5)		
Ru(3)-C(12)-C(13)	124.3(5)		
Ru(1)-H(1)-Ru(2)	110.9(1)		

mean Ru-C-O = 176.3

mean F-B-F = 109.3

cluster geometry is very similar to that of 38, with a μ_4-η^2-C=C(H)t-Bu moiety bound to a butterfly Ru_3Pt framework. The major alteration to the metal core is the elongation of the hinge Ru(1)-Ru(2) vector, which is 0.13Å longer in 39 than the corresponding distance in 38. Otherwise, corresponding metal framework separations in 38 and 39 vary by 0.054-0.007 Å. The hydride ligand was directly observed bridging the Ru(1)-Ru(2) edge. This position was also favoured by potential energy minimisation calculations,[271] and is in keeping with the significant elongation[303] of this vector compared with the hinge Ru-Ru vector in 38.

Fluxional behaviour of 39.

The carbonyl region of the variable temperature ^{13}C n.m.r spectrum of a ^{13}CO enriched sample of 39 is shown in Figure 81, while relevant parameters are cited in Table 44. It is evident that the introduction of the hydride ligand raises the barrier to carbonyl fluxionality in 39, compared with that observed in 38. Hence, at 298 K, 6 sharp resonances are observed, while 3 signals are broadened due to exchange. At 242 K, 9 sharp signals are observed, in accord with the low symmetry of 39. The presence of the hydride ligand facilitates the assignments of these resonances to particular carbonyl carbons in 39. Thus d and f are assigned to C(1)/C(5), trans to the hydride on the basis of the large coupling to H1 that these signals exhibit (J(H-C)= 13.2, 15.1Hz respectively). b,c,h and i are assigned to the 4 CO's cis to the hydride by similar considerations (J(H-C) ranges from 3.0 - 4.0Hz). Resonances a,e and g show no detectable coupling to H1 and are therefore assigned to the wingtip $Ru(CO)_3$ carbonyls. The ^{31}P couplings to a, e, and g are very similar to those observed for the corresponding $Ru(CO)_3$ carbonyls in 38, with 2 resonances, e and g, displaying a ca. 2Hz coupling, while a shows no resolvable ^{31}P coupling.

Figure 81 : CO region of VT ^{13}C NMR spectrum of
$[Ru_3Pt(\mu\text{-}H)(\mu_4\text{-}\eta^2\text{-}C{=}C(H)t\text{-}Bu)(dppe)(CO)_9]^+BF_4^-$

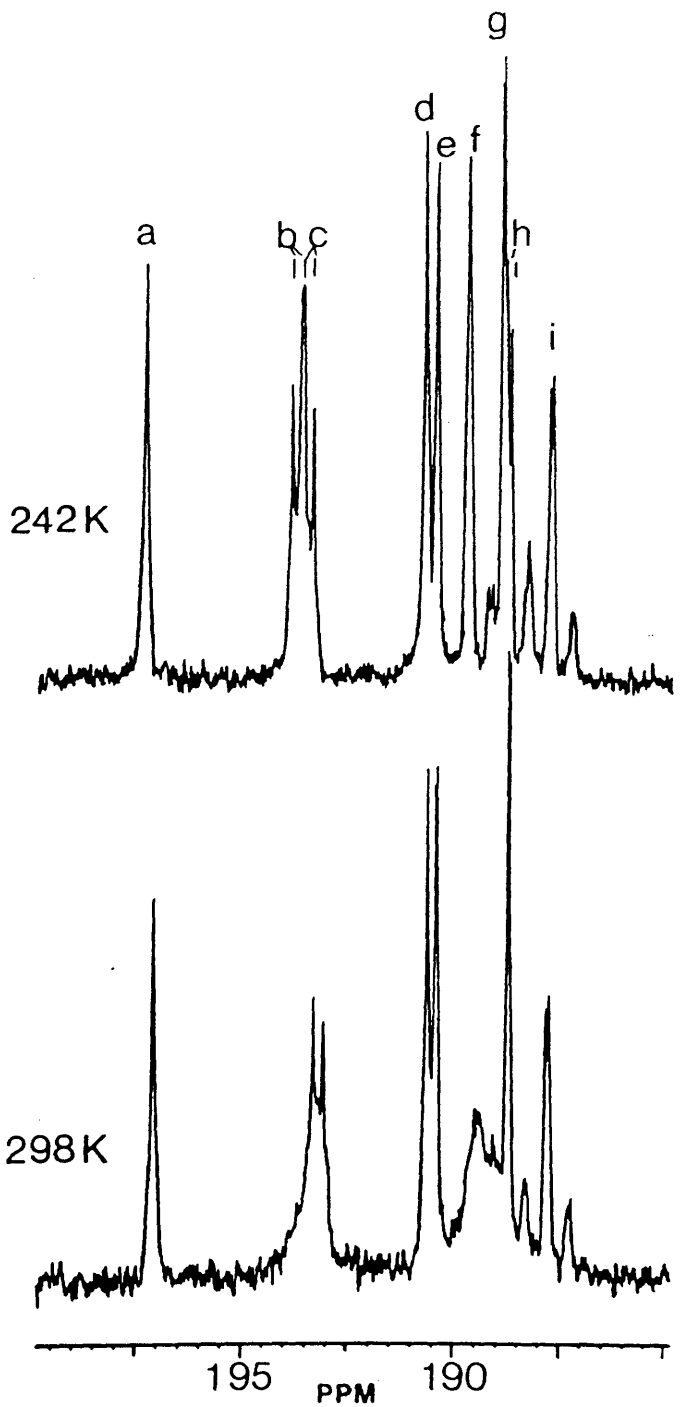

Table 44 : N.m.r. parameters for $[Ru_3Pt(\mu\text{-}H)(\mu_4\text{-}\eta^2\text{-}C{=}C(H)t\text{-}Bu)(dppe)(CO)_9]^+BF_4^-$

	^{13}C Data [a]			J/Hz			
Reson. [b]	p.p.m.	Mult. [c]	Assign. [d]	P-C	Pt-C	H1-C [d]	H12-C [d]
a	197.5	s	C8		12		
b	193.9	d	C2/C3	10.4		3.5	
c	193.7	d	C4/C6	11.9		3.0	
d	190.9	s	C5		7	13.2	
e	190.6	d	C7/C9	2.0			5.0
f	189.8	s	C1			15.1	
g	189.1	d	C7/C9	2.3			
h	188.9	d	C2/C3	5.2	44	4.0	
i	187.9	d	C4/C6	3.3	52	4.0	
	303.5 [e]	dd	C11	28,33			
	100.2 [e]	s	C12		73		

a) 242 K, CD_2Cl_2;

b) Figure 81

c) Multiplicities based on $^{13}C\{H\}$ spectra;

d) see Figure 80.

e) from 298 K spectrum.

These resonances are, hence, assigned to C(7)/C(9) (e and g) and C8(a). b,f and h are considerably broadened at 298 K and are assigned to the Ru(1) bound carbonyls on the basis of the steric arguements detailed for 38. Hence c,d, and i are assigned to the $Ru(CO)_3$ group on Ru(2).

3.4 The Reactions of $Ru_3Pt(\mu\text{-}H)(\mu_4\text{-}\eta^2\text{-}C{\equiv}Ct\text{-}Bu)(cod)(CO)_9$, 36, with other donor ligands; CO, CyNC, CH_2N_2.

The reaction of 36 with dppe led to the displacement of the labile cod ligand of 36 by a bidentate dppe moiety. A similar reaction was attempted with CO in the hope of obtaining the undecacarbonyl analogue of 36. However, treatment with CO led to the regeneration of $Ru_3(\mu\text{-}H)(\mu_3\text{-}\eta^2\text{-}C{\equiv}Ct\text{-}Bu)(CO)_9$, 35, and the formation of a brown-purple precipitate. This precipitate is insoluble in common organic solvents and appears to be a polymeric $[Pt_x(CO)_y]_n$ species, on the basis of i.r. and microanalytical data. The solid-state i.r. shows three bands in the carbonyl region at 2053, 1882 and 1822 cm^{-1}, the latter two bands represent bridging CO stretches. Microanalytical data indicated a Pt:CO ratio of ca. 2:1. Further characterisation of this species was not undertaken. 35 was characterised from i.r. spectra of the mother liquor.

On addition of CyNC to solutions of 36 at $-70^{o}C$ the orange colour of the starting material gives way to bright yellow. However, if this solution is warmed to $-20^{o}C$ the colour soon changes from bright yellow to dark brown. It did not prove possible to isolate any products from this solution and the reaction was not investigated further. The initial, bright yellow complex may be $Ru_3Pt(\mu\text{-}H)(\mu_4\text{-}\eta^2\text{-}C{\equiv}Ct\text{-}Bu)(CyNC)_2(CO)_9$.

Reaction of 36 with CH_2N_2 gave no tractable products and was not studied further.

3.5 The Reaction of $Ru_3Pt(\mu\text{-}H)(\mu_4\text{-}\eta^2\text{-}C{\equiv}Ct\text{-}Bu)(cod)(CO)_9$, 36, with $Os_3(\mu\text{-}H)_2(CO)_{10}$, 4.

The above results show that the cod ligand in complex 36 is easily displaced. In view of this, the reactivity of 36 towards cluster complexes was investigated with the aim of preparing novel Ru_3PtM_n systems. The reactions of $Fe_3(CO)_{12}$, and $Co_2(CO)_8$ with 36 gave no tractable products.

As outlined in Chapter 1, the unsaturated cluster $Os_3(\mu\text{-}H)_2(CO)_{10}$, 4, is reactive towards metal complexes containing labile ligands. With this in mind, the reaction of 36 with 4 was investigated in the hope of forming a Pt bridged Ru_3PtOs_3 cluster.

Addition of a toluene solution of 4 to 36 in the same solvent at ambient temperature resulted in a rapid colour change from orange to brown. Removal of solvent afforded red/brown crystals of $Os_3Pt(\mu\text{-}H)_2(\mu\text{-}CO)(cod)(CO)_9$, 40, and yellow crystals of 35. These crystals were separated mechanically. The latter product was unambiguously characterised by i.r. and ^1H n.m.r spectroscopy. The solution i.r. spectrum of 40, shows several bands in the terminal carbonyl stretching region (2087-1940 cm^{-1}) and a broad, weak band in the bridging CO region (1769 cm^{-1}). At 298 K, the ^1H n.m.r spectrum of 40 shows signals at 5.52 (J(Pt-H)=53Hz), 2.72-2.42 and -21.78 p.p.m. (J(Pt-H)=17.0, J(Os-H)= 21.6Hz) in the intensity ratio 2:4:1. These resonances correspond to the olefin and methylene protons of the cod ligand and two equivalent Os(μ-H)Os protons respectively. Two broad singlet olefinic proton reconances, at 5.70 (J(Pt-H)=61Hz) and 5.16 p.p.m. (J(Pt-H)=48Hz) are observed in the ^1H n.m.r spectrum at 203 K. This indicates that, at 298 K, the cod ligand undergoes rapid rotation which renders the olefinic protons equivalent, while at 203 K, this rotation is slow on the n.m.r

timescale. The resonance due to the two Os(μ-H)Os hydrides remains a sharp singlet throughout the temperature range, 203-298 K.

In order to fully delineate the structure of 40, a single crystal X-ray diffraction experiment was undertaken by Dr. L.J. Farrugia.

The molecular structure of 40 is shown in Figure 82, together with the crystallographic labelling scheme employed. Relevant bond lengths and angles are given in Table 45. The metal core of 40 adopts a *closo*-tetrahedral geometry, with Pt-Os separations varying between 2.714(1)-2.811(1)Å and Os-Os distances of 2.837(1)-2.952(1)Å. The calculated[271] hydride ligand positions span the Os(1)-Os(3) and Os(2)-Os(3) separations. This is in keeping with the ^{1}H n.m.r data, which indicates the hydrides span Os-Os edges. The Os(1)-Os(2) bond is symmetrically bridged by a carbonyl ligand, with Os(1)-C(1), Os(2)-C(1) distances of 2.17(2) and 2.10(2)Å respectively. The carbonyls trans to the μ-CO ligand form weak semi-bridging interactions with the Pt centre, with Pt---C(2), Pt---C(5) distances of 2.50(2) and 2.63(2)Å respectively, and Os(1)-C(2)-O(2), Os(2)-C(5)-O(5) angles of 160.7(2)° and 163.2(2)°. Similar weak semi-bridging interactions between Pt centres and CO ligands trans to μ-CH_2 (see Chapter 2 and refs 255,258) or μ-SO_2 (see Chapter 2) moieties have been observed in other tetrahedral Os_3Pt systems.

There are comparatively few clusters known with carbonyl bridged Os-Os edges (for recent examples see refs 214, 370, 371).

40 has a pseudo-mirror plane defined by Os(3), Pt, C(1), C(9). The overall molecular geometry of 40 closely resembles that found in the related cluster $Os_3Pt(\mu\text{-}H)_2(\mu\text{-}CH_2)(cod)(CO)_9$, reported by Norén and Sundberg[255] during the course of these studies. In this latter complex a μ-CH_2 ligand bridges an Os-Os vector instead of the μ-CO in

Figure 82 : Molecular structure of $Os_3Pt(\mu\text{-}H)_2(\mu\text{-}CO)(cod)(CO)_{10}$

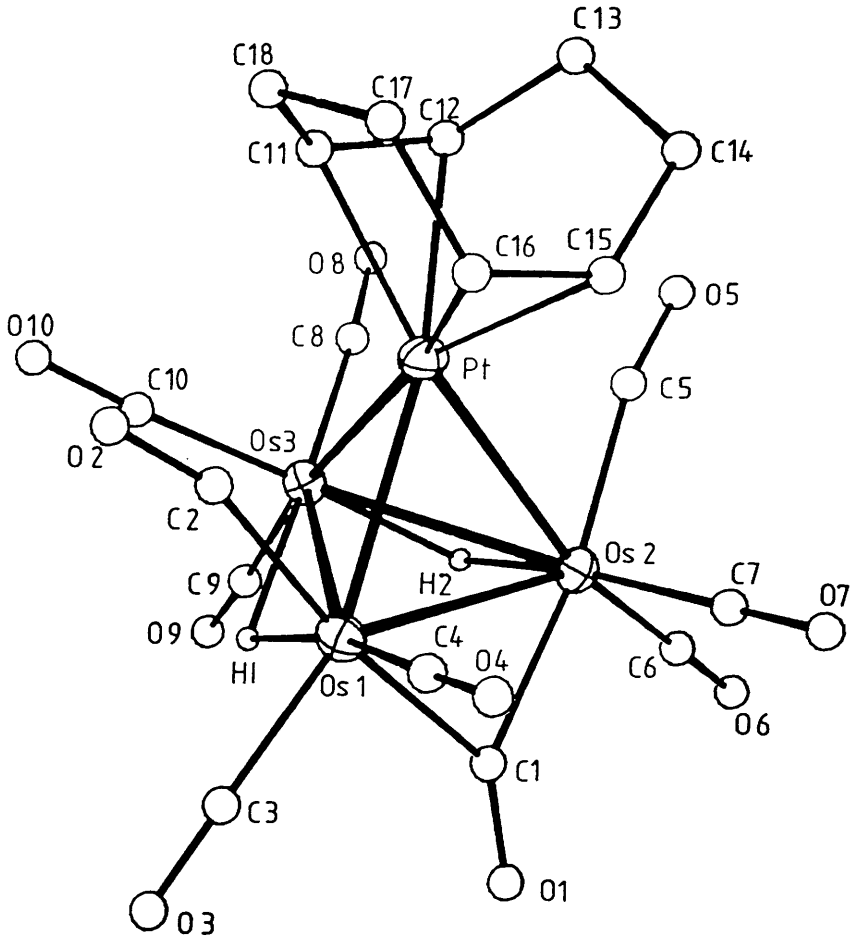

Table 45 : Selected bonds and angles for $Os_3Pt(\mu\text{-}H)_2(\mu\text{-}CO)(cod)(CO)_9$, 40

Bonds (Å)

Pt-Os(1)	2.730(1)	Pt-Os(2)	2.811(1)
Pt-Os(3)	2.714(1)	Pt-C(11)	2.190(17)
Pt-C(12)	2.203(16)	Pt-C(15)	2.303(17)
Pt-C(16)	2.30(2)	Os(1)-Os(2)	2.837(1)
Os(1)-Os(3)	2.919(1)	Os(2)-Os(3)	2.952(1)
Os(1)-C(1)	2.167(16)	Os(2)-C(1)	2.103(16)
C(11)-C(12)	1.39(3)	C(15)-C(16)	1.36(4)

mean of remaining Os-C = 1.918

mean C-O = 1.13

Angles (deg)

Os(1)-Pt-Os(2)	61.6(1)	Pt-Os(1)-Os(2)	60.6(1)
Os(1)-Pt-Os(3)	64.9(1)	Pt-Os(1)-Os(3)	57.3(1)
Os(2)-Pt-Os(3)	64.6(1)	Os(2)-Os(1)-Os(3)	61.7(1)
Pt-Os(2)-Os(3)	56.1(1)	Os(1)-Os(2)-Os(3)	60.5(1)
Pt-Os(2)-Os(1)	57.8(1)	Pt-Os(3)-Os(1)	57.8(1)
Pt-Os(3)-Os(2)	59.3(1)	Os(1)-Os(3)-Os(2)	57.8(1)
Os(1)-C(1)-Os(2)	83.3(6)	Os(1)-C(1)-O(1)	135.7(14)
Os(2)-C(1)-O(1)	141.0(14)	Os(1)-C(2)-O(2)	160.7(15)
Os(2)-C(5)-O(5)	163.2(15)	C(12)-C(11)-C(18)	127.6(16)
C(11)-C(12)-C(13)	121.7(17)	C(14)-C(15)-C(16)	124.3(19)
C(15)-C(16)-C(17)	122.6(16)		

Average of remaining Os-C-O angles = 177.3

complex 40. In both clusters, the cod ligand is asymmetrically bound to the Pt centre with the olefinic bond lying over the Pt-Os edge having significantly shorter Pt-C(olefin) separations than the olefinic bond lying over the $PtOs_2$ face.

Complex 40 has a valence electron count of 60 i.e. the normal electron count for tetrahedral clusters.[54,55,75] The Pt centre has a pseudo trigonal bipyramidal coordination geometry and, therefore, is an effective 18 electron centre.

In conclusion, the reaction of 4 with 36 does not yield the expected Os_3PtRu_3 cluster. Instead, the formation of 40 from 36 has been effected by formal cleavage of the Ru-Pt bond, yielding 35 and Pt(cod) fragments which add to 4. Similar scission of the Ru-Pt bond is observed in the reaction of 36 with CO and in the formation of $Pt\{Ru_3(\mu\text{-}H)(\mu_3\text{-}\eta^2\text{-}C{\equiv}Ct\text{-}Bu)(CO)_9\}_2$.[344] These observations suggest that, although the Ru-Pt distance in 36 (2.645(1) Å) is the shortest such separation reported, this bond is rather weak. Indeed, in the formation of 40, 36 could be considered as a Pt(cod)L, $[L{=}Ru_3(\mu\text{-}H)(\mu_3\text{-}\eta^2\text{-}C{\equiv}Ct\text{-}Bu)(CO)_9]$ unit, where L, rather than cod is the labile moiety.

As the synthesis of 40 involves the formal addition of a Pt(cod) fragment to 4, the reaction of $Pt(cod)_2$ with 4 was studied by ^1H n.m.r spectroscopy. This investigation indicated that, although 40 is formed, substantial quantities of unidentified coproducts are also formed with highfield proton resonances at -12.37(J(Pt-H)=24.3Hz) and -20.45p.p.m. The isolation of pure samples of 40 from this mixture did not prove possible as 40 decomposes on Florisil or alumina columns and is somewhat unstable in solution. Hence the synthetic route involving 36 is preferred.

Finally, $Os_3Pt(\mu\text{-}H)_2(cod)(CO)_{10}$, 40, bears a formal similarity to the 2 electron adducts of $Os_3Pt(\mu\text{-}H)_2(CO)_{10}(PCy_3)$, 19, by replacement of the Pt (cod) unit by $Pt(CO)(PCy_3)$. In the light of the EHMO

analysis of such adducts presented in Chapter 2.2.1 , it is interesting that 40 provides an example of a 60 electron *closo*-tetrahedral Os_3Pt cluster with a carbonyl moiety spanning an Os-Os edge. The EHMO calculations showed that, although the μ-CO *closo*-tetrahedral cluster is a stable configuration, one of the μ-COπ^* orbitals is not stabilised through interaction with the cluster. It was argued that this may be the reason for the CO adduct of 19 having a butterfly core, where COπ^* orbitals are stabilised through back bonding with metal "t_{2g}" orbitals. However, the structure of 40 suggests that the factors controlling the framework geometry adopted in 60 electron Os_3Pt systems are more complex, and may depend on the nature of the ancillary ligands on the Pt centre.

CHAPTER FOUR.

CHAPTER 4.

Crystallographic Analyses of $Os_3Pt(\mu\text{-}H)(\mu_4\text{-}\eta^2\text{-}C{\equiv}CPh)(CO)_{10}(PCy_3)$, 34; $Ru_3Pt(\mu\text{-}H)(\mu_4\text{-}\eta^2\text{-}C{\equiv}Ct\text{-}Bu)(cod)(CO)_9$, 36; and $[Ru_3Pt(\mu\text{-}H)(\mu_4\text{-}\eta^2\text{-}C{=}C(H)\text{-}t\text{-}Bu)(dppe)(CO)_9]^+BF_4^-$, 39.

Single crystal X-ray crystallography is probably the most important technique employed in the structural characterisation of cluster systems. With the development of high speed computers, X-ray diffraction studies of cluster complexes are now routinely performed. X-ray diffraction provides the most accessible means of determining the metal core geometries of cluster complexes and has been essential in the development of cluster bonding schemes.[54,55,57,75] In addition, the detailed information made available about the metal-ligand interactions have provided the basis for the cluster-surface analogy.[2-7]

However, there are particular problems associated with this technique which are worth bearing in mind:-

i) X-ray analysis is performed on a single crystal that may not be representative of the bulk sample.

ii) In molecules incorporating heavy atoms (e.g. Ru, Os, Pt), X-ray absorption effects can severely limit the accuracy with which positional and vibrational parameters of lighter atoms are determined.

iii) It is often difficult or impossible to locate transition metal hydride ligands as X-ray scattering is dominated by the heavy atom contribution. Indirect methods (e.g. potential energy minimisation procedures[271]) have been developed to overcome this problem.

iv) Crystallography only defines the solid-state structure, whereas the majority of cluster reactivity occurs in solution, where cluster fluxionality is frequently observed.

The majority of crystal structure analyses contained in this Thesis were performed by Dr. Louis J. Farrugia. However the structures of $Os_3Pt(\mu\text{-}H)(\mu_4\text{-}\eta^2\text{-}C{\equiv}CPh)(CO)_{10}(PCy_3)$, 34, $Ru_3Pt(\mu\text{-}H)(\mu_4\text{-}\eta^2\text{-}C{\equiv}Ct\text{-}Bu)(cod)(CO)_9$, 36, and $[Ru_3Pt(\mu\text{-}H)(\mu_4\text{-}\eta^2\text{-}C{=}C(H)t\text{-}Bu)(dppe)(CO)_9]^+BF_4^-$, 39, were determined by the author and these are described in this Chapter.

The structure analyses of complexes 34, 36 and 39 were performed using similar computational and experimental techniques outlined below.

Data Collection and Reduction.

The X-ray measurements were made with molybdenum radiation (λ=0.71069Å) using an Enraf-Nonius CAD-4F diffractometer equipped with a graphite monochromator. The unit cell dimensions were determined by refinement of setting angles ($\theta>12^\circ$) of 25 reflections. Data were collected at 298 K using the $\theta/2\theta$ scan mode. Space groups were determined by consideration of the symmetry of the lattice and the systematic absences of reflections.

For each reflection, the integrated intensity, I, and the standard deviation $\sigma_1(I)$ were determined from

$$I = C - 2(B_1+B_2)$$

$$\sigma_1(I) = [C + 4(B_1+B_2)]^{\frac{1}{2}}$$

where B_1 and B_2 are the counts measured in the first and last sixths of the scan range and C is the count measured for the remainder of the scan range. C was set to 0.95° for 34, 1.00° for 36 and $1.00^\circ + 0.34\tan\theta$ for 39. Reflections for which a preliminary scan gave

$\sigma_1(I)/I > \frac{1}{2}$ were considered weak and not examined further. For the remainder counting continued until $\sigma_1(I)/I < n$, (n = 0.02 for 34, 36; 0.03 for 39) or for N secs (N = 80 for 34; 90 for 36; 60 for 39), whichever required less time. The intensities of standard reflections were remeasured at intervals of ca. 2 hours throughout these experiments and no decay correction was considered necessary for 34, 36 or 39.

The integrated intensities, I, and their standard deviations $\sigma(I)$, where

$$\sigma^2(I) = \sigma_1^2(I) + (0.03\ I)^2$$

were corrected for both Lorentz-polarisation and absorption (DIFABS[372]) effects.

Structure Analyses.

In all analyses, the heavy atom positions were located by Patterson techniques and all other non-hydrogen atoms were located from subsequent electron density difference syntheses. Final positional and vibrational atomic parameters were obtained by full matrix least-squares minimisation of the function

$$\Sigma\ w(|F_o| - |F_c|)^2$$

with the weighting function $w = \sigma^{-2}(F_o)$ used and judged satisfactory. $\sigma(F_o)$ was estimated from counting statistics. Due to core storage limitations, for 34 and 39, parameters were divided into two blocks and each refined separately. Neutral atom scattering factors which compensate for anomalous dispersion were employed throughout.[373] Unweighted and weighted residuals, R and R_w, were determined by the expressions:

$$R = \frac{\Sigma|(|F_o| - |F_c|)|}{\Sigma|F_o|}$$

$$R_w = \left[\frac{\Sigma w(|F_o| - |F_c|)^2}{\Sigma w|F_o|^2} \right]^{\frac{1}{2}}$$

All non-hydrogen atoms were allowed anisotropic thermal motion except the oxygen of disordered Et_2O in 34, and the phenyl carbon atoms in 39. Hydride positions were obtained from difference Fourier maps for 36 and 39, as were the olefinic hydrogens of 36 and the vinylidene hydrogen in complex 39. All other hydrogens were included at calculated positions, assuming an Os-H distance of 1.85 Å in 34 and a C-H distance of 0.96 Å (for 34) or 1.00 Å (for 36 and 39). No hydrogen positional parameters were refined. The hydrogen isotropic temperature parameters were restricted to ca. 1.2 times those of their carbon atoms for 34, refined for 36, and fixed at 0.08 $Å^2$ for 39.

All calculations were performed on a GOULD-SEL 32/27 mini computer using the GX[374] program package.

i) The structure determination of $Os_3Pt(\mu\text{-}H)(\mu_4\text{-}\eta^2\text{-}C{\equiv}CPh)(CO)_{10}(PCy_3)$, 34.

Yellow crystals of 34 were grown at -20°C from a Et_2O solution containing a mixture of two complexes. The other, unidentified complex crystallised as small red prisms. These crystals were separated mechanically.

Details of the data collection and structure refinement are given in Table 46. 34 crystallises in a triclinic lattice, indicating the space group $P1$ or $P\bar{1}$. Analysis of the distribution of normalised structure factors favoured the centrosymmetric $P\bar{1}$ and this choice was confirmed by successful full-matrix refinement.

The refinement of 34 converged at R=0.031, R_w=0.042. In the final cycle of refinement the maximum (Δ/σ)=0.184, while the mean (Δ/σ)= 0.016. Difference syntheses showed residual electron density close to the centre of symmetry, 0 ½ 0. This was attributed to disordered

Table 46 : Experimental Data for Crystallographic Analysis of

$Os_3Pt(\mu\text{-}H)(\mu_4\text{-}\eta^2\text{-}C{\equiv}CPh)(CO)_{10}(PCy_3)$, 34.

Compd. formula	$C_{36}H_{39}O_{10}Os_3PPt$
M_r	1428.37
Space Group	$P\bar{1}$ (C_i^1 No.2)
Cryst. system	triclinic
a/Å	9.816(1)
b/Å	11.414(2)
c/Å	19.971(4)
α/deg	76.14(2)
β/deg	77.83(1)
γ/deg	87.68(1)
V/Å^3	2123.5(6)
Z	2
$D_{calc.}$/g cm^{-3}	2.24
F(000)	1312
μ(Mo-Kα), cm^{-1}	123.6
θ range/deg.	$2 \leqslant \theta \leqslant 25$
cryst. size/mm	0.32 x 0.32 x 0.28
range of trans. coeff. corr.	0.83 /1.17
no. of data collected	10861
no. of unique data	7451
std. reflections	200, 002
observability criterion n	
$I \geqslant n\sigma(I)$	3.0
no. of data in refinement	5444
no. of refined parameters	246/264
final R	0.031
R_w	0.042
largest remaining feature in elec. density map, eÅ^{-3}	+1.78(max) -1.52(min)
shift/esd in last cycle	0.18(max) 0.01(av.)

Et_2O solvent molecules. Although no satisfactory model for this disorder was obtained, the solvent oxygen atom O(S1), was included at 0 ½ 0 with an occupancy of ½ per asymmetric unit. The final difference synthesis shows three peaks close to this centre with $|\Delta\rho|$ of 1.59, 1.71 and 1.78 eA^{o-3}. The remaining peaks and troughs are located close to the metal centres and are of no chemical significance.

The molecular structure of 34 is shown in Figure 83, along with the atomic labelling scheme used. Atomic coordinates, anisotropic temperature factors, bond lengths and angles are listed in Tables 47, 48 49 and 50 respectively.

Complex 34 has a spiked triangular metal core consisting of a near equilateral Os_3 triangle (Os-Os bond lengths range 2.824(1)-2.845(1) Å; angles between 59.6(1) - 60.3(1)°) axially bonded at Os(1) by Pt(1) (angle between Pt(1)-Os(1) and normal to Os_3 triangle is 11.7°). The Pt-Os(2), Os(3) separations (4.308(1) and 4.070(1) Å respectively) are too long to be considered bonding. Potential energy minimisation calculations[271] position the hydride ligand at the Os(2)-Os(3) edge. The Pt(1)-Os(1), Os(1)-Os(2) and Os(1)-Os(3) distances (2.712(1), 2.845(1) and 2.824(1) Å respectively) fall within the expected ranges.[147,148,255]

The hydride bridged Os(2)-Os(3) separation (2.838(1) Å) is similar in magnitude to the unbridged Os-Os vectors and this may be attributed[338] to a balance between bond lengthening and bond shortening influences of the hydride and acetylide ligands respectively.

The Os(2) centre has a distorted octahedral coordination geometry, if the hydride bridged Os(2)-Os(3) vector is ignored. The angles Os(1)-Os(2)-C(7) = 165.4(3)°, Os(1)-Os(2)-C(12) = 75.4(3)°, and C(6)-Os(2)-C(12) = 166.3(4)° show the greatest deviation from idealised

Figure 83 : The molecular structure of $Os_3Pt(\mu\text{-}H)(\mu_4\text{-}\eta^2\text{-}C{\equiv}CPh)(CO)_{10}(PCy_3)$, 34.

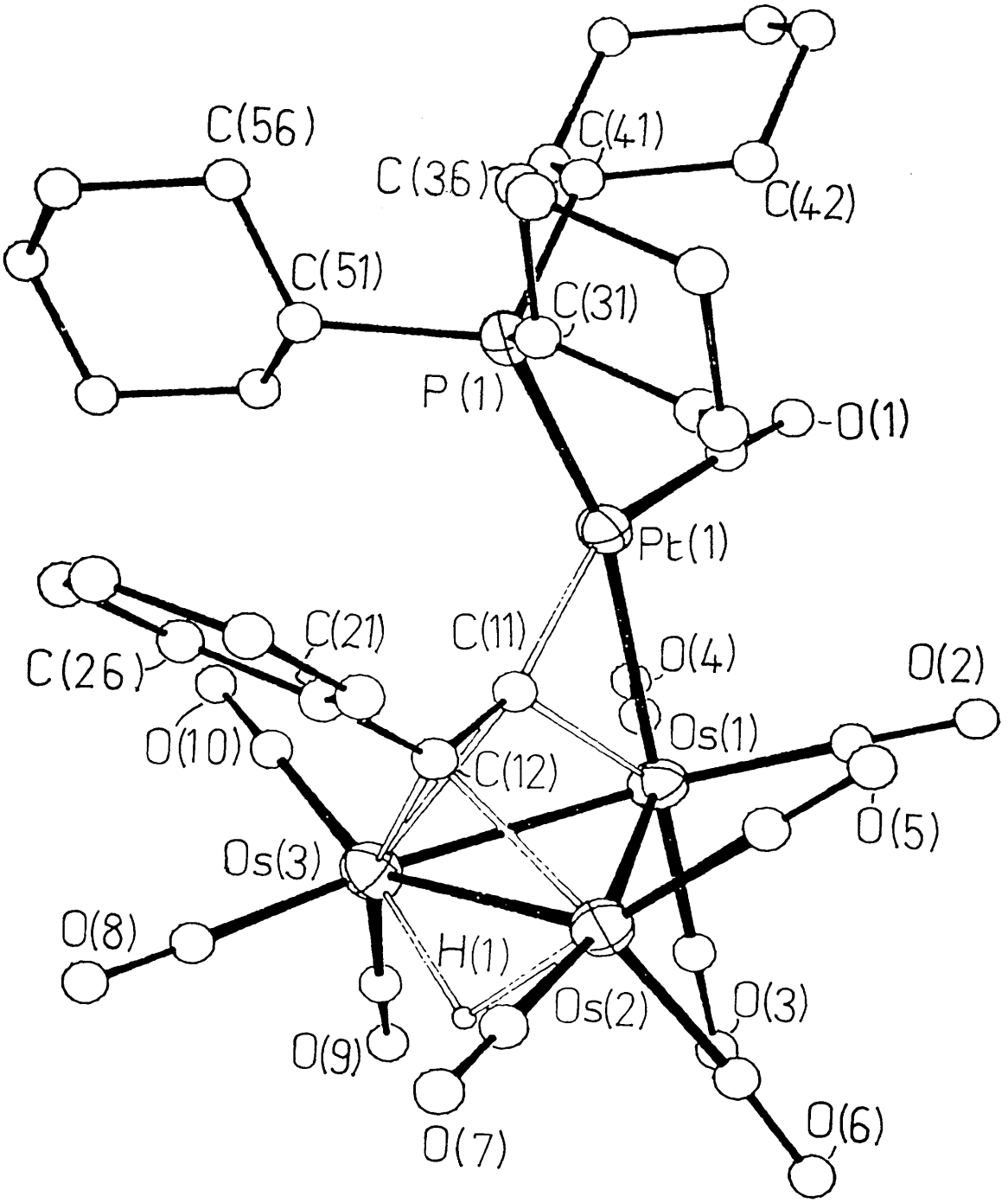

Table 47 : Final positional parameters (fractional coordinate) with esd's and equivalent isotropic thermal parameters, U ($Å^2$), for the complex $Os_3Pt(\mu\text{-}H)(\mu_4\text{-}\eta^2\text{-}C{\equiv}CPh)(CO)_{10}(PCy_3)$, 34

$U = {}^1/_3 \Sigma_i \Sigma_j U_{ij} a_i^* a_j^* a_i . a_j$

	X/A	Y/B	Z/C	U
Os(1)	.18450(5)	-.07838(4)	.23862(2)	.032
Os(2)	.27904(5)	-.08100(4)	.09418(2)	.033
Os(3)	-.00728(5)	-.11851(4)	.15884(2)	.036
Pt(1)	.20265(5)	-.31481(4)	.30280(2)	.030
P(1)	.2161(3)	-.5225(2)	.3140(1)	.028
O(1)	.2476(13)	-.2864(8)	.4422(5)	.099
O(2)	.4704(12)	-.0562(10)	.2702(6)	.098
O(3)	.1506(10)	.1898(7)	.1803(4)	.062
O(4)	.0036(13)	-.0708(8)	.3821(5)	.090
O(5)	.5625(9)	-.1757(8)	.1200(4)	.065
O(6)	.3811(10)	.1834(7)	.0459(4)	.064
O(7)	.3047(11)	-.1085(8)	-.0550(4)	.075
O(8)	-.1262(11)	-.1746(8)	.0411(5)	.073
O(9)	-.1612(12)	.1125(9)	.1755(6)	.105
O(10)	-.2339(11)	-.2570(10)	.2760(5)	.093
O(S1)	.50000	.00000	.50000	.18(1)
C(1)	.2334(15)	-.3027(9)	.3914(6)	.050
C(2)	.3595(15)	-.0653(11)	.2586(7)	.061
C(3)	.1657(14)	.0875(9)	.2000(6)	.047
C(4)	.0727(14)	-.0767(10)	.3281(6)	.050
C(5)	.4567(13)	-.1418(11)	.1091(6)	.048
C(6)	.3439(12)	.0816(10)	.0666(6)	.046
C(7)	.2959(12)	-.0987(10)	.0009(6)	.042
C(8)	-.0876(13)	-.1509(10)	.0850(6)	.046
C(9)	-.1055(14)	.0276(12)	.1683(7)	.064
C(10)	-.1487(14)	-.2075(12)	.2331(7)	.058
C(11)	.1693(10)	-.2425(8)	.2060(5)	.030
C(12)	.1649(12)	-.2476(8)	.1404(5)	.033
C(21)	.1572(13)	-.3557(9)	.1121(5)	.039
C(22)	.2706(13)	-.3904(10)	.0676(6)	.045
C(23)	.2648(16)	-.4897(11)	.0419(6)	.058
C(24)	.1455(19)	-.5577(11)	.0583(7)	.069
C(25)	.0278(17)	-.5265(11)	.1038(8)	.070
C(26)	.0393(14)	-.4286(10)	.1303(6)	.050
C(31)	.3499(11)	-.5601(9)	.2417(5)	.034
C(32)	.4754(13)	-.4739(9)	.2174(6)	.042
C(33)	.5754(14)	-.4983(11)	.1527(6)	.053
C(34)	.6203(13)	-.6293(11)	.1643(6)	.050
C(35)	.4991(14)	-.7132(11)	.1866(7)	.060
C(36)	.3991(12)	-.6899(10)	.2546(6)	.045
C(41)	.2573(12)	-.6090(8)	.3974(5)	.030
C(42)	.4043(11)	-.5785(9)	.4070(5)	.034
C(43)	.4376(12)	-.6527(10)	.4761(6)	.046
C(44)	.3239(15)	-.6428(12)	.5391(6)	.059
C(45)	.1859(15)	-.6758(10)	.5305(6)	.050
C(46)	.1477(12)	-.5999(10)	.4622(5)	.039
C(51)	.0527(11)	-.5900(9)	.3078(5)	.037
C(52)	.0283(12)	-.7250(9)	.3391(6)	.044
C(53)	-.1045(13)	-.7656(11)	.3237(7)	.056
C(54)	-.2293(13)	-.6966(11)	.3489(7)	.057
C(55)	-.2081(12)	-.5623(11)	.3196(7)	.051
C(56)	-.0751(12)	-.5191(10)	.3349(6)	.044
H(1)	.10732	-.01293	.08548	.19(8)

Table 48 : Anisotropic Thermal Parameters ($\mathring{A}^2$) in the form

$$\exp\ -2\pi^2\ (U_{11}h^2a^{*2}\ldots+2U_{12}hka^*b^*\ldots)$$ for complex 34.

	U11	U22	U33	U12	U13	U23
Os(1)	.0368(3)	.0265(2)	.0291(2)	-.0010(2)	-.0067(2)	-.0068(2)
Os(2)	.0305(3)	.0365(2)	.0279(2)	-.0022(2)	-.0037(2)	-.0047(2)
Os(3)	.0283(3)	.0391(3)	.0357(2)	.0044(2)	-.0067(2)	-.0090(2)
Pt(1)	.0315(3)	.0274(2)	.0278(2)	.0009(2)	-.0106(2)	-.0067(2)
P(1)	.023(2)	.032(1)	.026(1)	-.001(1)	-.006(1)	-.007(1)
O(1)	.16(1)	.07(1)	.07(1)	.02(1)	-.08(1)	-.03(1)
O(2)	.072(8)	.109(9)	.107(8)	-.015(7)	-.036(7)	-.026(7)
O(3)	.084(8)	.038(4)	.054(5)	.000(5)	-.005(5)	-.007(4)
O(4)	.12(1)	.06(1)	.07(1)	.01(1)	.04(1)	-.02(0)
O(5)	.031(5)	.081(6)	.068(6)	.011(5)	-.006(5)	.006(5)
O(6)	.059(7)	.050(5)	.071(6)	-.012(5)	.005(5)	-.015(4)
O(7)	.084(8)	.094(7)	.042(5)	0.000(6)	-.023(5)	-.024(5)
O(8)	.071(7)	.084(7)	.066(6)	.006(6)	-.041(6)	-.024(5)
O(9)	.096(9)	.085(7)	.138(10)	.059(7)	-.068(8)	-.061(7)
O(10)	.056(7)	.110(8)	.079(7)	.008(6)	.031(6)	.029(6)
C(1)	.07(1)	.03(1)	.04(1)	.01(1)	-.03(1)	-.01(0)
C(2)	.07(1)	.04(1)	.07(1)	-.01(1)	-.04(1)	0.00(1)
C(3)	.058(9)	.036(6)	.041(6)	-.004(6)	-.006(6)	-.011(5)
C(4)	.060(9)	.033(6)	.047(7)	-.002(6)	.006(7)	-.007(5)
C(5)	.037(8)	.063(8)	.036(6)	-.012(6)	.002(6)	-.008(6)
C(6)	.026(7)	.053(7)	.055(7)	-.001(6)	-.008(6)	-.018(6)
C(7)	.028(7)	.050(7)	.044(6)	-.007(6)	-.012(5)	-.005(5)
C(8)	.043(8)	.052(7)	.040(6)	.001(6)	-.014(6)	-.010(5)
C(9)	.040(8)	.066(8)	.084(10)	.023(7)	-.028(8)	-.036(7)
C(10)	.040(8)	.066(8)	.057(8)	.012(7)	-.004(7)	.001(6)
C(11)	.009(5)	.034(5)	.043(6)	-.004(4)	-.006(5)	-.010(5)
C(12)	.032(7)	.028(5)	.035(6)	.009(5)	-.004(5)	-.005(4)
C(21)	.051(8)	.034(6)	.030(6)	-.001(6)	-.014(6)	-.002(5)
C(22)	.043(8)	.041(6)	.048(7)	.005(6)	-.004(6)	-.016(5)
C(23)	.06(1)	.06(1)	.05(1)	.01(1)	-.01(1)	-.02(1)
C(24)	.11(1)	.05(1)	.05(1)	.00(1)	-.03(1)	-.02(1)
C(25)	.07(1)	.05(1)	.09(1)	-.01(1)	-.03(1)	-.03(1)
C(26)	.051(9)	.044(7)	.051(7)	.001(6)	-.010(7)	-.018(6)
C(31)	.023(6)	.042(6)	.031(6)	-.005(5)	.003(5)	-.010(5)
C(32)	.043(8)	.035(6)	.041(6)	-.005(6)	.005(6)	-.007(5)
C(33)	.047(9)	.063(8)	.039(7)	-.005(7)	.011(6)	-.005(6)
C(34)	.030(7)	.062(8)	.049(7)	.003(6)	.008(6)	-.015(6)
C(35)	.047(9)	.059(8)	.067(9)	.009(7)	.009(7)	-.034(7)
C(36)	.029(7)	.043(6)	.056(7)	-.011(5)	.005(6)	-.022(5)
C(41)	.039(7)	.028(5)	.019(5)	-.007(5)	-.003(5)	-.003(4)
C(42)	.026(6)	.040(6)	.032(5)	-.003(5)	-.005(5)	-.001(4)
C(43)	.032(7)	.060(7)	.043(6)	.000(6)	-.021(6)	-.003(5)
C(44)	.06(1)	.08(1)	.03(1)	0.00(1)	-.02(1)	-.01(1)
C(45)	.056(9)	.052(7)	.033(6)	-.003(7)	.008(6)	-.004(5)
C(46)	.027(6)	.048(6)	.038(6)	0.000(5)	.001(5)	-.017(5)
C(51)	.020(6)	.038(6)	.048(6)	.001(5)	-.003(5)	-.013(5)
C(52)	.030(7)	.033(6)	.065(8)	-.001(5)	-.011(6)	-.022(5)
C(53)	.029(7)	.057(8)	.079(9)	-.011(6)	-.006(7)	-.028(7)
C(54)	.033(8)	.064(8)	.069(8)	-.006(7)	-.001(7)	-.025(7)
C(55)	.026(7)	.055(7)	.067(8)	.002(6)	-.006(6)	-.017(6)
C(56)	.022(6)	.044(6)	.064(8)	.009(5)	-.014(6)	-.021(6)

Table 49 : Selected Bond lengths (Å) with esd's for $Os_3Pt(\mu\text{-}H)(\mu_4\text{-}\eta^2\text{-}C{\equiv}CPh)(CO)_{10}(PCy_3)$, 34.

Os(1)	Os(2)	2.845(1)	Os(1)	Os(3)	2.824(1)
Os(1)	Pt(1)	2.712(1)	Os(1)	C(2)	1.863(15)
Os(1)	C(3)	1.883(11)	Os(1)	C(4)	1.893(12)
Os(1)	C(11)	2.146(10)	Os(2)	Os(3)	2.838(1)
Os(2)	C(5)	1.907(13)	Os(2)	C(6)	1.900(12)
Os(2)	C(7)	1.894(11)	Os(2)	C(12)	2.149(10)
Os(2)	H(1)	1.851(1)	Os(3)	C(8)	1.926(11)
Os(3)	C(9)	1.922(14)	Os(3)	C(10)	1.919(13)
Os(3)	C(11)	2.397(10)	Os(3)	C(12)	2.227(11)
Os(3)	H(1)	1.853(1)	Pt(1)	P(1)	2.328(3)
Pt(1)	C(1)	1.893(12)	Pt(1)	C(11)	2.002(10)
P(1)	C(31)	1.856(11)	P(1)	C(41)	1.838(10)
P(1)	C(51)	1.846(11)	O(1)	C(1)	1.113(15)
O(2)	C(2)	1.173(19)	O(3)	C(3)	1.154(13)
O(4)	C(4)	1.163(16)	O(5)	C(5)	1.139(16)
O(6)	C(6)	1.181(14)	O(7)	C(7)	1.134(14)
O(8)	C(8)	1.116(15)	O(9)	C(9)	1.117(17)
O(10)	C(10)	1.121(17)	C(11)	C(12)	1.335(14)
C(12)	C(21)	1.485(14)	C(21)	C(22)	1.379(17)
C(21)	C(26)	1.385(18)	C(22)	C(23)	1.359(17)
C(23)	C(24)	1.37(3)	C(24)	C(25)	1.40(3)
C(25)	C(26)	1.364(18)	C(31)	C(32)	1.529(16)
C(31)	C(36)	1.520(16)	C(32)	C(33)	1.525(17)
C(33)	C(34)	1.519(18)	C(34)	C(35)	1.481(18)
C(35)	C(36)	1.570(18)	C(41)	C(42)	1.559(16)
C(41)	C(46)	1.520(15)	C(42)	C(43)	1.529(15)
C(43)	C(44)	1.519(18)	C(44)	C(45)	1.48(2)
C(45)	C(46)	1.540(16)	C(51)	C(52)	1.526(15)
C(51)	C(56)	1.537(16)	C(52)	C(53)	1.514(17)
C(53)	C(54)	1.492(19)	C(54)	C(55)	1.509(18)
C(55)	C(56)	1.528(16)			

Table 50 : Selected Bond Angles (deg) with esd's for

$Os_3Pt(\mu\text{-}H)(\mu_4\text{-}\eta^2\text{-}C{\equiv}CPh)(CO)_{10}(PCy_3)$, **34**

Os(2) - Os(1) - Os(3)	60.1(1)	Os(2) - Os(1) - Pt(1)	101.6(1)
Os(2) - Os(1) - C(2)	96.9(5)	Os(2) - Os(1) - C(3)	82.2(4)
Os(2) - Os(1) - C(4)	164.1(5)	Os(2) - Os(1) - C(11)	60.7(3)
Os(3) - Os(1) - Pt(1)	94.6(1)	Os(3) - Os(1) - C(2)	156.3(4)
Os(3) - Os(1) - C(3)	86.8(4)	Os(3) - Os(1) - C(4)	104.2(4)
Os(3) - Os(1) - C(11)	55.7(3)	Pt(1) - Os(1) - C(2)	84.4(4)
Pt(1) - Os(1) - C(3)	176.1(4)	Pt(1) - Os(1) - C(4)	81.2(4)
Pt(1) - Os(1) - C(11)	46.9(3)	C(2) - Os(1) - C(3)	95.8(6)
C(2) - Os(1) - C(4)	99.0(6)	C(2) - Os(1) - C(11)	110.2(5)
C(3) - Os(1) - C(4)	94.9(5)	C(3) - Os(1) - C(11)	136.2(5)
C(4) - Os(1) - C(11)	114.2(5)	Os(1) - Os(2) - Os(3)	59.6(1)
Os(1) - Os(2) - C(5)	92.4(4)	Os(1) - Os(2) - C(6)	94.4(4)
Os(1) - Os(2) - C(7)	165.4(4)	Os(1) - Os(2) - C(12)	75.4(3)
Os(1) - Os(2) - H(1)	83.5(1)	Os(3) - Os(2) - C(5)	139.6(4)
Os(3) - Os(2) - C(6)	116.3(4)	Os(3) - Os(2) - C(7)	106.1(4)
Os(3) - Os(2) - C(12)	50.8(3)	Os(3) - Os(2) - H(1)	40.0(1)
C(5) - Os(2) - C(6)	92.6(5)	C(5) - Os(2) - C(7)	98.3(5)
C(5) - Os(2) - C(12)	96.8(5)	C(5) - Os(2) - H(1)	174.6(4)
C(6) - Os(2) - C(7)	94.9(5)	C(6) - Os(2) - C(12)	166.4(5)
C(6) - Os(2) - H(1)	84.3(4)	C(7) - Os(2) - C(12)	93.5(5)
C(7) - Os(2) - H(1)	86.3(4)	C(12) - Os(2) - H(1)	85.5(3)
Os(1) - Os(3) - Os(2)	60.3(1)	Os(1) - Os(3) - C(8)	162.9(4)
Os(1) - Os(3) - C(9)	92.5(4)	Os(1) - Os(3) - C(10)	99.8(4)
Os(1) - Os(3) - C(11)	47.7(3)	Os(1) - Os(3) - C(12)	74.7(3)
Os(1) - Os(3) - H(1)	84.0(1)	Os(2) - Os(3) - C(8)	102.9(4)
Os(2) - Os(3) - C(9)	113.7(4)	Os(2) - Os(3) - C(10)	149.0(4)
Os(2) - Os(3) - C(11)	58.6(3)	Os(2) - Os(3) - C(12)	48.4(3)
Os(2) - Os(3) - H(1)	40.0(1)	C(8) - Os(3) - C(9)	98.0(6)
C(8) - Os(3) - C(10)	93.9(6)	C(8) - Os(3) - C(11)	122.7(5)
C(8) - Os(3) - C(12)	91.8(5)	C(8) - Os(3) - H(1)	84.0(4)
C(9) - Os(3) - C(10)	89.0(6)	C(9) - Os(3) - C(11)	139.3(5)
C(9) - Os(3) - C(12)	161.5(5)	C(9) - Os(3) - H(1)	82.1(5)
C(10) - Os(3) - C(11)	90.4(5)	C(10) - Os(3) - C(12)	106.0(5)
C(10) - Os(3) - H(1)	170.5(4)	C(11) - Os(3) - C(12)	33.3(4)
C(11) - Os(3) - H(1)	98.5(3)	C(12) - Os(3) - H(1)	83.3(3)
Os(1) - Pt(1) - P(1)	157.8(1)	Os(1) - Pt(1) - C(1)	100.8(4)
Os(1) - Pt(1) - C(11)	51.5(3)	P(1) - Pt(1) - C(1)	101.2(4)
P(1) - Pt(1) - C(11)	106.5(3)	C(1) - Pt(1) - C(11)	152.3(5)
Pt(1) - P(1) - C(31)	111.1(4)	Pt(1) - P(1) - C(41)	114.7(4)
Pt(1) - P(1) - C(51)	113.1(4)	C(31) - P(1) - C(41)	107.1(5)
C(31) - P(1) - C(51)	104.9(5)	C(41) - P(1) - C(51)	105.3(5)
Pt(1) - C(1) - O(1)	174.4(11)	Os(1) - C(2) - O(2)	179.0(12)
Os(1) - C(3) - O(3)	176.0(10)	Os(1) - C(4) - O(4)	177.3(10)
Os(2) - C(5) - O(5)	177.3(11)	Os(2) - C(6) - O(6)	175.9(10)
Os(2) - C(7) - O(7)	179.2(11)	Os(3) - C(8) - O(8)	175.1(11)
Os(3) - C(9) - O(9)	178.0(13)	Os(3) - C(10) - O(10)	178.1(12)
Os(1) - C(11) - Os(3)	76.6(3)	Os(1) - C(11) - Pt(1)	81.6(4)
Os(1) - C(11) - C(12)	124.4(8)	Os(3) - C(11) - Pt(1)	135.2(5)
Os(3) - C(11) - C(12)	66.3(6)	Pt(1) - C(11) - C(12)	152.7(8)
Os(2) - C(12) - Os(3)	80.8(4)	Os(2) - C(12) - C(11)	93.2(7)
Os(2) - C(12) - C(21)	130.5(8)	Os(3) - C(12) - C(11)	80.4(7)
Os(3) - C(12) - C(21)	125.8(9)	C(11) - C(12) - C(21)	128.6(9)
C(12) - C(21) - C(22)	120.9(11)	C(12) - C(21) - C(26)	122.5(11)
C(22) - C(21) - C(26)	116.6(10)	C(21) - C(22) - C(23)	121.2(12)
C(22) - C(23) - C(24)	121.2(13)	C(23) - C(24) - C(25)	119.6(12)
C(24) - C(25) - C(26)	117.3(14)	C(21) - C(26) - C(25)	123.9(12)
Os(2) - H(1) - Os(3)	100.0(1)		

octahedral coordination, all other angles being within $\pm 8^{o}$ of 90^{o} or 180^{o}. Os(1) and Os(3) are seven coordinate metal centres and the geometry about these sites is irregular.

The coordination about Pt(1) is distorted square planar, with the largest deviation from the mean plane defined by Os(1), Pt(1), P(1), C(1) and C(11) being 0.036 Å for the Os(1) centre. Thus Pt(1) acts as a 16 electron metal.

If the μ_4-η^2 acetylide function is considered a 5 electron donor ligand[326] 34 has 62 valence electrons. This is consistent with a spiked triangular metal framework containing a 16 electron Pt centre (for example $Os_3Pt(\mu\text{-}H)_2(\mu_4\text{-}C)(CO)_{10}(PCy_3)$[250] and $Os_3Pt(\mu\text{-}CH_2)(CO)_{11}(PPh_3)_2$[254] are both 62 electron spiked triangular clusters).

The acetylide moiety binds to the cluster core in a twisted μ_4-η^2 fashion. The C(11)-C(12) vector makes an angle of 80^{o} with the Os(2)-Os(3) edge. Consequently the C(11)-Os(2) distance of 2.59(1) Å is 0.20 Å longer than the C(11)-Os(3) separation and can be considered non-bonding. The variation in C(12)-Os(2), Os(3) distances (2.15(1) and 2.23(1) Å respectively) is much less significant.

Details of structurally defined spiked triangular clusters containing a μ_4-η^2 acetylide function are listed in Table 51. These complexes show considerable variation in the angle between the exo metal-metal bond and the normal to the M_3 triangle (range from 7.1 - 24.8^{o}). Furthermore, the angle between the C≡C axis and the bridged M-M vector varies between 69-89.5^{o}, which suggests that the μ_4-η^2 coordination mode in these systems is a flexible one. In contrast, in clusters containing the μ_3-C≡CR functionality, perpendicular μ_3-η^2-C≡CR coordination is more common.[34-36, 178]

The C(11)-C(12) separation of 1.34(1) Å is similar to that of other μ_4-η^2 C≡CR distances (Table 51) while the Os(1)-C(11)-C(12) and

Table 51 : Some bonding parameters of μ_4-η^2-C≡CR moieties in spiked triangular clusters.*

Cluster	Å C_α-C_β	degrees M(2)-C_α-C_β	C_α-C_β-R	A	B	Ref.
34	1.34(1)	124.4(8)	128.6(9)	11.7	80	This work
36	1.332(7)	129.3(4)	131.1(5)	10.9	81.5	This work
37	1.332(8)	129.4(5)	135.2(6)	7.1	88.7	This work
$Co_2FeRu(CCPh)(Cp)(CO)_{10}$	1.37(2)	126.1(9)	129(1)	24.8	69	327
$Co_2RuW(CCPh)(Cp)(CO)_{11}$	1.30(1)	137.2(7)	135(1)		80	327
$Co_2NiRu(CCMe)(Cp)(CO)_8(PPh_3)$	1.33(1)	140.7	141.4	10.1	87	328
$CoMo_2Ru(CCMe)(Cp)_2(CO)_9$	1.335(6)	129.5	132.1		73	328
$Fe_2Ni_2(\mu\text{-}PPh_2)(CCPh)(Cp)_2(CO)_5$	1.313(8)	141.7	136.6		89.5	326
Average	1.33	132.3	133.6			

A - angle between M(1)-M(2) bond and normal to M_3 triangle

B - angle between C≡C and M(3)-M(4)

*Parameters refer to

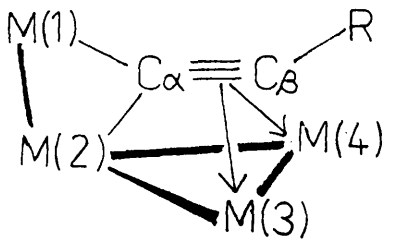

C(11)-C(12)-C(21) angles of 124.4(8)° and 128.6(9)° are slightly more acute than corresponding angles in other systems quoted in Table 51.

The PtL_2 fragment is isolobal with CH_2,[108] thus the $Pt(L)_2CCPh$ unit may be regarded as a μ_3-η^3 platina-allenyl function. Interestingly, in the complexes $Ru_3(\mu\text{-}H)[\mu_3\text{-}\eta^3\text{-}CH(Me)=C=C(Et)](CO)_9$,[334] 41, and $Ru_3(\mu\text{-}PPh_2)[\mu_3\text{-}\eta^3\text{-}CH_2=C=C(i\text{-}Pr)](L)(CO)_7$, (L=CO, 42, μ-CH_2, 43),[276] which contain μ_3-η^3 allenyl moieties, the central carbon atom is bound to only two metal centres. Similarly, in 34, C(11) binds only to the Os(1) and Os(3) sites of the Os_3 triangle. Moreover, consistent with this analogy, the Pt(1)-C(11) distance of 2.00(1)Å is similar to reported Pt-carbene separations,[375] and the C(11)-C(12) separation (1.34(1) Å) resembles the corresponding bond lengths in 42 and 43 (1.352(8), 1.340(9) Å respectively).[276] The Pt-C(11)-C(12) angle (152.7(8)°) is somewhat larger than the $R_2\underline{C}=\underline{C}=\underline{C}H$ angles in 41 — 43 (142.3-146.8°).[276,334] The bonding mode of the "platina-allenyl" fragment to the Os_3 framework is shown in Figure 84.

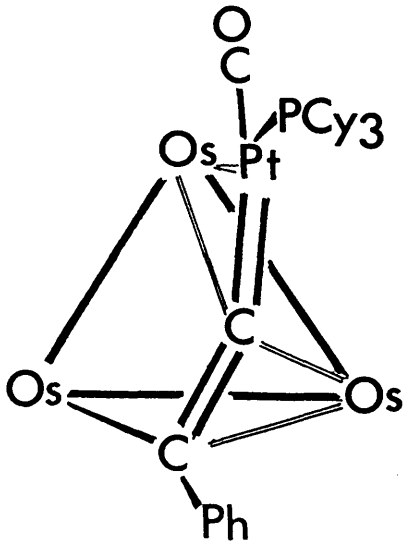

Figure 84 : Platina-allenyl unit bonding to Os_3 core in 34.

The carbonyl ligands in 34 are essentially linear with M-C-O varying between 174(1)-179(1)°, mean = 177°. The Os-CO distances range from 1.863(15) - 1.926(11) Å with an average of 1.900 Å while the Pt-CO separation is 1.893(11) Å. C-O separations vary between 1.113(15)-1.181(14) Å, mean = 1.114 Å. These M-CO and C-O distances are similar to those reported for other Os_3Pt cluster systems.[147,148,250,255]

The coordination about P(1) is approximately tetrahedral with angles ranging between 104.9(5)-114.7(3)°. The bond lengths and angles between the carbon atoms of the phenyl (1.36(2)-1.40(2) Å; 117(1)-124(1)°) and cyclohexyl (1.48(2)-1.57(2) Å; 110(1)-112(1)°) rings are within the normal ranges for aromatic and alkyl functions respectively.

4(ii) The molecular structure of $Ru_3Pt(\mu\text{-}H)(\mu_4\text{-}\eta^2\text{-}C{\equiv}Ct\text{-}Bu)(cod)(CO)_9$, 36

Dark orange/brown crystals of 36 were grown from petroleum ether (40°-60°) at -20°C. Experimental details of data collection and structure refinement are given in Table 52. Systematic absences ($h0l$, $h+l$ = 2n+1; $0k0$, = 2n+1) uniquely determined the space group $P2_1/n$. The hydride and olefinic hydrogen locations were determined from difference Fourier maps.

Refinement converged at R = 0.023 (R_w = 0.030). In the final cycle of refinement the largest (Δ/σ) = 0.11, while the mean (Δ/σ) = 0.02. The final difference map was essentially featureless with the largest remaining peaks and troughs adjacent to the metal centres.

The molecular structure of 36 and the atomic labelling scheme employed are depicted in Figure 85. Atomic coordinates, anisotropic temperature factors, bond lengths and angles are given in Tables 53,54, 55 and 56 respectively. The metal framework of 36 has a spiked triangular geometry, with a Pt centre bonded to the Ru(2) site (Pt-Ru(2)= 2.645(1) Å)of an essentially equilateral Ru_3 triangle (Ru-Ru separations

Table 52 : Experimental data for Crystallographic Analysis of $Ru_3Pt(\mu\text{-}H)(\mu_4\text{-}\eta^2\text{-}C{\equiv}Ct\text{-}Bu)(cod)(CO)_9$

Compd. formula	$C_{23}H_{22}O_9Ru_3Pt$
Mr.	940.72
space group	$P2_1/n$ (No. 14,
cryst. system	monoclinic
a/Å	11.283(3)
b/Å	17.843(2)
c/Å	13.625(3)
α/deg	
β/deg	94.06(2)
γ/deg	
V/Å^{-3}	2736(1)
Z	4
D_{calcd}/g cm^{-3}	2.28
F(000)	1768
μ(Mo-Kα), cm^{-1}	67.9
θ range/deg	$2 \leqslant \theta \leqslant 25$
cryst. size mm	0.3 x 0.3 x 0.2
range of trans coeff corr.	0.86/1.20
no. of data collected	5259
no. of unique data	4813
std reflections	$\bar{5}53$, $\bar{1}\bar{8}\bar{5}$, $2\bar{9}4$
observability criterion	
$I \geqslant n\sigma(I)$	3.0
no. of data in refinement	3815
final *R*	0.023
R_w	0.030
largest remaining feature in elec. density map eÅ^{-3}	+0.85(max), -0.73(min)
shift/esd in last cycle	0.11(max) 0.02(av.)

Figure 85 : The molecular structure of $Ru_3Pt(\mu\text{-}H)(\mu_4\text{-}\eta^2\text{-}C{\equiv}Ct\text{-}Bu)(cod)(CO)_9$, 36.

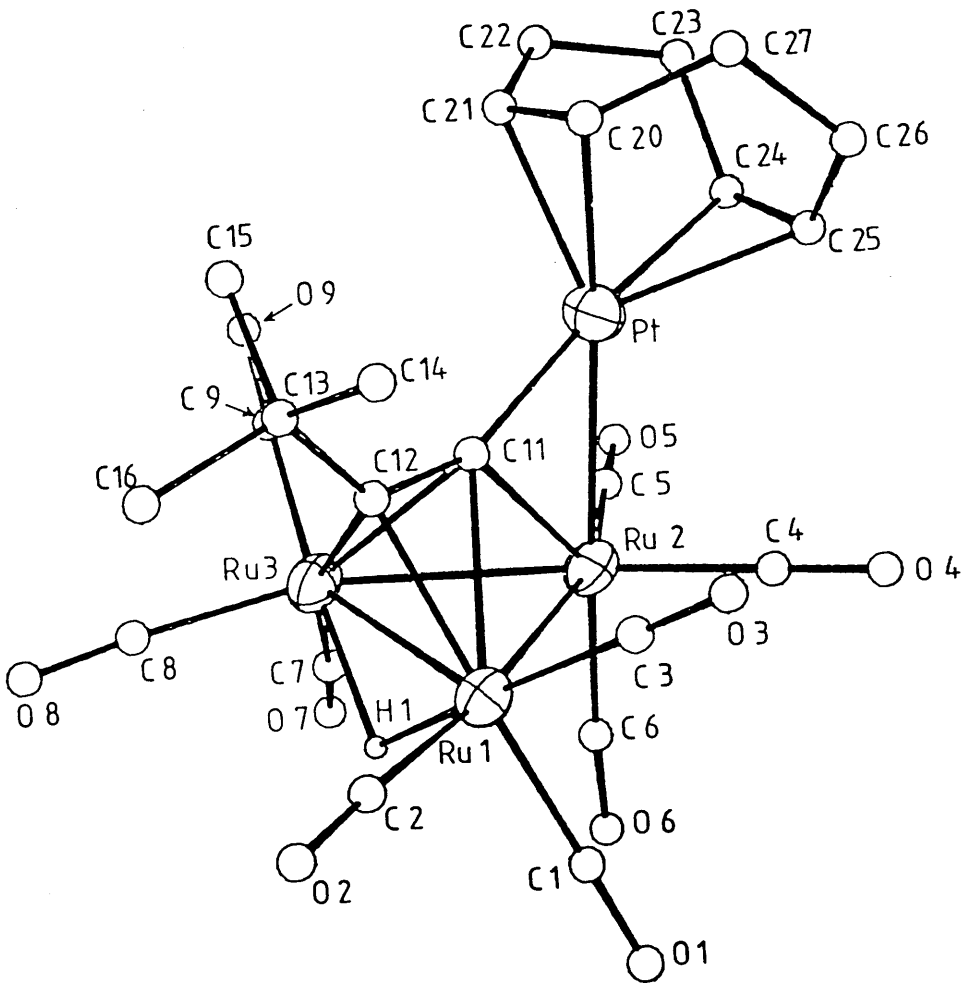

Table 53 : Final positional parameters (fractional coordinate) and isotropic thermal parameters ($\AA^2$) with their esd's for $Ru_3Pt(\mu\text{-}H)(\mu_4\text{-}\eta^2\text{-}C{\equiv}Ct\text{-}Bu)(cod)(CO)_9$, 36

$$U = {}^1/3 \ \Sigma_i\Sigma_j U_{ij} a_i^* a_j^* a_i.a_j.$$

	X/A	Y/B	Z/C	U
Pt	.04155(2)	.13782(1)	-.22039(2)	.038
Ru(1)	.37146(4)	.19974(2)	.68362(3)	.036
Ru(2)	.24216(4)	.19933(2)	.85247(3)	.035
Ru(3)	.37037(4)	.07216(2)	.80512(3)	.035
O(1)	.5093(6)	.3391(3)	.7578(4)	.089
O(2)	.5369(4)	.1757(3)	.5191(4)	.076
O(3)	.1912(5)	.2932(3)	-.4380(4)	.083
O(4)	-.1166(5)	-.3455(3)	.1975(4)	.083
O(5)	-.1339(5)	-.1551(3)	-.0415(3)	.080
O(6)	.4534(5)	.2724(3)	-.0321(4)	.088
O(7)	.4919(6)	.0896(3)	1.0115(4)	.095
O(8)	.5608(4)	-.0332(3)	.7363(4)	.085
O(9)	.2074(5)	-.0486(3)	.8734(4)	.084
C(1)	.4572(6)	.2879(4)	.7334(5)	.056
C(2)	.4733(5)	.1831(3)	.5806(5)	.051
C(3)	.2589(5)	.2593(3)	-.3931(4)	.050
C(4)	-.1630(6)	-.2910(4)	.1757(5)	.055
C(5)	-.1719(6)	-.1712(3)	.0307(4)	.051
C(6)	.3775(6)	.2429(3)	-.0786(5)	.055
C(7)	.4452(6)	.0854(3)	.9349(5)	.060
C(8)	.4860(6)	.0048(3)	.7595(5)	.053
C(9)	.2703(6)	-.0033(4)	.8487(4)	.050
C(11)	-.2997(4)	-.6233(3)	.2313(3)	.032
C(12)	-.2291(4)	-.5976(3)	.1645(4)	.035
C(13)	-.2563(5)	-.5483(3)	.0721(4)	.040
C(14)	-.3224(7)	-.5959(4)	-.0073(4)	.067
C(15)	-.3337(6)	-.4820(3)	.0967(5)	.056
C(16)	-.1432(6)	-.5152(4)	.0329(5)	.059
C(20)	.0964(5)	-.0953(4)	.3287(5)	.058
C(21)	.0756(6)	-.0408(4)	.2597(5)	.066
C(22)	.1495(7)	-.0259(5)	.1735(7)	.094
C(23)	.2011(7)	-.0930(6)	.1284(6)	.099
C(24)	.1162(6)	-.1586(6)	.1191(6)	.083
C(25)	.1159(6)	-.2143(5)	.1850(7)	.077
C(26)	.1901(7)	-.2178(5)	.2831(8)	.097
C(27)	.2043(7)	-.1446(5)	.3377(5)	.075
H(1)	.457(5)	.158(3)	-.233(4)	.04(1)

Table 54 : Anisotropic Thermal Parameters ($\AA^2$) in the form

$$\exp\ -2\pi^2(U_{11}h^2a^{*2}\ldots+2U_{12}hka^*b^*\ldots)$$ for complex 36.

	U11	U22	U33	U12	U13	U23
Pt	.0328(1)	.0452(1)	.0354(1)	-.0006(1)	.0037(1)	-.0099(1)
Ru(1)	.0365(2)	.0279(2)	.0433(2)	-.0006(2)	.0046(2)	.0031(2)
Ru(2)	.0394(2)	.0283(2)	.0368(2)	-.0027(2)	.0017(2)	-.0073(2)
Ru(3)	.0400(2)	.0265(2)	.0388(2)	.0013(2)	-.0058(2)	.0012(2)
O(1)	.105(4)	.058(3)	.105(4)	-.041(3)	.016(4)	-.020(3)
O(2)	.073(3)	.076(3)	.080(3)	-.001(3)	.037(3)	.008(3)
O(3)	.077(3)	.064(3)	.106(4)	.020(3)	-.014(3)	.030(3)
O(4)	.095(4)	.037(3)	.117(4)	.022(3)	.011(3)	.008(3)
O(5)	.103(4)	.094(4)	.045(3)	-.008(3)	.022(3)	.004(3)
O(6)	.076(3)	.092(4)	.094(4)	-.028(3)	-.022(3)	-.025(3)
O(7)	.144(5)	.070(4)	.064(3)	-.005(4)	-.058(3)	0.000(3)
O(8)	.059(3)	.067(3)	.130(5)	.015(3)	.003(3)	-.018(3)
O(9)	.093(4)	.067(3)	.092(4)	-.028(3)	.001(3)	.034(3)
C(1)	.059(4)	.041(4)	.070(4)	-.006(3)	.015(3)	.001(3)
C(2)	.049(3)	.044(3)	.061(4)	-.003(3)	.010(3)	.009(3)
C(3)	.053(4)	.038(3)	.059(4)	0.000(3)	.008(3)	.010(3)
C(4)	.057(4)	.046(4)	.063(4)	-.004(3)	.007(3)	-.007(3)
C(5)	.062(4)	.044(3)	.047(4)	-.002(3)	.007(3)	-.012(3)
C(6)	.061(4)	.045(4)	.058(4)	-.007(3)	-.005(3)	-.012(3)
C(7)	.073(4)	.042(4)	.063(4)	.000(3)	-.012(4)	.004(3)
C(8)	.049(4)	.040(3)	.069(4)	.002(3)	-.011(3)	.003(3)
C(9)	.060(4)	.046(4)	.043(3)	.002(3)	-.005(3)	.008(3)
C(11)	.041(3)	.022(2)	.031(2)	.002(2)	-.005(2)	.003(2)
C(12)	.032(3)	.031(3)	.040(3)	-.004(2)	.001(2)	-.003(2)
C(13)	.042(3)	.042(3)	.037(3)	-.004(3)	.002(2)	.011(2)
C(14)	.087(5)	.072(5)	.042(3)	-.017(4)	-.010(3)	.011(3)
C(15)	.058(4)	.049(4)	.062(4)	.008(3)	.008(3)	.024(3)
C(16)	.060(4)	.059(4)	.059(4)	-.001(3)	.017(3)	.023(3)
C(20)	.037(3)	.079(5)	.056(4)	-.005(3)	-.009(3)	-.023(4)
C(21)	.046(4)	.073(5)	.078(5)	-.017(4)	-.003(3)	-.023(4)
C(22)	.053(4)	.102(7)	.126(8)	-.031(5)	.004(5)	.029(6)
C(23)	.076(6)	.144(9)	.078(5)	-.021(6)	.035(5)	-.009(6)
C(24)	.044(4)	.150(8)	.057(4)	-.011(5)	.019(3)	-.041(5)
C(25)	.051(4)	.086(6)	.094(6)	.017(4)	.019(4)	-.037(5)
C(26)	.061(5)	.090(6)	.138(8)	.024(5)	-.003(5)	.006(6)
C(27)	.054(4)	.104(7)	.067(5)	.002(4)	-.006(4)	-.003(4)

Table 55 : Selected Bond Lengths (Å) with esd's for

$Ru_3Pt(\mu\text{-}H)(\mu_4\text{-}\eta^2\text{-}C{\equiv}Ct\text{-}Bu)(cod)(CO)_9$, 36

Pt - Ru(2)	2.645(1)	Pt - C(11)	1.969(6)
Pt - C(20)	2.202(7)	Pt - C(21)	2.221(8)
Pt - C(24)	2.358(8)	Pt - C(25)	2.317(8)
Ru(1) - Ru(2)	2.810(1)	Ru(1) - Ru(3)	2.815(1)
Ru(1) - C(1)	1.943(7)	Ru(1) - C(2)	1.899(7)
Ru(1) - C(3)	1.910(7)	Ru(1) - C(11)	2.488(5)
Ru(1) - C(12)	2.154(6)	Ru(1) - H(1)	1.62(6)
Ru(2) - Ru(3)	2.791(1)	Ru(2) - C(4)	1.890(7)
Ru(2) - C(5)	1.895(7)	Ru(2) - C(6)	1.902(7)
Ru(2) - C(11)	2.164(5)	Ru(3) - C(7)	1.920(7)
Ru(3) - C(8)	1.911(7)	Ru(3) - C(9)	1.881(7)
Ru(3) - C(11)	2.291(5)	Ru(3) - C(12)	2.198(5)
Ru(3) - H(1)	1.91(6)	O(1) - C(1)	1.124(9)
O(2) - C(2)	1.149(8)	O(3) - C(3)	1.121(9)
O(4) - C(4)	1.134(9)	O(5) - C(5)	1.139(8)
O(6) - C(6)	1.154(9)	O(7) - C(7)	1.138(9)
O(8) - C(8)	1.143(9)	O(9) - C(9)	1.142(9)
C(11) - C(12)	1.332(7)	C(12) - C(13)	1.548(8)
C(13) - C(14)	1.528(9)	C(13) - C(15)	1.522(9)
C(13) - C(16)	1.536(9)	C(20) - C(21)	1.361(11)
C(20) - C(27)	1.500(11)	C(21) - C(22)	1.512(12)
C(22) - C(23)	1.484(14)	C(23) - C(24)	1.512(14)
C(24) - C(25)	1.340(13)	C(25) - C(26)	1.527(13)
C(26) - C(27)	1.506(13)		

Table 56 : Selected Bond Angles (deg) with esd's for

$Ru_3Pt(\mu\text{-}H)(\mu_4\text{-}\eta^2\text{-}C{\equiv}Ct\text{-}Bu)(cod)(CO)_9$, 36

Ru(2)	- Pt -	C(11)	53.5(2)	Ru(2)	- Pt -	C(20)	160.0(2)
Ru(2)	- Pt -	C(21)	153.3(2)	Ru(2)	- Pt -	C(24)	112.1(3)
Ru(2)	- Pt -	C(25)	109.0(3)	C(11)	- Pt -	C(20)	110.3(3)
C(11)	- Pt -	C(21)	110.9(3)	C(11)	- Pt -	C(24)	163.5(3)
C(11)	- Pt -	C(25)	151.2(3)	C(20)	- Pt -	C(21)	35.8(3)
C(20)	- Pt -	C(24)	85.4(3)	C(20)	- Pt -	C(25)	80.0(3)
C(21)	- Pt -	C(24)	78.6(4)	C(21)	- Pt -	C(25)	93.3(3)
C(24)	- Pt -	C(25)	33.3(4)	Ru(2)	- Ru(1) -	Ru(3)	59.5(1)
Ru(2)	- Ru(1) -	C(1)	89.5(2)	Ru(2)	- Ru(1) -	C(2)	168.8(2)
Ru(2)	- Ru(1) -	C(3)	94.9(2)	Ru(2)	- Ru(1) -	C(11)	47.7(2)
Ru(2)	- Ru(1) -	C(12)	78.3(2)	Ru(2)	- Ru(1) -	H(1)	74.9(19)
Ru(3)	- Ru(1) -	C(1)	118.2(2)	Ru(3)	- Ru(1) -	C(2)	109.7(2)
Ru(3)	- Ru(1) -	C(3)	137.9(2)	Ru(3)	- Ru(1) -	C(11)	50.7(2)
Ru(3)	- Ru(1) -	C(12)	50.4(2)	Ru(3)	- Ru(1) -	H(1)	40.7(19)
C(1)	- Ru(1) -	C(2)	94.1(3)	C(1)	- Ru(1) -	C(3)	92.0(3)
C(1)	- Ru(1) -	C(11)	136.8(3)	C(1)	- Ru(1) -	C(12)	166.5(3)
C(1)	- Ru(1) -	H(1)	82.5(19)	C(2)	- Ru(1) -	C(3)	95.5(3)
C(2)	- Ru(1) -	C(11)	128.9(3)	C(2)	- Ru(1) -	C(12)	96.9(3)
C(2)	- Ru(1) -	H(1)	95.1(19)	C(3)	- Ru(1) -	C(11)	87.1(3)
C(3)	- Ru(1) -	C(12)	94.6(3)	C(3)	- Ru(1) -	H(1)	168.4(19)
C(11)	- Ru(1) -	C(12)	32.3(2)	C(11)	- Ru(1) -	H(1)	89.9(19)
C(12)	- Ru(1) -	H(1)	88.7(19)	Pt	- Ru(2) -	Ru(1)	100.0(1)
Pt	- Ru(2) -	Ru(3)	91.1(1)	Pt	- Ru(2) -	C(4)	84.4(2)
Pt	- Ru(2) -	C(5)	78.9(2)	Pt	- Ru(2) -	C(6)	172.4(2)
Pt	- Ru(2) -	C(11)	47.1(2)	Ru(1)	- Ru(2) -	Ru(3)	60.3(1)
Ru(1)	- Ru(2) -	C(4)	95.5(2)	Ru(1)	- Ru(2) -	C(5)	163.8(2)
Ru(1)	- Ru(2) -	C(6)	87.6(2)	Ru(1)	- Ru(2) -	C(11)	58.3(2)
Ru(3)	- Ru(2) -	C(4)	154.4(2)	Ru(3)	- Ru(2) -	C(5)	103.5(2)
Ru(3)	- Ru(2) -	C(6)	92.0(2)	Ru(3)	- Ru(2) -	C(11)	53.3(2)
C(4)	- Ru(2) -	C(5)	100.4(3)	C(4)	- Ru(2) -	C(6)	95.6(3)
C(4)	- Ru(2) -	C(11)	108.3(3)	C(5)	- Ru(2) -	C(6)	93.6(3)
C(5)	- Ru(2) -	C(11)	113.2(3)	C(6)	- Ru(2) -	C(11)	139.3(3)
Ru(1)	- Ru(3) -	Ru(2)	60.2(1)	Ru(1)	- Ru(3) -	C(7)	115.0(2)
Ru(1)	- Ru(3) -	C(8)	106.6(2)	Ru(1)	- Ru(3) -	C(9)	142.4(2)
Ru(1)	- Ru(3) -	C(11)	57.2(2)	Ru(1)	- Ru(3) -	C(12)	49.0(2)
Ru(1)	- Ru(3) -	H(1)	33.6(16)	Ru(2)	- Ru(3) -	C(7)	83.6(2)
Ru(2)	- Ru(3) -	C(8)	164.6(2)	Ru(2)	- Ru(3) -	C(9)	100.2(2)
Ru(2)	- Ru(3) -	C(11)	49.2(2)	Ru(2)	- Ru(3) -	C(12)	78.0(2)
Ru(2)	- Ru(3) -	H(1)	72.0(16)	C(7)	- Ru(3) -	C(8)	96.4(3)
C(7)	- Ru(3) -	C(9)	91.8(3)	C(7)	- Ru(3) -	C(11)	131.0(3)
C(7)	- Ru(3) -	C(12)	160.4(3)	C(7)	- Ru(3) -	H(1)	87.2(16)
C(8)	- Ru(3) -	C(9)	95.2(3)	C(8)	- Ru(3) -	C(11)	132.6(3)
C(8)	- Ru(3) -	C(12)	99.5(3)	C(8)	- Ru(3) -	H(1)	92.6(17)
C(9)	- Ru(3) -	C(11)	85.5(3)	C(9)	- Ru(3) -	C(12)	98.2(3)
C(9)	- Ru(3) -	H(1)	172.2(17)	C(11)	- Ru(3) -	C(12)	34.4(2)
C(11)	- Ru(3) -	H(1)	89.3(16)	C(12)	- Ru(3) -	H(1)	80.6(16)
Ru(1)	- C(1) -	O(1)	176.5(7)	Ru(1)	- C(2) -	O(2)	177.4(6)
Ru(1)	- C(3) -	O(3)	178.6(6)	Ru(2)	- C(4) -	O(4)	176.5(7)
Ru(2)	- C(5) -	O(5)	177.2(6)	Ru(2)	- C(6) -	O(6)	174.5(6)
Ru(3)	- C(7) -	O(7)	176.4(6)	Ru(3)	- C(8) -	O(8)	175.4(6)
Ru(3)	- C(9) -	O(9)	178.2(6)	Pt	- C(11) -	Ru(1)	139.1(3)
Pt	- C(11) -	Ru(2)	79.4(2)	Pt	- C(11) -	Ru(3)	131.2(3)
Pt	- C(11) -	C(12)	151.1(4)	Ru(1)	- C(11) -	Ru(2)	74.0(2)
Ru(1)	- C(11) -	Ru(3)	72.0(2)	Ru(1)	- C(11) -	C(12)	59.9(3)
Ru(2)	- C(11) -	Ru(3)	77.5(2)	Ru(2)	- C(11) -	C(12)	129.0(4)
Ru(3)	- C(11) -	C(12)	69.0(3)	Ru(1)	- C(12) -	Ru(3)	80.6(2)
Ru(1)	- C(12) -	C(11)	87.8(4)	Ru(1)	- C(12) -	C(13)	130.7(4)
Ru(3)	- C(12) -	C(11)	76.6(4)	Ru(3)	- C(12) -	C(13)	130.6(4)
C(11)	- C(12) -	C(13)	131.1(5)	Pt	- C(20) -	C(21)	72.8(4)
Pt	- C(20) -	C(27)	112.6(5)	C(21)	- C(20) -	C(27)	125.1(6)
Pt	- C(21) -	C(20)	71.3(5)	Pt	- C(21) -	C(22)	107.6(6)
C(20)	- C(21) -	C(22)	125.8(7)	Pt	- C(24) -	C(23)	109.2(6)
Pt	- C(24) -	C(25)	71.7(5)	C(23)	- C(24) -	C(25)	123.3(8)
Pt	- C(25) -	C(24)	75.0(5)	Pt	- C(25) -	C(26)	102.8(6)
C(24)	- C(25) -	C(26)	126.1(8)	Ru(1)	- H(1) -	Ru(3)	105.7(28)

vary between 2.791(1)-2.815(1) Å). The Pt-Ru(1), Ru(3) distances (4.180(1) and 3.883(1) Å respectively) are clearly non-bonding. The Pt-Ru(2) vector makes an angle of 10.9° with the normal to the Ru triangle. Hence the Pt atom can be considered to be pseudo-axially ligated to Ru(2). The Pt-Ru separation compares well with that observed in the related complex 37 (2.681(1) Å). These are somewhat shorter than previously reported Ru-Pt distances (range 2.707-2.858 Å), [335,336,345] though comparisons are complicated by the variety of ligands that span these bonds.

The overall cluster geometry of 36 resembles that of the spiked triangular $M_3Pt(\mu_4\text{-}\eta^2\text{-}C{\equiv}CR)$ complexes 34 (M = Os, R = Ph), and 37 (M = Ru, R = t-Bu).

The directly observed hydride ligand spans the Ru(1)-Ru(3) edge, this position being consistent with the HYDEX[271] calculated hydride location. The hydride bridged Ru(1)-Ru(3) vector (2.815(1) Å) is only slightly longer than the other Ru-Ru separations (2.810(1) and 2.791(1) Å). A similar situation is observed in complexes 34, and 37.

Assuming the $\mu_4\text{-}\eta^2\text{-}C{\equiv}Ct\text{-}Bu$ moiety to be a 5 electron donor, 36 has a 62 valence electron count, which is consistent with a spiked triangular metal framework incorporating a 16 electron Pt centre.[250,254]

The coordination of the $\mu_4\text{-}\eta^2\text{-}C{\equiv}Ct\text{-}Bu$ moiety to the cluster framework is similar to that observed in 34 (see Section 4(i)). The C≡C axis is inclined at an angle of 81.5° to the Ru(1)-Ru(3) edge and, consequently, the Ru(3)-C(11) vector (2.291(5) Å) is significantly shorter than the Ru(1)-C(11) distance (2.488(5) Å). The difference in the Ru(1)-C(12) (2.154(6) Å) and Ru(3)-C(12) (2.198(5) Å) separations is much less pronounced. A similar acetylide twist is observed in 34, and it has been suggested (section 4(i)) that the $Pt(L)_2CCR$ fragment

can be regarded as a platina-allenyl unit coordinated to an Os_3 core. However, the μ_4-η^2-C≡CR coordination in the dppe substituted analogue of 36, complex 37, is near perpendicular (angle between C≡C axis and bridged Ru-Ru bond = 88.7°) which suggests that the platina-allenyl analogy may not be relevant and other factors e.g. crystal packing forces may influence the solid state geometries of these clusters. In support of this, ^{13}C n.m.r data for 36 imply that the molecule has mirror symmetry even at low temperature, which suggests that the twist deformation observed in the solid-state may not persist in solution.

The Ru-C_α distances in 36 are greater than corresponding separations reported for $Ru_3(\mu_3$-η^2C≡CR) systems, while Ru-C_β separations are rather similar (see ref. 276). The C_α atom is thus displaced towards the Pt centre in 36 resulting in a relatively short Pt-C(11) distance of 1.969(6) Å. A similar effect is observed in 34 and 37 (corresponding Pt-C_α separations : 2.00(1) and 1.985(6) Å respectively).

The C_α-C_β distance in 36 (1.332(7) Å) is similar to that observed in other μ_4-η^2-C≡CR systems (see Table 51). In keeping with observations by Carty and coworkers,[276] these separations are slightly greater than the C_α-C_β distances in μ_3-η^2-C≡CR complexes. The Ru(2)-C(11)-C(12) and C(11)-C(12)-C(13) bend back angles in 36 (129.0(4)° and 131.1(5)° respectively) are more acute than those observed in μ_3-acetylide complexes.[276] These factors suggest the perturbation of acetylide carbon atoms towards sp^2 character is more pronounced in μ_4 than μ_3 acetylides.

The cod ligand is asymmetrically bonded to the Pt centre, with the exo Pt-C (olefin) distances (2.358(8), 2.317(8) Å) being greater than the Pt-C (olefin) separations endo to the cluster (2.202(7), 2.221(8) Å). Similar asymmetry is observed in the Pt-P

bond lengths in 37 (endo Pt-P = 2.267(2) Å; exo Pt-P = 2.304(2) Å). This effect may be attributed to the differing trans influences of the Pt-Ru and Pt-C_α bonds.

The Ru-CO bond lengths (range : 1.881(7) - 1.943(7) Å, mean : 1.906 Å), C-O distances (range : 1.121(8)-1.154(8) Å, mean : 1.138 Å) and Ru-C-O angles(range:174.5(6)-178.6(6)°, mean : 176.7°) fall within expected ranges for terminal carbonyl moieties.

4(iii) Molecular Structure of $[Ru_3Pt(\mu\text{-}H)(\mu_4\text{-}\eta^2\text{-}C{=}C(H)t\text{-}Bu)(dppe)(CO)_9]^+ BF_4^-$, 39.

Orange prisms of $[Ru_3Pt(\mu\text{-}H)(\mu_4\text{-}\eta^2\text{-}C{=}C(H)t\text{-}Bu)(dppe)(CO)_9]^+ BF_4^-$ were grown from a 1:1 mixture of CH_2Cl_2/Et_2O at ambient temperature. Experimental details of data collection and refinement are given in Table 57. Complex 39 crystallises in a triclinic unit cell, and consideration of the distribution of normalised structure factors favoured the centrosymmetric space group $P\bar{1}$. This was confirmed by successful solution and refinement of the structure.

The carbon atoms of the phenyl rings were constrained as rigid, planar hexagons (C-C = 1.395 Å) and refined with isotropic thermal parameters. The hydride and vinylidene proton locations were derived from electron density difference maps. Refinement converged at R = 0.035, R_w = 0.044. The final electron density difference map shows residual electron density close to the BF_4^- anion and the phenyl groups in addition to the metal centres.

The structure of the cation $[Ru_3Pt(\mu\text{-}H)(\mu_4\text{-}\eta^2\text{-}C{=}C(H)t\text{-}Bu)(dppe)(CO)_9]^+$ is shown in Figure 86 along with the atomic labelling scheme employed. Atomic coordinates, anisotropic temperature factors, bond lengths and angles are given in Tables 58,59, 60 and 61 respectively.

The metal core of 39 has a butterfly geometry with the Pt

Table 57 : Experimental Data for Crystallographic Analysis of $[Ru_3Pt(\mu\text{-}H)(\mu_4\text{-}\eta^2\text{-}C{=}C(H)t\text{-}Bu)(dppe)(CO)_9]^+BF_4^-$

Compd. formula	$C_{41}H_{35}BF_4O_9P_2PtRu_3$
M_r.	1318.8
space group	$P\bar{1}$ (No.2, C_i^1)
cryst. system	triclinic
a/Å	10.189(4)
b/Å	14.329(4)
c/Å	15.596(9)
α/deg	97.70(4)
β/deg	94.72(4)
γ/deg	98.75(3)
V/Å^{-3}	2218(2)
Z	2
D_{calc}/g cm^{-3}	1.97
F(000)	1268
μ(Mo-K_α), cm^{-1}	43.0
θ range/deg	$2 \leq \theta \leq 25$
cryst. size mm	0.33 x 0.4 x 0.5
range of trans coeff corr.	0.85-1.33
no. of data collected	8253
no. of unique data	7786
standard reflections	$\bar{5}\bar{2}1$, $2\bar{7}\bar{3}$, $\bar{5}21$
observability criterion, $I \geq n\sigma(I)$	3.0
no. of data in refinement	6293
no. of refined parameters	301/337
final R	0.035
R_w	0.044
largest remaining feature in elec. density map, eÅ^{-3}	+1.32(max) -1.25(min)
shift/esd in last cycle	0.11(max) 0.02(av)

Figure 86 : The structure of the cation $[Ru_3Pt(\mu\text{-}H)(\mu_4\text{-}\eta^2\text{-}C{=}C(H)t\text{-}Bu)(dppe)(CO)_9]^+$

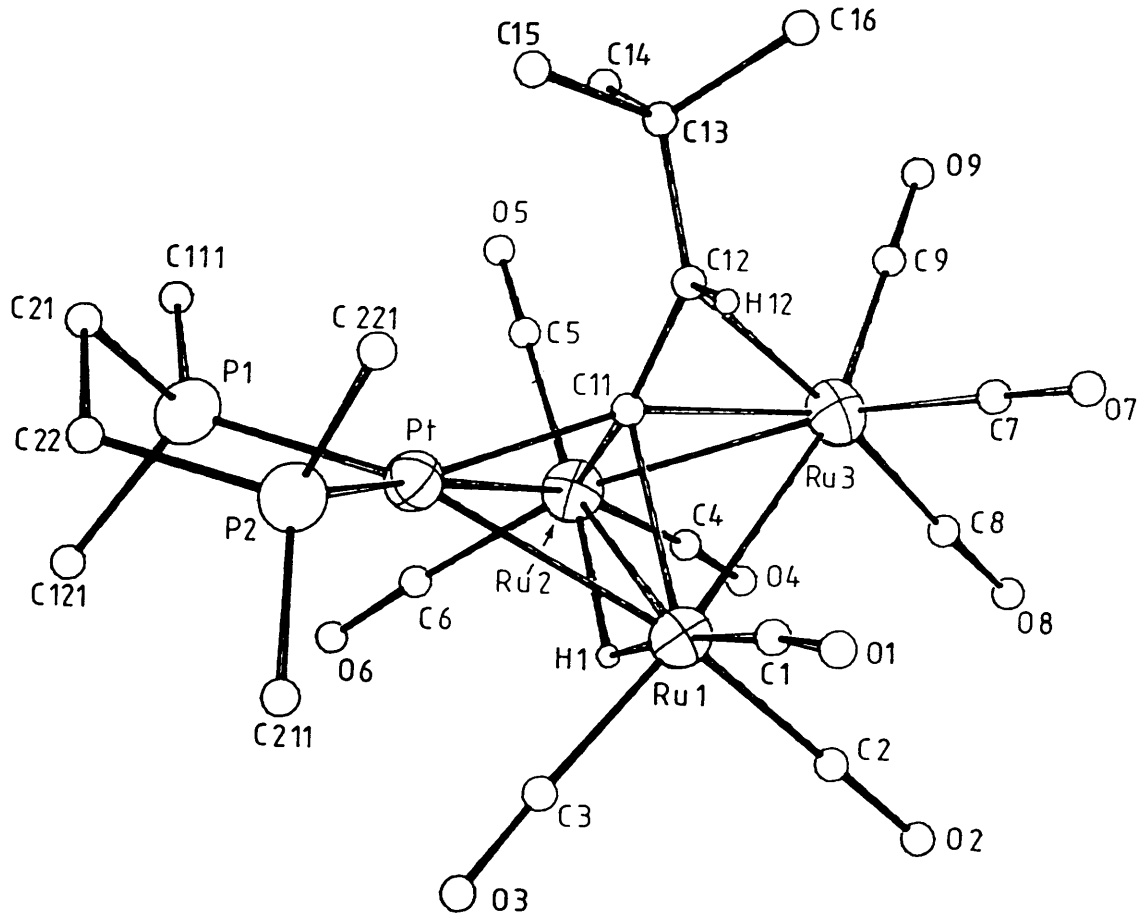

Table 58 : Final positional parameters (fractional coordinate) and isotropic thermal parameters ($\AA^2$) with their esd's for $[Ru_3Pt(\mu\text{-}H)(\mu_4\text{-}\eta^2\text{-}C{=}C(H)t\text{-}Bu)(dppe)(CO)_9]^+BF_4^-$, 39

$U = {}^1/3\ \Sigma_i\Sigma_j U_{ij} a_i^* a_j^* a_i . a_j .$

	X/A	Y/B	Z/C	U
Pt	.86414(3)	.23767(2)	.25959(2)	.032
Ru(1)	.98509(5)	.07541(4)	.24844(3)	.036
Ru(2)	.79242(6)	.09807(4)	.11428(3)	.037
Ru(3)	.74911(6)	-.05436(4)	.21215(4)	.041
B	.4505(14)	.3520(8)	.7475(7)	.075
F(1)	.4726(7)	.2725(4)	.7020(5)	.123
F(2)	.3610(7)	.3325(5)	.8048(5)	.131
F(3)	.4347(11)	.4146(6)	.6995(5)	.183
F(4)	.5669(11)	.3924(9)	.7968(6)	.229
P(1)	.79403(18)	.36982(12)	.21934(11)	.040
P(2)	.94655(17)	.33657(11)	.38617(11)	.036
C(1)	1.0288(8)	.0550(6)	.3643(5)	.060
C(2)	1.0758(8)	-.0265(5)	.2061(5)	.055
C(3)	1.1336(7)	.1749(5)	.2508(5)	.056
C(4)	.7947(8)	-.0036(6)	.0215(5)	.055
C(5)	.6151(9)	.1096(6)	.0734(5)	.057
C(6)	.8631(9)	.1973(5)	.0504(5)	.060
C(7)	.7759(9)	-.1216(5)	.3083(6)	.065
C(8)	.8175(8)	-.1470(5)	.1355(6)	.061
C(9)	.5725(9)	-.1187(5)	.1712(5)	.058
C(11)	.7790(6)	.0936(4)	.2481(4)	.033
C(12)	.6898(7)	.0638(4)	.3065(5)	.046
C(13)	.5476(8)	.0748(5)	.3196(5)	.060
C(14)	.4619(8)	.0831(6)	.2352(7)	.073
C(15)	.5518(8)	.1686(6)	.3796(6)	.071
C(16)	.4817(9)	-.0066(7)	.3621(6)	.074
C(21)	.7715(7)	.4430(4)	.3205(4)	.044
C(22)	.9013(7)	.4533(4)	.3778(4)	.045
C(111)	.6460(7)	.3612(7)	.1464(5)	.049(2)
C(112)	.5201(7)	.3383(5)	.1744(3)	.061(2)
C(113)	.4056(4)	.3318(4)	.1170(4)	.078(3)
C(114)	.4169(6)	.3483(6)	.0315(4)	.077(3)
C(115)	.5429(6)	.3712(4)	.0036(3)	.078(3)
C(116)	.6574(5)	.3776(5)	.0610(4)	.068(2)
C(121)	.9210(6)	.4479(4)	.1762(3)	.045(2)
C(122)	.8991(6)	.5404(5)	.1687(6)	.070(2)
C(123)	.9997(7)	.6061(4)	.1445(6)	.081(3)
C(124)	1.1223(5)	.5794(3)	.1278(2)	.078(3)
C(125)	1.1442(6)	.4869(4)	.1353(6)	.072(2)
C(126)	1.0435(7)	.4212(4)	.1595(6)	.055(2)
C(211)	1.1257(5)	.3584(6)	.4166(5)	.040(2)
C(212)	1.1830(4)	.3213(3)	.4861(2)	.059(2)
C(213)	1.3215(5)	.3363(5)	.5050(4)	.079(3)
C(214)	1.4026(5)	.3885(5)	.4542(4)	.075(3)
C(215)	1.3453(4)	.4255(3)	.3847(3)	.067(2)
C(216)	1.2068(5)	.4105(6)	.3658(5)	.056(2)
C(221)	.8678(6)	.2992(4)	.4789(3)	.041(2)
C(222)	.8860(8)	.2115(3)	.5033(6)	.063(2)
C(223)	.8293(7)	.1816(4)	.5755(5)	.086(3)
C(224)	.7545(5)	.2395(3)	.6234(2)	.071(2)
C(225)	.7363(8)	.3272(3)	.5990(5)	.065(2)
C(226)	.7930(6)	.3571(4)	.5268(5)	.052(2)

Table 58 cont....

O(1)	1.0639(8)	.0402(5)	.4310(4)	.098
O(2)	1.1315(7)	-.0853(4)	.1834(5)	.085
O(3)	1.2248(6)	.2315(4)	.2503(5)	.089
O(4)	.8020(7)	-.0598(4)	-.0358(4)	.082
O(5)	.5129(6)	.1140(5)	.0426(4)	.081
O(6)	.9068(8)	.2507(4)	.0101(4)	.096
O(7)	.7950(8)	-.1556(5)	.3673(5)	.113
O(8)	.8547(7)	-.2040(4)	.0914(4)	.085
O(9)	.4648(6)	-.1570(4)	.1442(4)	.080
H(1)	.96430	.09420	.14660	.080
H(12)	.74590	.06430	.37640	.080

Table 59 : Anisotropic Thermal Parameters ($Å^2$) in the form

$\exp - 2\pi^2 (U_{11}h^2a^{*2} \ldots + 2U_{12}hka^*b^* \ldots .)$ for complex 39.

	U11	U22	U33	U12	U13	U23
Pt	.0323(1)	.0303(1)	.0309(1)	.0064(1)	.0049(1)	.0051(1)
Ru(1)	.0320(3)	.0345(3)	.0414(3)	.0080(2)	.0042(2)	.0061(2)
Ru(2)	.0410(3)	.0377(3)	.0300(3)	.0080(2)	.0049(2)	.0042(2)
Ru(3)	.0412(3)	.0322(3)	.0465(3)	.0015(2)	.0044(3)	.0068(2)
B	.102(9)	.060(6)	.058(6)	.008(6)	.019(6)	.014(5)
F(1)	.119(6)	.099(5)	.152(6)	.027(4)	.067(5)	.020(4)
F(2)	.102(5)	.142(6)	.144(6)	.017(4)	.062(5)	.008(5)
F(3)	.26(1)	.16(1)	.14(1)	.12(1)	.04(1)	.08(1)
F(4)	.175(9)	.339(15)	.129(7)	-.122(10)	-.029(7)	.028(8)
P(1)	.042(1)	.040(1)	.039(1)	.014(1)	.008(1)	.010(1)
P(2)	.0362(9)	.0343(8)	.0360(9)	.0067(7)	.0043(7)	.0033(7)
C(1)	.059(5)	.063(5)	.056(5)	.027(4)	.007(4)	.004(4)
C(2)	.047(4)	.047(4)	.068(5)	.013(4)	-.004(4)	.002(4)
C(3)	.039(4)	.047(4)	.077(5)	.012(4)	.008(4)	-.008(4)
C(4)	.055(5)	.062(5)	.043(4)	.002(4)	.003(4)	.003(4)
C(5)	.054(5)	.066(5)	.045(4)	.011(4)	-.006(4)	.002(4)
C(6)	.077(6)	.056(5)	.045(4)	.019(4)	.021(4)	.010(4)
C(7)	.067(6)	.044(4)	.078(6)	-.008(4)	-.002(5)	.020(4)
C(8)	.063(5)	.040(4)	.077(6)	.008(4)	.008(4)	.004(4)
C(9)	.067(6)	.047(4)	.057(5)	.004(4)	.008(4)	.005(4)
C(11)	.032(3)	.028(3)	.037(3)	.006(3)	.000(3)	.005(2)
C(12)	.047(4)	.035(3)	.054(4)	.001(3)	.016(3)	.007(3)
C(13)	.040(4)	.060(5)	.074(5)	0.000(4)	.017(4)	0.000(4)
C(14)	.047(5)	.068(5)	.098(7)	.013(4)	.001(5)	0.000(5)
C(15)	.049(5)	.081(6)	.079(6)	.013(4)	.021(4)	-.007(5)
C(16)	.056(5)	.083(6)	.077(6)	-.006(5)	.029(5)	.009(5)
C(21)	.047(4)	.040(3)	.044(4)	.017(3)	.005(3)	.005(3)
C(22)	.053(4)	.039(4)	.040(4)	.009(3)	.005(3)	.003(3)
O(1)	.134(7)	.107(5)	.055(4)	.062(5)	0.000(4)	.021(4)
O(2)	.075(4)	.062(4)	.114(5)	.035(3)	.013(4)	-.007(4)
O(3)	.059(4)	.054(4)	.147(6)	-.007(3)	.038(4)	-.005(4)
O(4)	.105(5)	.074(4)	.060(4)	.021(4)	.019(4)	-.017(3)
O(5)	.064(4)	.096(5)	.077(4)	.024(4)	-.017(4)	.008(4)
O(6)	.150(7)	.066(4)	.074(4)	.023(4)	.053(5)	.032(3)
O(7)	.129(7)	.100(5)	.100(5)	-.016(5)	-.036(5)	.066(5)
O(8)	.081(5)	.060(4)	.106(5)	.020(3)	.017(4)	-.018(4)
O(9)	.057(4)	.082(4)	.090(5)	-.011(3)	-.011(3)	-.002(4)

Table 60 : Selected Bond Lengths (Å) with esd's for

$[Ru_3Pt(\mu\text{-}H)(\mu_4\text{-}\eta^2\text{-}C{=}C(H)t\text{-}Bu)(dppe)(CO)_9]^+BF_4^-$, 39

Pt	- Ru(1)	2.784(1)	Pt	- Ru(2)	2.782(1)
Pt	- P(1)	2.269(2)	Pt	- P(2)	2.286(2)
Pt	- C(11)	2.092(6)	Ru(1)	- Ru(2)	2.835(1)
Ru(1)	- Ru(3)	2.774(1)	Ru(1)	- C(1)	1.896(9)
Ru(1)	- C(2)	1.917(8)	Ru(1)	- C(3)	1.910(8)
Ru(1)	- C(11)	2.155(7)	Ru(1)	- H(1)	1.648(1)
Ru(2)	- Ru(3)	2.830(1)	Ru(2)	- C(4)	1.915(8)
Ru(2)	- C(5)	1.904(9)	Ru(2)	- C(6)	1.928(8)
Ru(2)	- C(11)	2.112(7)	Ru(2)	- H(1)	1.793(1)
Ru(3)	- C(7)	1.911(9)	Ru(3)	- C(8)	1.915(9)
Ru(3)	- C(9)	1.909(9)	Ru(3)	- C(11)	2.089(6)
Ru(3)	- C(12)	2.278(7)	B	- F(1)	1.320(13)
B	- F(2)	1.354(15)	B	- F(3)	1.262(14)
B	- F(4)	1.361(17)	P(1)	- C(21)	1.825(7)
P(1)	- C(111)	1.791(8)	P(1)	- C(121)	1.812(6)
P(2)	- C(22)	1.820(7)	P(2)	- C(211)	1.816(6)
P(2)	- C(221)	1.814(5)	C(1)	- O(1)	1.131(11)
C(2)	- O(2)	1.121(10)	C(3)	- O(3)	1.138(10)
C(4)	- O(4)	1.135(10)	C(5)	- O(5)	1.125(11)
C(6)	- O(6)	1.118(11)	C(7)	- O(7)	1.113(12)
C(8)	- O(8)	1.128(11)	C(9)	- O(9)	1.167(11)
C(11)	- C(12)	1.400(10)	C(12)	- C(13)	1.508(11)
C(12)	- H(12)	1.187(8)	C(13)	- C(14)	1.547(13)
C(13)	- C(15)	1.525(12)	C(13)	- C(16)	1.515(13)
C(21)	- C(22)	1.510(10)			

Table 61 : Selected Bond Angles (deg) with esd's for

$[Ru_3Pt(\mu\text{-}H)(\mu_4\text{-}\eta^2\text{-}C{=}C(H)t\text{-}Bu)(dppe)(CO)_9]^+BF_4^-$, 39

Ru(1) - Pt - Ru(2)	61.2(1)	Ru(1) - Pt - P(1)	158.6(1)
Ru(1) - Pt - P(2)	109.4(1)	Ru(1) - Pt - C(11)	50.0(2)
Ru(2) - Pt - P(1)	104.8(1)	Ru(2) - Pt - P(2)	170.6(1)
Ru(2) - Pt - C(11)	48.9(2)	P(1) - Pt - P(2)	84.1(1)
P(1) - Pt - C(11)	134.6(2)	P(2) - Pt - C(11)	126.2(2)
Pt - Ru(1) - Ru(2)	59.3(1)	Pt - Ru(1) - Ru(3)	95.6(1)
Pt - Ru(1) - C(1)	106.6(3)	Pt - Ru(1) - C(2)	162.5(3)
Pt - Ru(1) - C(3)	77.8(3)	Pt - Ru(1) - C(11)	48.0(2)
Pt - Ru(1) - H(1)	76.6(1)	Ru(2) - Ru(1) - Ru(3)	60.6(1)
Ru(2) - Ru(1) - C(1)	149.9(3)	Ru(2) - Ru(1) - C(2)	108.4(3)
Ru(2) - Ru(1) - C(3)	106.8(3)	Ru(2) - Ru(1) - C(11)	47.7(2)
Ru(2) - Ru(1) - H(1)	36.2(1)	Ru(3) - Ru(1) - C(1)	97.9(3)
Ru(3) - Ru(1) - C(2)	87.5(3)	Ru(3) - Ru(1) - C(3)	167.3(3)
Ru(3) - Ru(1) - C(11)	48.2(2)	Ru(3) - Ru(1) - H(1)	86.9(1)
C(1) - Ru(1) - C(2)	90.0(4)	C(1) - Ru(1) - C(3)	94.4(4)
C(1) - Ru(1) - C(11)	102.4(3)	C(1) - Ru(1) - H(1)	173.9(3)
C(2) - Ru(1) - C(3)	95.6(4)	C(2) - Ru(1) - C(11)	134.9(3)
C(2) - Ru(1) - H(1)	86.4(3)	C(3) - Ru(1) - C(11)	125.7(3)
C(3) - Ru(1) - H(1)	81.0(3)	C(11) - Ru(1) - H(1)	83.6(2)
Pt - Ru(2) - Ru(1)	59.4(1)	Pt - Ru(2) - Ru(3)	94.4(1)
Pt - Ru(2) - C(4)	163.5(3)	Pt - Ru(2) - C(5)	105.4(3)
Pt - Ru(2) - C(6)	84.7(3)	Pt - Ru(2) - C(11)	48.2(2)
Pt - Ru(2) - H(1)	74.8(1)	Ru(1) - Ru(2) - Ru(3)	58.6(1)
Ru(1) - Ru(2) - C(4)	106.0(3)	Ru(1) - Ru(2) - C(5)	151.3(3)
Ru(1) - Ru(2) - C(6)	110.7(3)	Ru(1) - Ru(2) - C(11)	49.0(2)
Ru(1) - Ru(2) - H(1)	32.9(1)	Ru(3) - Ru(2) - C(4)	82.6(3)
Ru(3) - Ru(2) - C(5)	102.3(3)	Ru(3) - Ru(2) - C(6)	167.1(3)
Ru(3) - Ru(2) - C(11)	47.3(2)	Ru(3) - Ru(2) - H(1)	82.6(1)
C(4) - Ru(2) - C(5)	91.1(4)	C(4) - Ru(2) - C(6)	94.5(4)
C(4) - Ru(2) - C(11)	129.7(3)	C(4) - Ru(2) - H(1)	88.7(3)
C(5) - Ru(2) - C(6)	90.4(4)	C(5) - Ru(2) - C(11)	102.3(3)
C(5) - Ru(2) - H(1)	175.1(3)	C(6) - Ru(2) - C(11)	132.9(3)
C(6) - Ru(2) - H(1)	84.7(3)	C(11) - Ru(2) - H(1)	81.6(2)
Ru(1) - Ru(3) - Ru(2)	60.8(1)	Ru(1) - Ru(3) - C(7)	96.7(3)
Ru(1) - Ru(3) - C(8)	96.2(3)	Ru(1) - Ru(3) - C(9)	165.1(3)
Ru(1) - Ru(3) - C(11)	50.2(2)	Ru(1) - Ru(3) - C(12)	77.9(2)
Ru(2) - Ru(3) - C(7)	156.4(3)	Ru(2) - Ru(3) - C(8)	97.4(3)
Ru(2) - Ru(3) - C(9)	104.8(3)	Ru(2) - Ru(3) - C(11)	48.0(2)
Ru(2) - Ru(3) - C(12)	80.6(2)	C(7) - Ru(3) - C(8)	91.8(4)
C(7) - Ru(3) - C(9)	97.1(4)	C(7) - Ru(3) - C(11)	113.1(3)
C(7) - Ru(3) - C(12)	88.1(4)	C(8) - Ru(3) - C(9)	89.0(4)
C(8) - Ru(3) - C(11)	138.6(3)	C(8) - Ru(3) - C(12)	174.1(4)
C(9) - Ru(3) - C(11)	118.3(3)	C(9) - Ru(3) - C(12)	96.9(4)
C(11) - Ru(3) - C(12)	37.1(3)	F(1) - B - F(2)	110.6(9)
F(1) - B - F(3)	111.4(10)	F(1) - B - F(4)	107.0(11)
F(2) - B - F(3)	119.3(12)	F(2) - B - F(4)	105.6(9)
F(3) - B - F(4)	101.7(11)	Pt - P(1) - C(21)	105.5(3)
Pt - P(1) - C(111)	121.3(4)	Pt - P(1) - C(121)	113.8(2)
C(21) - P(1) - C(111)	107.5(4)	C(21) - P(1) - C(121)	101.8(3)
C(111) - P(1) - C(121)	105.1(4)	Pt - P(2) - C(22)	107.9(3)
Pt - P(2) - C(211)	118.4(3)	Pt - P(2) - C(221)	112.1(2)
C(22) - P(2) - C(211)	105.6(4)	C(22) - P(2) - C(221)	104.6(3)
C(211) - P(2) - C(221)	107.1(4)	Ru(1) - C(1) - O(1)	174.3(8)
Ru(1) - C(2) - O(2)	178.0(8)	Ru(1) - C(3) - O(3)	177.1(7)
Ru(2) - C(4) - O(4)	175.4(8)	Ru(2) - C(5) - O(5)	174.4(8)
Ru(2) - C(6) - O(6)	175.9(8)	Ru(3) - C(7) - O(7)	175.7(8)
Ru(3) - C(8) - O(8)	177.5(8)	Ru(3) - C(9) - O(9)	178.3(7)
Pt - C(11) - Ru(1)	81.9(3)	Pt - C(11) - Ru(2)	82.9(3)
Pt - C(11) - Ru(3)	160.4(4)	Pt - C(11) - C(12)	119.9(5)
Ru(1) - C(11) - Ru(2)	83.3(3)	Ru(1) - C(11) - Ru(3)	81.6(3)
Ru(1) - C(11) - C(12)	127.0(5)	Ru(2) - C(11) - Ru(3)	84.7(3)
Ru(2) - C(11) - C(12)	142.0(5)	Ru(3) - C(11) - C(12)	78.8(4)
Ru(3) - C(12) - C(11)	64.1(4)	Ru(3) - C(12) - C(13)	124.3(5)
Ru(3) - C(12) - H(12)	108.6(5)	C(11) - C(12) - C(13)	134.4(7)
C(11) - C(12) - H(12)	111.5(6)	C(13) - C(12) - H(12)	106.9(6)
C(12) - C(13) - C(14)	113.9(7)	C(12) - C(13) - C(15)	107.5(7)
C(12) - C(13) - C(16)	110.3(7)	C(14) - C(13) - C(15)	105.7(7)
C(14) - C(13) - C(16)	110.2(7)	C(15) - C(13) - C(16)	109.1(7)
P(1) - C(21) - C(22)	105.7(5)	P(2) - C(22) - C(21)	110.3(5)
Ru(1) - H(1) - Ru(2)	110.9(1)		

centre occupying a wing tip position. The vinylidene moiety spans the open butterfly face, with the C_α atom, C(11) bonded to all four metal centres and the C=C bond formally π-bonded to the wing tip Ru(3) site. The directly observed hydride ligand spans the hinge Ru(1)-Ru(2) edge. Apart from the perturbation introduced by this hydride (see below), complex 39 has a very similar cluster geometry to 38, the parent, unprotonated system. With the exception of the hinge Ru(1)-Ru(2) bond, corresponding inter-metal separations in the two complexes differ by only 0.007 - 0.054 Å. The elongation of the Ru(1)-Ru(2) vector in 39 (2.708(1) Å in 38, *cf* 2.835(1) Å in 39) can be ascribed to the bond lengthening effect of the bridging hydride.[303] Furthermore, in order to accommodate this hydride, the carbonyl ligands cis to H(1) are splayed back in 39 compared with the corresponding CO groups in 38 (hinge Ru-Ru-C angles are 5.8 - 18.6° greater in 39 than 38).

The hinge-wing tip Ru-Ru separations differ significantly from each other with Ru(1)-Ru(3) = 2.774(1) Å and Ru(2)-Ru(3) = 2.830(1) Å. Moreover, the Ru(3)-Ru(2)-C(5) and Ru(2)-Ru(3)-C(9) angles (102.3(3)° and 104.8(3)° respectively) are larger than the Ru(3)-Ru(1)-C(1), Ru(1)-Ru(3)-C(7) angles (97.9(3)° and 96.7(3)° respectively). This asymmetry may be due to the steric requirements of the bulky t-Bu group which lies over the Ru(2)-Ru(3) edge. Similarly, in complex 38, the Ru-Ru hinge - wing tip vector cisoid to the t-Bu function is 0.024 Å (12σ) longer than the corresponding transoid edge.

The Pt-Ru separations in 39 (2.784(1), 2.782(1) Å) are essentially identical whereas, in 38, significant asymmetry is observed (Pt-Ru = 2.730(1), 2.792(1) Å).

The coordination about the Pt atom approximates to square planar if the C(11)-Pt vector is ignored. The greatest deviation from the mean plane defined by Pt,Ru(1), Ru(2),P(1) and P(2) is

0.203(2) Å for the P(1) centre. Furthermore, the sum of bond angles about Pt is 359.5°, as shown in Figure 87. Hence it is expected that the Pt centre acts as a 16 electron metal.

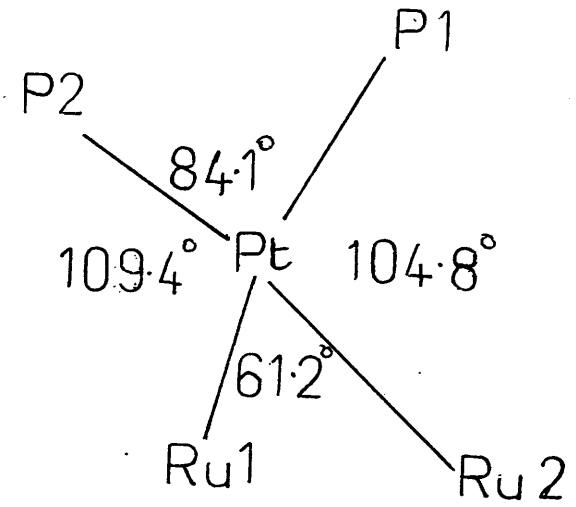

Figure 87. The coordination about the Pt centre in 39.

Assuming the μ_4-η^2 coordinated vinylidene moiety to be a 4 electron donor, 39 has 60 valence electrons, as expected for a butterfly cluster incorporating a 16 electron Pt centre.[148,258] The P.S.E.P.T is obeyed if C(11), the C_α atom of the vinylidene moiety, is considered a skeletal atom, but C(12), the C_β centre, is assumed to be a bridging exo ligand. This gives 6 SEP's which is consistent with the distorted *closo*-trigonal bipyramidal geometry defined by Pt,Ru(1),Ru(2),Ru(3) and C(11).

The coordination of the μ_4-η^2-C=C(H)t-Bu moiety in 39 is similar to that observed in 38 and several other butterfly cluster systems : $Os_3Ni(\mu\text{-}H)(\mu_4\text{-}\eta^2\text{-}C{=}C(H)t\text{-}Bu)(Cp)(CO)_9$,[352] 44;

$Ru_3Ni(\mu\text{-}H)(\mu_4\text{-}\eta^2\text{-}C{\equiv}C(H)R)(Cp)(CO)_9$, [R = t-Bu,[350] 45; i-Pr,[351] 46]; $Co_3Fe(\mu\text{-}CO)_2(\mu_4\text{-}\eta^2\text{-}C{\equiv}CH_2)(Cp)(CO)_7$,[353] 47; and $Ru_4(\mu\text{-}PPh_2)(\mu_3\text{-}OH)(\mu_4\text{-}\eta^2\text{-}C{\equiv}C(H)i\text{-}Pr)(CO)_{10}$[354], 48. The $C_\alpha\text{-}C_\beta$ separation in 39 (1.40(1) Å) falls within the range (1.39-1.44 Å) observed in 38, 44-48.[350-354] These vectors are somewhat longer than the C≡C distances observed for $\mu_4\text{-}\eta^2\text{-}C{\equiv}CR$ functions (Table 51), in keeping with the increased formal bond order in acetylide c.f. vinylidene moieties.

C(11) is approximately equidistant from the four metal centres (C(11)-M ranges 2.089(6)-2.155(7) Å), while the wing tip M-C_β, Ru(3)-C(12) distance of 2.278(7) Å compares well with corresponding separations in 38 (2.297(11) Å), 44 (2.25(2) Å),[352] 45 (2.227(10) Å),[350] and 46 (2.219(6) Å).[351]

The dihedral butterfly angle in 39 (117.8(1)°) is identical to that of 38 and similar to those observed in 44 (117.1°)[352]; 45 (116.6°)[350]; and 46 (118.3°)[351], while complexes 47 [353] and 48 [354] have more open butterfly frameworks, (dihedral angles 124° and 143.7° respectively).

The carbonyl ligands are terminally bound (M-C-O range 174.3(8)-178.3(7)°, mean 176.3°). Ru-CO and C-O bond lengths fall within the expected ranges (Ru-CO distances vary between 1.896(8) - 1.928(8) Å; mean 1.912 Å; C-O range 1.114(12) - 1.167(11) Å; mean 1.131 Å).

The bonding parameters of the dppe group are similar to those observed in 38.

The BF_4^- anion is well separated from the cluster cation; the C(7)-F(1) separation of 3.05(1) Å is the shortest inter-ion distance. The coordination about B is distorted tetrahedral with F-B-F angles varying between 101(1) - 119(1)°.

CHAPTER FIVE.

CHAPTER 5.

EXPERIMENTAL SECTION.

All manipulations were carried out under dry oxygen-free nitrogen using standard vacuum line/Schlenk tube techniques. Solvents were freshly distilled prior to use and were dried under dinitrogen by distillation over the following reagents:

a) diethyl ether and tetrahydrofuran were distilled over sodium/benzophenone.

b) light petroleum was distilled from an alloy of sodium/potassium

c) toluene was distilled from sodium

d) methylene chloride was distilled over calcium hydride

Light petroleum refers to that fraction with a boiling point of 40-60^{o}C. Chromatography was generally performed under nitrogen on Florisil (BDH, 100-200 mesh) columns made up in light petroleum.

Elemental analyses were performed by the Microanalytical Unit in the Department of Chemistry, University of Glasgow.

Infra-red spectra were recorded on a Perkin-Elmer 983 spectrometer using CaF_2 solution cells of 0.1mm path length.

^{1}H, ^{31}P and ^{13}C n.m.r spectra were recorded on Varian XL100 or Bruker WP200SY spectrometers. N.m.r samples were prepared under N_2 in deoxygenated deuterated solvents. ^{1}H and ^{13}C chemical shifts were generally referenced to internal solvent signals and are given relative to tetramethylsilane, while ^{31}P chemical shifts are referenced to external 85% H_3PO_4.

Dynamic n.m.r spectra were simulated using the program DNMR3,[376] which was locally adapted to allow for exchanging ^{195}Pt satellites. Thermodynamic parameters were determined from the rate data using standard methods.[377] N.m.r probe temperatures were calibrated using the methanol chemical shift method[378] and are

considered accurate to ±2K.

The following reagents were prepared by literature methods; $Os_3Pt(\mu\text{-}H)_2(CO)_{10}(PCy_3)$,[147]; ^{13}CO enriched $Os_3Pt(\mu\text{-}H)_2(CO)_{10}(PCy_3)$[265]; [PPN]SCN[366] $Ru_3(\mu\text{-}H)(\mu_3\text{-}\eta^2\text{-}C{\equiv}Ct\text{-}Bu)(CO)_9$[337]; $Os_3(\mu\text{-}H)_2(CO)_{10}$[79]; $Pt(cod)_2$[379]

Solutions of diazomethane in Et_2O were prepared using an Aldrich Diazald kit.

Solutions of Li(C≡CPh) were prepared immediately prior to use by treatment of PhC≡CH (typically 0.065g in 20ml of Et_2O) with n-BuLi (1.2ml of a 0.54M solution in hexanes). ^{13}CO enriched $Ru_3(\mu\text{-}H)(\mu_3\text{-}\eta^2\text{-}C{\equiv}Ct\text{-}Bu)(CO)_9$ was prepared by maintaining a toluene solution at 90°C under an atmosphere of ^{13}CO (99% ^{13}C, Cambrian Gases) for 5 days.

t-BuNC, CyNC, $HBF_4.Et_2O$, PhC≡CH, n-BuLi (approx 0.6M solution in hexanes), NEt_3 and pyridine - (Aldrich Chemicals); SO_2 - (BDH Chemicals); and CF_3COOH -(Lancaster Syntheses) were used as received. Dppe (Aldrich Chemicals) was recrystallised from ethanol prior to use. $SnCl_2$ was obtained as the dihydrate (Aldrich Chemicals) and dehydrated by treatment with acetic anhydride.

A sample of 1,1,3,3 tetramethyl-2-thiocarbonyl cyclohexane was kindly supplied by Dr. U. Behrens, Hamburg University

Extended Hückel Calculations

Extended Hückel calculations[86,380] were carried out using the programs ICON8 and FMO.[209] Orbital exponents and H_{ii}'s for Pt[175] and Ru[381] were obtained from published work. The geometry of Z was taken from the crystal structure of 19a[147] and idealised to C_s symmetry. Bond distances (Å) were as follows: Ru-Ru = 2.78, Pt-Ru = 2.83, Pt-P = 2.37, P-H = 1.42, Ru-H = 1.85, Pt-H = 1.85; distances involving CO's Ru-C = 1.90, Pt-C = 1.86, C-O = 1.15; for interactions of Z with

CH_2, Ru-C = 2.15, C-H = 1.0; and with CO, Ru-C = 2.15. All calculations were carried out on an ICL 2988. Orbital contour plots (at intervals of 0.05, 0.1, 0.2, 0.5, 0.8eau^{-3}) were drawn using the program PSI77.[382]

N.m.r Studies of the Reaction of $Os_3Pt(\mu\text{-}H)_2(CO)_{10}(PCy_3)$ with RNC, (R = t-Bu; R = Cy).

In a typical experiment a solution of $Os_3Pt(\mu\text{-}H)_2(CO)_{10}(PCy_3)$ (0.054g, 0.041 mmol) in $CDCl_3$ (0.5ml) was treated with CyNC (0.1ml of a 0.4M solution in $CDCl_3$) at 273K. The green colour of the solution rapidly gave way to yellow. The resulting solution contained a mixture of isomers of $Os_3Pt(\mu\text{-}H)_2(CO)_{10}(CyNC)(PCy_3)$ that were characterised spectroscopically. Similar experimental procedure was used for the addition of RNC (R = t-Bu, Cy) at 273 and 195K.

$Os_3Pt(\mu\text{-}H)_2(CO)_{10}(t\text{-}BuNC)(PCy_3)$: I.R (KBr disc) for isomer A: ν_{max} CN 2180 (br, w) ν_{max}CO, 2080 (w), 2060(m), 2035(s), 2015(sh), 2005(vs), 1980(s), 1960(s), 1930(m). Anal. Calcd for $C_{33}H_{44}NO_{10}Os_3PPt$:C,28.08; H, 3.14. Found C, 28.40; H, 3.26. ^1H NMR ($CDCl_3$, 233K): Isomer A; δ-9.74 (d,1H,Os(μ-H)Pt, J(Pt-H) = 567, J(P-H) = 14.6Hz), -17.57 (s,1H, Os(μ-H)Os). Isomer B; δ -11.60 (d,1H,Os(μ-H)Pt, J(Pt-H) = 503, J(P-H) = 10.8Hz), -17.60 (s,1H,Os(μ-H)Os). Isomer C; δ -9.65 (d,1H, Os(μ-H)Pt, J(P-H) = 12.0Hz), -18.98 (s,1H,Os(μ-H)Os).

$Os_3Pt(\mu\text{-}H)_2(CO)_{10}(CyNC)(PCy_3)$: ^1H, ^{31}P and ^{13}C NMR parameters for Isomer A are given in Table 21. ^1H NMR ($CDCl_3$,233K): Isomer B; δ -11.59 (d,1H,Os(μ-H)Pt, J(Pt-H) = 503, J(P-H) = 11Hz), -17.56 (d, 1H,Os(μ-H)Os, J(Pt-H) = 26, J(P-H) = 1.5Hz). Isomer C; δ -9.70(d, Os(μ-H)Pt, J(Pt-H) = 570, J(P-H) = 15Hz), -18.94 (s, Os(μ-H)Os, J(Pt-H) = 16Hz).

Preparation of $Os_3Pt(\mu\text{-}H)_2(CO)_9(RNC)(PCy_3)$, R = t-Bu, 26a; R = Cy, 26b.

A solution of $Os_3Pt(\mu\text{-}H)_2(CO)_{10}(PCy_3)$ (0.153g, 0.12mmol) in light petroleum (50ml) was treated with CyNC (0.6ml of a 0.2M solution in light petroleum). The dark green colour of the solution gave way to yellow and the solution was refluxed under a dinitrogen purge for 90 minutes. Concentration of the resulting dark green solution afforded crystals of complex 26b, R = Cy,(0.139g, 84% yield.) IR (cyclohexane) ν_{max} CN 2177(br); ν_{max} CO 2064(m), 2035(s), 2012(s), 1983(s), 1959(m), 1952(m), 1935(w) cm^{-1}. For NMR parameters see Table 23

Anal. Calcd. for $C_{34}H_{46}NO_9Os_3PPt$: C, 28.98; H, 3.29; N, 0.99.
Found: C, 29.09; H, 3.11; N, 0.92%.

In a similar manner treatment of $Os_3Pt(\mu\text{-}H)_2(CO)_{10}(PCy_3)$ (0.154g, 0.116mmol) with t-BuNC afforded complex 26a, (0.143g, 87% yield). IR (cyclohexane) ν_{max} CN 2169(br); ν_{max}CO 2064(m), 2035(s), 2012(s), 1983(s), 1958(m), 1952(m), 1935(w) cm^{-1}. ^1H NMR ($CDCl_3$, 233K) δ 1.78 - 1.24 (m,42H, C_6H_{11} and CH_3), -7.99 (s,1H,Os(μ-H)Os, J(Pt-H) = 5.7Hz), -11.47 (d,1H, Os(μ-H)Pt, J(Pt-H) = 539, J(P-H) = 9.4Hz).

Anal. Calcd. for $C_{32}H_{44}O_9Os_3NPPt$: C, 27.78; H, 3.20; N, 1.01; P, 2.24.
Found: C, 27.73; H, 3.10; N, 0.93; P, 2.76%

Addition of CO to $Os_3Pt(\mu\text{-}H)_2(CO)_9(RNC)(PCy_3)$, R = t-Bu, Cy.

Reaction conditions identical for $Os_3Pt(\mu\text{-}H)_2(CO)_9(RNC)(PCy_3)$, R = t-Bu, Cy. In a typical reaction, a solution of $Os_3Pt(\mu\text{-}H)_2(CO)_9$-$(RNC)(PCy_3)$, R = t-Bu, Cy, was treated with CO at 195K. The dark green colour of the solution rapidly changed to yellow. ^1H NMR showed essentially quantitative conversion to isomer A of $Os_3Pt(\mu\text{-}H)_2(CO)_{10}$-$(RNC)(PCy_3)$, R = t-Bu, Cy. Similar treatment at 298K gave identical results.

Preparation of $Os_3Pt(\mu\text{-}H)_2(\mu\text{-}CH_2)(CO)_9(CyNC)(PCy_3)$, 27.

A solution of $Os_3Pt(\mu\text{-}H)_2(CO)_9(CyNC)(PCy_3)$ (0.150g, 0.107mmol) in toluene (15ml) was treated dropwise with a solution of diazomethane in diethyl ether at 273K, until the dark green colour of the starting material gave way to an orange solution. Evaporation of this solution *in vacuo*, and recrystallisation of the residue from diethyl ether afforded red crystals of complex 27, (0.127g, 83%). IR (cyclohexane) ν_{max} CN 2181(br); ν_{max} CO 2068(m), 2047(s), 2016(s), 1989(s), 1973(s), 1954(m), 1950(m), 1925(m) cm^{-1}; ^1H NMR ($CDCl_3$, 298K), 7.02 (m,1H,CH_2), 6.61 (d of d,1H,CH_2, J(H-H) = 6.0 and 2.3Hz), 3.96-1.12(m,44H,C_6H_{11}), -15.87 (d,1H,Os(μ-H)Pt, J(Pt-H) = 534, J(P-H) = 7.3Hz), -21.82 (d,1H, Os(μ-H)Os, J(Pt-H) = 22Hz, J(H-H) = 2Hz). ^{13}C NMR data given in Table 25. Anal. Calcd. for $C_{35}H_{48}O_9Os_3NPPt$: C, 29.54; H, 3.37; N, 0.98. Found C, 29.79; H, 3.22; N, 0.79%.

Preparation of $Os_3Pt(\mu\text{-}H)_2(\mu\text{-}SO_2)(CO)_{10}(PCy_3)$, 28.

A solution of $Os_3Pt(\mu\text{-}H)_2(CO)_{10}(PCy_3)$ (0.20g, 0.15mmol) in methylene chloride (5ml) was saturated with SO_2 by rapid passage of the gas, and the solution allowed to stand for 30 mins. Light petroleum (ca. 5ml) was added and the solution was maintained at -20°C overnight. Dark red crystals of complex 28 were obtained (0.11g, 53% yield): IR (KBr disc) ν_{max} CO 2100(w), 2080 (vs), 2060 (s), 2040 (s), 2018 (s), 1995 (m), 1985 (s), 1956 (m), ν_{max} SO 1195(vw), 1040(s) cm^{-1}. For ^1H and ^{31}P NMR data see Table 28. ^{13}C NMR (CD_2Cl_2, 295K) CO region, ^{13}CO enriched sample, δ 179.4 (d,1C, J(P-C) = 8.0Hz), 176.8 (s,1C), 174.2 (d,1C,J(P-C) = 8.3Hz), 172.8 (s,1C), 172.2(s,1C), 172.17 (s,1C), 172.0 (s,1C), 169.5 (s,1C, J(Pt-C) = 28Hz), 161.7 (d,1C J(P-C) = 1.3Hz, J(H-C) = 12Hz), 159.3 (d,1C, J(P-C) = 6.3Hz, J(Pt-C) = 1560, J(H-C) = 33Hz). Anal. Calcd for $C_{28}H_{35}O_{12}Os_3PPtS$: C, 24.15; H, 2.53. Found:

C, 24.33; H, 2.31%

NMR data for species A is given in Table 27. ^{1}H and ^{31}P NMR parameters for species B-G are listed in Table 28.

NMR data for species H. ^{1}H (CD_2Cl_2, 213K) δ -16.05 (d,H1, Os (μ-H)Os, J(H-H) = 1.4Hz); -16.14 (d,H2, Os(μ-H)Os, J(H-H) = 1.4Hz); ^{13}C (CD_2Cl_2, 198K) ^{13}CO enriched sample, CO region δ 176.4 (J(H2-C) = 10.3Hz), 175.3 (J(H1-C) = 4.8Hz), 174.3 (J(H1-C) = 7.3Hz), 171.9 (J(H2-C) = 3.0Hz), 169.6 (J(H2-C) = 3.4Hz), 166.7 (J(H1-C) = 4.6, J(H2-C) = 4.6Hz), 164.2 (J(H1-C) = 2.2Hz), 163.8 (J(H1-C) = 10.2, J(H2-C) = 4.7Hz), 158.1 (J(H1-C) = 3.8, J(H2-C) = 11.7Hz).

Preparation of $Os_3PtSn(\mu\text{-}H)_2(CO)_{10}(Cl)(OEt_2)(SnCl_3)(PCy_3)$, 29.

$Os_3Pt(\mu\text{-}H)_2(CO)_{10}(PCy_3)$ (0.056g, 0.043mmol) in methylene chloride (2.5ml) was treated with 0.086mmol of $SnCl_2$ (0.43ml of a 0.2M solution of anhydrous $SnCl_2$ in tetrahydrofuran). 0.5ml of diethyl ether was carefully added forming a layer on top of the resulting orange solution. On standing at -20°C for 12h, bright orange crystals of complex 29 were obtained (0.064g, 85% yield): IR (cyclohexane), ν_{max} CO 2103(w), 2059(m), 2047(s), 2042(sh), 2032(w), 2017(w), 2011(sh), 1987(w) cm^{-1}; for NMR parameters see Table 29. Anal. Calcd. for $C_{32}H_{45}Cl_4O_{11}Os_3PPtSn_2$: C, 21.58; H, 2.55. Found C, 21.92; H, 2.24% (crystals suffer rapid solvent loss).

Preparation of $[Os_3Pt(\mu\text{-}H)_3(CO)_{10}(PCy_3)]^+BF_4^-$, 30.

A solution of $Os_3Pt(\mu\text{-}H)_2(CO)_{10}(PCy_3)$ (0.20g, 0.15mmol) in methylene chloride (20ml) was treated with $HBF_4.Et_2O$ (ca. 0.1ml). Careful addition of diethyl ether in 1ml aliquots until the mother-liquor is almost colourless afforded dark green crystals of 30 (0.20g, 94% yield). IR(CH_2Cl_2) ν_{max} CO 2130(sh), 2124(m), 2096(vs), 2084(vs), 2068(s), 2046(m), 2026(s), 2004(w) cm^{-1}. NMR parameters are given in Table 33 Anal. Calcd for $C_{28}H_{36}BF_4O_{10}Os_3PPt$: C, 23.75; H, 2.59; P, 2.19. Found : C, 23.73; H, 2.12; P, 2.49%.

Preparation of $[Os_3Pt(\mu\text{-}H)_3(CO)_9(CyNC)(PCy_3)]^+BF_4^-$, 31.

$Os_3Pt(\mu\text{-}H)_2(CO)_9(CyNC)(PCy_3)$ (0.06g, 0.043mmol) in CH_2Cl_2 (1.5ml) was treated with excess $HBF_4.Et_2O$. The solution changed colour from dark green to dark purple and the product identified spectroscopically. IR (CH_2Cl_2) ν_{max} CN 2202(br), ν_{max} CO 2111(m), 2088 (vs), 2062(vs), 2036(s), 2019(s), 1990 (m) cm^{-1}. ^1H NMR ($CDCl_3$, 298K) δ 3.81 - 2.36 (m,44H,C_6H_{11}), -13.13(s,1H,Os(μ-H)Os), -13.29 (d, 1H, Os(μ-H)Pt, J(Pt-H) = 547, J(P-H) = 7.2Hz), -13.47 (s,1H,Os(μ-H)Os, J(Pt-H) = 21Hz); ^{31}P NMR ($CDCl_3$, 298K) δ 65.6 (J(Pt-P) = 2456Hz).

Preparation of $[Os_3Pt(\mu\text{-}H)_3(\mu\text{-}CH_2)(CO)_9(CyNC)(PCy_3)]^+CF_3COO^-$, 32.

$Os_3Pt(\mu\text{-}H)_2(\mu\text{-}CH_2)(CO)_9(CyNC)(PCy_3)$ in $CDCl_3$ (0.5ml) was treated with excess CF_3COOH. ^1H NMR ($CDCl_3$, 298K), highfield region, δ -17.73 (d,1H,Os(μ-H)Pt, J(Pt-H) = 490Hz), -21.67 (s,2H,Os(μ-H)Os, J(Pt-H) = 11Hz).

Preparation of $Os_3Pt(\mu_3\text{-}S)_2[\eta^1\text{-}CCC(CH_3)_2CH_2.CH_2.CH_2.C(CH_3)_2](CO)_9(PCy_3)$, 33.

A solution of $Os_3Pt(\mu\text{-}H)_2(CO)_{10}(PCy_3)$ (0.133g, 0.101mmol) in toluene (15ml) was treated with a threefold excess of 1,1,3,3 tetramethyl-2-thiocarbonyl cyclohexane (2.0ml of a 0.153M solution in light petroleum). The reaction mixture was heated to 90°C under reduced pressure for 22h by which time the colour of the solution had changed from dark green to brown. Volatile material was removed *in vacuo* and the toluene soluble residues chromatographed. Elution with light petroleum separated 14 products. The first of these was an unidentified pale yellow band, which was followed by a red band containing the major product, complex 33. With the exception of 33, all other products remain uncharacterised. After recrystallisation from light petroleum the yield of complex 33 was 6.5% (0.007g). IR(cyclohexane) ν_{max} CO 2069 (m), 2045 (vs), 2032(m), 2023(m), 1977(s), 1971(s), 1961(w), 1946(vw), cm^{-1}. ^1H NMR ($CDCl_3$, 298K) δ 2.36 - 0.84 (m,51H, C_6H_{11}, $C_{11}H_{18}$); ^{31}P NMR ($CDCl_3$, 223K) δ 36.1 (s,J(Pt-P) = 2771Hz). Anal. Calcd. for $C_{38}H_{51}O_9Os_3PPtS_2$: C, 30.17; H, 3.39. Found C, 30.73; H, 3.35%.

Reaction of $Os_3Pt(\mu\text{-}H)_2(CO)_{10}(PCy_3)$ with [PPN]SCN.

A solution of $Os_3Pt(\mu\text{-}H)_2(CO)_{10}(PCy_3)$, (0.075g, 0.057mmol) in CH_2Cl_2 was treated dropwise with [PPN]SCN in CH_2Cl_2 until the green colour of the starting material gave way to yellow (required 6.0ml of a 0.02M solution). Spectroscopic data were obtained from reaction mixtures. IR(CH_2Cl_2) ν_{max} CN 2121(br,w); ν_{max} CO 2080(vw), 2060(sh), 2054(m), 2040(sh), 2033(s), 2010(br,s), 1995(sh), 1970(sh), 1962(br,m), 1920(br,w). ^1H NMR parameters are given in text.

Preparation of $Os_3Pt(\mu\text{-}H)(\mu_4\text{-}\eta^2\text{-}C{\equiv}CPh)(CO)_{10}(PCy_3)$, 34

A stirred solution of $Os_3Pt(\mu\text{-}H)_2(CO)_{10}(PCy_3)$ (0.102g, 0.077mmol) in Et_2O (60ml) was treated with a slight excess of $Li(C{\equiv}CPh)$ (2.5mls of a 0.032M solution in Et_2O) at -20°C. The green colour of the starting material rapidly gave way to orange. This solution was treated with excess (ca. 0.1ml) CF_3COOH. The volatiles were removed *in vacuo* and the Et_2O soluble residues chromatographed. Eluting with 1:20 CH_2Cl_2:light petroleum gave an orange band followed by a green and a yellow band. These two latter products remain uncharacterised. Recrystallisation of the first band in Et_2O at -20°C afforded a mixture of yellow crystals of 34 (0.011g, 10%) and red crystals which were separated by crystal picking. The red complex remains uncharacterised, Spectroscopic data for 34: IR(cyclohexane) ν_{max} CO 2086(m), 2062(s), 2042(vs), 2022(m), 2004(m), 1993(m), 1964(w) cm^{-1}. ^1H NMR ($CDCl_3$, 235K) δ 7.39 - 7.03 (m,5H,C_6H_5), 1.75 - 0.88 (m,33H, C_6H_{11}), -20.42 (s,1H,Os(μ-H)Os). ^{31}P NMR ($CDCl_3$, 295K), δ 49.2 (s,J(Pt-P) = 3988 Hz). Anal. Calcd for $C_{36}H_{39}O_{10}Os_3PPt$: C, 30.27; H, 2.75. Found C, 32.24; H, 2.77%

Preparation of $Ru_3Pt(\mu\text{-}H)(\mu_4\text{-}\eta^2\text{-}C{\equiv}Ct\text{-}Bu)(cod)(CO)_9$, 36.

0.766g (1.9mmol) of $Pt(cod)_2$ in toluene (5ml) was added dropwise to a stirred solution of $Ru_3(\mu\text{-}H)(\mu_3\text{-}\eta^2\text{-}C{\equiv}Ct\text{-}Bu)(CO)_9$, 35, (1.18g, 1.9mmol) in toluene (30ml) at 0°C. The yellow colour of the solution gives way to dark brown over 25 mins. The volatiles were removed *in vacuo* and the residue chromatographed. After elution of unreacted 35, the product was eluted with light petroleum as a bright orange band. Removal of the solvent and recrystallisation from Et_2O gave orange crystals of complex 36, (0.98g, 56% yield).

IR (cyclohexane); ν_{max} CO 2080(m), 2069(vw), 2057(s), 2023(vs), 2006(m), 1999(m), 1970(w), 1953(w) cm^{-1}. ^{1}H NMR ($CD_3C_6D_5$, 233K) δ 6.02 (s,2H,CH=CH, J(Pt-H) = 49Hz), 5.28 (s,2H,CH=CH, J(Pt-H) = 71Hz), 1.62 (br,s,8H,CH_2), 1.30 (s,9H,CH_3), -19.25 (s,1H,Ru(μ-H)Ru, J(Pt-H)= 6.4Hz); ^{13}C NMR (CD_2Cl_2, 220K), δ 209.4 (s,1C, C≡Ct-Bu, J(Pt-C) = 1621Hz), 121.9 (s,1C, C≡Ct-Bu, J(Pt-C) = 224Hz), 105.2 (s,2C, CH=CH, J(Pt-C) = 60, J(H-C) = 159Hz), 92.4 (s,2C,CH=CH, J(Pt-C) = 134, J(H-C) = 155Hz), 39.8 (s,1C, $C(CH_3)_3$), 32.5 (s,3C,$C(CH_3)_3$, J(H-C) = 125Hz), 30.3 (s,2C,CH_2 J(Pt-C) = 20, J(H-C) = 122Hz), 29.0 (s,2C,CH_2, J(H-C) = 127Hz). For carbonyl parameters see Table 38. Anal. Calcd. for $C_{23}H_{22}O_9Ru_3Pt$: C, 29.36; H, 2.36. Found : C, 29.57; H, 2.06%.

Reaction of $Ru_3Pt(\mu\text{-}H)(\mu_4\text{-}\eta^2\text{-}C{\equiv}Ct\text{-}Bu)(cod)(CO)_9$ with bis(diphenylphosphino) ethane.

Bis(diphenylphosphino) ethane (0.110g, 0.278mmol) in diethyl ether (10ml) was added to a stirred solution of $Ru_3Pt(\mu\text{-}H)(\mu_4\text{-}\eta^2\text{-}C{\equiv}Ct\text{-}Bu)(cod)(CO)_9$ (0.261g, 0.278 mmol) in diethyl ether (30ml). The orange colour of 36 rapidly gave way to red. After 15 mins the volatiles were removed and the residue chromatographed. Elution with light petroleum separated an orange band which, after recrystallisation from diethyl ether at -20°C, gave orange crystals of $Ru_3Pt(\mu\text{-}H)(\mu_4\text{-}\eta^2\text{-}CCt\text{-}Bu)(dppe)(CO)_9$, 37 (0.102g, 30% yield). IR (cyclohexane) ν_{max} CO 2073 (m), 2050 (s), 2017 (s), 1999 (m), 1987 (m), 1962 (vw), 1951 (w) cm^{-1}. ^{1}H NMR ($CDCl_3$, 233K) δ 7.76-7.32 (m,20H,C_6H_5), 2.40-2.15 (m,4H,CH_2), 0.74 (s,9H,CH_3), -19.12 (s,1H,Ru(μ-H)Ru); ^{31}P NMR ($CDCl_3$, 233K) δ 51.8 (d, 1P, J(P-P) = 17.3, J(Pt-P) = 2643Hz), 46.5(d, 1P,J(P-P) = 17.3, J(Pt-P) = 4152 Hz); ^{13}C NMR (CD_2Cl_2, 233K) δ 228.3 (dd, 1C, C≡Ct-Bu, J(P-C) = 15,75Hz), 134.3-128.3 (m,24C,C_6H_5), 123.7 (d,1C, C≡Ct-Bu, J(P-C) = 5, J(Pt-C) = 178Hz), 39.8 (s,1C,$C(CH_3)_3$), 32.1(m,1C,CH_2), 31.9 (s,

3C, C($\underline{C}H_3)_3$), 28.1 (m,1C,CH_2); for carbonyl parameters see Table 40. Anal. Calcd. for $C_{41}H_{34}O_9P_2Ru_3Pt$: C, 40.01; H, 2.78. Found: C, 40.30; H, 2.75%.

On further elution with light petroleum/methylene chloride (1:1 mixture), a dark red band separated which on recrystallisation from methylene chloride/light petroleum at -20°C, gave red crystals of $Ru_3Pt(\mu_4\text{-}\eta^2\text{-}C{=}C(H)t\text{-}Bu)(dppe)(CO)_9$, 38 (0.215g, 63% yield). IR (cyclohexane) ν_{max} CO 2061(s), 2018(s), 2005(vs), 1996(m), 1974(w), 1963(w), 1951 (w) cm^{-1}. ^1H NMR ($CDCl_3$, 298K) δ 7.82 - 7.23 (m, 20H, C_6H_5), 5.75 (dd, 1H, C=C($\underline{H}$)t-Bu, J(P-H) = 4.5, 5.0Hz), 2.8 - 1.9 (m,4H, CH_2), 0.56 (s,9H,CH_3); ^{31}P NMR ($CDCl_3$, 243K) δ 55.5 (J(Pt-P) = 3452Hz), 52.7 (J(Pt-P) = 3600Hz), as AB quartet (J(P-P) = 19Hz); ^{13}C NMR (CD_2Cl_2, 295K) δ 319.7 (t,1C,$\underline{C}$=C(H)t-Bu, J(P-C) = 27Hz), 136.0-128.7 (m,24C,C_6H_5); 100.3 (s,1C,C=$\underline{C}$(H)t-Bu, J(Pt-C) = 73Hz), 39.0 (s,1C,$\underline{C}(CH_3)_3$), 33.1 (s, 3C,C($\underline{C}H_3)_3$), 29.9 (dd,1C,CH_2, J(P-C) = 38, 13Hz), 25.9(dd, 1C, CH_2, J(P-C) = 36, 13Hz); for carbonyl parameters see Table 42. Anal. Calcd. for $C_{41}H_{34}O_9P_2Ru_3Pt$: C, 40.01; H, 2.78. Found C, 40.37; H, 2.74%.

Kinetic Study of Transformation of $Ru_3Pt(\mu\text{-}H)(\mu_4\text{-}\eta^2\text{-}C{\equiv}Ct\text{-}Bu)(dppe)(CO)_9$, 37, to $Ru_3Pt(\mu_4\text{-}\eta^2\text{-}C{=}C(H)t\text{-}Bu)(dppe)(CO)_9$, 38.

The progress of the isomerisation of 37 to 38 was monitored using ^1H NMR spectroscopy. $CDCl_3$ solutions of samples were maintained at a constant temperature of 296(±1)K. The relative concentrations of 37 and 38 were determined from the intensities of the C($C\underline{H}_3$) resonances (assuming equal T_1's). Initial concentrations of the three samples were:- a) complex 37, 0.017M; b) complex 37, 0.017M with NEt_3 0.019M; and c) complex 37, 0.019M, with pyridine 0.052M.

Rate constants for the isomerisation to equilibrium were

determined from plots of $\ell n[a_e/(a_e-x)]$ against t,[383] where a_e is the equilibrium concentration of 38 and x is the concentration of 38 at time t. The gradient of the plots were determined by a least squares fit to the data points. Equilibrium concentrations of 37 and 38 were measured after 5 days, and no signals other than those due to 37 and 38 were detectable.

Reaction of $Ru_3Pt(\mu\text{-}H)(\mu_4\text{-}\eta^2\text{-}C{\equiv}Ct\text{-}Bu)(cod)(CO)_9$ with CO.

CO was rapidly passed through a solution of $Ru_3Pt(\mu\text{-}H)(\mu_4\text{-}\eta^2\text{-}C{\equiv}Ct\text{-}Bu)(cod)(CO)_9$ (0.05g) in CH_2Cl_2 (5ml). The solution turned from orange to dark brown and a brown/purple precipitate formed (ca. 0.01g). The mother liquor contained $Ru_3(\mu\text{-}H)(\mu_3\text{-}\eta^2\text{-}C{\equiv}Ct\text{-}Bu)(CO)_9$ as shown by IR spectra. Data on precipitate: IR (KBr disc) 2053 (vs), 1882 (s), 1822 (m), 474 (w), 405 (w) cm^{-1}. Anal. Found C, 2.0; H, 0.0%.

Preparation of $[Ru_3Pt(\mu\text{-}H)(\mu_4\text{-}\eta^2\text{-}C{=}C(H)t\text{-}Bu)(dppe)(CO)_9]^+BF_4^-$, 39.

A CH_2Cl_2 (10ml) solution of $Ru_3Pt(\mu_4\text{-}\eta^2\text{-}C{=}C(H)t\text{-}Bu)(dppe)(CO)_9$ (0.15g, 0.12mmol) was treated with an excess of $HBF_4.Et_2O$. The solution changed colour rapidly from dark red to light orange-yellow. Addition of Et_2O (ca. 10ml) precipitated complex 39, (0.14g, 0.11mmol, 92% yield) as bright orange crystals. IR (CH_2Cl_2) ν_{max} CO 2095(s), 2071 (vs), 2059 (s), 2032 (m), 2023 (m), 2000 (w,sh) cm^{-1}. ^1H NMR (CD_2Cl_2, 295K) δ 7.90-7.27 (m, 20H, C_6H_5), 5.72 (t,1H,C=C(H)t-Bu, J(P-H) = 4.7Hz), 2.8-2.0 (m,4H,CH_2), 0.77 (s,9H,t-Bu), -20.34 (t,1H, Ru(μ-H)Ru, J(Pt-H) = 13, J(P-H) = 2.9Hz); ^{31}P NMR (CD_2Cl_2, 298K) δ 55.1 (d,J(Pt-P) = 3345Hz), 53.2 (d,J(Pt-P) = 3448Hz) as AB quartet (J(P-P) = 19Hz); ^{13}C NMR (CD_2Cl_2, 298K) δ 303.5 (dd, 1C, C=C(H)t-Bu, J(P-C) = 28,23Hz), 136.3-127.6 (m,24C, C_6H_5), 100.2 (s,1C,C=C(H)t-Bu, J(Pt-C) = 73Hz),

39.8 (s,1C,$\underline{C}(CH_3)_3$), 33.7 (s,3C,$C(\underline{CH}_3)_3$), 30.7 (dd, 1C,CH_2, J(Pt-C) = 50, J(P-C) = 38,10Hz), 26.9 (dd,1C,CH_2, J(Pt-C) = 39, J(P-C) = 38,11Hz); for carbonyl parameters see Table 44. Anal. Calcd. for $C_{41}H_{35}BF_4O_9P_2Ru_3Pt$: C, 37.34; H, 2.68. Found: C, 37.32; H, 2.67%

Preparation of $Os_3Pt(\mu\text{-}H)_2(\mu\text{-}CO)(cod)(CO)_9$, 40

$Ru_3Pt(\mu\text{-}H)(\mu_4\text{-}\eta^2\text{-}C{\equiv}Ct\text{-}Bu)(cod)(CO)_9$, (0.127g, 0.132mmol) and $Os_3(\mu\text{-}H)_2(CO)_{10}$, (0.1165g, 0.137mmol) were dissolved in the minimum amount of toluene (ca. 5ml). Standing this solution at ambient temperatures for 12h afforded yellow crystals of $Ru_3(\mu\text{-}H)(\mu_3\text{-}\eta^2\text{-}C{\equiv}Ct\text{-}Bu)(CO)_9$, in addition to large well-formed red/brown crystals of complex 40, (0.081g, 53% yield). As 40 decomposed on chromatographic columns, the products were separated by crystal picking. Spectroscopic data for 40; IR (CH_2Cl_2) ν_{max} CO, 2087 (m), 2062 (vs), 2038 (s), 2005 (s), 1980 (sh), 1940 (w,br), 1769 (w,br) cm^{-1}. ^1H NMR (CD_2Cl_2, 298K), δ 5.52 (s,br,4H, CH=CH, J(Pt-H) = 53Hz), 2.72-2.42 (m,br,CH_2), -21.78 (s,Os(μ-H)Os, J(Pt-H) = 17.0, J(Os-H) = 21.6Hz).

Reaction of $Os_3(\mu\text{-}H)_2(CO)_{10}$ with $Pt(cod)_2$

Equimolar quantities of $Os_3(\mu\text{-}H)_2(CO)_{10}$, (0.042g, 0.049mmol) and $Pt(cod)_2$, (0.022g, 0.053mmol) were dissolved in CD_2Cl_2. ^1H NMR (295K) of the reaction mixture after 30 min at 295K showed highfield resonances due to $Os_3Pt(\mu\text{-}H)_2(\mu\text{-}CO)(cod)(CO)_9$ and unreacted $Os_3(\mu\text{-}H)_2(CO)_{10}$ in addition to resonances due to the unidentified complexes A: δ -12.38 (s,J(Pt-H) = 24.3Hz) and B: δ -20.45 (s). Intensity ratio of hydride signals of $Os_3(\mu\text{-}H)_2(CO)_{10}$:$Os_3(\mu\text{-}H)_2(\mu\text{-}CO)(cod)(CO)_9$:A:B is 8.8:6.0:1.0:1.8.

Reaction of $Os_3Pt(\mu\text{-}H)_2(\mu\text{-}CO)(cod)(CO)_9$ with CO.

A solution of $Os_3Pt(\mu\text{-}H)_2(\mu\text{-}CO)(cod)(CO)_9$ in $CDCl_3$ was treated with CO. The solution changes colour from brown to yellow. ^1H NMR data for reaction mixture (CD_2Cl_2, 224K) δ 5.52 (4H,CH=CH), 2.31 (8H,CH_2), -19.22 (s,2H,Os(μ-H)Os, J(Pt-H) = 22.6Hz). Minor coproduct with highfield resonance at δ -8.99 (s) also present.

REFERENCES.

REFERENCES

1. 'Advanced Inorganic Chemistry', F.A.Cotton and G. Wilkinson, Wiley, Chichester, 5th Edition, 1988.

2. E.L. Muetterties, Science, 1977, 196, 839.

3. M.G. Thomas, B.F. Beier and E.L. Muetterties, J. Am. Chem. Soc., 1976, 98, 1296.

4. E.L. Muetterties, T.N. Rhodin, E. Band, C.F. Brucker and W.R. Pretzer, Chem. Rev., 1979, 79, 91.

5. L.L. Kesmodel, L.H. DuBois and G.A. Somarjai, J. Chem. Phys., 1979, 70, 2180.

6. M.M. Hills, J.E. Parmeter and W.H. Weinberg, J. Am. Chem. Soc., 1987, 109, 597.

7. J.E. Parmeter, M.M. Hills and W.H. Weinberg, J. Am. Chem. Soc., 1986, 108, 3563.

8. M. Moskovits, Acc. Chem. Res., 1979, 12, 229.

9. 'Metal Clusters in Catalysis', eds. B.C. Gates, L. Guczi and H. Knozinger, Elsevier, Amsterdam, 1986.

10. E.L. Muetterties and M.J. Krause, Angew. Chem., Int. Ed. Engl., 1983, 22, 135.

11. R. Whyman in ref 19, Ch.8, p.545.

12. A.J. Deeming and S. Hasso, J. Organomet. Chem., 1976, 114, 313.

13. M. Castiglioni, R. Giordano and E. Sappa, J. Organomet. Chem., 1987, 319, 167.

14. R.M. Laine, R.G. Rinker and P.C. Ford, J. Am. Chem. Soc., 1977, 99, 252.

15. P.C. Ford, Acc. Chem. Res., 1981, 14, 31.

16. J. Venter, M. Kaminsky, G.L. Geoffroy and M.A. Vannice, J. Catal., 1987, 103, 450.

17. S. Uchiyama and B.C. Gates, J. Catal, 1988, 110, 388.

18. B.F.G. Johnson and J. Lewis, Adv. Inorg. Chem. Radiochem., 1981, 24, 255.

19. 'Transition Metal Clusters', ed. B.F.G. Johnson, Wiley, Chichester, 1980.

20. 'Metal Clusters' ed. M. Moskovits, Wiley, Chichester, 1986.

21. H. Vahrenkamp, Adv. Organomet. Chem, 1983, 22, 169.

22. R.D. Adams and I.T. Horváth, Prog. Inorg.Chem., 1985, 33, 127.

23. M.D. Vargas and J.N. Nicholls, Adv. Inorg. Chem. Radiochem, 1986, 30, 123.

24. W.L. Gladfelter and G.L. Geoffroy, Adv. Organomet. Chem., 1980, 18, 207.

25. D.H. Roberts and G.L. Geoffroy in "Comprehensive Organometallic Chemistry", eds. G. Wilkinson, F.G.A. Stone and E.W. Abel, Pergamon, Oxford, 1982, Vol. 6, Ch.40, p.763.

26. P. Lemoine, Coord. Chem. Rev., 1988, 83, 169.

27. M. McPartlin and D.M.P. Mingos, Polyhedron, 1984, 3, 1321.

28. S.M. Owen, Polyhedron, 1988, 7, 253.

29. M.O. Albers, D.J. Robinson and N.J. Coville, Coord. Chem. Rev., 1986, 69, 127.

30. C.E. Housecroft, Polyhedron, 1987, 6, 1935.

31. E. Sappa, A. Tiripicchio, A.J. Carty and G.E. Toogood, Prog. Inorg. Chem., 1987, 35, 437.

32. H.D. Kaesz, C.B. Knobler, M.A. Andrews, G. van Buskirk, R. Szostak, C.E. Strouse, Y.C. Lin and A. Mayr, Pure and Appl. Chem., 1982, 54, 131.

33. K. Burgess, Polyhedron, 1984, 3, 1175.

34. A.J. Carty, Pure and Appl. Chem., 1982, 54, 113.

35. E. Sappa, A. Tiripicchio and P. Braunstein, Chem. Rev., 1983, 83, 203.

36. P. R. Raithby and M.J. Rosales, Adv. Inorg. Chem. Radiochem., 1985, 29, 169.

37. J.S. Bradley, Adv. Organomet. Chem., 1983, 22, 1.

38. W.L. Gladfelter, Adv. Organomet. Chem., 1985, 24, 41.

39. B.F.G. Johnson, in ref. 19. Ch. 1, p.2.

40. J. A. Connor, in ref. 19, Ch.5, p.345.

41. A. Shojaie and J.D. Atwood, Organometallics, 1985, 4, 187.

42. A. Poë, and V.C. Sekhar, Inorg. Chem., 1985, 24, 4376.

43. C.W. Bradford and R.S. Nyholm, J. Chem. Soc., Dalton Trans., 1973, 529.

44. A. J. Deeming, R.E. Kimber and M. Underhill, J. Chem. Soc., Dalton Trans, 1973, 2589.

45. G.J. Gainsford, J.M. Guss, P.R. Ireland, R. Mason, C.W. Bradford and R.S. Nyholm, J. Organomet. Chem., 1972, 40, C70.

46. M.J. Mays and P.D. Gavens, J. Organomet. Chem., 1977, 124, C37.

47. M.J. Mays and P.D. Gavens, J. Chem.Soc., Dalton Trans, 1980, 911.

48. M.J. Mays and P.D. Gavens, J. Organomet Chem., 1979, 177, 443.

49. A.J. Poë and M.V. Twigg, J. Chem. Soc., Dalton Trans, 1974, 1860.

50. A.J. Poë and M.V. Twigg, Inorg. Chem., 1974, 13, 2983.

51. P.R. Raithby in ref 19, Ch. 2, p.5.

52. G.L. Geoffroy, in ref. 9, Ch.2, p.21.

53. N.W. Sidgwick and R.W. Bailey, Proc. R. Soc., London Ser.A, 1934, 144, 521.

54. K. Wade, in ref. 19, Ch. 3, p.193.

55. D.M.P. Mingos, Nature Phys. Sci (London), 1972, 236, 99.

56. L.R. Martin, F.W.B. Einstein and R.K. Pomeroy, Organometallics, 1988, 7, 294.

57. K. Wade, Adv. Inorg. Chem. Radiochem., 1976, 18, 1.

58. A.J. Stone, Inorg. Chem., 1981, 20, 563.

59. D.M.P. Mingos, Acc. Chem. Res, 1984, 17, 311.

60. D.M.P. Mingos, J. Chem. Soc., Chem. Commun, 1983, 706.

61. K.P. Hall and D.M.P. Mingos, Prog. Inorg. Chem., 1984, 32, 281.

62. D.M.P. Mingos and R.W.M. Wardle, Transition Met. Chem., 1985, 10, 441.

63. K.P. Hall, D.I. Gilmour and D.M.P. Mingos, J. Organomet. Chem., 1984, 268, 275.

64. D.M.P. Mingos and D.G. Evans, J. Organomet Chem., 1983, 251, C13.

65. D.M.P. Mingos and D.G.Evans, J. Organomet. Chem., 1982, 240, 321.

66. D.M.P. Mingos J. Chem. Soc., Chem. Commun, 1985, 1352.

67. N.M. Boag, J. Chem. Soc., Chem. Commun, 1988, 617.

68. G. Longini, P. Chini, L.D. Lower and L.F. Dahl, J. Am. Chem. Soc., 1975, 97, 5034.

69. B.K. Teo, Inorg. Chem., 1984, 23, 1251.

70. B.K. Teo, G. Longini and F.R.K. Chung, Inorg. Chem, 1984, 23, 1257.

71. B.K. Teo, Inorg. Chem., 1984, 23, 1627.

72. B.K. Teo, Inorg. Chem., 1985, 24, 4209.

73. D.M.P. Mingos, Inorg. Chem., 1985, 24, 114.

74. B.K. Teo, Inorg. Chem., 1985, 24, 115.

75. J. W.Lauher, J. Am. Chem. Soc., 1978, 100, 5305.

76. B.K. Teo, J. Chem. Soc., Chem. Commun, 1983, 1362.

77. D.M.P. Mingos and L. Zhenyang, J. Chem. Soc., Dalton Trans, 1988, 1657.

78. B.F.G. Johnson, J. Lewis and P. Kilty, J. Chem. Soc., A., 1968, 2859.

79. S.A.R. Knox, J.W. Koepke, M.A. Andrews and H.D. Kaesz J. Am. Chem. Soc., 1975, 97, 3942.

80. M. R. Churchill, F.J. Hollander and J.P. Hutchinson, Inorg. Chem., 1977, 16, 2697.

81. V.F. Allen, R. Mason and P.B. Hitchcock, J. Organomet. Chem., 1977, 140, 297.

82. A.G. Orpen, A.V. Rivera, D. Pippard, G.M. Sheldrick and K.D. Rouse, J. Chem. Soc., Chem. Commun, 1978, 723.

83. R.W. Broach, and J.M. Williams, Inorg. Chem., 1979, 18, 314.

84. D.E. Sherwood and M.B. Hall, Inorg. Chem., 1982, 21, 3458.

85. J.R. Shapley, J.B. Keister, M.R. Churchill and B.G. De Boer, J. Am. Chem. Soc., 1975, 97, 4145.

86. R. Hoffmann and W.N. Lipscomb, J. Chem. Phys., 1962, 36, 3179.

87. M.R. Churchill and B.G. De Boer, Inorg. Chem., 1977 16, 878.

88. J.B. Keister and J.R. Shapley, Inorg. Chem., 1982, 21, 3304.

89. R.D. Adams and N.M. Golembeski, J. Am. Chem. Soc., 1979, 101, 2579.

90. M.R. Churchill and B.G. De Boer, Inorg. Chem., 1977, 16, 2379.

91. R.D. Adams and N.M. Golembeski, Inorg. Chem., 1979, 18, 1909.

92. S. Kennedy, J.J. Alexander and S.G. Shore, J. Organomet. Chem., 1981, 219, 385.

93. A.J. Deeming, S. Donovan-Mtunzi, S.E. Kabir, A.J. Arce and Y. De Sanctis, J. Chem. Soc., Dalton Trans., 1987, 1457.

94. A. J. Deeming, Adv. Organomet. Chem., 1986, 26, 1.

95. J.B. Keister and J.R. Shapley, J. Organomet Chem., 1975, 85, C29.

96. A.J. Deeming, S. Hasso and M. Underhill, J. Chem. Soc., Dalton Trans., 1975, 1614.

97. A.D. Clauss, M. Tachikawa, J.R. Shapley and C.G. Pierpont, Inorg. Chem., 1981, 20, 1528.

98. M. Tachikawa, J.R. Shapley and C.G. Pierpont, J. Am. Chem. Soc., 1975, 97, 7172.

99. G. Ferraris and G. Gervasio, J. Chem. Soc., Dalton Trans., 1974, 1813.

100. M. Valle, G. Cetini, O. Gambina and E. Sappa, Atti. Acad. Sci., Torino, 1969, 105, 913.

101. R.B. Calvert and J.R. Shapley, J. Am. Chem. Soc., 1977, 99, 5225.

102. R.B. Calvert and J.R. Shapley, J. Am. Chem. Soc., 1978, 100, 7726.

103. R.B. Calvert, J.R. Shapley, A.J. Shultz, J.M. Williams, S.L. Suib and G.D. Stucky, J. Am. Chem. Soc., 1978, 100, 6240.

104. A.J. Shultz, J.M. Williams, R.B. Calvert, J.R. Shapley and G.D. Stucky, Inorg. Chem., 1979, 18, 319.

105. W.A.Herrmann, Adv. Organomet.Chem., 1981, 20, 159.

106. C.J. Cardin, D.J. Cardin, H.E. Parge and J.M. Power, J. Chem. Soc., Chem. Commun., 1984, 609.

107. G.D. Jarvinen and R.R. Ryan, Organometallics, 1984, 3, 1434.

108. R. Hoffmann, Angew. Chem., Int. Ed. Engl., 1982, 21, 711.

109. K.A. Azam and A.J. Deeming, J. Chem. Soc., Chem. Commun., 1977, 472.

110. K.A. Azam, A.J. Deeming and I.P. Rothwell, J. Chem. Soc., Dalton Trans, 1981, 91.

111. A.J. Arce and A.J. Deeming, J. Chem. Soc., Chem. Commun., 1982, 364.

112. B.F.G. Johnson, D.A. Kaner, J. Lewis and P.R. Raithby J. Organomet. Chem., 1981, 215, C33.

113. K. Burgess, B.F.G. Johnson, D.A. Kaner, J. Lewis, P.R. Raithby, S.N. Azman and B. Syedd-Mustaffa, J. Chem. Soc., Chem. Commun., 1983, 455.

114. A.J. Deeming and S.E. Kabir, J. Organomet. Chem., 1988, 340, 359.

115. R.E. Benfield, B.F.G. Johnson, J. Lewis, P.R. Raithby, C. Zuccaro and K. Henrick, Acta. Crystallogr. Sect. B, 1979, 35, 2210.

116. J.A. Clucas, M.M. Harding and A.K. Smith, J. Chem. Soc., Chem. Commun., 1985, 1280.

117. B.F.G Johnson, D.A. Kaner, J. Lewis and P.R. Raithby J. Chem. Soc., Chem. Commun., 1981, 753.

118. M. Fajardo, M.P. Gomez-sal, H.D. Holden, B.F.G Johnson, J. Lewis, R.C.S. McQueen and P.R. Raithby, J. Organomet. Chem., 1984, 267, C25.

119. R.D. Adams, N.M. Golembeski and J.P. Selegue, Inorg. Chem., 1981, 20, 1242.

120. R.D. Adams and N.M. Golembeski, J.Am. Chem. Soc., 1979, 101, 1306.

121. R.D. Adams and J.P. Selegue, J. Organomet Chem., 1980, 195, 223.

122. R.D. Adams, N.M. Golembeski and J.P. Selegue, J. Am. Chem. Soc., 1981, 103, 546.

123. S.C. Brown and J. Evans, J. Chem. Soc., Dalton Trans, 1982, 1049.

124. J.A. Clucas, D.F. Foster, M.M. Harding and A.K. Smith J. Chem. Soc., Chem. Commun., 1984, 949.

125. J.A. Clucas, M.M. Harding and A.K. Smith, J. Chem. Soc., Chem. Commun., 1985, 1280.

126. M.I. Bruce, E. Horn, O. bin Shawkataly, M.R. Snow, E.R.T. Tiekink and M.L. Williams, J. Organomet. Chem., 1986, 316, 187.

127. J.A. Clucas, P.A. Dolby, M.M. Harding and A.K. Smith, J. Chem. Soc., Chem. Commun., 1987, 1829.

128. R.A. Bartlett, C.J. Cardin, D.J. Cardin, G.A. Lawless, J.M. Power, and P.P. Power, J. Chem. Soc., Chem. Commun., 1988, 312.

129. D.G. Evans and D.M.P. Mingos, Organometallics, 1983, 2, 435.

130. A. Choplin, M. Leconte, J.M. Bassat, S. Shore and W.L. Hsu, J. Mol. Catal., 1983, 21, 389.

131. J.R. Budge, B.F. Lücke, B.C. Gates and J. Toran, J. Catal, 1985, 91, 272.

132. E. Sappa, A.M. Manotti Lanfredi and A. Tiripicchio, J. Organomet. Chem., 1981, 221, 93.

133. M. Castiglioni, E. Sappa, M. Valle, M. Lanfranchi and A. Tiripicchio, J. Organomet. Chem., 1983, 241, 99.

134. M. Castiglioni, R. Giordano, E. Sappa, A. Tiripicchio and M. Tiripicchio-Camellini, J. Chem. Soc., Dalton Trans, 1986, 23.

135. M. Castiglioni, R. Giordano and E. Sappa, J. Organomet. Chem., 1988, 342, 111.

136. M.R. Churchill, C. Bueno, W.L. Hsu, J.S. Plotkin and S.G. Shore, Inorg. Chem., 1982, 21, 1958.

137. G.L. Geoffroy, J.R. Fox, E. Burkhardt, H.C. Foley, A.P. Harley and R. Rosen, Inorg. Synth. 1982, 21, 57.

138. A.L. Rhiengold, B.C. Gates, J.P. Scott and J.R. Budge J. Organomet. Chem., 1987, 331, 81.

139. S. Bhaduri, B.F.G. Johnson, J. Lewis, P.R. Raithby and D.J. Watson, J. Chem. Soc., Chem. Commun., 1978, 343.

140. M.R. Churchill, C. Bueno, S. Kennedy, J.C. Bricker, J.S. Plotkin and S.G. Shore, Inorg. Chem., 1982, 21, 627.

141. L.Y. Hsu, W.L. Hsu, D.Y. Jan, A.G. Marshall and S.G. Shore, Organometallics, 1984, 3, 591.

142. S.G. Shore, W.L. Hsu, C.R. Weisenberger, M.L. Caste, M.R. Churchill, and C. Bueno, Organometallics, 1982, 1, 1405.

143. S.G. Shore, W.L. Hsu, M.R. Churchill and C. Bueno J. Am. Chem. Soc., 1983, 105, 655.

144. D.Y. Jan, L.Y. Hsu, W.L. Hsu and S.G. Shore, Organometallics, 1987, 6, 274.

145. L.Y. Hsu, W.L. Hsu, D.Y. Jan and S.G. Shore, Organometallics, 1986, 5, 1041.

146. L.J. Farrugia, J.A.K. Howard, P. Mitrprachachon, F.G.A. Stone and P. Woodward, J. Chem. Soc., Dalton Trans, 1981, 171.

147. L.J. Farrugia, J.A.K. Howard, P. Mitrprachachon, F.G.A. Stone and P. Woodward, J. Chem. Soc., Dalton Trans, 1981, 155.

148. L.J. Farrugia, J.A.K. Howard, P. Mitrprachachon, F.G.A. Stone and P. Woodward, J. Chem. Soc., Dalton Trans, 1981, 162.

149. J. Lewis, R.B.A. Pardy and P.R. Raithby, J. Chem. Soc., Dalton Trans, 1982, 1509.

150. R.D. Adams, I.T. Horvàth and B.E. Segmueller, Organometallics, 1982, 1, 1537.

151. L.J. Farrugia, A.G. Orpen and F.G.A. Stone, Polyhedron, 1983, 2, 171.

152. A.B. Antonova, S.V. Kovalenko, E.D. Korniyets, A.A. Johansson, Y.T. Struchkov and A.I. Yanovsky, J. Organomet. Chem., 1984, 267, 299.

153. R.D. Adams and J.P. Selegue in "Comprehensive Organometallic Chemistry", eds. G. Wilkinson, F.G.A. Stone and E.W. Abel, Pergamon Press, Oxford, 1982, Vol. 4, p. 967.

154. A. Bertolucci, M. Freni, P. Romiti, G. Ciani, A. Sironi and V.G. Albano, J. Organomet. Chem., 1976, 113, C61.

155. G. Ciani, G. D'Alfonso, M. Freni, P. Romiti, A. Sironi and A. Albinati, J. Organomet. Chem., 1977, 136, C49.

156. G. Ciani, G. D'Alfonso, M. Freni, P. Romiti and A. Sironi, J. Organomet. Chem., 1982, 226, C31.

157. T. Beringhelli, G. Ciani, G.D'Alfonso, A. Sironi and M. Freni, J. Organomet. Chem., 1982, 233, C46.

158. G. Ciani, G.D'Alfonso, M. Freni, P. Romiti and A. Sironi, J. Organomet. Chem., 1980, 186, 353.

159. T. Beringhelli, G.D'Alfonso, M. Freni, G. Ciani, M. Moret and A. Sironi, J. Organomet. Chem., 1988, 339, 323.

160. G. Ciani, G.D'Alfonso, M. Freni, P. Romiti and A. Sironi, J. Organomet. Chem., 1981, 219, C23.

161. R. Bonfichi, G. Ciani, G.D'Alfonso, P. Romiti and A. Sironi, J. Organomet. Chem., 1982, 231, C35.

162. T. Beringhelli, G.D'Alfonso, G. Ciani and H. Molinari, Organometallics, 1987, 6, 194.

163. T. Beringhelli, G. Ciani, G.D'Alfonso, H. Molinari, A. Sironi and M. Freni, J. Chem. Soc., Chem. Commun., 1984, 1327.

164. T. Beringhelli, G. Ciani, G. D'Alfonso, H. Molinari and A. Sironi, Inorg. Chem., 1985, 24, 2666.

165. T. Beringhelli, G. Ciani, G. D'Alfonso and M. Freni, J. Organomet. Chem., 1986, 311, C51.

166. M.R. Churchill, P.H. Bird, H.D. Kaesz, R. Bau and B. Fontal, J. Am. Chem. Soc., 1968, 90, 7135.

167. T. Beringhelli, G. Ciani, G.D'Alfonso, P. Romiti, A. Sironi and M. Freni, Inorg. Chem., 1984,23,2849.

168. T.Beringhelli, G.D'Alfonso, M. Freni, G. Ciani, A. Sironi and H. Molinari, J. Chem. Soc., Dalton Trans, 1986, 2691.

169. T. Beringhelli, G. Ciani, G.D'Alfonso, V. De Maldé and M. Freni, J. Chem. Soc., Chem. Commun., 1986, 735.

170. J.F. Blount, L.F. Dahl, C. Hoogzand and W. Hubel, J. Am. Chem. Soc., 1966, 88, 292.

171. D. Osella, R. Gobetto, P. Montangero, P. Zanello and A. Cinquantini, Organometallics, 1986, 5, 1247.

172. A.J. Carty, N.J. Taylor and E. Sappa, Organometallics, 1988, 7, 405.

173. R. Mason and K.M. Thomas, Ann. N.Y. Acad. Sci., 1974, 239, 225.

174. R.J. Goudsmit, B.F.G. Johnson, J. Lewis, P.R. Raithby and M.J. Rosales, J. Chem. Soc., Dalton Trans, 1983, 2257.

175. B.E.R. Schilling and R. Hoffmann, J. Am. Chem. Soc., 1979, 101, 3456.

176. J.F. Halet, J.Y. Saillard, R. Lissillour, M.J. McGlinchey and G. Jaouen, Inorg. Chem., 1985, 24, 218.

177. G. Granozzi, E. Tondello, M. Casarin, S. Aime and D. Osella, Organometallics, 1983, 2, 430.

178. J.A. Hriljac and D.F. Shriver, J.Am. Chem. Soc., 1987, 109, 6010.

179. A.D. Clauss, J.R. Shapley, C.N. Wilker and R. Hoffmann, Organometallics, 1984, 3, 619.

180. V. Busetti, G. Granozzi, S. Aime, R. Gobetto and D. Osella, Organometallics, 1984, 3, 1510.

181. L. Busetto, J.C. Jeffery, R.M. Mills, F.G.A. Stone, M. Went and P. Woodward, J. Chem. Soc., Dalton Trans, 1983, 101.

182. C.G. Pierpont, Inorg. Chem., 1977, 16, 639.

183. D. Boccardo, M. Botta, R. Gobetto, D. Osella, A. Tiripicchio and M. Tiripicchio Camellini, J. Chem. Soc., Dalton Trans, 1988, 1249.

184. S. Aime, L. Milone, D. Osella, A. Tiripicchio and A.M. Manotti Lanfredi, Inorg. Chem., 1982, 21, 501.

185. E. Roland, W. Bernhardt and H. Vahrenkamp, Chem. Ber., 1985, 118, 2858.

186. P. Braunstein, J. Rose and O. Bars, J. Organomet. Chem., 1983, 252, C101.

187. F. van Gastel, S.A. MacLaughlin, M. Lynch, A.J. Carty, E. Sappa, A. Tiripicchio and M. Tiripicchio Camellini J. Organomet Chem., 1987, 326, C65.

188. F.W.B. Einstein, K.G. Tyers, A.S. Tracey and D. Sutton, Inorg. Chem., 1986, 25, 1631.

189. E. Sappa, J. Organomet. Chem., 1987, 323, 83.

190. S. Aime, R. Bertoncello, V. Busetti, R. Gobetto, G. Granozzi and D. Osella, Inorg. Chem., 1986, 25, 4004.

191. A.D. Clauss, J.R. Shapley, and S.R. Wilson, J.Am. Chem. Soc., 1981, 103, 7386.

192. T. Jaeger, S. Aime and H. Vahrenkamp, Organometallics, 1986, 5, 245.

193. H.H. Ohst and J.K. Kochi, Organometallics, 1986, 5, 1359.

194. R.D. Adams, J.E. Babin and M. Tasi, Inorg. Chem., 1986, 25, 4514.

195. J.F. Halet, R. Hoffmann and J.Y. Saillard, Inorg. Chem., 1985, 24, 1695.

196. H. Vahrenkamp and D. Walter, Organometallics, 1982, 1, 874.

197. J.S. Field, R.J. Haines and D.N. Smit, J. Organomet. Chem., 1982, 224, C49.

198. J.S. Field, R.J. Haines, D.N. Smit, K. Natarajan, O. Scheidsteger and G. Huttner, J. Organomet. Chem., 1982, 240, C23.

199. J.S. Field, R.J. Haines and D.N. Smit, J. Chem. Soc., Dalton Trans, 1988, 1315.

200. J.S. Field, R.J. Haines, E. Minshall and D.N. Smit, J. Organomet. Chem., 1986, 310, C69.

201. T. Jaeger and H. Vahrenkamp, Z. Naturforsch.B:Anorg. Chem., Org. Chem., 1986, 41B(6), 789.

202. E.G. Bryan, B.F.G. Johnson and J. Lewis, J. Chem. Soc., Dalton Trans., 1977, 1328.

203. M. Tachikawa and J.R. Shapley, J. Organomet. Chem., 1977, 124, C19.

204. M.O. Albers and N.J. Colville, Coord. Chem. Rev., 1984, 53, 227.

205. C.J. Cardin, D.J. Cardin, N.B. Kelly, G.A. Lawless and M.B. Power, J. Organomet. Chem., 1988, 341, 447.

206. G.A. Foulds, B.F.G. Johnson and J. Lewis, J. Organomet. Chem., 1985, 296, 147.

207. B.F.G. Johnson, J. Lewis and D. Pippard, J. Organomet. Chem., 1978, 145, C4.

208. P.A. Dawson, B.F.G. Johnson, J. Lewis, J. Puga, P.R. Raithby and M.J. Rosales, J. Chem. Soc., Dalton Trans, 1982, 233.

209. J. Howell, A. Rossi, D. Wallace, K. Haraki and R. Hoffmann, Q.C.P.E, 1977, 10, 344.

210. B.F.G. Johnson, J. Lewis and D.A. Pippard, J. Chem. Soc., Dalton Trans., 1981, 407.

211. K. Dahlinger, A.J. Poë, P.K. Sayal and V.C. Sekhar, J. Chem. Soc., Dalton Trans., 1986, 2145.

212. S.B. Colbran, F.J. Lahoz, P.R. Raithby, J. Lewis, B.F.G. Johnson and C.J. Cardin, J. Chem. Soc., Dalton Trans, 1988, 173.

213. R.J. Goudsmit, J.G. Jeffrey, B.F.G. Johnson, J. Lewis R.C.S. McQueen, A.J. Sanders and J.C. Lin, J. Chem Soc., Chem. Commun., 1986, 24.

214. C.J. Cardin, D.J. Cardin, G.A. Lawless, J.M. Power, M.B. Power and M.B. Hursthouse, J. Organomet. Chem., 1987, 325, 203.

215. G.A. Foulds, B.F.G. Johnson, J. Lewis and R.M. Sorrell, J. Chem. Soc., Dalton Trans., 1986, 2515.

216. J.R. Shapley, G.A. Pearson, M. Tachikawa, G.E. Schmidt, M.R. Churchill and F.J. Hollander, J.Am. Chem. Soc., 1977, 99, 8064.

217. R.D. Adams, I.T. Horváth and P. Mathur, Organometallics, 1984, 3, 623.

218. E.J. Ditzel, B.F.G. Johnson, J. Lewis, P.R. Raithby and M.J. Taylor, J. Chem. Soc., Dalton Trans., 1985, 555.

219. A.J. Arce, A.J. Deeming, M.B. Hursthouse and N.P.C. Walker, J. Chem. Soc., Dalton Trans, 1987, 1861.

220. B.F.G. Johnson, J. Lewis and T.I. Odiaka, J. Organomet. Chem., 1986, 307, 61.

221. A.J. Deeming, A.J. Arce, Y. De Sanctis, P.A. Bates and M.B. Hursthouse, J. Chem. Soc., Dalton Trans, 1987, 2935.

222. B.F.G. Johnson, J. Lewis, P.R. Raithby and S.W. Swankey, J. Organomet. Chem., 1982, 231, C65.

223. J.R. Shapley, A.C. Sievert, M.R. Churchill and H.J. Wasserman, J. Am. Chem. Soc., 1981, 103, 6975.

224. E.D. Morrison, G.L. Geoffroy, A.L. Rheingold and W.C. Fultz, Organometllics, 1985, 4, 1413.

225. E.D. Morrison, G.R. Steinmetz, G.L. Geoffroy, W.C. Fultz and A.L. Rheingold, J.Am. Chem. Soc., 1984, 106, 4783.

226. E.D. Morrison, S.L. Bassner and G.L. Geoffroy, Organometallics, 1986,5, 408.

227. E.J. Ditzel, M.P. Gómez-Sal, B.F.G. Johnson, J. Lewis, and P.R. Raithby, J. Chem. Soc., Dalton Trans., 1987, 1623.

228. B.F.G. Johnson, R. Khattar, J. Lewis, P.R. Raithby and D.N. Smit, J. Chem. Soc., Dalton Trans, 1988, 1421.

229. C. Couture and D.H. Farrar, J.Chem.Soc., Chem Commun., 1985, 197.

230. B.F.G. Johnson, J. Lewis, M.McPartlin, J. Morris, G.L. Powell, P.R. Raithby and M.D. Vargas, J. Chem. Soc., Chem. Commun., 1986, 429.

231. J.A. Clucas, R.H. Dawson, P.A. Dolby, M.M. Harding K. Pearson and A.K. Smith, J. Organomet. Chem., 1986, 311, 153.

232. M.I. Bruce, Coord. Chem. Rev., 1987, 76, 1, and refs therein.

233. M. Arewgoda, B.H. Robinson and J. Simpson, J. Am. Chem Soc., 1983, 105, 1893.

234. J. Pursiainen, T.A. Pakkanen and J. Jääskeläinen, J. Organomet. Chem., 1985, 290, 85.

235. M.I. Bruce, M.J. Liddell, C.A. Hughes, B.W. Skelton and A.H. White, J. Organomet. Chem., 1988, 347, 157.

236. M.I. Bruce, M.J. Liddell, C.A. Hughes, J.M. Patrick, B.W. Skelton and A.H. White, J. Organomet. Chem., 1988, 347, 181.

237. M.I. Bruce, M.J. Liddell, O.Bin Shawkataly, C.A. Hughes, B.W. Skelton and A.H. White, J. Organomet. Chem., 1988, 347, 207.

238. M.I. Bruce, J.G. Matisons, J.M. Patrick, A.H. White and A.C. Willis, J.Chem.Soc., Dalton Trans., 1985, 1223.

239. M.I. Bruce, D.C. Kehoe, J.G. Matisons, B.K. Nicholson, P.H. Rieger and M.L. Williams, J.Chem. Soc., Chem. Commun., 1982, 442.

240. G. Lavigne and H.D. Kaesz, J.Am.Chem.Soc., 1984, 106, 4647.

241. G. Lavigne and H.D. Kaesz in ref. 9., Ch.4, p.43.

242. H. Vahrenkamp, E.J. Wucherer and D. Wolters, Chem. Ber., 1983, 116, 1219.

243. M.I. Bruce, G. Shaw and F.G.A. Stone, J. Chem. Soc., Dalton Trans, 1972, 1781.

244. L.J. Farrugia, J.A.K. Howard, P. Mitrprachachon, F.G.A. Stone and P. Woodward, J. Chem. Soc., Dalton Trans., 1981, 1274.

245. R.D. Adams, T.S.A. Hor, Inorg. Chem., 1984, 23, 4723.

246. C. Couture, D.H. Farrar and R.J. Goudsmit, Inorg. Chim. Acta., 1984, 89, L29.

247. C. Couture and D.H. Farrar, J. Chem. Soc., Dalton Trans, 1987, 2245.

248. C. Couture and D.H. Farrar, J. Chem. Soc., Dalton Trans, 1987, 2253.

249. R.D. Adams, T.S.A. Hor, and I.T. Horváth, Inorg. Chem., 1984, 23, 4733.

250. L.J. Farrugia, A.D. Miles and F.G.A. Stone, J. Chem. Soc., Dalton Trans, 1985, 2437.

251. B.F.G. Johnson, D.A. Kaner, J. Lewis, P.R. Raithby and M.J. Taylor, Polyhedron, 1982, 1, 105.

252. R.D. Adams, J.E. Babin, R. Mathab and S. Wang, Inorg. Chem., 1986, 25, 1623.

253. R.D. Adams, I.T. Horváth and S. Wang, Inorg. Chem., 1986, 25, 1617.

254. G.D. Williams, M.C.Lieszovszky, C.A. Mirkin and G.L. Geoffroy, Organometallics, 1986, 5, 2228.

255. B. Norén and P. Sundberg, J. Chem. Soc., Dalton Trans, 1987, 3103.

256. P. Sundberg, J. Chem. Soc., Chem. Commun, 1987, 1307.

257. M.R. Churchill and F.J. Hollander, Inorg. Chem., 1979, 18, 843.

258. L.J. Farrugia, M. Green, D.R. Hankey, M. Murray, A.G. Orpen and F.G. A. Stone, J. Chem. Soc., Dalton Trans, 1985, 177.

259. T.A. Albright, J.K. Burdett and M.-H Whangbo, "Orbital Interactions in Chemistry", Wiley-Interscience Chichester, 1985.

260. P. Ewing and L.J. Farrugia, New. J. Chem., 1988, 12, 409.

261. H. Pepermans, C. Hoogzand and P. Geerlings, J. Organomet. Chem., 1986, 306, 395.

262. R.D. Adams and N.M. Golembeski, Inorg. Chem., 1979, 18, 2255.

263. Y. Chi, J.R. Shapley, M.R. Churchill and Y-J.Li, Inorg. Chem., 1986, 25, 4165.

264. S. Aime, D. Osella, L. Milone and E. Rosenberg, J. Organomet. Chem., 1981, 213, 207.

265. P. Ewing, L.J. Farrugia and D.S. Rycroft, Organometallics, 1988, 7, 859.

266. A.A. Koridze, O.A. Kizas, N.E. KoloboVa, P.V. Petrovskii and E.I. Fedin, J. Organomet. Chem., 1984, 265, C33.

267. (a) E.C. Constable, B.F.G. Johnson, J. Lewis, G.N. Pain and M.J. Taylor, J. Chem. Soc., Chem. Commun., 1982, 754. (b) S.B. Colbran, B.F.G. Johnson, F.J. Lahoz, J. Lewis, and P.R. Raithby, J. Chem. Soc., Dalton Trans, 1988, 1199.

268. J.S. Holmgren, J.R. Shapley and P.A. Belmonte, J. Organomet. Chem., 1985, 284, C5.

269. P.M. Treichel, Adv. Organomet. Chem., 1973, 11, 21.

270. M. Green, J.A.K. Howard, M. Murray, J.L. Spencer and F.G.A. Stone, J. Chem. Soc., Dalton Trans., 1977, 1509.

271. A.G. Orpen, J. Chem. Soc., Dalton Trans, 1980, 2509.

272. L.R. Beanan and J.B. Keister, Organometallics, 1985, 4, 1713.

273. R. Ugo and R. Psaro, J. Mol. Catal., 1983, 20, 53.

274. J.S. Holmgren, J.R. Shapley, S.R. Wilson and W.T. Pennington, J. Am. Chem. Soc., 1986, 108, 508.

275. D. Nucciarone, N.J. Taylor, A.J. Carty, A. Tiripicchio M. Tiripicchio-Camellini and E. Sappa, Organometallics 1988, 7, 118.

276. D. Nucciarone, S.A. MacLaughlin, N.J. Taylor and A.J. Carty, Organometallics, 1988, 7, 106.

277. D.M.P. Mingos, Transition Met. Chem., 1978, 3, 1.

278. G.J. Kubas, Inorg. Chem., 1979, 18, 182.

279. R.R. Ryan, G.J. Kubas, D.C. Moody and P.G. Eller, Struct. Bonding. (Berlin), 1981, 46, 47.

280. P.L. Bogdan, M. Sabat, S.A. Sunshine, C. Woodcock and D.F. Shriver, Inorg. Chem., 1988, 27, 1904.

281. D. Braga, R. Ros and R. Roulet, J. Organomet. Chem. 1985, 286, C8.

282. C.E. Briant, D.G. Evans and D.M.P. Mingos, J. Chem. Soc., Dalton Trans, 1986, 1535.

283. C.E. Briant, B.R.C. Theobald and D.M.P. Mingos, J. Chem. Soc., Chem. Commun., 1981, 963.

284. S.G. Bott, O.J. Ezomo and D.M.P. Mingos, J. Chem. Soc., Chem. Commun., 1988, 1046.

285. D.M.P. Mingos and R.W.M. Wardle, J. Chem. Soc., Dalton Trans., 1986, 73.

286. B.E.R. Schilling, R. Hoffmann and D.L. Lichtenberger J.Am. Chem. Soc., 1979, 101, 585.

287. L.J. Farrugia, to be published.

288. C.S. Browning, D.H. Farrar, R.R. Gukathasan and S.A. Morris, Organometallics, 1985, 4, 1750.

289. This complex has been structurally characterised by D.M.P. Mingos, et al (private communcation).

290. N. Vistwanathan, E.D. Morrison, G.L. Geoffroy, S.J. Geib and A.L. Rheingold, Inorg. Chem., 1986, 25, 3100.

291. R.D. Adams and W.L. Yang, J. Am. Chem. Soc., 1983, 105, 235.

292. C.J. Cardin, D.J. Cardin, J.M. Power and M.B. Hursthouse, J. Am. Chem. Soc., 1985, 107, 505.

293. A. Albinati, U. von Gunten, P.S. Pregosin and H.J. Ruegg, J. Organomet. Chem., 1985, 295, 239.

294. L.J. Guggenberger, J. Chem. Soc., Chem. Commun., 1968, 9, 13.

295. Y.I. Yermakov and B.N. Kuznetsov, J. Mol. Catal., 1980, 9, 13.

296. L. Guczi in ref 9, Ch. 10, p. 547.

297. B.F.G. Johnson, personal communication.

298. J. Knight and M.J. Mays, J. Chem. Soc., A, 1970, 2967.

299. A.J. Deeming, K.I. Hardcastle and S.E. Kabir, J. Chem. Soc., Dalton Trans, 1988, 827.

300. J. Powell, A. Rossi, D. Wallace, K. Faraki and R. Hoffmann, Q.C.P.E, 1977, 10, 344.

301. E.G. Bryan, W.G. Jackson, B.F.G. Johnson, J.W. Kelland, J. Lewis and K.T. Schropp, J. Organomet. Chem., 1976, 108, 385.

302. A.A. Koridze, O.A. Kizas, N.M. Astakhova, P.V. Petrovskii, and Y.K. Grishin, J. Chem. Soc., Chem. Commun., 1981, 853.

303. R.G. Teller and R. Bau, Struct. Bonding (Berlin), 1981, 44, 1.

304. M.A. Gallop, B.F.G. Johnson and J. Lewis, J. Chem. Soc., Chem. Commun., 1987, 1831.

305. G.A. Morris and R.J. Freeman, J. Mag. Reson., 1978, 29, 433.

306. M. Green, J.A.K. Howard, R.N. Mills, G.N. Pain, F.G.A. Stone and P. Woodward, J. Chem. Soc., Chem. Commun., 1981, 869.

307. E. Band and E.L. Muetterties, Chem. Rev., 1978, 78, 639.

308. R.D. Adams, Acc. Chem. Res., 1983, 16, 67.

309. R.D. Pergola, L. Garlaschelli, S. Martinengo, F. de martin, M. Manassero and M. Sansoni, Gazz. Chim. Ital., 1987, 117, 245.

310. R.D. Pergola, L. Garlaschelli, S. Martinengo, F. de martin, M. Manassero and N. Masciocchi, J. Chem. Soc., Dalton Trans, 1988, 2307.

311. R.D. Adams and Z. Dawoodi, J. Am. Chem. Soc., 1981, 103, 6510.

312. K. Seitz and U. Behrens, J. Organomet. Chem., 1985, 294, C9.

313. D. Wormsbächer, R. Drews, F. Edelmann and U. Behrens, J. Organomet. Chem., 1984, 270, 93.

314. D. Wormsbächer, F. Edelmann and U. Behrens, J. Organomet. Chem., 1986, 312, C53.

315. K. Seitz and U. Behrens, J. Organomet Chem., 1988, 345, 351.

316. D. Wormsbächer, F. Edelmann and U. Behrens, Chem. Ber., 1981, 114, 153.

317. W.R. Roper, J.M. Waters, L.J. Wright and F. von Muers J. Organomet. Chem., 1980, 201, C27.

318. H. Umland and U. Behrens, J. Organomet. Chem., 1983, 273, C39.

319. D.E. Fjare, J.A. Jenson and W.L. Gladfelter, Inorg. Chem., 1983, 22, 1774.

320. K. Nakamoto, "Infrared and Raman Spectra of Inorganic and Coordination Compounds", 4th Ed. Wiley-Interscience Chichester, 1986, p.283.

321. A.H. Norbury, Adv. Inorg. Chem. Radiochem, 1975, 17, 232.

322. D. Nuel, F. Dahan and R. Mathieu, Organometallics, 1985, 4, 1436.

323. Y. Chi and J.R. Shapley, Organometallics, 1985, 4, 1900.

324. W.-Y. Yeh and J.R. Shapley, J. Organomet. Chem., 1986, 315, C29.

325. J. Suades, F. Dahan and R. Mathieu, Organometallics, 1988, 7, 47.

326. C. Weatherell, N.J. Taylor, A.J. Carty, E. Sappa and A. Tiripicchio, J. Organomet. Chem., 1985, 291, C9.

327. E. Roland, W. Bernhardt and H. Vahrenkamp, Chem. Ber., 1986, 119, 2566.

328. W. Bernhardt and H. Vahrenkamp, J. Organomet. Chem., 1988, in press.

329. J.K.M. Saunders, and B.K. Hunter, "Modern NMR Spectroscopy", Oxford University Press, Oxford, Ch.7.

330. G.E. Hawkes, L.Y. Lian, E.W. Randall, K.D. Sales and S. Aime, J. Chem. Soc., Dalton Trans, 1985, 225.

331. W.E. Lindsell, N.M. Walker and A.S.F. Boyd, J. Chem. Soc., Dalton Trans, 1988, 675.

332. A.J. Carty, N.J. Taylor, E. Sappa and A. Tiripicchio, Inorg. Chem., 1983, 22, 1871.

333. M. Lanfranchi, A. Tiripicchio, E. Sappa, S.A. Maclaughlin and A.J. Carty, J. Chem. Soc., Chem. Commun., 1982, 538.

334. G. Gervasio, D. Osella and M. Valle, Inorg. Chem., 1976, 15, 1221.

335. M.I. Bruce, J.G. Matisons, B.W. Skelton and A.H. White, Aust. J. Chem., 1982, 35, 687.

336. D.L. Davies, J.C. Jeffery, D. Miguel, P. Sherwood and F.G.A. Stone, J. Chem. Soc., Chem. Commun., 1987, 454.

337. E. Sappa, O. Gambino, L. Milone and G. Cetini, J. Organomet. Chem., 1972,39, 169.

338. M. Catti, G. Gervasio and S.A. Mason, J. Chem. Soc., Dalton Trans, 1977, 2260.

339. G. Granozzi, E. Tondello, R. Bertoncello, S. Aime and D. Osella, Inorg. Chem., 1983, 22, 744.

340. S.A. MacLaughlin, J.P. Johnston, N.J. Taylor, A.J. Carty and E. Sappa, Organometallics, 1983, 2, 352.

341. E. Boyer, A.J. Deeming and S.E. Kabir, J. Chem. Soc., Chem. Commun., 1986, 577.

342. K. Henrick, M.McPartlin, A.J. Deeming, S. Hasso and P.J. Manning, J. Chem. Soc., Dalton Trans, 1982, 899.

343. S. Aime and A.J. Deeming, J. Chem. Soc., Dalton Trans, 1983, 1807.

344. L.J. Farrugia, unpublished results.

345. A. Modinos and P. Woodward, J. Chem. Soc., Dalton Trans, 1975, 1534.

346. A.J. Carty, A.A. Cherkas and L.H. Randall, Polyhedron, 1988, 7, 1045.

347. M. Green, J.A.K. Howard, J.L. Spencer and F.G.A. Stone, J. Chem. Soc., Dalton Trans, 1977, 271.

348. M. Green, J.A.K. Howard, M. Murray, J.L. Spencer, and F.G.A. Stone, J. Chem. Soc., Dalton Trans, 1977, 1509.

349. J.G. Verkade and J.A. Mosbo in "Methods in Stereochemical Analysis; Phosphorus-31 n.m.r spectroscopy in Stereochemical Analysis of Organic Compounds and Metal Complexes", eds. J.G. Verkade, L.D. Quin, V.C.H Weinheim, 1987; Vol. 8, Ch. 13, pp 425-463.

350. E. Sappa, A. Tiripicchio and M. Tiripicchio-Camellini, Inorg. Chem. Acta., 1980, 41, 11.

351. A.J. Carty, N.J. Taylor, E. Sappa and A. Tiripicchio Inorg. Chem., 1983, 22, 1871.

352. E. Sappa, A. Tiripicchio and M. Tiripicchio-Camellini J. Organomet. Chem., 1983, 246, 287.

353. P. Brun, G.M. Dawkins, M. Green. R.M. Mills, J.-Y. Salaun, F.G.A. Stone and P. Woodward, J. Chem. Soc., Dalton Trans, 1983, 1357.

354. A.J. Carty, S.A. MacLaughlin and N.J. Taylor, J. Chem. Soc., Chem. Commun., 1981, 476.

355. M.I. Bruce and A.G. Swincer, Adv. Organomet. Chem., 1983, 22, 59.

356. W. Bernhardt and H. Vahrenkamp, Angew. Chem. Int. Ed., (Engl.), 1984, 23, 141.

357. Y.N. Al-Obaidi, M. Green, N.D. White and G.E. Taylor J. Chem. Soc., Dalton Trans, 1982, 319.

358. J. Silvestre, and R. Hoffmann, Helv. Chim. Acta., 1985, 68, 1461.

359. F.J. Garcia Alonso, A. Höhn, J. Wolf, H. Otto and H. Werner, Angew. Chem. Int. Ed. (Engl.), 1985, 24, 406.

360. A. Höhn, H. Otto, M. Dziallas and H. Werner, J. Chem. Soc., Chem. Commun., 1987, 852.

361. H. Werner, J. Wolf, F.J. Garcia Alonso, M.L. Ziegler and O. Serhadli, J. Organomet. Chem., 1987, 336, 397.

362. M. Cree-Uchiyama, J.R. Shapley and G.M. St. George, J. Am. Chem. Soc., 1986, 108, 1316.

363. D.G. VanderVelde, J.S. Holmgren and J.R. Shapley, Inorg. Chem., 1987, 26, 3077.

364. H.-J. Kneuper and J.R. Shapley, Organometallics, 1987, 6, 2455.

365. W.-Y. Yeh, H.-J. Kneuper and J.R. Shapley, Polyhedron, 1988, 7, 961.

366. A. Martinsen and J. Songstad, Acta Chem. Scand. A., 1977, 31, 645.

367. C.E. Megiris, P. Berlowitz, J.B. Butt and H.H. Kung, Surf. Sci., 1985, 159, 184.

368. M.M. Hills, J.E. Parmeter and W.H. Weinberg, J. Am. Chem. Soc., 1987, 109, 4224.

369. G.A. Somarjai, Surf. Sci., 1979, 89, 496.

370. R.D. Adams and S. Wang, Organometallics, 1986, 5, 1272.

371. R.D. Adams, J.E. Babin, R. Mathab and S. Wang, Inorg. Chem., 1986, 25, 1623.

372. N. Walker and D. Stuart, Acta. Crystallogr. Sect. A., Found crystallogr. 1983, A39, 158.

373. "International Tables for X-Ray Crystallography", Kynoch Press, Birmingham, 1974, Vol. 4.

374. P.R. Mallinson and K.W. Muir, J. Appl. Cryst., 1985, 18, 51.

375. F.R. Hartley in "Comprehensive Organometallic Chemistry", eds. G. Wilkinson, F.G.A. Stone and E.W. Abel, Pergamon Press, Oxford, 1982, Vol. 6., p.471.

376. D.A. Kleier and G. Binsch, Q.C.P.E., 1970, 11, 165.

377. J. Sandstrom, "Dynamic NMR Spectroscopy", Academic Press, New York, 1982.

378. A.L. Van Geet, Anal. Chem., 1970, 42, 679.

379. J.L. Spencer, Inorg. Synth. 1979, 19, 213.

380. R. Hoffmann, J. Chem. Phys., 1963, 39, 1397.

381. D.L. Thorn and R. Hoffmann, Inorg. Chem., 1978, 17, 126.

382. W.L. Jorgenson, "PSI77", Q.C.P.E., 1977, 10, 340.

383. see K.J. Laidler, "Chemical Kinetics", Harper and Row, New York, 3rd edition, 1987, Ch.2, p.29.